UNIVERSIDAD NACIONAL AUTÓNOMA DE MÉXICO

PROGRAMA DE POSGRADO EN CIENCIAS DE LA TIERRA

CENTRO DE GEOCIENCIAS

AMBIENTE TECTONICO DEL MARGEN OCCIDENTAL DE OAXAQUIA EN EL CRETACICO INFERIOR Y SU RELACION CON LA GEODINAMICA REGIONAL

T E S I S

QUE PARA OPTAR POR EL GRADO DE:

DOCTOR EN CIENCIAS DE LA TIERRA

P R E S E N T A

MARIA ISABEL SIERRA ROJAS

TUTOR

Dr. ROBERTO STANLEY MOLINA GARZA

CENTRO DE GEOCIENCAS, UNAM

MIEMBROS DEL COMITÉ TUTOR:

Dr. José Luis Sánchez Zavala, Instituto de Geología, UNAM.

Dr. Timothy Lawton, CGeo, UNAM.

Querétaro, Junio de 2018

Declaración de Ética

“Declaro conocer el Código de Ética de la Universidad Nacional Autónoma de México, plasmado en la legislación Universitaria. Con base en de las definiciones de integridad y honestidad ahí especificadas, aseguró mediante mi firmar al alcance que el presente trabajo es original y enteramente de mi autoría. Toda la actividad de, o referencias a, la obra de otros autores aparecerán de vida y adecuadamente señaladas, así como acreditadas mediante los recursos editoriales convencionales”.

MARIA ISABEL SIERRA ROJAS

INDICE GENERAL

RESUMEN

Los sistemas depositacionales del Cretácico Temprano al suroeste de Oaxaquia fueron controlados por procesos tectónicos asociados a la formación de arcos continentales y la acreción de arcos de islas. El régimen tectónico en el que se desarrollaron las cuencas sedimentarias en el suroeste de México en el Cretácico Temprano es inferido a partir de la composición de los productos terrígenos depositados, así como su edad de depósito, y ambiente sedimentario. Igualmente, el análisis de circones detríticos en las cuencas de Zicapa y Tentzo y la correlación con cuencas contemporáneas como Zapotitlán y Chivillas permite proponer un escenario tectónico para el Cretácico Inferior en el margen occidental de Oaxaquia. Proponemos entonces el desarrollo de cuencas de arco en la porción más occidental de Oaxaquia en la Plataforma Guerrero-Morelos (cuenca de Zicapa), y cuencas extensionales al este en posición de tras-arco (Cuenca de Tentzo, Zapotitlán y Chivillas), las cuales registran tasas rápidas de extensión. Finalmente, por medio de un análisis paleomagnético, de magnetoestratigrafía y magnetismo de rocas en la cuenca de Zicapa, fue posible constreñir la edad de depósito de esta formación al Barremiano. Rotaciones en el eje vertical de aproximadamente 70° en sentido antihorario indican que la región de la Plataforma Guerrero-Morelos fue afectada por fallamiento lateral izquierdo posterior al Barremiano. Dicha rotación es atribuida la deformación en la región de Tierra Colorada y La Venta y de la rotación de bloques en la plataforma Guerrero-Morelos.

Palabras clave: Cretácico Inferior, Oaxaquia, sedimentología, proveniencia, paleomagnetismo.

ABSTRACT

Depositional systems from the Early Cretaceous in southwestern Oaxaquia were influenced by tectonic processes associated with initiation of a continental arc and subsequent island arc accretion. During the Early Cretaceous, a series of basins was born in this geotectonic context that record crustal extension, magmatism, and basement exhumation. Compositional analysis of the terrigenous products deposited in these basins, determination of depositional age, and interpretation of depositional environment permits interpretation of the tectonic regime in which the basins were developed. Detrital zircon analyses from the Zicapa and Tentzo basins were correlated with analyses in the Chivillas basin, which provides insight into the tectonic scenario for the western margin of Oaxaquia during the Early Cretaceous. I propose the development of an arc in the westernmost margin of Oaxaquia (Zicapa arc), and a series of back-arc basins in the east (Tentzo, Zapotitlán, and Chivillas basins), which recorded fast extension rates. Finally, through a paleomagnetic, magnetostratigraphic, and rock-magnetism study of the Zicapa Formation, I was able to constrain the age of the strata deposited during Early Cretaceous to the Barremian. Counterclockwise vertical- axis rotations of ca. 70° indicate that the Guerrero-Morelos platform was affected by left-lateral deformation after the Barremian. Such rotation is attributed to deformation in the Tierra-Colorada and La Venta area, and to block rotations in the Guerrero- Morelos platform.Key words: Lower Cretaceous, Oaxaquia, sedimentology, provenance, paleomagnetism.

CAPITULO 1. GENERALIDADES

1.1. INTRODUCCIÓN

La Cordillera de Norte América es uno de los orógenos convergentes más estudiados en el mundo. Esta región contiene un largo registro de magmatismo de arco, acreción de arco de islas y deformación contráctil de retro-arco (Dickinson, 2004). En la literatura, esta historia ha sido explicada como el resultado de una subducción continua desde el occidente de la placa Farallón durante el Mesozoico (e.g. Busby, 2004) y como el acoplamiento episódico de arcos de islas a la trinchera Norte América-Farallón. En ese sentido, Sigloch and Mihalynuk (2013) basados en tomografías del manto invocaron sistemas de múltiples arcos-fosas, similares a los presentes en el Pacífico occidental actual. Para validar dichos modelos, es necesario evidencias en el registro en los continentes. Mientras que el registro de magmatismo y acreción en el occidente de Canadá, Estados Unidos, y en la Península de Baja California es conocido con bastante detalle (Monger et al., 1982; Gabrielse y Yorath, 1989; Dickinson, 2004; Kimbrough y Moore, 2003; Kimbrought et al., 2014), el entendimiento del magmatismo de arco, polaridad de subducción y acreción de terrenos en la parte más sur de la Cordillera de Norte América en México y Centro América es aún fragmentario. Este estudio trata de aliviar esa carencia de información.

El registro de magmatismo en el margen continental en Mexico inicia en el Pérmico, disminuye durante el Triásico (Torres et al. 1999; Solari et al. 2001; Dickinson and Lawton, 2001; Kirsch et al. 2012; Ortega-Obregón et al., 2013) y se intensifica en el Jurásico (Lawton y Molina-Garza, 2014 y referencias en el mismo). En el Jurásico el magmatismo corresponde al arco Nazas (Dickinson and Lawton, 2001; Bartolini et al., 2003; Lawton y Molina, 2014). Además del magmatismo del Jurásico Temprano a Medio asociado al arco de Nazas (Pantoja- Alor, 1972; Anderson et al., 1991; Jones et al., 1995; Barboza-Gudiño et al., 1998, 1999, 2004, 2008; Bartolini, 1998; Blickwede, 2001; Bartolini et al., 2003) y del evento magmático del

Jurásico Tardío del oeste de México asociado al terreno Guerrero (Centeno-García et al., 2003; Kimbrough y Moore, 2003; Vega-Granillo et al., 2008; Valencia et al., 2013), existen reportes de magmatismo y metamorfismo en la zona sur de Oaxaquia en el Terreno Cuicateco en el Jurásico (Alaniz-Alvarez et al., 1996) (Figura 1.3).

En parte, debido a la escasez de datos y especialmente a la limitada exposición del registro geológico de ese período, la evolución Jurásico a Cretácico del oeste de México es en varios sentidos controversial. Este registro ha sido interpretado, por ejemplo, en términos de doble subducción de la placa Mezcalera bajo Norte América y bajo un arco intra-oceánico, formando así el Arco Nazas en el margen continental y el Superterreno Guerrero en el oeste (Freydier et al., 2000; Dickinson and Lawton, 2001; Lawton and Molina-Garza, 2014; (Figura 1.1A). Sin embargo, la polaridad de la subducción bajo el superterreno Guerrero no ha sido constreñido por los datos disponibles actualmente. Así mismo, diferentes escenarios de subducción han sido propuestos. Por ejemplo, Talavera-Mendoza et al. (2007) proponen la existencia de hasta cuatro sistemas arco-fosa, en una configuración con subducción de diferentes polaridades (Figura 1.1B). Modelos con una única subducción hacia el este también han sido propuestos (Busby, 2004; Elías et al., 2000; Martini et al., 2011; Martini et al., 2014). Estos modelos invocan la apertura y cierre de una cuenca de tras-arco entre el arco Guerrero y el bloque continental Mexicano (Figura 1.1C).

Así entonces, el estado actual de nuestro conocimiento sobre la evolución geológica del Jurásico-Cretácico se puede resumir a partir de una arco Jurásico continental en el margen occidental de Pangea, el cual se extiende desde California hasta Ecuador, que en México se refiere como el arco Nazas con la Formación del mismo nombre y secuencias correlacionables.

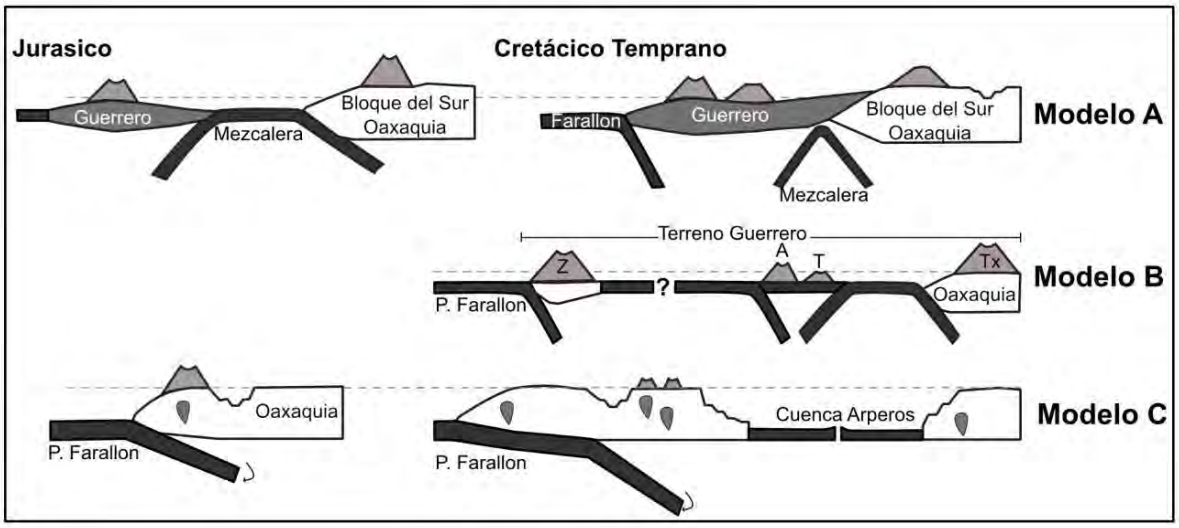

Figura 1.1. Modelos tectónicos alternativos para la evolución del occidente de México y el Terreno Guerrero. Modelo A. Doble subducción (Freydier et al., 2000; Dickinson and Lawton, 2001; Lawton and Molina-Garza, 2014). Modelo B. Varios Sistemas arco-fosa (Talavera-Mendoza et al., 2007). Modelo C. Una Subducción unidireccional hacia el este (Busby, 2004; Elías et al., 2000; Martini et al., 2011; Martini et al., 2014; Ortega-Flores et al., 2014). Z: Zihutanejo A: Arcelia, T: Teloloapan, Tx: Taxco.

En el margen continental, en Oaxaquia, sobre el arco Nazas en el norte de México se desarrolla una secuencia sedimentaria de margen pasivo que incluye las Formaciones Zuloaga y La Casita (Lawton y Molina-Garza, 2014), por lo que se ha interpretado la migración de ese magmatismo hacia el oeste (Dickinson y Lawton, 2001). Mientras que en el sur de México el registro de magmatismo parece ser continuo desde el Jurásico Medio (Ignimbrita las Lluvias y Unidad Diquiyú), al Jurásico Superior (trabajo aquí reportado, Sierra et al., 2016), al Neocomiano (Esquisto Taxco, Fm. Chapolapa, entre otras aquí reportado; Sierra y Molina, 2014). Por lo que parece haber un registro continuo.

En la región la montaña de Guerrero, durante en Jurásico Medio, una serie magmática félsica con firma geoquímica de arco, Ignimbrita Las Lluvias, está emplazada en Oaxaquia, donde contemporáneamente es depositado el Grupo Tecocoyunca en un ambiente extensional (Campa-Uranga et al., 2004). Hacia la región Mixteca, depósitos continentales de cuencas extensionales (Formaciones

Ayuquila y Tecomazuchil) son intrusionadas por el tronco de Chilixtlahuaca, un cuerpo alargado de 5 km de extensión cuya edad es de ca. 164 Ma (Campos-Madrigal et al., 2013). Un evento termal es registrado en las migmatitas del Complejo Ayú en la región Mixteca (Helbig et al., 2012), el cual ha sido interpretado como asociado a extensión en una cuenca de tras-arco durante el rompimiento de Pangea.

En el oeste de México también parece haber un registro continuo de magmatismo. Recientes datos de petrología ígnea, geocronología y paleomagnetismo de plutones anteriores al Cinturón Batolítico Peninsular en el área de Vizcaíno en Baja California (Torres- Carrillo et al., 2016) demuestran la presencia de un arco Jurásico Medio a Superior en un margen tectónico con un basamento diferente al del Arco nazas. Este arco es el registro más antiguo de magmatismo de arco en el límite oeste del Superterreno Guerrero. Sobre el arco Jurásico de Vizcaíno se emplaza durante el Cretácico el Arco Alisitos, cuyas cámaras magmáticas forman el Cinturón Batolítico Peninsular (Torres Carrillo et al., 2016). A su vez, Alisitos se acrecionó al margen de Norte América en el Albiano-Cenomaniano (Johnson et al., 2003; Molina-Garza et al. 2014; Torres- Carrillo et al. 2016). Esto lleva entonces al planteamiento general del siguiente problema. Los registros de magmatismo Jurásico-Cretácio de Oaxaquia (arco Nazas y sur de México) y de Baja California (arco San Andrés/Vizcaíno y Alisitos) se pueden atribuir a un mismo margen convergente como sugieren Martini y Ortega-Gutiérrez (2016) ¿o son dos límites convergentes diferentes?

Así, de norte a sur, uno de los elementos clave para la evaluación de modelos geodinámicos en el oeste de México es el registro de magmatismo de arco en el margen continental durante el Cretácico Temprano. Magmatismo continental del Cretácico Temprano se ha propuesto en California-Baja California, en el arco Santiago Peak (Schmidt et al., 2014; Torres-Carrillo et al., 2016). Este magmatismo puede corresponder a la migración de magmatismo al oeste que proponen Dickinson y Lawton (2001) por "*slab-roll back*". En el sur de México, el magmatismo

de arco continental que fue originalmente considerado pre-Jurásico, pero ahora se ha demostrado su edad Cretácico Temprano (Delgado-Argote y López-Martínez, 1992; Campa-Uranga et al., 2012; Solari et al., 2007; Campa-Uranga et al., 2004). El registro de magmatismo en el sur de México y su contexto tectono-estratigráfico son el enfoque principal de este trabajo.

La evolución Sistema Cordillerano de México durante el Jurásico y Cretácico Temprano también se caracterizó por el desarrollo de cuencas extensionales (Figura 1.2). Estas cuencas las podemos dividir en dos grandes familias: aquellas asociadas al magmatismo de arco en el margen Pacífico y las asociadas a la extensión asociada a la apertura del Golfo de México (GdM). La migración hacia el oeste del magmatismo como producto del retroceso del slab de Farallón ha sido invocado para explicar el origen del sistema del “Borderland rift” (Dickinson y Lawton, 2001), este incluye la cuenca de Bisbee, la fosa de Chihuahua y la cuenca de Sabinas en el norte de México (Figura 1.2) que se desarrollan en un ambiente de tras-arco transtensional (e.g., Dickinson y Lawton, 2001; Haenggi, 2001).

Aunque este modelo satisface la evolución de las cuencas, existen otros eventos geodinámicos que afectan esta región y que a su vez pueden haber jugado un papel importante en su evolución. A medida que Norteamérica y Suramérica se separaran, se abre la cuenca del proto-Caribe (Pindell y Kennan, 2009). Incluso el GdM ha llegado a ser interpretado como una cuenca extensional desarrollada en el flanco continental del arco Nazas (Stern y Dickinson, 2010). La parte sur del Sistema Cordillerano se puede considerar entonces como un lugar donde el magmatismo del margen convergente del Pacífico interactúa en espacio y tiempo con la extensión y el desarrollo del margen pasivo del Atlántico durante el Mesozoico (GdM).

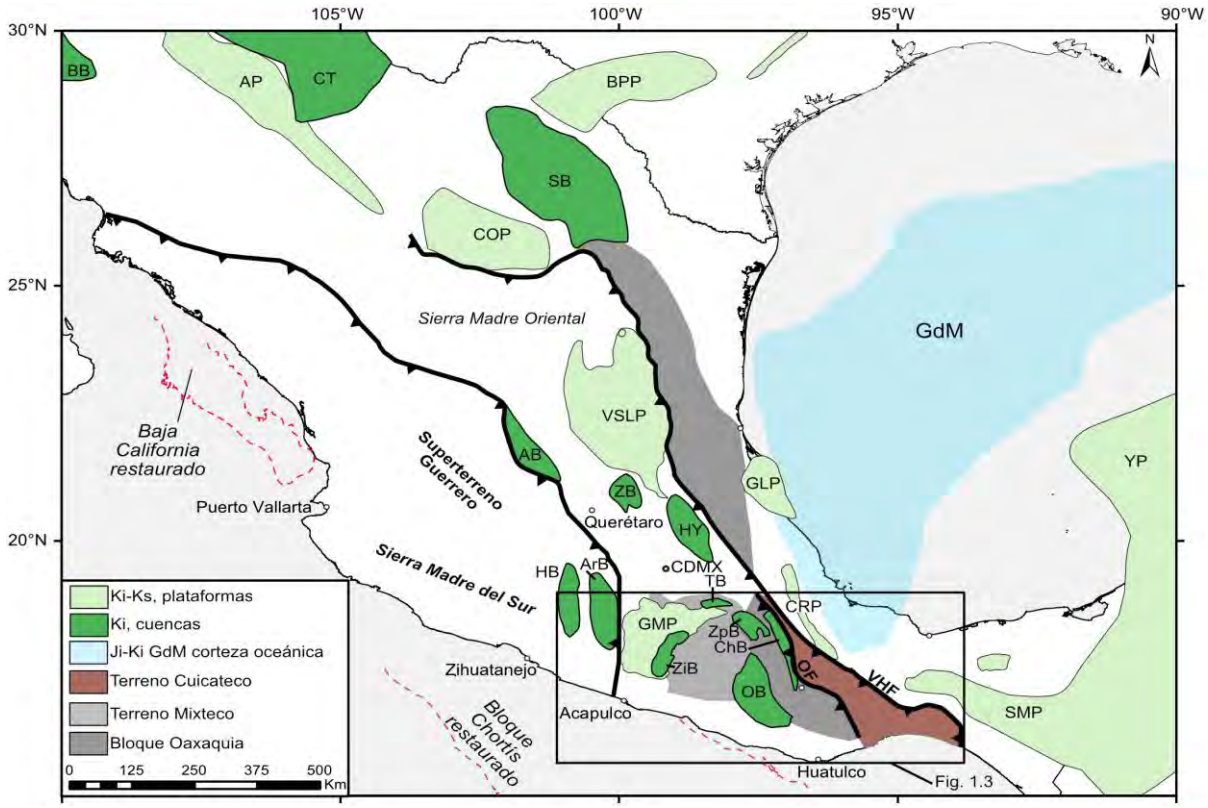

Figura 1.2. Mapa de México mostrando algunos elementos fisiográficos del Jurásico-Cretácico. Basamento Precámbrico a Paleozoico de los bloques Oaxaquia y terreno Mixteco se muestran en gris; la cuenca del Golfo de México (GdM) en azul; Terreno Cuicateco en café; Plataforma de carbonatos del Albiano al Cenomaniano en verde claro; cuencas del Cretácico Inferior en verde oscuro; las líneas rojas punteadas representan Baja California (Ferrari et al., 2013) y Chortís (Rogers et al., 2007) restaurados. AP: Plataforma Aldama; COP: Plataforma de Coahuila; BPP: Plataforma Burro- Peyotes; VSLP: Plataforma Valles-San Luis Potosí; GLP: Plataforma Golden Lane; GMP: Plataforma Guerrero-Morelos; CRP: Plataforma Córdoba; SMP: Plataforma Sierra Madre; YP: Plataforma Yucatan; OF: Falla Oaxaca; VHF: Falla Vista Hermosa: BB: Cuenca de Bisbee; CT: Cuenca de Chihuahua; SB: Cuenca de Sabinas; HY: Cuenca de Huayacocotla; AB: Cuenca de Arperos; ZB: Cuenca de Zimapán; HB: Cuenca de Huetamo; ArB: Cuenca de Arcelia; ZiB: Cuenca de Zicapa; ZpB: Cuenca de Zapotitlán; CB: Cuenca de Chivillas; OB: Cuenca de Oaxaca; TB, Cuenca de Tentzo.

El depósito en ambientes extensionales continuó durante el Cretácico Temprano. El evento más notable, aunque controversial, es el desarrollo de la cuenca de Arperos-Arcelia, pero incluye también los depósitos de la cuenca Cuicateca y depósito en ambientes extensionales continentales. La cuenca de Arperos registra, por ejemplo, magmatismo de oceanización asociados con depósitos marinos profundos entre el Jurásico Superior y el Cretácico Inferior desde Sinaloa y Zacatecas hasta el norte de Guerrero respectivamente (Martini et al., 2011; Ortega-Flores et al., 2014; Martini et al., 2014; Figura 1.1, Modelo C). La importancia paleogeográfica de la cuenca de Arperos-Arcelia radica en que separa asociaciones de arco del Superterreno Guerrero al oeste, de asociaciones petrotectónicas asociadas al margen continental de México al este. Los modelos de su evolución son controversiales ya que esta cuenca se ha considerado una cuenca oceánica (Freydier et al., 2000; entre otros) o una cuenca de tras-arco (Pindel y Kennan, 2009; Martini et al., 2014). Aquí se concluye que la gran mayoría de las cuencas del sur de México en ambientes continentales se desarrollan en en ambiente tectonoestratigráfico de tras-arco. Los modelos regionales implican que las cuencas del sur de México desarrollan en el tras-arco de un arco continental sin relación con la cuenca de Arperos.

La acreción y acoplamiento del Superterreno Guerrero al margen continental de México, y por lo consiguiente, el cierre de la cuenca de Arperos-Arcelia, ha sido interpretado del Hauteriviano-Albiano (Martini et al., 2011; Martini et al., 2014). En este trabajo se demuestra que después del evento de acreción, las cuencas extensionales en el sur de México desarrollan renovada subsidencia (Sierra-Rojas et al., 2016) que cesa hacia el Aptiano-Albiano. En este período México fue cubierto de norte a sur por extensas plataformas de carbonatos separadas por depósitos de cuenca; este proceso continúa en el Albiano y Cenomaniano (Ferrusquia-Villafranca, 1976; Ortega-González y Lambarria-Silva, 1991; Wilson y Ward, 1993; Hernández-Romano et al., 1997; Lopez-Doncel, 2003; Ortuño-Alzate et al., 2003). Los depósitos de plataforma están representados en el sur de México de oeste a este por las formaciones Morelos, Teposcolula y Orizaba (Figura 1.2) y los

depósitos de cuenca por las formaciones Miahuatepec, Tamaulipas y unidades correlacionables. Los depósitos de plataforma sobreyacen un registro de sedimentación y magmatismo en ambientes continentales del Cretácico Inferior y no están asociados a magmatismo.

Hacia el oriente de la falla de Oaxaca, en la región correspondiente al Terreno Cuicateco (Figuras 1.2 y 1.3), eventos de magmatismo y metamorfismo han sido registrados en el Jurásico Tardío a Cretácico Temprano (Delgado-Argote et al., 1992; Ángeles-Moreno, 2006; Coombs, 2016). Su relación con la cuenca de Arperos y con las cuencas extensionales y sistemas de arco del Cretácico Temprano es también un tema de debate. La formación de la cuenca Cuicateca, dónde se deposita la Formación Chivillas, se ha interpretado como tipo *pull-apart*, la cual es asociada a la formación del proto-caribe (Carfantan, 1981: Pindellet al., 1988), o a la apertura del GdM (Mendoza-Rosales et al., 2010). Una de las preguntas fundamentales es entonces si el magmatismo Jurásico del sur de México es parte de un registro continuo de convergencia en el margen occidental de Oaxaquia desde el Pérmico hasta el Cretácico, lo cual tendría implicaciones geodinámicas importantes.

Varios de los modelos geotectónicos han supuesto que el magmatismo asociado a subducción del Jurásico Tardío y Cretácico Temprano se limita a la existencia de un arco o arcos de islas en el superterrerno Guerrero, con manifestaciones en Mexico continental por cambios en el ángulo de subducción (e.g., Martini et al., 2011). Por ello la estratigrafía del Sur de México durante el Cretácico Temprano es considerado clave para entender la evolución de la parte occidental de Norte América y el orógeno Cordillerano. En este trabajo analizamos el registro estratigráfico Jurásico-Cretácico de Oaxaquia en su paleo margen pacífica hacia la paleo margen atlántica, desde la Plataforma Guerrero-Morelos (Formación Zicapa) a las cuencas de Tentzo y Chivillas (formaciones Atzompa y Chivillas) en el bloque conformado por los terrenos Mixteco y Oaxaca. En estas zonas enfocamos el trabajo de investigación en las formaciones Zicapa y Atzompa, específicamente en el registro sedimentario

y magmático asociado a subducción (Figura 1.4), en los ambientes de depósito, estudios de proveniencia y asi como paleogeografía, paleomagnetismo y geocronología. Con estos estudios tratamos de entender la relación entre el desarrollo de las cuencas extensionales con los procesos geodinámicos activos desde el Jurásico Tardío hasta el Cretácico Temprano (magmatismo y extensión).

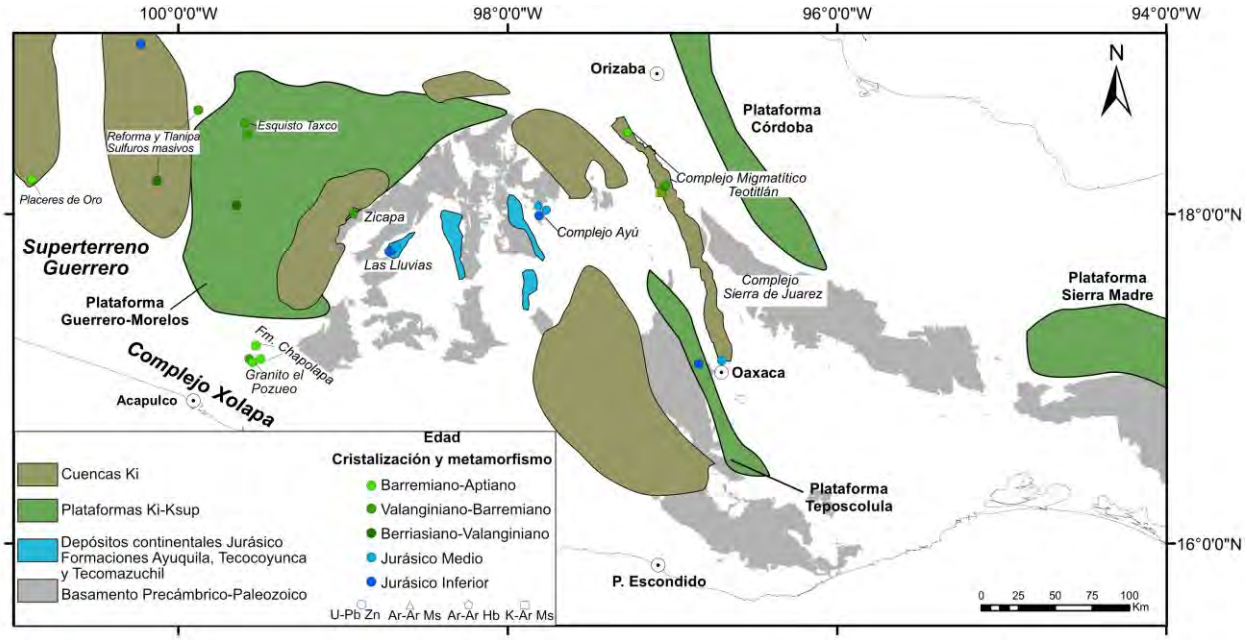

Figura 1.3. Contexto geotectónico del sur de México. Se muestran en polígonos el basamento cristalino pre-Mesozoico (Complejo Acatlán y Complejo Oaxaqueño), las cuencas del Jurásico y Cretácico Temprano, las plataformas de carbonatos del Aptiano-Cenomaniano. Las edades de cristalización y metamorfismo de algunos cuerpos ígneos y metamórficos son indicadas en colores. Ignimbrita Las Lluvias (Campa-Uranga et al., 2004), Complejo Ayú (Helbig et al., 2012), Complejo Migmatítico de Teotitlán y Sierra de Juarez (Delgado-Argote et al., 1992; Ángeles-Moreno, 2006), Formación Chapolapa (Campa e Iriondo, 2004; Hernández-Treviño et al., 2004), El Pozuelo (Solari et al., 2007), Esquisto Taxco (Campa-Uruanga e Iriondo 2004; Campa-Uruanga et al., 2012), Formación Zicapa (Fitz-Diaz et al., 2001), Sulfuros masivos Tlanipa y Reforma (Mortensen et al., 2008), Plutón Placeres de Oro (Martini et al., 2009).

El capítulo dos de esta tesis corresponde a la definición estratigráfica de la Formación Zicapa en la región de la plataforma Guerrero-Morelos. En él redefinimos estratigráficamente la formación con base en evidencias de campo, definimos el ambiente de depósito, y la proveniencia de los sedimentos, y asignamos una edad para el magmatismo que caracteriza a la Formación Zicapa, definiendo con base en los datos nuevos y la correlación estratigráfica el arco de Zicapa (Sierra-Rojas y Molina-Garza, 2014).

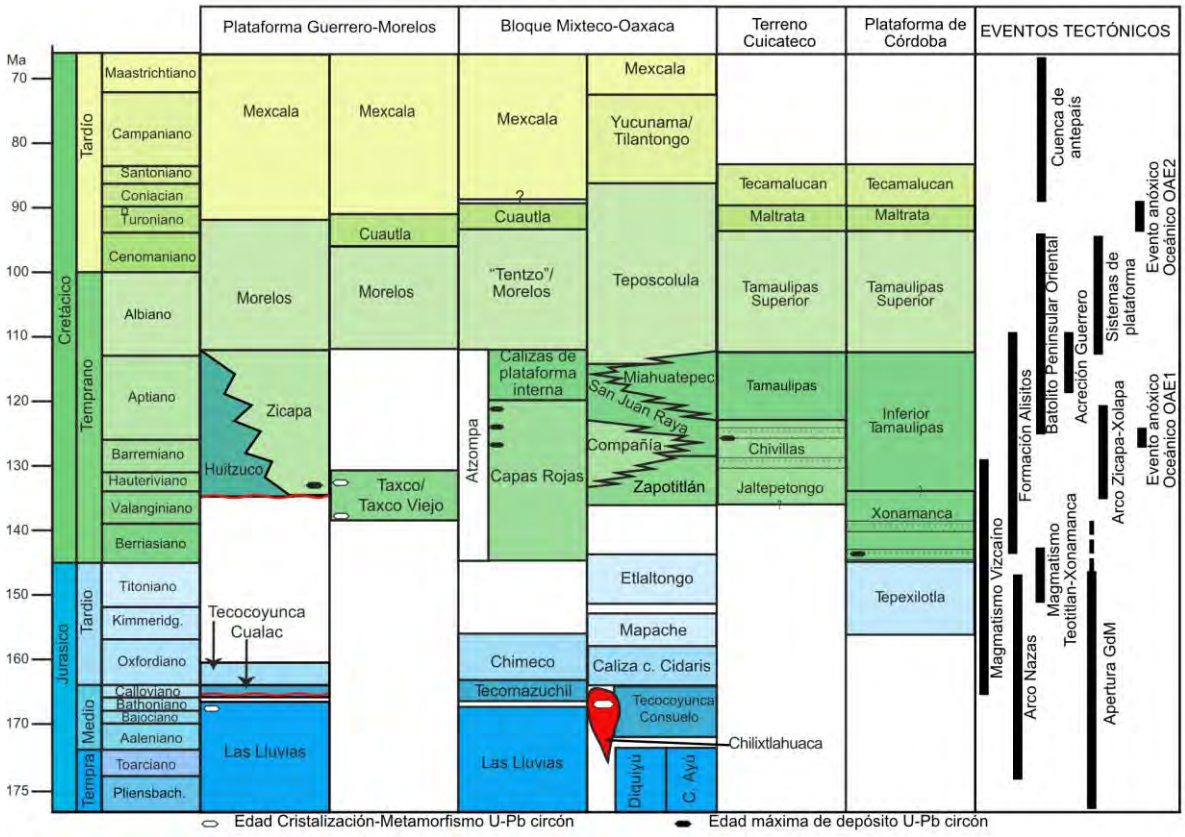

Figura 1.4. Correlación del Suroeste al este de las unidades Mesozoicas del sur de México. Las columnas de cada región son generalizadas a partir de varios autores. Plataforma Guerrero–Morelos (Hernández-Romano et al.1997; Campa et al. 2012; Sierra-Rojas and Molina-Garza 2014), Bloque Mixteco-Oaxaca (López-Ticha, 1985; Campos-Madrigal et al., 2008; Monroy-Fernández y Sosa-Patrón, 1984; Sierra-Rojas et al., 2016), Terreno Cuicateco (Ortega-González y Lambarria-Silva, 1991; Ortuño-Arzate et al., 2003; Angeles-Moreno, 2006; Mendoza-Rosales, 2010; Coombs, 2016).

El capítulo tres trata sobre la Formación Atzompa depositada en la cuenca de Tentzo como parte del sistema de cuencas extensionales del sur de México en el Cretácico Temprano. Con base en análisis de proveniencia y análisis de facies sedimentarias, se determina que la cuenca de Tentzo es una cuenca extensional de tras-arco, la cual registra la transición desde ambientes continentales fluviales y lacustres hacia una plataforma de carbonatos desde el Barremiano hasta el Aptiano (Sierra-Rojas et al., 2016). Igualmente, determinamos la conexión entre la cuenca de Tentzo con la cuenca de Chivillas al este.

En el capítulo cuatro, el énfasis está en el paleomagnetismo y las propiedades magnéticas de las capas rojas de la Formación Zicapa. Con base en sus propiedades y en la temporalidad de la adquisición de la magnetización en estas rocas, probamos la confiabilidad del uso de datos paleomagnéticos en capas rojas para ser utilizados en modelos paleogeográficos. También establecemos la relación paleogeográfica entre el sur de México y el resto de Norteamérica.

1.2. HIPOTESIS DE TRABAJO

El registro estratigráfico del Cretácico Temprano en el sur de México ocurre en relación paleogeográfica cercana a un arco continental en el margen paleo-Pacífico de México. El arco continental es un arco extensional que lleva a la evolución de una cuenca de tras-arco.

1.3. OBJETIVOS

Objetivo General

Determinar la relación entre la tectónica, el magmatismo y la sedimentación durante el Cretácico Temprano en el borde occidental de Oaxaquia previo al desarrollo del margen pasivo del Aptiano-Cenomaniano en el sur de México.

Objetivos específicos

- Caracterizar sedimentológicamente las unidades sedimentarias del Cretácico Inferior en Oaxaquia, específicamente las formaciones Zicapa, Atzompa, Caltepec y Chivillas.
- Analizar las áreas de procedencia de las areniscas del Cretácico Temprano por medio de circones detríticos y petrografía de areniscas, lo cual permitirá correlacionar con las unidades correspondientes a la paleolatitud obtenida.
- Inferir a partir del análisis de litofacies y proveniencia de sedimentos las características paleogeográficas de las cuencas de Zicapa y Tentzo.
- Determinar las paleolatitudes para las cuencas de Zicapa y Tentzo y para la Formación Caltepec en el Cretácico Temprano.
- Establecer columnas de polaridad magnética para la Formación Zicapa en secciones de referencia.

CAPITULO 2.

La Formación Zicapa del sur de México: revisión estratigráfica, sedimentología y ambientes sedimentarios.

Sierra-Rojas, M.I. y Molina-Garza, 2014, La Formación Zicapa del sur de México: revisión estratigráfica, sedimentología y ambientes sedimentarios, Revista Mexicana de ciencias Geológicas, V. 31(2), 174-189.

Contribuciones individuales:

Maria Isabel Sierra-Rojas: Planteamiento del problema y trabajo de campo, levantamiento de columnas estratigráficas, toma de muestras. Preparación de muestras para análisis geocronológicos y obtención de datos geocronológicos, procesado de datos, petrografía de areniscas y análisis modales, análisis sedimentológico y de facies sedimentarias. Elaboración de mapas y figuras, redacción del manuscrito.

Roberto Molina-Garza: Planteamiento del problema y asesoría general del proyecto. Trabajo de campo, supervisión en obtención de datos de campo, revisión y orientación en la interpretación de datos y revisión del manuscrito.

La Formación Zicapa del sur de México: revisión estratigráfica, sedimentología y ambientes sedimentarios

María Isabel Sierra-Rojas y Roberto Stanley Molina-Garza

Centro de Geociencias, Universidad Nacional Autónoma de México, Campus Juriquilla, Querétaro 76230, México.
misierra@geociencias.unam.mx

RESUMEN

El Cretácico Inferior del oeste de México se ha interpretado como el registro de magmatismo y sedimentación en un sistema de arco de islas separado de la margen continental por una cuenca marginal, al este de la cual se desarrolló un sistema de plataformas calcáreas sobre el basamento metamórfico pre-Mesozoico. Las características sedimentológicas y las relaciones de facies de las rocas de la Formación Zicapa en el norte de Guerrero y sur de Puebla, permiten inferir la presencia de magmatismo calcialcalino en el occidente del núcleo continental de México en el Cretácico Temprano, previo al desarrollo de la plataforma Guerrero-Morelos en el Albiano. La Formación Zicapa registra un ambiente de sedimentación continental cercano a la costa con evidencias de, al menos, una transgresión y presencia de volcanismo intermedio de ~130 Ma. Para mejorar el conocimiento de la estratigrafía del sur de México en el Cretácico Inferior, se propone dividir la Formación Zicapa en cinco miembros: el Miembro Cerro La Cruz, compuesto por un conglomerado basal, el Miembro San Juan de las Joyas, de carácter calcáreo, el Miembro Ajuatetla, de carácter siliciclástico y de ambiente transicional marino, el Miembro San Andrés, de carácter volcanosedimentario y el Miembro río Poblano, dominado por limolita y lutita roja con algunas intercalaciones de caliza. La edad máxima de depósito de la Formación Zicapa fue determinada con base en análisis U-Pb por ablasión láser de circones detríticos, obteniendo una edad para la parte media de la formación (Miembro San Andrés) de 133±1.3 Ma. Junto con unidades como las formaciones Chapolapa, Xonamanca y Atzompa, la Formación Zicapa apoyan la interpretación de la margen oeste de Oaxaquia como una margen convergente durante el Barremiano-Aptiano.

Palabras clave: facies sedimentarias; volcanismo calcialcalino; Cretácico Temprano; Formación Zicapa; México.

ABSTRACT

The Lower Cretaceous of western Mexico has been interpreted as the record of magmatism and sedimentation in an island arc system, separated of the continental margin by a marginal basin, east of which a system of carbonate platforms was developed on the pre-Mesozoic basement. The sedimentological characteristics and facies relations of the Zicapa Formation in northern Guerrero and southern Puebla allow us to infer the presence of calc-alkaline magmatism in western margin of mainland Mexico during the Early Cretaceous, prior to the development of the Albian Guerrero-Morelos platform. The Zicapa Formation deposited in a continental environment near the coast with the presence of ~130 Ma intermediate volcanism and evidences of, at least, one transgression. To improve the knowledge of the Early Cretaceous stratigraphy of southern Mexico, we suggest to divide the Zicapa Formation into five members: the Cerro La Cruz Member which consists of a basal conglomerate, San Juan de las Joyas Member, made of limestone, the Ajuatetla Member of siliciclastic and transitional marine environment, the San Andrés Member with volcanosedimentary character and the río Poblano Member, dominated by red siltstone and shale interbedded with some limestone. The maximum depositional age for the medium part (San Andrés Member) of the Zicapa Formation is 133±1.3 Ma, from detrital zircon U-Pb laser-ablation geochronology. Strata of the Chapolapa, Atzompa, and Xonamanca formations, together with the Zicapa Formation support interpretation of a convergent margin in western Oaxaquia during Barremian-Aptian time.

Key words: sedimentary facies; calcalkaline volcanism; Early Cretaceous; Zicapa Formation; Mexico.

INTRODUCCIÓN

El Cretácico Temprano del oeste de México se caracteriza por el registro de magmatismo y sedimentación en un sistema de arco de islas separado de la margen continental por una cuenca marginal, al este de la cual se desarrolló un sistema de plataformas calcáreas sobre un basamento pre-Mesozoico (Martini *et al.*, 2011). Este es el caso de la plataforma Guerrero-Morelos del Albiano en Guerrero, construida en la margen occidental del terreno Mixteco (Figura 1). Al oeste de dicha plataforma existe el registro de volcanismo de arco y sedimentación peri-arco del Terreno Compuesto Guerrero (Centeno-García *et al.*, 2003; Centeno-García *et al.*, 2008). Subyaciendo a las rocas calcáreas de la Plataforma Guerrero-Morelos, aflora la Formación Zicapa (de Cserna *et al.*, 1980), objetivo del presente estudio, en el que mostramos que magmatismo calcialcalino está presente en las secuencias del Barremiano-Aptiano del terreno Mixteco. En trabajos previos sobre la Formación Zicapa se reporta principalmente su ubicación, paleontología y descripciones litológicas (de Cserna *et al.,* 1980; Figueroa-Catalán y Gómez-Martínez, 2010 y Pantoja-Alor, 1990).

A nivel regional, para el sur de México, se puede considerar que el registro sedimentario del intervalo Berriasiano-Barremiano en la

Sierra-Rojas, M.I., Molina-Garza, R.S., 2014, La Formación Zicapa del sur de México: revisión estratigráfica, sedimentología y ambientes sedimentarios: Revista Mexicana de Ciencias Geológicas, v. 31, núm. 2, p. 174-189.

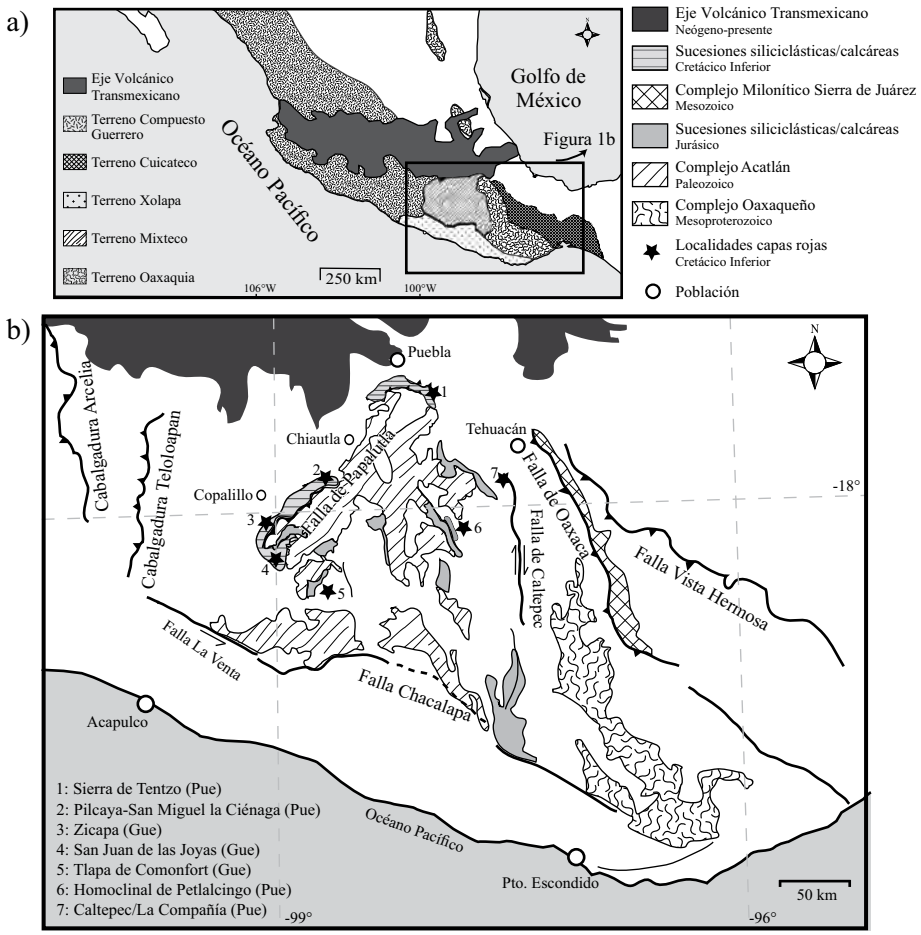

Figura 1. Mapa geológico simplificado del sur de México. El mapa de la parte superior muestra los terrenos tectonoestratigráficos de México (Modificado de Keppie *et al.*, 2004). El mapa inferior muestra la distribución de las rocas del basamento mesoproterozico y paleozoico y las coberturas sedimentarias mesozoicas (Modificado de Ferrari *et al.*, 2007). Las estrellas marcan las localidades del Cretácico Inferior en el terreno Mixteco. Las localidades 2 y 4, se encuentran en las Figuras 3 y 9.

margen Mixteco/Oaxaquia, representa una pieza clave para entender la historia geológica de esta región. En el presente trabajo abordamos el aspecto de los ambientes de depósito, la presencia de volcanismo andesítico y los posibles escenarios paleogeográficos para el depósito de la Formación Zicapa, lo cual permitirá entender de mejor manera los procesos tectónicos que ocurrieron en el suroccidente de México.

Además de conocer los ambientes de depósito en un área y en un tiempo específicos, nuestro trabajo permitió analizar las posibles áreas fuente de los sedimentos, su relación con la tectónica local o regional y correlacionar regionalmente con otras unidades en ambientes sedimentarios y tectónicos similares.

La integración de cartografía geológica, sedimentología y geocronología permitió proponer un modelo de transición tectónica durante el Cretácico Inferior en el sur de México. El análisis de facies fue fundamental para determinar un ambiente de sedimentación transicional marino, con aporte inicial de sedimentos con procedencia continental, desde los macizos metamórficos circundantes, y un aporte posterior de fuentes volcánicas que dominó la composición del sedimento durante un período que antecede la formación de la plataforma Guerrero-Morelos. Se propone también una revisión de la nomenclatura estratigráfica de la Formación Zicapa para incluir intervalos de depósitos calcáreos e intervalos de volcanismo y depósitos volcaniclásticos no incluidos en la definición original de la formación. De acuerdo con esta revisión, se propone definir formalmente la Formación Zicapa en cinco miembros que pueden ser correlacionados en dos localidades diferentes, lo que facilita, además, la correlación regional.

LOCALIZACIÓN Y MÉTODOS

La Formación Zicapa del Cretácico Inferior (de Cserna *et al.*, 1980) aflora en la Sierra Madre del Sur, en la región de la Montaña de Guerrero, desde el sur de Puebla hasta el sur de Guerrero, en las inmediaciones de la ciudad de Chilpancingo. Su localidad tipo fue propuesta al sur del poblado de Zicapa (de Cserna *et al.*, 1980), ubicado en el municipio de Copalillo, estado de Guerrero, sobre el curso del río Mezcala, conocido en el área como río Poblano. En esta localidad la Formación Zicapa está compuesta por capas rojas de arenisca, lutita, conglomerado polimíctico, con presencia de capas decimétricas a métricas de caliza, marga y, localmente, rocas volcánicas y volcaniclásticas (Fitz-Díaz, 2001; Fitz-Díaz *et al.*, 2002; Figueroa-Catalán y Gómez-Martínez, 2010).

El presente trabajo se basa en el análisis detallado de la Formación Zicapa en dos localidades: una en la localidad de Pilcaya-San Miguel la Ciénaga en la cuenca alta del río Balsas, cerca de Chiautla de Tapia, estado de Puebla; la otra en San Juan de las Joyas, al norte del estado de Guerrero y cerca de la localidad tipo (Figura 1). Este estudio presenta la integración de datos litológicos y sedimentológicos colectados

Tabla 1. Litofacies presentes en la Sección Pilcaya-San Miguel la Ciénaga y San Juan de las Joyas, Formación Zicapa. Modificado de Miall (1996) y Smith (1986).

Código litofacies	Tamaño de grano	Estructuras sedimentarias	Interpretación
Bmm	Guijarros y bloques angulosos	Brecha masiva, soportada por matriz, sin gradación	Flujos de gravedad, abanico aluvial, flujo de escombros
Gmm	Gujarros a bloques	Masivas, sin imbricación, soportada por matriz,	Flujos de masa depositados por flujos hiperconcentrados
Gh	Guijas y Guijarros	Estratificación horizontal, imbricación	Depósitos residuales, barras longitudinales, depósitos bien clasificados
Gh(a)	Guijas y Guijarros	Estratificación horizontal de clastos volcánicos	Depósitos residuales, barras longitudinales, depósitos bien clasificados
Gp	Guijas y Guijarros	Estratificación cruzada plana	Barras transversales, barras deltaicas a partir de barras remanentes
St	Arena fina a muy gruesa	Estratificación cruzada festonada individual o agrupada	Dunas tridimensionales
Sp	Arena fina a conglomerática	Estratificación cruzada plana	Dunas bidimensionales, régimen de flujo inferior
Sm	Arena fina a gruesa	Laminación masiva o tenue	Depósito de flujos de gravedad
Sh	Arena fina a muy fina	Laminación plana paralela, tabular	Plataforma de mareas
Sm (a)	Arena fina a media, localmente conglomerática con predominio de líticos	Masivas, mal clasificadas. Espesor de 0.3 a 4 metros. Contacto neto en la base	Depósito de flujo piroclástico, de grano fino; depósito epiclástico
Sr	Arena muy fina a gruesa	Laminación cruzada y rizaduras	Rizaduras (flujo inferior)
Ss	Arena fina a muy gruesa, escasamente conglomerática	Marcas de fondo de canal amplios y someros	Relleno de canal
Fl	Arena, limo o lodo	Laminación fina y rizaduras muy pequeñas	Llanura de inundación, canales abandonados o depósitos de inundaciones menguantes
Fl*	Arena muy fina, limo, arcilla	Laminación con icnofósiles	Plataforma de mareas
Fr	Arena, muy fina, limo, arcilla	Masivas, con materia orgánica	Suelos incipientes
Lm	Calizas *packstone*/*wackstone*	Capas tabulares de calizas con fósiles y fragmentos de fósiles	Plataformas interiores
Lch	*Mudstone*/*wackestone* con carofitas	Capas tabulares masivas con fósiles de carofitas y gasterópodos	Calizas de agua dulce. Lagunas continentales
Bc	Brechas de caliza	Fragmentos angulosos de caliza y matriz ocre	Plataformas de emersión
Ta, La	Ceniza o *lapilli*	Estratificación horizontal, gradación inversa, normal o ambas	Depósitos de caída piroclástica

durante tres campañas; se construyeron las columnas estratigráficas y se muestrearon diez secciones estratigráficas a lo largo de terracerías, brechas y algunos pequeños arroyos. Por la calidad de los afloramientos, no fue posible hacer una análisis completo de variaciones laterales de facies, sin embargo, dada la continuidad de la mayoría de las secciones compuestas, sí fue posible documentar de forma general los patrones de distribución de facies.

El análisis sedimentológico de la Formación Zicapa incluyó la identificación de litología, estructuras sedimentarias, espesores, geometría de las capas y presencia de material fósil; tras analizar las relaciones inter- e intra-capa, se definieron las facies sedimentarias y sus asociaciones. Se utilizó la metodología sugerida por Miall (1996) para facies fluviales, la de Smith (1987) para las facies volcánicas y volcaniclásticas, y se propusieron nuevos códigos para las facies carbonatadas (Tabla 1). Cada una de las litofacies definidas fue, posteriormente, agrupada en asociaciones de facies, para así interpretar el ambiente de depósito.

Por otro lado, el estudio de circones detríticos tiene una amplia aplicación en la sedimentología, ya que lleva a determinar la edad máxima de depósito, reconocer hiatos en el registro geológico y determinar las características de las fuentes o proveniencia, permitiendo evaluar reconstrucciones paleogeográficas regionales (Fedo *et al.*, 2003).

La metodología utilizada para el análisis de circones consistió en el muestreo de areniscas de grano medio y brechas andesíticas, las cuales fueron trituradas en prensa hidraúlica y tamizadas hasta obtener una fracción menor de 125 µm. Esta fracción fue sometida a separación por gravedad en la mesa Wilfley, obteniendo así los minerales densos de la muestra. Finalmente, la muestra se sometió a separación magnética con equipo Frantz y por líquidos pesados. El montaje de la probeta se hizo manualmente, acomodando aleatoriamente todos los circones sin hacer selección, para evitar el sesgo en la muestra. Los circones fueron analizados para obtener relaciones isotópicas y edades en un espectrómetro de masa de plasma inductivamente acoplado en el Centro de Geociencias, UNAM Campus Juriquilla. El procedimiento analítico se describe en Gehrels *et al.* (2008). Los datos fueron reducidos utilizando el programa Isoplot 4.15 (Ludwig, 2012).

CONTEXTO GEOLÓGICO

En el sur de México se reconoce un núcleo continental conformado por los basamentos metamórficos de los terrenos Oaxaquia y Mixteco (Figura 1). El basamento del terreno Mixteco está con-

formado por el Complejo Acatlán, un complejo polimetamórfico paleozoico compuesto por dos unidades litotectónicas: la unidad estructuralmente inferior corresponde a rocas metasedimentarias de bajo grado, y la superior se compone de metasedimentos, rocas máficas y ultramáficas eclogitizadas que están cubiertas tectónicamente por migmatitas y granitos de alta presión (Ortega-Gutiérrez *et al.*, 1994; Ortega-Gutiérrez *et al.*, 1999; Keppie *et al.*, 2008). El Pérmico tardío en la margen occidental del terreno Mixteco se caracteriza por el depósito de una secuencia clástica y carbonatada, en un ambiente marino epicontinental somero, cuyo contenido fósil restringe su edad al Guadalupiano (Juárez-Arriaga, 2006; Corona-Esquivel, 1981); esta secuencia cubre discordantemente las rocas metamórficas del Complejo Acatlán en la región de Olinalá. Hacia el oriente, en la región de Caltepec, en los límites entre los terrenos Mixteco y Zapoteco, se depositó la secuencia siliciclástica de la Formación Matzitzi del Leonardiano (Centeno-García *et al.*, 2009). En otras regiones de la Mixteca el registro del Pérmico corresponde a la Formación Tecomate (Keppie *et al.*, 2004).

En la región de Olinalá, al occidente del terreno Mixteco, aflora localmente la Ignimbrita Las Lluvias (Figura 2) del Jurásico Medio (Campa-Uranga e Iriondo, 2004), la cual está cubierta por rocas sedimentarias continentales marinas del Conglomerado Cualac y el Grupo Tecocoyunca del Jurásico Medio. El registro estratigráfico del Jurásico Superior del sur de México corresponde a sedimentación en ambientes marinos someros (Padilla y Sánchez, 2007; López-Ticha, 1985). No existe registro de volcanismo en el terreno Mixteco durante ese tiempo, y es hasta el Cretácico Temprano que se presenta volcanismo calcialcalino asociado a sedimentación clástica marina y continental, como es el caso de la Formación Chapolapa al sur de Chilpancingo (Hernández-Treviño *et al.*, 2004; Campa-Uranga e Iriondo, 2004; Solari *et al.*, 2007), la Formación Zicapa, en las cercanías de la falla Papalutla (Fitz-Díaz *et al.*, 2002), la "Roca Verde Taxco Viejo" y el Esquisto Taxco (Campa-Uranga e Iriondo, 2004; Talavera-Mendoza *et al.*, 2007).

Durante el Cretácico Temprano, en el terreno Mixteco, se presentan formaciones con asociaciones de facies transicionales subaéreas a marinas someras (Formación Atzompa, Formación Zicapa, Anhidrita Huitzuco y Formación Acahuizotla), las cuales registran una transición continua hacia una plataforma de carbonatos en el Albiano (Formación Morelos). El depósito de las calizas de la Formación Morelos generan una rampa que profundiza hacia el oeste (Hernández-Romano *et al.*, 1997), en la que es notable la ausencia de material volcánico. La sedimentación calcárea en la plataforma es interrumpida durante el Turoniano-Coniaciano por el depósito de la sucesión clástica marina de la Formación Mexcala (Hernández-Romano *et al.*, 1997).

El volcanismo registrado en la Formación Zicapa fue reconocido por Guzmán (1950) quien define una secuencia compuesta por tobas, areniscas y conglomerados finos de cuarzo, de origen continental o litoral. Una descripción más reciente y completa de la composición, petrografía y edades fue realizada por Fitz-Díaz (2001) y Fitz-Díaz *et al.* (2002), quienes reconocieron rocas volcánicas intercaladas en la Formación Zicapa y asignan una edad Cretácico Temprano para esta formación. En trabajos recientes realizados en la localidad tipo de la Formación Zicapa, se describen en detalle derrames basálticos, tobas y brechas volcánicas intercalados con lentes y capas de calizas arrecifales (Figueroa-Catalán y Gómez-Martínez, 2010). En la localidad de San Juan de las Joyas, los mismos autores describen igualmente la presencia de rocas volcánicas intercaladas con calizas y areniscas en la Formación Zicapa, lo cual ha sido corroborado en el presente trabajo.

Además de las rocas volcánicas reportadas en la Formación Zicapa en Guerrero y en el sur de Puebla, existe evidencia de dicho magmatismo en la margen norte del terreno Mixteco. En la Sierra de Tentzo, al sur de la ciudad de Puebla, en la parte basal de la unidad de capas rojas que subyace a calizas del Albiano (Monroy-Fernández y Sosa-Patrón, 1984) o Formación El Tentzo (Zepeda-Martínez, 2013), se presentan clastos de hasta 30 cm de andesita, basalto y felsitas. Esta unidad es correlacionable con la Formación Zicapa por posición estratigráfica y características litológicas. Estas relaciones estratigráficas evidencian una sedimentación marina transicional contemporánea con un volcanismo calcialcalino.

FORMACIÓN ZICAPA

Nomenclatura estratigráfica

Se hizo la revisión de la nomenclatura estratigráfica de la Formación Zicapa debido al carácter informal de su definición original (de Cserna *et al.*, 1980) y a las diferencias que se encontraron durante el desarrollo de nuestro trabajo con la definición original, así como con otros trabajos (de Cserna *et al.,* 1980, Fitz-Díaz *et al.*, 2002; Figueroa-Catalán y Gómez-Martínez, 2010). Las diferencias substanciales en las observaciones y mediciones de litología y espesores realizadas en este trabajo y que nos llevan a proponer formalmente la redefinición de la Formación Zicapa, de acuerdo a la Guía Estratigráfica Norteamericana (Barragán *et al.*, 2010) son: (1) la definición original se publicó en un medio inapropiado para ese fin; (2) carece de la descripción de rocas volcánicas intercaladas; y, (3) no reconoce la secuencia de calizas en la base de la formación.

Antecedentes

Los lechos rojos asociados a calizas en la región de la montaña de Guerrero fueron notados previamente a la primera definición de la Formación Zicapa (Guzmán, 1950). de Cserna *et al.* (1980) denomina como Formación Zicapa a una secuencia de capas rojas continentales con intervalos de caliza marina. En la localidad tipo tiene un espesor de 700 m donde su base está un contacto por falla con esquistos del Complejo Acatlán, mientras que su contacto superior es transicional con las calizas de la Formación Morelos. En dicha descripción de la sección tipo están ausentes los niveles volcánicos y volcaniclásticos de esta formación. Un trabajo extenso que documenta ampliamente las características petrográficas y sedimentológicas de la Formación Zicapa fue realizado por Figueroa-Catalán y Gómez-Martínez (2010). En dicho trabajo interpretaron que la Formación Zicapa se depositó en una cuenca de *rift,* con base en la procedencia de sedimentos por análisis petrográficos.

La Formación Zicapa ha sido interpretada como sedimentación continental en ambientes transicionales cercanos a la costa, con facies asociadas a regresiones y transgresiones marinas. La extensión durante el depósito, a su vez, ha sido asociada a: (1) la apertura del Golfo de México (Salinas-Prieto, 1986; Cerca, 2004), (2) sedimentación basal de aulacógenos (Fitz-Díaz *et al.*, 2002) y (3) evolución sedimentaria de una secuencia de *rift* (Figueroa-Catalán y Gómez-Martínez, 2010). Ninguno de esos modelos está plenamente soportado, aunque todos coinciden en asociar a la Formación Zicapa a un ambiente tectónico extensional.

Definición y Localidad Tipo

De acuerdo con lo anterior y acorde a los lineamientos del Código Estratigráfico Norteamericano (Barragán *et al.*, 2010) se propone una redefinición de la Formación Zicapa como unidad litoestratigráfica formal en la categoría de formación y se propone la localidad San Juan de las Joyas como localidad tipo. Esta formación se divide en cinco miembros: Miembro Cerro La Cruz, Miembro San Juan de las Joyas, Miembro Ajuatetla, Miembro San Andrés y finalmente en la cima, el Miembro río Poblano. La localidad tipo definida por de Cserna *et al.* (1980), se localiza a 10 km al norte de la Localidad San Juan de las Joyas

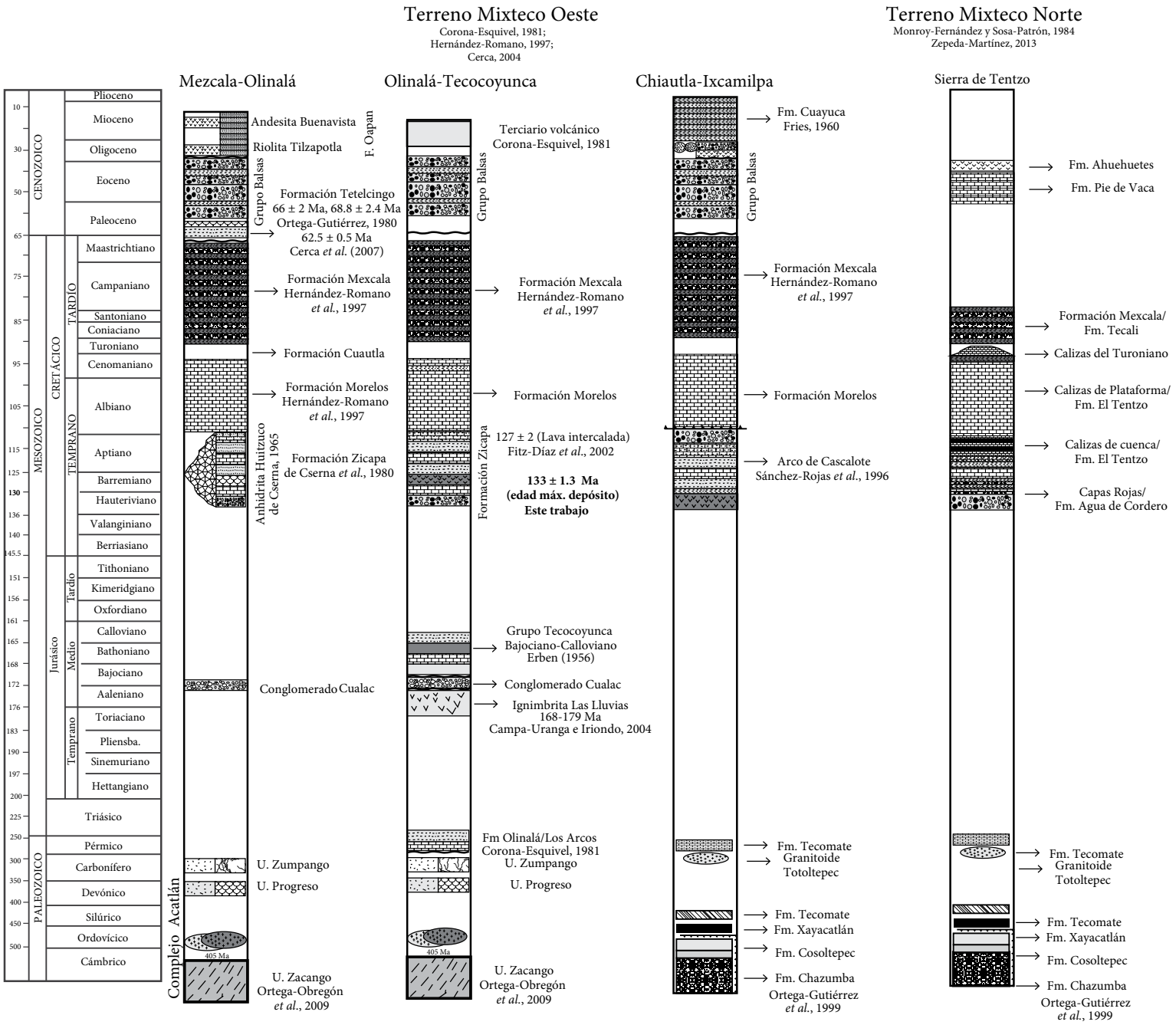

Figura 2. Correlación estratigráfica entre unidades del terreno Mixteco.

y está bien definida en cuanto a características sedimentológicas y relaciones estratigráficas por Figueroa-Catalán y Gómez-Martínez (2010), por lo cual se propone mantener a ésta como sección de referencia.

Localidad San Juan de las Joyas

Esta localidad se encuentra ubicada en el estado de Guerrero, entre el río Poblano al norte y Chilapa de Álvarez al sur. Geológicamente se encuentra sobre el terreno Mixteco, estando aproximadamente a 8 km al suroeste de la cabalgadura de Papalutla (Cerca *et al.*, 2007), falla que pone en contacto el Complejo Acatlán con la Formación Morelos (Figura 3).

La exposición de la Formación Zicapa en los alrededores de San Juan de las Joyas no es un afloramiento continuo de toda la formación, pero permite levantar desde la base hasta la cima, varias columnas representativas para cada uno de los miembros aquí definidos, cubriendo todo el espesor de la formación. Se levantaron cuatro columnas estratigráficas de la base a la cima, separadas geográficamente por una distancia menor a 1 km. La unidad basal se encuentra en el cerro La Cruz, una unidad intermedia, cerca de Ajuatetla, una unidad media volcaniclástica, en el cerro San Andrés y finalmente una unidad superior, en el camino al río Poblano (Figure 3). Las columnas fueron levantadas sobre los flancos de un anticlinal cuyo plano axial (N20°E) pasa aproximadamente a 1 km al este de la población de San Juan de las Joyas. Las columnas levantadas en el cerro La Cruz, el cerro San Andrés y el camino al río Poblano están en el flanco oeste del anticlinal, mientras que la columna levantada cerca de Ajuetetla se encuentra en el flanco este de la estructura (Figura 3). En la localidad de San Juan de las Joyas la Formación Zicapa tiene un espesor total de 560 m (Figura 4).

Miembro Cerro La Cruz. La base de la secuencia de la Formación Zicapa, en el cerro La Cruz está en contacto con el Conglomerado Cualac, el cual a su vez está en contacto discordante sobre filitas del Complejo Acatlán. La parte inferior de la secuencia, con un espesor de 30 metros, se caracteriza por una brecha basal matriz soportada con clastos angulosos con diámetros entre 3 a 10 cm, compuestos de filitas y cuarzo lechoso, intercalada con areniscas líticas y conglomerados de igual composición y clastos subredondeados. El contacto con el miembro suprayacente es transicional y está marcado con la aparición de margas y lodos calcáreos.

Miembro San Juan de las Joyas. Este miembro con un espesor total de 140 m aflora, al igual que el miembro basal, en el camino al cerro de la Cruz. Está compuesto, en la base, por areniscas muy finas, margas y un paquete significativo de 100 m de *packstone* en capas gruesas de 1 a 1.5 m de espesor, con abundantes fósiles de bivalvos y gasterópodos, intercaladas con *mudstone* y localmente, con capas finas de lodolitas calcáreas (Figura 5). Esta intercalación de calizas en la base, es un rasgo notorio que permite delimitar la base de dicho miembro. Esta secuencia es seguida por intercalaciones de areniscas líticas, conglomerados con clastos de areniscas, *packestone* con foraminíferos y clastos de cuarzo lechoso intercalados con estratos tabulares de limolitas rojas.

Miembro Ajuatetla. Este miembro aflora pobremente en la zona del poblado de San Juan de las Joyas y en la terracería hacia el poblado de Ajuatetla. El contacto de este miembro con el miembro subyacente es

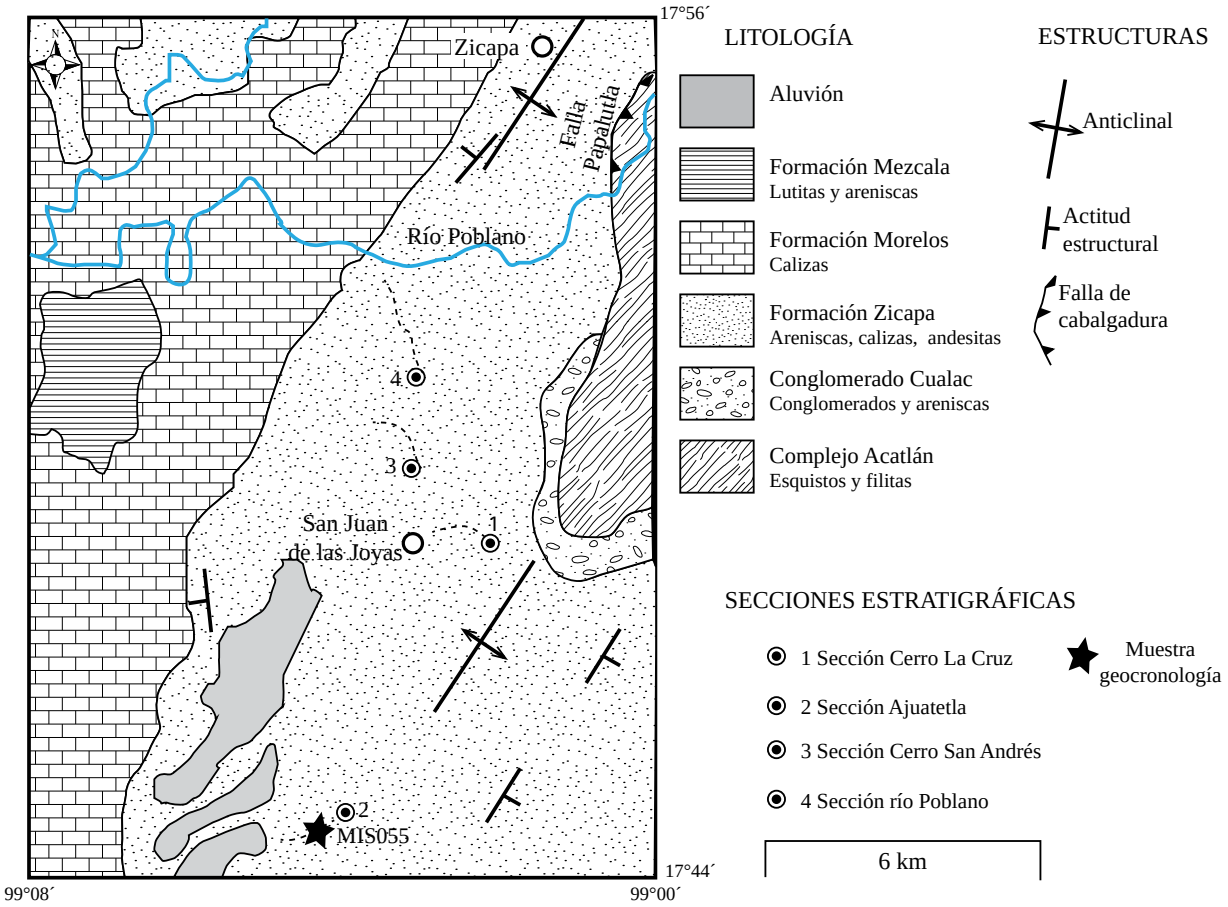

Figura 3. Mapa geológico de la localidad San Juan de las Joyas. Se marcan las secciones estratigráficas compuestas levantadas con línea punteada. (Modificado de Campa-Uranga *et al.*, 1998).

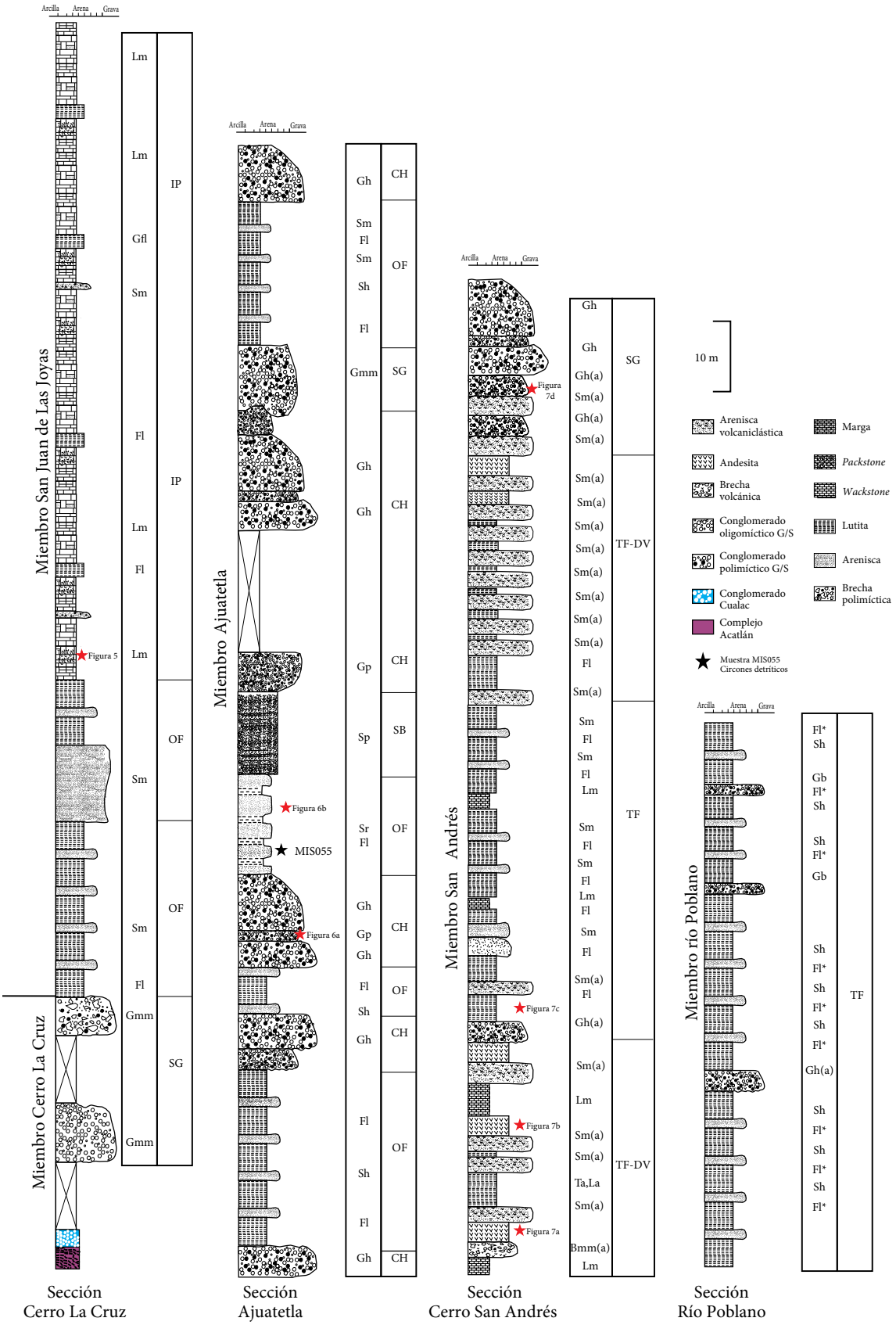

Figura 4. Columna estratigráfica compuesta y facies de la Formación Zicapa en la localidad San Juan de las Joyas. De izquierda a derecha, se describen las secciones de la base a la cima. Los códigos de litofacies corresponden a la Tabla 1 y las asociaciones de facies a la Tabla 2. Las estrellas rojas muestran la localización de las Figuras 5, 6 y 7.

Tabla 2. Descripción e interpretación de los elementos de arquitectura de las facies de la Formación Zicapa (Modificado de Miall, 1996).

Elemento de arquitectura	Tamaño de grano	Descripción	Interpretación
Canales (CH)	Conglomerados de guijas y guijarros, areniscas de grano fino a grueso	Geometría lenticular con base erosiva; Gh, Gp, St, Sp, Sm, y Sr	Rellenos de canales de gravas y arenas
Barras de gravas (GB)	Conglomerados soportados por clastos, de gránulos a guijarros, interestratificadas con areniscas	Geometría tabular y en lentes con una extensión lateral de hasta 10 m; Gco, Gt y Gp	Barras longitudinales relativamente pequeñas
Barras de acreción aguas abajo (DA)	Conglomerados de gránulos a guijas y areniscas de grano fino a grueso	Geometría de cuña, de extensión moderada (hasta decenas de metros); Gh, Sm, St, Ss	Acreción río abajo de barras de arenas y gravas
Sedimentos de flujos por gravedad (SG)	Conglomerados soportados por matriz, de guijarros a bloques	Pueden estar interestratificados con barras de gravas y de arenas; Gm	Flujos de gravedad
Barras de arenas (SB)	Areniscas de grano fino a grueso	Geometría de cuña o tabulares, con superficies erosivas y extensión lateral de hasta 50 m; St, Sm, Sr y Sm	Rellenos de canales, dunas y sedimentos de planicie de inundación (*crevasse splay*)
Sedimentos finos de llanura de inundación (OF)	Limolitas y areniscas de grano muy fino	Geometría tabular con una extensión lateral no mayor de 200 metros; Sr, Fl y Fl*	Depósitos de llanura de inundación
Calizas de agua dulce (FL)	Calizas con carofitas intercaladas con limolitas pardas y brechas de calizas	Geometría tabular a lenticular, límites abruptos con capas subyacentes; Lch, FL	Lagunas en ambientes fluviales
Plataforma interior (IP)	*Packstone*/*wackstone*, brechas de gránulos a bloques angulares con matriz roja a ocre	Capas tabulares a cuñas; Lm, B, Fl, Sc	Calizas de plataforma interior
Llanura de mareas (TF)	Limolitas laminadas con bioturbación, areniscas calcáreas	Capas tabulares de amplia extensión lateral; Fl*, Fl, Sh	Llanura de mareas

transicional y se observa a lo largo del arroyo que cruza al norte de la localidad de San Juan de las Joyas y en el camino de terracería hacia la población. En este sitio se compone de capas heterolíticas de estratos tabulares de areniscas de grano medio con estratificación plana-paralela y rizaduras, intercaladas con lutitas moradas tabulares con facies de *Thallasynoides* y algunos estratos de conglomerados medianamente bien seleccionados con clastos de caliza, cuarzo y roca metamórfica, con diámetro máximo de 2 cm y estratificación cruzada tipo canal (Figura 6). Las areniscas son ligeramente conglomeráticas mostrando gradación normal. El miembro Ajuatetla tiene un espesor de 160 m.

Miembro San Andrés. Este miembro aflora de forma continua en el camino al cerro San Andrés, y se caracteriza por la presencia de derrames de andesitas con autobrechas en la base y tobas intercaladas con areniscas, rocas epiclásticas y algunas capas delgadas (30 cm) de calizas tipo *mudstone* a *grainstone* (Figura 7). Hacia la cima, la secuencia se vuelve de grano más grueso, incorporando conglomerados tabulares a lenticulares en capas de 1 m, compuestos de clastos medianamente redondeados de rocas volcánicas, cuarzo lechoso y cuarcitas, que se intercalan con areniscas masivas de grano medio, en capas de 70 cm a 1 m. El Miembro San Andrés tiene un espesor total de 140 m.

Las rocas volcánicas de la Formación Zicapa son andesitas porfídicas con fenocristales de andesina y cuarzo accesorio, con una textura microlítica y pilotaxítica (Figura 8). Estas andesitas se presentan en derrames masivos, con espesores de 20 a 30 metros en la localidad de San Juan de las Joyas y en Zicapa; en ambas localidades están asociadas a una autobrecha volcánica basal compuesta por fragmentos de andesita. Los derrames de lava están asociados a capas de tobas de lapilli y ceniza con gradación inversa, lo cual sugiere un medio de sedimentación acuoso.

Miembro río Poblano. La parte superior de la sección, con un espesor de 92 m, aflora al oeste de la población de San Juan de las Joyas, en el camino hacia el río Poblano. Se caracteriza por el predominio de limolitas y lutitas rojas tabulares con espesores entre 0.5 y 1.0 m, con presencia de icnofósiles (*Skolithos*); están intercaladas con areniscas de grano fino, con laminación tenue a masivas, en espesores promedio de 0.5 metros. Se presentan escasos conglomerados soportados por guijas de rocas volcánicas, calizas y roca metamórfica, y geometría lenticular. El contacto con las calizas de la Formación Morelos que le sobreyace es transicional, y aunque no fue posible tener acceso a él por la topografía, se le pudo observar en el río Poblano, donde la actitud estructural de las capas de lutitas y calizas son concordantes.

Localidad Pilcaya-San Miguel la Ciénaga

Esta localidad se localiza al sur de Puebla en la terracería que conduce de Pilcaya a San Miguel la Ciénaga (Figura 9). En esta zona, al noroeste de la cabalgadura de Papalutla, la Formación Zicapa se encuentra en discordancia angular sobre el Complejo Acatlán presentando una diferencia en la litología basal entre esta zona y la región de San Juan de las Joyas, marcada por la ausencia de material derivado de la secuencia jurásica y la presencia de calizas de agua dulce.

La sección 1 tiene un espesor de 35 m (Figura 10) y está constituida por el Miembro Cerro La Cruz, compuesto por una brecha basal soportada por matriz, con líticos metamórficos angulosos, en discordancia angular con el Complejo Acatlán y el Miembro San Juan de las Joyas, que incluye calcarenitas con laminación cruzada a escala decimétrica, estratos de 1 a 1.5 metros de *wackestone* de agua dulce con fósiles de carofitas, gasterópodos y ostreidos, y brechas de caliza. La sección 2 tiene un espesor de 70 m, se encuentra estratigráficamente en un nivel superior con relación a la Sección 1, e incluye una intercalación de conglomerados masivos, areniscas rojas con estratificación cruzada tipo canal, areniscas con rizaduras, limolitas con restos de plantas y calcarenitas del Miembro Ajuatetla. A este conjunto le sigue una secuencia dominada por lutitas rojas masivas intercaladas con estratos tabulares de 30 cm de espesor de arenitas volcánicas y arcosas con rizaduras en la cima correspondientes al Miembro San Andrés. Finalmente, la sección 3 localizada al sur, en el poblado de San Miguel

Figura 5. Intercalaciones de calizas tipo *wackestone* con lodo calcáreo en la base del Miembro Cerro La Cruz. En la imagen del lado derecho se observan fósiles de bivalvos fragmentados.

la Ciénaga, tiene un espesor de 75 m y está caracterizada, al igual que la sección 1, por el Miembro Cerro La Cruz, compuesto por una brecha basal soportada por matriz con líticos metamórficos, en contacto de falla con el Complejo Acatlán. Sobreyaciendo transicionalmente al Miembro Cerro la Cruz, se encuentra el Miembro Ajuatetla caracterizado por secuencias de capas heterolíticas de limolitas y lutitas rojas con bioturbación e icnofacies de *Skolithos* intercaladas con litarenitas con estratificación cruzada burda, separadas por capas de conglomerados masivos, soportados por granos.

Procedencia y Edad

Con el fin de determinar edades máximas de depósito, se hicieron análisis con el método U/Pb en circones, de dos muestras de arenisca en los miembros Ajuatetla (MIS055) y San Andrés (0118-3c).

La muestra MIS055 se colectó en la localidad San Juan de las Joyas, en la base del Miembro Ajuatetla (Figuras 3 y 4). Esta es una arcosa lítica con fragmentos de cuarzo policristalino de origen metamórfico, cuarzo monocristalino con extinción ondulante y recta, albita, feldespato potásico, esquisto, intraclastos de caliza recristalizada y arenisca, líticos volcánicos felsíticos, sin matriz y con abundante cemento. Para los análisis de geocronología detrítica (n=126) se definieron cuatro familias morfológicas (Figura 11a). La primera familia corresponde a circones euhedrales, bipiramidales, translúcidos; la segunda familia son circones euhedrales rosas, la tercera familia son circones redondeados de tamaño variable y la cuarta familia son circones de gran tamaño, en colores de pardo a rosa, redondeados a subredondeados. En cuanto a las edades obtenidas, se encontraron cinco familias de circones concordantes (Figura 11b) con las siguientes edades: una familia del Paleo-Mesoproterozoico (~1.7 y 1.0 Ga, 66 granos), Neoproterozoico (~875 -570 Ma, 12 granos), Ordovícico-Silúrico (~480 Ma, 2 granos), Pérmico-Triásico (~290-220 Ma, 13 granos), Jurásico Temprano (~178 Ma, 2 circones) y una edad del Jurásico Tardío (152-149 Ma, 2 granos). La edad máxima de depósito se determinó por el circón más joven en 149 Ma.

La muestra 0118-3c se colectó en el Miembro San Andrés en la Sección 2 de la localidad Pilcaya-San Miguel la Ciénaga (Figuras 9, 10). Ésta es una arenisca volcaniclástica de grano medio, compuesta por plagioclasa, cuarzo policristalino de origen metamórfico, feldespato, esquisto e intraclastos de caliza recristalizada; carece de matriz y contiene abundante cemento de calcita. Para análisis de circones detríticos (n=76) se agruparon en tres familias morfológicas (Figura 12a). La primera familia la más abundante, de circones pequeños, euhedrales, transparentes y traslúcidos; la segunda familia corresponde a circones medianamente retrabajados de color rosa pálido a

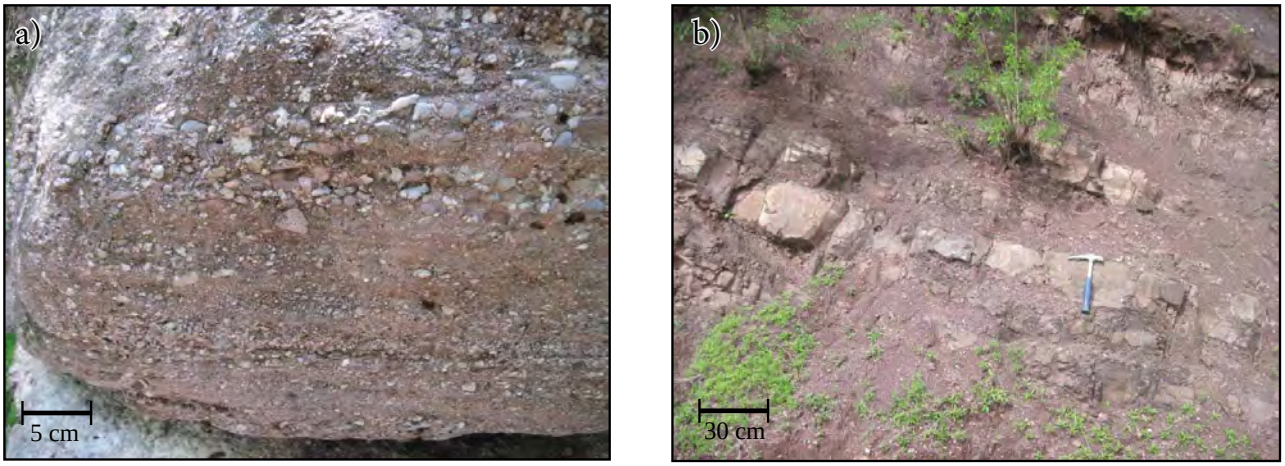

Figura 6. Miembro Ajuatetla: a) Conglomerados con estratificación cruzada; b) intercalaciones de areniscas y limolitas rojas tabulares.

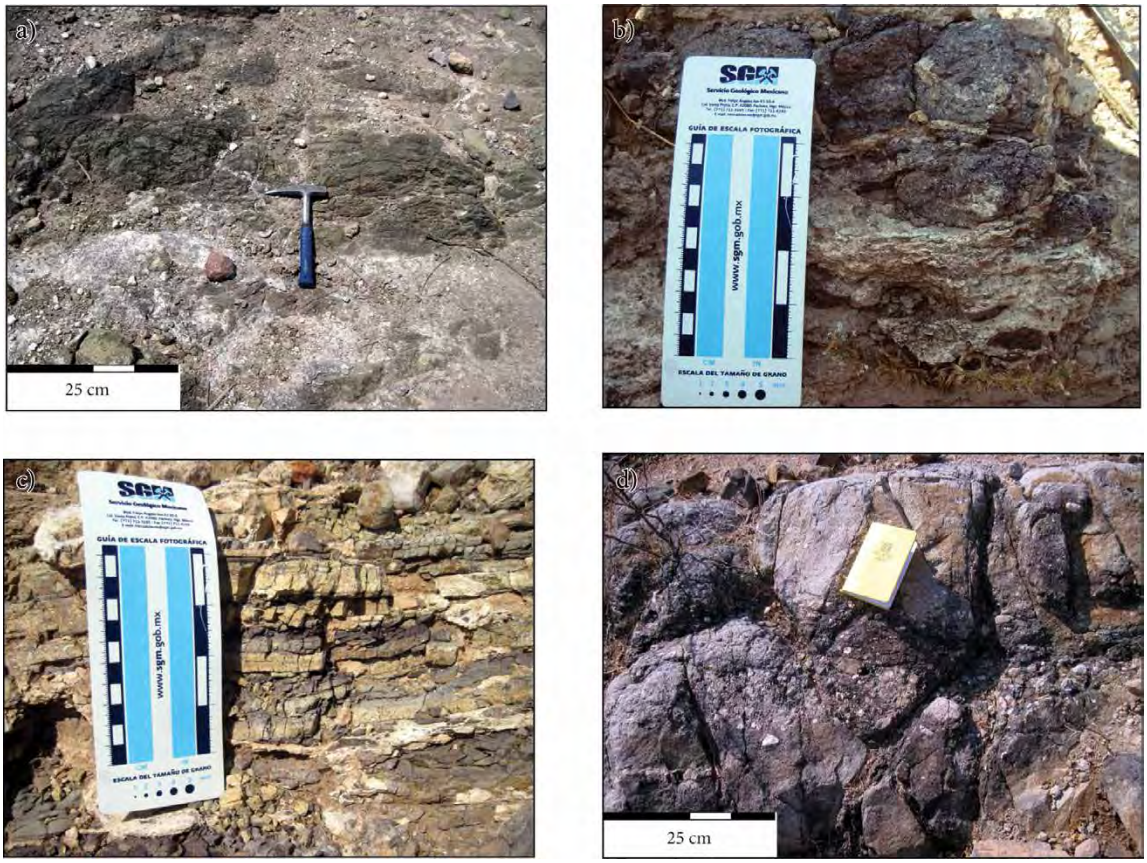

Figura 7. Características de las rocas del Miembro San Andrés: a) brecha andesítica en la base; b) lavas andesíticas intercaladas; c) horizonte de tobas de ceniza y lapilli; d) arenisca conglomerática en la cima del miembro.

transparentes y una tercera familia de circones redondeados de color rosa a rojo, de tamaño variable. En cuanto a las edades obtenidas se encontraron cinco familias de edad (Figura 12b, 12c): una población mayoritaria del Cretácico Temprano (~148–131 Ma, 35 granos) y poblaciones del Paleo-Mesoproterozoico (~1.6 y 1.0 Ga, 11 granos), Neoproterozoico (un circón 682 Ma), Ordovícico-Silúrico (un circón 480 Ma), Pérmico-Triásico (~260-240 Ma, dos granos) y Jurásico (153–190 Ma, siete circones). Para esta muestra se determinó una edad máxima de depósito como el promedio ponderado de la población más joven de 133 ± 1.3 Ma (n=7 granos), la cual corresponde al límite Valanginiano-Hauteriviano en una población de circones con edades entre 131 y 148 m. a.

Fitz-Díaz *et al.* (2002) reportaron una edad de 127 ± 2 Ma por $^{40}Ar/^{39}Ar$ en roca total para una andesita asignada a la Formación Zicapa en el arroyo Piedras Grandes, aguas arriba de la localidad de Mezquitlán en Guerrero (Figura 9), a 1 km al oeste de la falla de Papalutla (E. Fitz, comunicación personal, 2012). En el presente trabajo, se muestreó en esa localidad (MIS107) una brecha volcánica de color verde, compuesta por clastos entre 15 y 30 cm, angulosos, de composición variable entre andesita y dacita, embebidos en una matriz volcánica verde cloritizada. Dicha roca fue fechada mediante el método U/Pb en circón por ablasión láser, obteniendo una discordancia con la edad reportada por Fitz-Díaz *et al.* (2002). La edad obtenida arroja dos poblaciones de edades concordantes (Figura 13), una con circones entre 66 y 71 Ma (n=5 circones) y una edad máxima de depósito de 66.3 ± 4 Ma, y otra población con circones concordantes entre 122 y 141 Ma (n=11), un grano de circón ~80 Ma y otro de ~480 Ma. Aunque el depósito es del Cretácico Tardío, algunos de los clastos incorporados en la brecha son del Cretácico Temprano y fueron derivados localmente de la Formación Zicapa. La edad determinada por Fitz-Díaz *et al.* (2002) correspondería al fechamiento de uno de estos clastos. No se puede descartar la hipótesis de que la fecha reportada por el método Ar/Ar en roca total pueda corresponder a una mezcla de edades entre volcanismo de la Formación Zicapa y la Formación Tetelcingo, de edad entre 66 y 68 Ma (método K-Ar; Ortega-Gutiérrez, 1980) y Ar-Ar (Cerca *et al.*, 2007) entre 66 y 68 Ma.

Correlación

La Formación Zicapa ha sido correlacionada al norte del terreno Mixteco con la Formación Atzompa (Tarango, 1968, en Monroy-Fernández y Sosa-Patrón, 1984) que aflora en la Sierra de Tentzo y denominada por Monroy-Fernández y Sosa-Patrón (1984) como Capas Rojas del Neocomiano y por Zepeda-Martínez (2013) como Formación Agua de Cordero. Esta formación al igual que la Formación Zicapa, cuenta con conglomerados intercalados con areniscas y lodolitas de facies transicionales, las cuales pasan gradualmente a calizas someras con fauna del Barremiano-Aptiano (Monroy-Fernández y Sosa-Patrón, 1984; Zepeda-Martínez, 2013). Hacia el sur de las localidades estudiadas, las capas rojas de la Formación Zicapa son correlacionadas con la Formación Chapolapa en las localidades de El Ocotito y Quechultenango en Guerrero (Salinas-Prieto, 1986). Regionalmente y basados en la edad y características ambientales, la Formación Zicapa puede ser correlacionada con las formaciones de ambiente costero como La Compañía y Agua de Cordero de la Cuenca de Zapotitlán (Mendoza-Rosales, 2010). La Formación Zicapa también ha sido reconocida en el homoclinal de Petlalcingo (Figura 1), entre Huajuapan

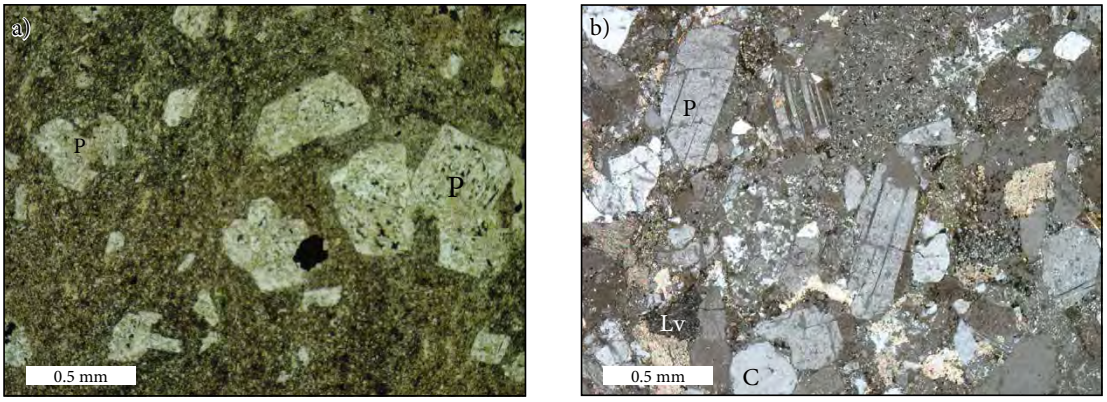

Figura 8. Características petrográficas del Miembro San Andrés: a) Andesita porfídica con fenocristales de plagioclasa subidiomórfica con abundantes inclusiones de magnetita en una matriz microlítica (luz polarizada); b) arenisca volcaniclástica con abundantes fragmentos líticos volcánicos (Lv), cristales subangulosos de plagioclasa (p) y fragmentos de cuarzo (C) (luz polarizada).

de León y Acatlán de Osorio (Pérez-Ibargüengoitia *et al.*, 1965), donde se caracteriza por conglomerados con abundante madera silicificada. Volcanismo contemporáneo a la Formación Zicapa ocurre también en la Formación Xonamanca de la sierra de Zongolica, donde se asigna al Barremiano por su posición estratigráfica (Carrasco *et al.*, 1975).

El registro de magmatismo del Cretácico Temprano en la margen de Oaxaquia parece extenderse desde la región de San Luis Potosí hasta el sur de Guerrero. En la sierra de Pinos, Zacatecas, lavas andesíticas están intercalada con calizas (Dávalos-Elizondo, 2011), que se asignan a la Formación Taraises con base en la presencia del amonite *Thurmanniceras thurmani* del Valanginiano (González-Arreola, comunicación personal, 2011). Igualmente, con base en la edad del magmatismo es posible correlacionar las formaciones San Juan de la Rosa y Trancas, en la región central de Querétaro (Ortega-Flores *et al.*, 2013), con la Formación Zicapa. Estas unidades se caracterizan por contener un registro de magmatismo félsico con edades entre 127 y 150 Ma en la margen de Oaxaquia. Capas rojas del Cretácico Inferior que subyacen calizas de la plataforma de Actopan, en el sur de Hidalgo (Abascal y Murillo-Muñetón, 2013), también son correlacionables con la Formación Zicapa.

ANÁLISIS DE FACIES

El análisis sedimentológico realizado en la Formación Zicapa se basó en la identificación de litología, estructuras sedimentarias, espesores, geometría de las capas y presencia de material fósil, lo cual permitió analizar las relaciones inter- e intracapa, y definir las facies sedimentarias (Tablas 1 y 2). Para la Formación Zicapa se definieron asociaciones de facies o la arquitectura de los elementos característicos de ambientes continentales (CH, GB, DA, SG y SB) y ambientes transicionales deltaicos a costeros (OF, IP, TF).

DISCUSIÓN

Ambientes sedimentarios: análisis e interpretación

Con base en las asociaciones de facies y la arquitectura de facies, fue posible determinar los ambientes de depósito de la Formación Zicapa en las dos localidades estudiadas. La unidad basal en ambas secciones consta de facies conglomeráticas y brechas características de flujos por gravedad (asociación de facies SG), los cuales se asocian directamente a la creación del espacio de acomodación por actividad tectónica en un ambiente continental. Al sur de Tlapa de Comonfort, a las afueras de la ciudad, la Formación Zicapa se encuentra en contacto por falla con areniscas y lutitas del Jurásico Medio. Las características litológicas de la Formación Zicapa sugieren que el fallamiento fue contemporáneo con el depósito. Dicho fallamiento pudo haber favorecido la incursión marina que caracteriza al Miembro San Juan de las Joyas y el subsecuente desarrollo de plataformas internas de carbonatos, seguido por facies de llanura de marea con desarrollo de *Skolithos* (asociación de facies OF, IP, TF). Las incursiones marinas registradas en la Formación Zicapa se caracterizan por alternancias de calizas arenosas y margas con *packstone*, lo cual representa períodos de incursión marina en un ambiente donde existió el aporte de sedimentos detríticos. En la localidad Pilcaya-San Miguel la Ciénaga, las calizas del Miembro San Juan de las Joyas son de agua dulce, y sobreyacen facies de llanura de inundación. Estas asociaciones de facies se atribuyen a desarrollo de lagunas en los sistemas fluviales incipientes, generadas por efectos de represado y aumento del nivel base de depósito, en contraste con la localidad San Juan de las Joyas, donde las condiciones de agua fueron propicias para el establecimiento de pequeños arrecifes. En otras localidades, las plataformas calcáreas de la Formación Zicapa fueron destruidas dejando solo como evidencia, algunas brechas de emergencia. Estas brechas se pueden observar, por ejemplo, al sur de la ciudad de Tlapa de Comonfort (Figura 1).

Aunque es clara la relación entre fallamiento, el depósito de facies de flujo por gravedad y la creación de espacio de acomodación, la presencia de facies marinas en la localidad San Juan de las Joyas intercaladas con facies continentales, permite formular la hipótesis de que el Miembro San Juan de las Joyas pudiera corresponder a un evento transgresivo global. Los candidatos incluyen el evento Ap3 del Aptiano inferior, el evento Bar5, de finales del Barremiano, o un evento Ha7 del Hauteriviano (Haq *et al.*, 1987; Haq *et al.*, 1988). Tomando en cuenta la edad máxima de depósito de 133 ± 1.3 Ma (edad promedio para siete circones concordantes e interpretados como cercanos a la edad de depósito) del Miembro San Andrés que sobreyace al Miembro San Juan de las Joyas, el escenario más probable es que la plataforma interna se halla desarrollado entre el Hauteriviano-Barremiano (Ha7) previo al volcanismo, ya que el límite entre estos pisos se sitúa en 130 m. a.. Aunque el evento de sedimentación previo al volcanismo es una gruesa formación de calizas, éste no es el único evento presente en la secuencia. En la base del Miembro San Andrés, en la localidad San Juan de las Joyas, se encuentran capas lenticulares de caliza de 30 cm de espesor máximo, espaciadas sucesivamente cada 20 metros (Figura 3), intercaladas con andesitas, tobas y areniscas volcaniclásticas. Estas

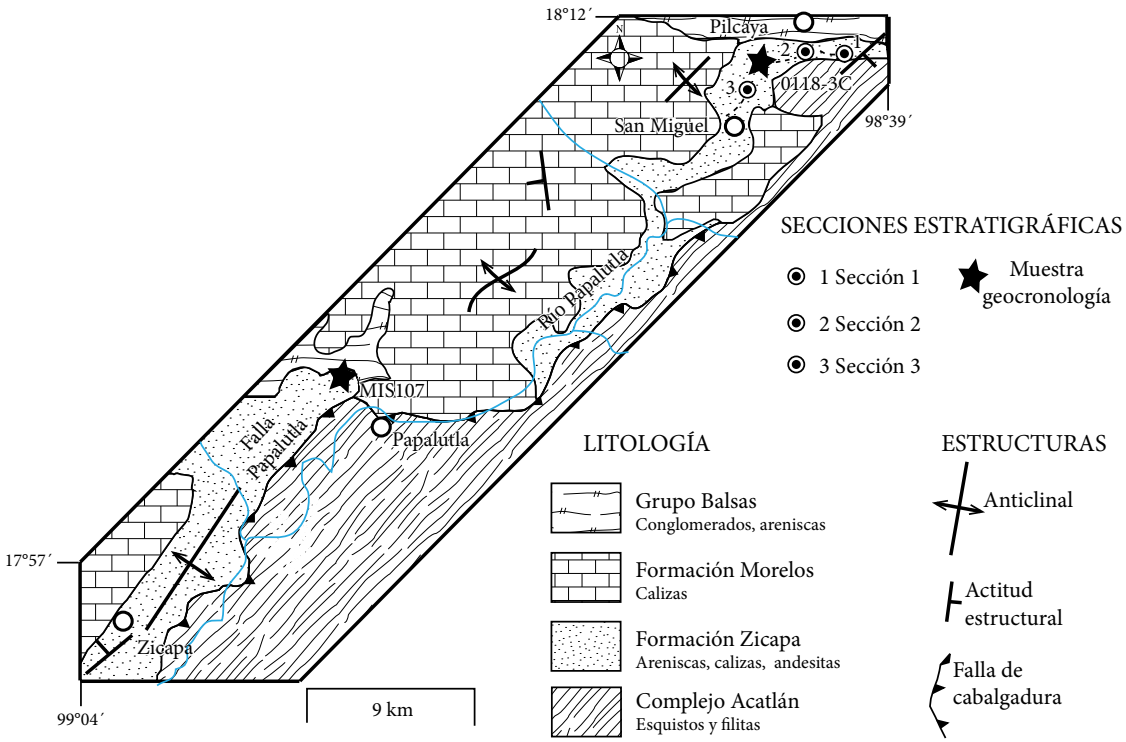

Figura 9. Mapa geológico de la localidad Pilcaya-San Miguel la Ciénaga. Se marcan las secciones estratigráficas compuestas con línea punteada (modificado de Rivera-Carranza *et al.*, 1998).

calizas pueden representar, a su vez, un evento transgresivo contemporáneo con el volcanismo más acorde con los eventos Ap3 o Ap4.

La parte media de la Formación Zicapa, en el Miembro SanAndrés, muestra un aporte significativo de brechas volcánicas, flujos de lava andesítica, tobas de ceniza y lapilli, así como areniscas volcaniclásticas de ambiente costero. El brechamiento de las lavas andesíticas en los bordes sugiere que estas rocas volcánicas fueron depositadas en un ambiente submarino somero. Se desconoce la localización de los aparatos volcánicos, fuente de dicho volcanismo, sin embargo se descarta que se localicen al norte ya que el espesor de las rocas volcánicas disminuye en esa dirección, y el volcanismo está solo presente en las areniscas volcaniclásticas.

La actividad volcánica cesa para originarse un depósito de limolitas y lutitas con facies de *Skolithos*, y lentes de caliza intercalados con areniscas tabulares masivas y conglomerados, correspondientes a un ambiente de marea. Finalmente, la sedimentación de lodolitas cambia gradualmente hacia el desarrollo de la plataforma de carbonatos de la Formación Morelos. La naturaleza del contacto entre las formaciones Zicapa y Morelos sugiere que ocurrieron varios intentos para establecer la plataforma, evidentes por la presencia de brechas de emersión en su base.

En trabajos previos (de Cserna *et al.*, 1980) se propuso una variación lateral de facies entre la Formación Zicapa y la Anhidrita Huitzuco, localizada al oeste, donde ésta última correspondería a facies lagunares mientras que la Formación Zicapa, a facies de laguna costera. En el presente trabajo se observaron variaciones laterales de facies entre las localidades Pilcaya-San Miguel la Ciénaga, que se interpreta como más cercano al continente y San Juan de las Joyas con mayor influencia marina. Dichas localidades se encuentran a una distancia de 45 km de sur a norte, siguiendo el rumbo de las estructuras contráctiles y del contacto con el Complejo Acatlán, el cual se asume como un elemento paleogeográfico preservado. Aunque no tenemos evidencias de campo en el presente trabajo para refutar la relación de la Formación Zicapa con la Anhidrita Huitzuco como una variación lateral de facies, consideramos que la presencia de la falla de Papalutla entre ambas localidades, pudo afectar los sistemas de depósito, la cual jugó un papel importante como elemento paleogeográfico durante el tiempo de depósito de ambas formaciones.

CONCLUSIONES

La Formación Zicapa se depositó entre un ambiente continental y uno marino, donde la creación de espacio para su depósito está directamente relacionado con actividad tectónica. Hacemos notar que la extensión cortical en el Cretácico Inferior es una característica que es posible reconocer desde el norte de México, como en las cuenca de Sabinas y la fosa de Chihuahua (Haenggi, 2001; Eguiluz, 2011), hasta el sur de México en las cuencas Cuicateca (Mendoza-Rosales *et al.*, 2010), Zapotitlán y Zicapa (este estudio). La Formación Zicapa registra un ambiente de sedimentación continental cercano a la costa, con evidencias de por lo menos una, y posiblemente múltiples transgresiones. Es posible que una de esas transgresiones corresponda con el evento Ha7 (Hauteriviano), registrado en el Miembro San Juan de las Joyas.

Se propone dividir la Formación Zicapa en cinco miembros: el Miembro Cerro La Cruz, compuesto por un conglomerado basal, el Miembro San Juan de las Joyas de carácter calcáreo, el Miembro Ajuatetla de carácter siliciclástico y de ambiente transicional marino, el Miembro San Andrés de carácter volcanosedimentario y el Miembro río Poblano, dominado por limolitas y lutitas rojas con algunas intercalaciones de caliza.

Entre las localidades Pilcaya-San Miguel la Ciénaga y San Juan de las Joyas, la Formación Zicapa registra una variación lateral de facies, de

norte a sur. La localidad Pilcaya-San Miguel la Ciénaga muestra facies más cercanas al continente, donde los efectos de incursiones marinas, ya sea por efectos tectónicos o eustáticos, no fueron suficientes para desarrollar plataformas internas de carbonatos, como en el caso de la localidad San Juan de las Joyas.

La edad máxima de depósito del Miembro Ajuatetla de la Formación Zicapa, es Titoniano, la cual es la edad del circón más joven en el depósito, mientras que para el Miembro San Andrés, es el Hauteriviano-Barremiano. Esto permite afirmar que los miembros Cerro La Cruz, San Juan de las Joyas y Ajuatetla se depositaron después del Jurásico Tardío y durante el Hauteriviano, previo al volcanismo presente en la Formación Zicapa. A su vez, circones detríticos en la Formación Zicapa en la localidad de Pilcaya registran evidencia de actividad magmática entre 131 y 148 Ma.

La parte media a superior de la Formación Zicapa se depositó en un ambiente transicional marino de forma contemporánea con volcanismo intermedio que afectó el margen suroccidental del núcleo continental de México durante el Cretácico Temprano (Hauteriviano). Dicho volcanismo intermedio se correlaciona con el volcanismo de la Formación Chapolapa y el Complejo Xolapa (Solari *et al.*, 2007), al sur de la zona de estudio. Con los datos actuales no es posible concluir si este volcanismo es atribuido a arco o *rift*, sin embargo se puede correlacionar con eventos extensionales debido a las facies de capas rojas y conglomerados y brechas basales.

La edad de la Formación Zicapa reportada por Fitz-Díaz *et al.* (2002) cartográficamente no corresponde a dicha formación sino a la Formación Tetelcingo, con una edad máxima de depósito de 68 Ma. No obstante, los depósitos de esta unidad contienen evidencia de magmatismo en la región de Papalutla con una edad aproximada entre 141 y 122 Ma (Berriasiano-Aptiano). En el presente estudio se sugiere que la presencia de material volcánico en el Miembro San Andrés de la Formación Zicapa, compuesto por derrames de lavas y tobas, tienen un significado geológico mayor al que se le ha dado en trabajo anteriores y permite ubicar a la Formación Zicapa en el marco geotectónico de una margen convergente en el suroeste de México para el Cretácico Inferior.

Otras manifestaciones de magmatismo del Cretácico Inferior incluyen andesitas intercaladas en calizas de la Formación Taraises (Dávalos-Elizondo, 2011). Incluye también unidades volcaniclásticas como la Formación San Juan de la Rosa, de carácter turbidítico, la cual presenta estratos de rocas volcánicas con edades de 139 Ma (Dávila-Alcocer *et al.*, 2009) y rocas volcanosedimentarias con edades máximas de 127 Ma, una población de circones entre el Jurásico Tardío y el Cretácico Temprano (Ortega-Flores *et al.*, 2013) y en San Miguel Allende (Ortiz-Hernández *et al.*, 2002), cuya edad está definida por su contenido faunístico. Eso lleva a proponer que el magmatismo (supra-subducción) del Cretácico Temprano en la margen del subcontinente Oaxaquia fue un evento regional, extendiéndose desde Zacatecas hasta Guerrero y posiblemente el Bloque Chortis, como han propuesto Talavera-Mendoza *et al.* (2007).

AGRADECIMIENTOS

Agradecemos al Programa de Apoyo a Proyectos de Investigación (PAPIIT: IN104511-3), Carlos Ortega-Obregón por el apoyo técnico en el Laboratorio de Estudios Isotópicos del Centro de Geociencias y

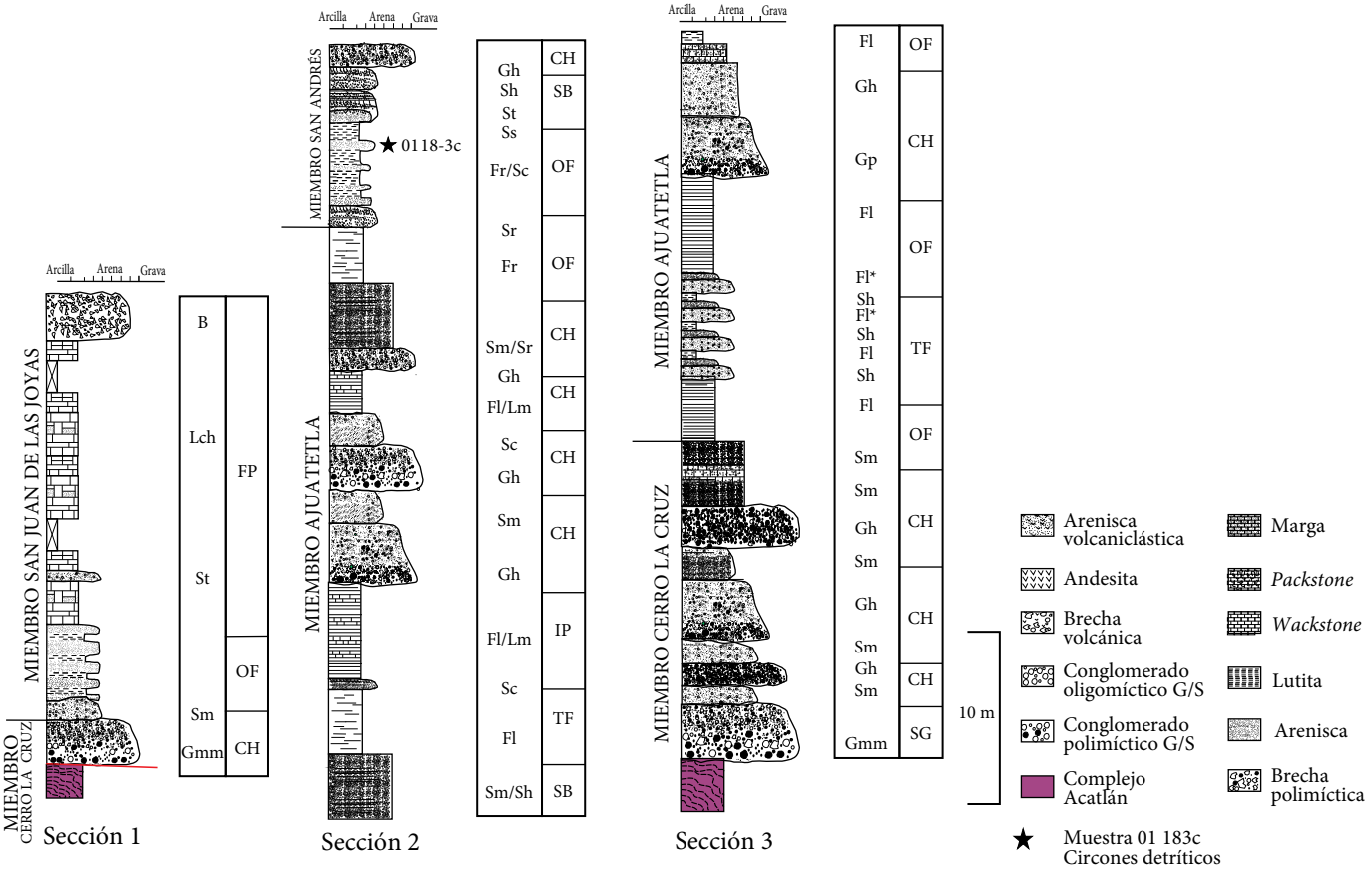

Figura 10. Columna estratigráfica compuesta y asociación de facies de la Formación Zicapa en la localidad Pilcaya-San Miguel la Ciénaga. Los códigos de litofacies corresponden a la Tabla 1, y las asociaciones de facies, a la Tabla 2.

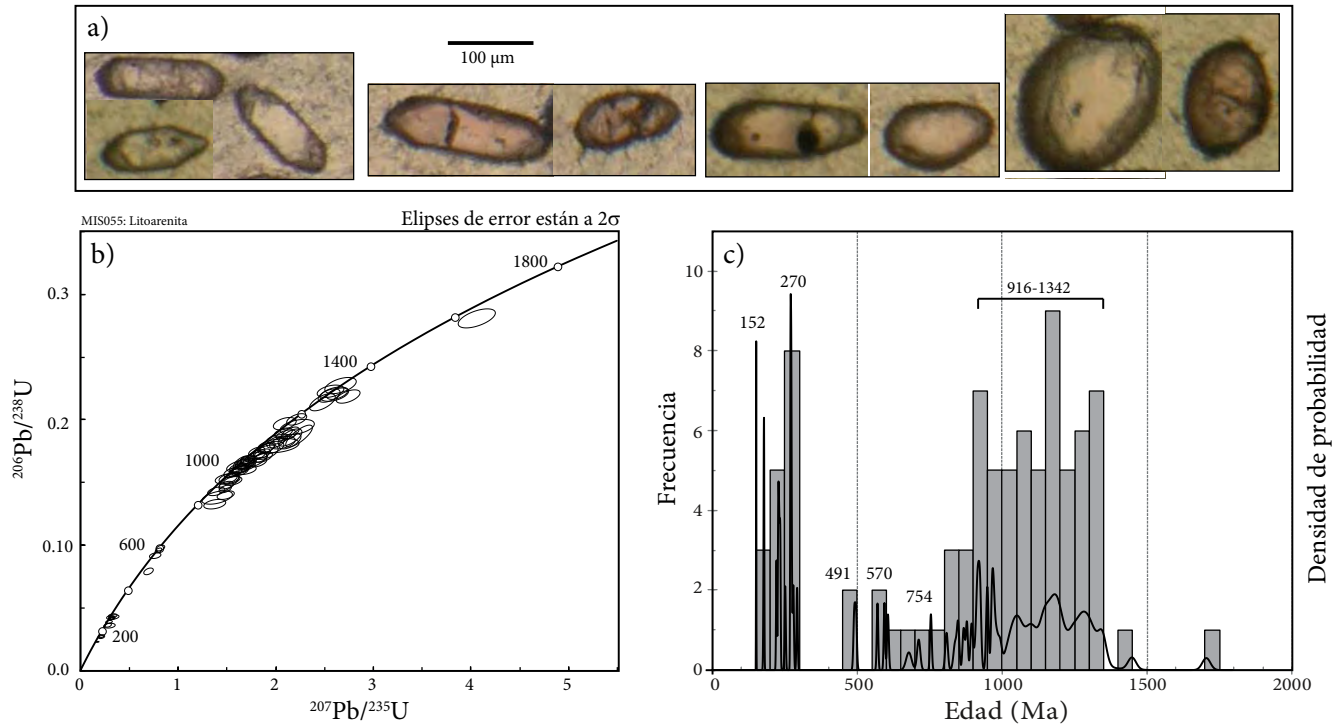

Figura 11. Geocronología de circones detríticos de litarenita de la localidad San Juan de las Joyas, Miembro Ajuatetla (17°45'35.50"N, 99° 5'10.65"W). a) Características de las cuatro familias morfológicas de circones; b) Diagrama de concordia Wetherill mostrando las edades de los circones detríticos de la muestra MIS055; c) Diagrama de densidad de probabilidad para las edades de los circones detríticos de la muestra MIS055. Todos los errores tienen una desviación estándar de 2σ.

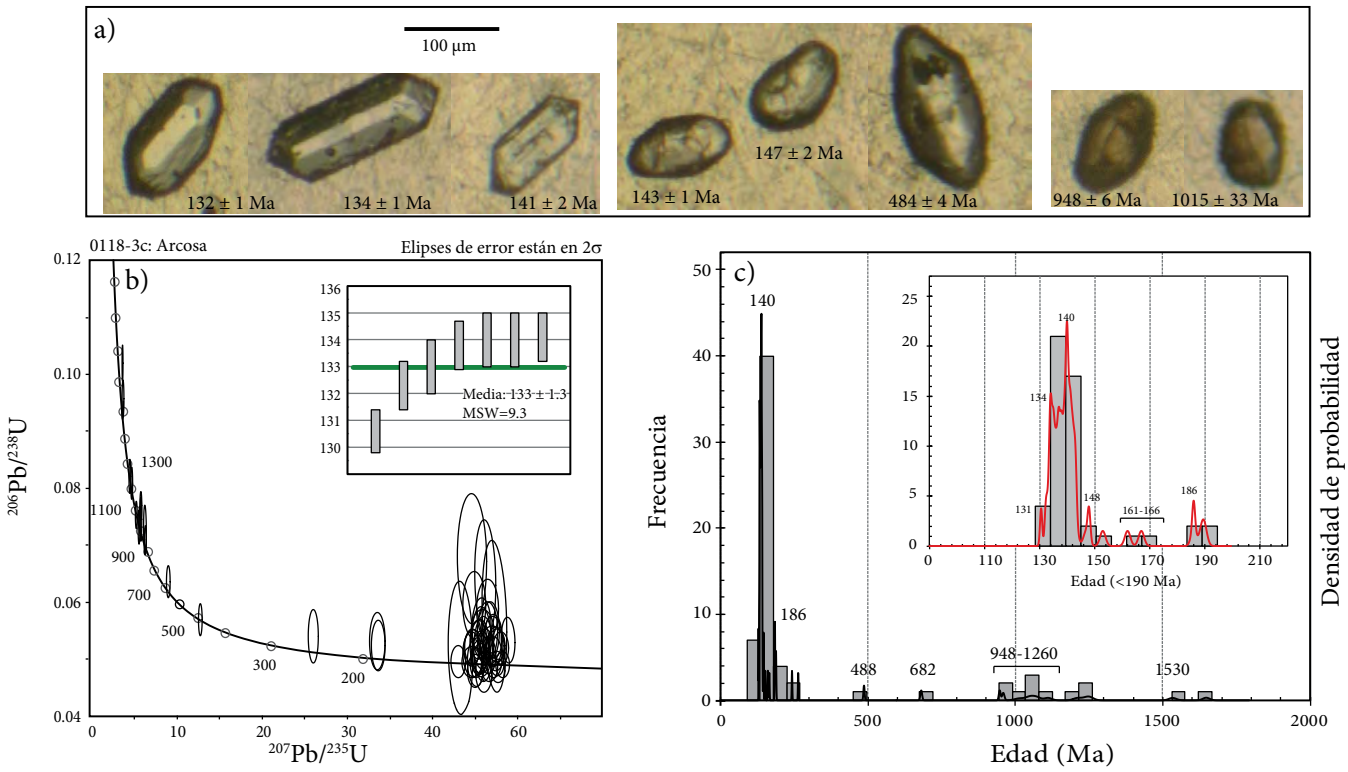

Figura 12. Geocronología de circones detríticos de arenisca volcaniclástica de la localidad Pilcaya-San Miguel la Ciénaga, Miembro San Andrés (18°12'16.77"N, 98°42'24.04"W). (a) Características de las tres familias morfológicas de circones; b) Diagrama de concordia Tera-Wasserburg mostrando las poblaciones de edad de la muestra MIS055. En el pequeño recuadro se muestra el promedio ponderado de los siete circones más jóvenes (edad máxima de depósito); (c) Diagrama de densidad de probabilidad para las edades de los circones detríticos de la muestra 0118-3c. En detalle, el diagrama de densidad de probabilidad de los circones Jurásico-Cretácico Temprano. Todos los errores tienen una desviación estándar de 2σ.

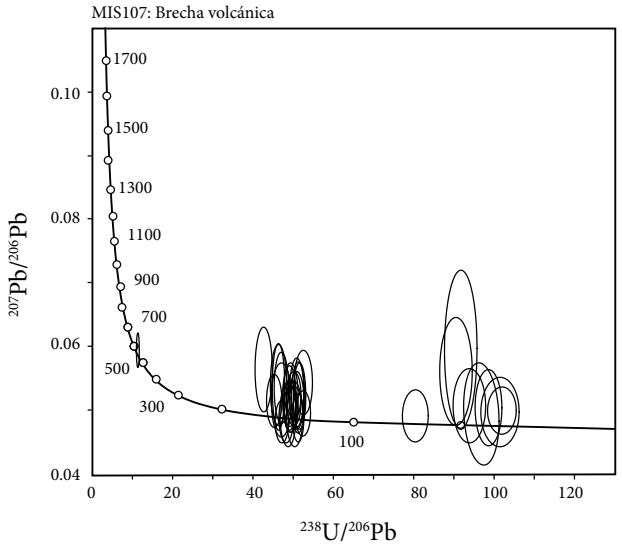

Figura 13. Diagrama de concordia Tera-Wasserburg mostrando las poblaciones de edad de la brecha volcánica de Mezquitlán (MIS107) perteneciente a la Formación Tetelcingo (18°2'3.11"N, 98°56'17.66"W).

a Juan Tomás Vázquez-Ramírez por el apoyo en la preparación de las láminas delgadas. Al Dr. Timothy Lawton por sus importantes aportes en la sedimentología, muchas gracias. Este trabajo se benefició de los comentarios de los árbitros de la revista, Mariano Elías, Elena Centeno y un árbitro anónimo.

REFERENCIAS

Abascal, G., Murillo-Muñetón, G., 2013, Preliminary Sequence stratigraphy framework of the SW part of the Actopan Platform, Lower Cretaceous, Hidalgo, Mexico, *in* American Geophysical Union, Meeting of The Americas, Cancún, México, <http:/moa.agu.org/2013/eposters/eposter/pp51a-02/>.

Barragán, R., Campos-Madrigal, E., Ferrusquía-Villafranca, I., López-Palomino, I., Tolson, G., 2010, Código estratigráfico norteamericano: Universidad Nacional Autónoma de México, Instituto de Geología, Boletín 117, 48 pp.

Campa-Uranga, M.F., Iriondo A., 2004, Significado de dataciones cretácicas de los arcos volcánicos de Taxco, Taxco el Viejo y Chapolapa, en la evolución de la Plataforma Guerrero Morelos: IV Reunión Nacional de Ciencias de la Tierra, Juriquilla, Querétaro, Sociedad Geológica Mexicana, Libro de Resúmenes, 76.

Campa-Uranga, M.F., García-Díaz, J.L., Bustamante-García, J., Torreblanca-Castro, T., Aguilera-Martínez., M.A., Vergara-Martínez, A., 1998, Carta Geológico-Minera Chilpancingo E14-8, escala 1:250,000: Pachuca, Hidalgo, México, Consejo de Recursos Minerales, 1 mapa.

Carrasco, B., Flores, V., Gody, D., 1975, Tobas del Cretácico Inferior del área de Fortín-Zongolica, Estado de Veracruz: Revista del Instituto Mexicano del Petróleo, 7(1), 7-27.

Centeno-García, E., Corona-Chávez, P., Talavera-Mendoza, O., Iriondo, A., 2003, Geologic and tectonic evolution of the western Guerrero terrane-a transect from Puerto Vallarta to Zihuatanejo, Mexico, *en* Geologic transects across Cordilleran Mexico, Guidebook for the field trips of the 99th Geological Society of America Cordilleran Section Annual Meeting, Puerto Vallarta, Jalisco, Mexico: Universidad Nacional Autónoma de México, Instituto de Geología, Publicación Especial, 1, 201- 228.

Centeno-García E., Guerrero-Suástegui, M., Talavera-Mendoza O., 2008, The Guerrero Composite Terrane of western Mexico: Collision and subsequent rifting in a suprasubduction zone: Geological Society of America Special Paper, 436, 279-308, doi:10.1130/2008.2436(13).

Centeno-García, E., Silva-Romo, G., Mendoza-Rosales, C., 2009, Sedimentología de la Formación Matzitzi (Paleozoico superior) y significado de sus componentes volcánicos, región de Los Reyes Metzontla-San Luis Atolotitlán, Estado de Puebla: Revista Mexicana de Ciencias Geológicas, 26(1), 18-36.

Cerca, M., 2004, Deformación y magmatismo Cretácico tardío-Terciario temprano en la zona de la Plataforma Guerrero-Morelos: Guerrero, México: Juriquilla, Querétaro, Universidad Nacional Autónoma de México, tesis de doctorado, 175 pp.

Cerca, M., Ferrari, L., López-Martínez, M., Martiny, B., Iriondo, A., 2007, Late Cretaceous shortening and early Tertiary shearing in the central Sierra Madre del Sur, southern Mexico: Insights into the evolution of the Caribbean-North American plate interaction: Tectonics, 26(3), 1-34.

Corona-Esquivel, R.J., 1981, Estratigrafía de la región de Olinalá-Tecocoyunca, noreste del Estado de Guerrero: Revista del Instituto de Geología, Universidad Nacional Autónoma de México, 5(1), 17-24.

Dávalos-Elizondo, E., 2011, Análisis estructural del complejo volcano-tectónico de Pinos, Zacatecas, México: Linares, Nuevo León, Universidad Autónoma de Nuevo León, tesis de licenciatura, 136 pp.

Dávila-Alcocer, V., Centeno-García, E., Valencia, V., Fitz-Díaz, E., 2009, Una nueva interpretación de la estratigrafía de la región de Tolimán, Estado de Querétaro: Boletín de la Sociedad Geológica Mexicana, 61, 491-497.

de Cserna, Z., 1965, Reconocimiento geológico de la Sierra Madre del Sur, entre Chilpancingo y Acapulco, estado de Guerrero: Universidad Nacional Autónoma de México, Instituto de Geología, Boletín, 62, 77 pp.

de Cserna, Z., Ortega G.F., Palacios, N.M., 1980, Reconocimiento geológico de la parte central de la cuenca del alto Río Balsas, estados de Guerrero y Puebla, *en* V Convención Geológica Nacional, Libro Guía de la Excursión a la parte alta de la Cuenca del Alto Rio Balsas, estados de Guerrero y Puebla: México, Sociedad Geológica Mexicana, 1-33.

Eguiluz, S., 2011, Secuencias estratigráficas del Berriasiano-Aptiano en la Cuenca de Sabinas: su significado en el entendimiento de la evolución geológica del noreste mexicano: Boletín de la Sociedad Geológica Mexicana, 63(2), 285-311.

Erben, H.K., 1956, El Jurásico Inferior de México y sus amonitas, *en* XX Congreso Geológico Internacional: México D. F., Universidad Nacional Autónoma de México, Instituto de Geología, 20, 393 pp.

Fedo, C.M., Sircombe, K.N., Rainbird, R.H., 2003, Detrital zircon analysis of the sedimentary record, *en* Hanchar, J.M. and Hoskin, P.W.O. (eds.), Zircon: Experiments, Isotopes, and Trace Element Investigations: Mineralogical Society of America, Reviews in Mineralogy, 10(53), 277-303.

Ferrari, L., Morán, D., González, E., 2007, Actualización del Mapa Geológico de México a escala 1:4,000,000, Nuevo Atlas Nacional de México: Instituto de Geografía, Universidad Nacional Autónoma de México, 1 mapa.

Figueroa-Catalán, A., Gómez-Martínez, G.A., 2010, Estratigrafía, Petrografía y Procedencia de la formación Zicapa (Cretácico Temprano) en la Región de Zicapa y San Juan de Las Joyas, Guerrero, México: Taxco, Guerrero, Universidad Autónoma de Guerrero, tesis de licenciatura, 103 pp.

Fitz-Díaz, E., 2001, Evolución estructural del sinclinorio de Zacango en el límite oriental de la Plataforma Guerrero-Morelos, Guerrero, México: México, D. F., Instituto Politécnico Nacional, tesis de licenciatura, 103 pp.

Fitz-Díaz, E., Campa-Uranga, M.F., López-Martínez, M., 2002, Fechamiento de las lavas andesíticas de la Formación Zicapa, en el límite oriental de la Plataforma Guerrero-Morelos, *en* III Reunión Nacional de Ciencias de la Tierra (Resumen): GEOS, 22(2), 178-179.

Fries, C.Jr., 1960, Geología del estado de Morelos y de partes adyacentes de México y Guerrero, región central meridional de México: Universidad Nacional Autónoma de México, Boletín del Instituto de Geología, 60, 236 pp.

Gehrels, G.E., Valencia, V.A., Ruiz, J., 2008, Enhanced precision, accuracy, efficiency, and spatial resolution of U-Pb ages by laser ablation–multicollector–inductively coupled plasma–mass spectrometry: Geochemistry Geophysics Geosystems, 9(3), 13 p., Q03017, DOI: 10.1029/2007GC001805.

Guzmán, E.J., 1950, Geología del noroeste de Guerrero: Boletín de la Asociación Mexicana de Geólogos Petroleros, 2, 95-156.

Haenggi, W., 2001, Tectonic history of the Chihuahua trough, Mexico and adjacent USA, Part I: the pre-Mesozoic setting: Boletín de la Sociedad Geológica Mexicana, 54, 28-66.

Haq, B.U., Hardenbol, J., Vail, P.R., 1987, Chronology of fluctuating sea

levels since the Triassic: Science, 235, 1156-1167, DOI: 10.1126/science.235.4793.1156.

Haq, B.U., Hardenbol, J., Vail, P.R., 1988, Mesozoic and Cenozoic chronostratigraphy and cycles of sea-level change, *en* Wilgus, C.K., Hastings, B.S., Kendall, C.G.S.C., Posamentier, H.W., Ross, C.A., Van Wagoner, J.C. (eds.), Sea level changes: an integrated approach: Tulsa, Oklahoma, Society of Economic Paleontologists and Mineralogists (Society for Sedimentary Geology), Special Publication, 42, 71-108.

Hernández-Romano, U., Aguilera-Franco, N., Martínez-Medrano, M., Barceló-Duarte, J., 1997, Guerrero-Morelos Platform drowning at the Cenomanian-Turonian boundary, Huitziltepec area, Guerrero State, southern Mexico: Cretaceous Research, 18, 661-686.

Hernández-Treviño, T., Torres de León, R., Solís-Pichardo, G., Schaaf, P., Hernández-Bernal, M., Morales-Contreras, J., 2004, Edad de la Formación Chapolapa en la localidad de río Cochoapa, al oeste del Ocotito, estado de Guerrero, *en* Reunión de la Unión Geofísica Mexicana, Puerto Vallarta, Jal., México: GEOS, 24, 179.

Juárez-Arriaga, E., 2006, Marco de estratigrafía de secuencias para la sucesión estratigráfica terrígeno-carbonatada del Paleozoico Superior en el área de Olinalá, Guerrero, México: Universidad Nacional Autónoma de México, tesis de maestría, 93 pp.

Keppie, J.D., 2004, Terranes of Mexico revisited: A 1.3 billion year odyssey: International Geology Review, 46(9), 765-794.

Keppie, J.D., Sandberg, C.A., Miller, B.V., Sánchez-Zavala, J.L., Nance, R.D., Poole, F.G., 2004, Implications of latest Pennsylvanian to Middle Permian paleontological and U-Pb SHRIMP data from the Tecomate Formation to re-dating tectonothermal events in the Acatlán Complex, southern Mexico: International Geology Review, 46(8), 745-753.

Keppie, J.D., Dostal, J., Murphy, J.B., Nance, R.D., 2008, Synthesis and tectonic interpretation of the westernmost Paleozoic Variscan orogen in southern Mexico: From rifted Rheic margin to active Pacific margin: Tectonophysics, 461(1-4), 277-290.

López-Ticha, D., 1985, Revisión de la estratigrafía y potencial petrolero de la Cuenca de Tlaxiaco: Boletín Asociación Mexicana de Geólogos Petroleros, 37(1), 49-92.

Ludwig, K.R., 2012, User's manual for Isoplot 3.75, A geochronological toolkit for Microsoft Excel: Berkeley Geochronology Center Special Publication, 5.

Martini, M., Mori, L., Solari, L., Centeno-García, E., 2011, Sandstone provenance of the Arperos Basin (Sierra de Guanajuato, central Mexico): Late Jurassic-Early Cretaceous back-arc spreading as the foundation of the Guerrero terrane: The Journal of Geology, 119, 597-617.

Mendoza-Rosales, C., 2010, Estratigrafía y facies de las cuencas cretácicas de Puebla y su significado tectónico: Universidad Nacional Autónoma de México, tesis doctoral, 190 pp.

Mendoza-Rosales, C., Centeno-García, E., Silva-Romo, G., Campos-Madrigal., E., Bernal., J.P., 2010, Barremian rift-related turbidites and alkaline volcanism in southern Mexico and their role in the opening of the Gulf of Mexico: Earth and Planetary Science Letters, 295, 419-434.

Miall, A.D., 1996, The Geology of Fluvial Deposits: Berlin, Springer-Verlag, 581 pp.

Monroy-Fernández, M.G., Sosa-Patrón, A.A., 1984, Geología de la Sierra de Tentzo, Pue., borde norte del Terreno Mixteco: Boletín de la Sociedad Geológica Mexicana, 45(1-2), 43-71.

Ortega-Flores, B., Solari, L., Lawton, T.F., 2013, Detrital-zircon record of a major Middle Triassic-Early Cretaceous provenance shift, central Mexico: demise of Gondwanan continental fluvial systems and onset of back-arc volcanism and sedimentation: International Geology Review, 56, 237-261, DOI:10.1080/00206814.2013.844313.

Ortega-Gutiérrez, F., 1980, Rocas volcánicas del Maastrichtiano en el área de San Juan Tetelcingo, Estado de Guerrero, *en* V Convención Geológica Nacional, Libro Guía de la Excursión a la parte alta de la Cuenca del Alto Río Balsas, estados de Guerrero y Puebla: México, Sociedad Geológica Mexicana, 34-38.

Ortega-Gutiérrez, F., Sedlock, R.L., Speed, R.C., 1994, Phanerozoic tectonic evolution of Mexico, *en* Speed, R.C. (ed.), Phanerozoic evolution of North American continent ocean transitions: Boulder, Colorado, Geological Society of America, The Decade of North American Geology Summary Volume to accompany the DNAG Continent-Ocean Transects Series, 265-306.

Ortega-Gutiérrez, F., Elías-Herrera, M., Reyes-Salas, M., Macías-Romo, C., López, R., 1999, Late Ordovician–Early Silurian continental collision orogeny in southern Mexico and its bearing on Gondwana–Laurentia connections: Geology, 27(8), 719-722.

Ortega-Obregón, C., Keppie, J.D., Murphy, J.B., Lee, J.K.W., Ortega-Rivera, A., 2009, Geology and geochronology of Paleozoic rocks in western Acatlán Complex, southern Mexico: evidence for contiguity across an extruded high-pressure belt and constraints on Paleozoic reconstructions: Geological Society of America Bulletin, 121(11-12), 1678-1694.

Ortiz-Hernández, L.E., Flores-Castro, K., Acevedo-Syoval, O., 2002, Petrographic and geochemical characteristics of upper Aptian calc-alkaline volcanism in San Miguel Allende, Guanajuato State, Mexico: Revista Mexicana de Ciencias Geológicas, 19(2), 81-90.

Padilla y Sánchez, R.J., 2007, Evolución geológica del sureste mexicano desde el Mesozoico al presente en el contexto regional del Golfo de México: Boletín de la Sociedad Geológica Mexicana, 59(1), 19-42.

Pantoja-Alor, J., 1990, Redefinición de las unidades estratigráficas de la secuencia mesozoica de la región de Huetamo-Altamirano, estados de Michoacán y Guerrero (resumen), *en* X Convención Geológica Nacional: México, D.F., Sociedad Geológica Mexicana, 66.

Perez-Ibargüengoitia, J.M., Hokuto-Castillo, A., de Cserna, Z., 1965, Reconocimiento geológico del área Petlalcingo-Santa Cruz, Municipio de Acatlán, Estado de Puebla: Paleontología Mexicana 21, 1-22 .

Rivera-Carranza, E., De la Teja-Segura, M.A., Miranda-Huerta, A., Lemus-Bustos, O., Motolinea-García, O., León-Ayala, V., Moctezuma-Salgado, M.D., 1998, Carta Geológico-Minera Cuernavaca E14-5, escala 1:250,000: Pachuca, Hidalgo, México, Consejo de Recursos Minerales, 1 mapa.

Salinas-Prieto, J.C., 1986, Estudio Geológico de la Porción Occidental de la Región de la Montaña, Estado de Guerrero, México: México, D. F., Instituto Politécnico Nacional, tesis profesional, 85 pp.

Sánchez-Rojas, L.E., Sabanero-Sosa, M.H., Salinas-Prieto, J.C., Talavera-Mendoza, O., Campa, M.F., 1996, Carta geológico-minera y geoquímica de Chiautla, estado de Puebla, Tomo I: Consejo de Recursos Minerales y Escuela Regional de Ciencias de la Tierra, Universidad Autónoma de Guerrero, Informe técnico, 93 pp.

Smith, G., 1987, The influence of explosive volcanism on fluvial sedimentation; the Deschutes Formation (Neogene) in central Oregon: Journal of Sedimentary Petrology, 57(4), 613-629.

Solari, L., Torres de León, R., Hernández-Pineda, G., Solé, J., Solís-Pichardo, G., Hernández-Treviño, T., 2007, Tectonic significance of Cretaceous-Tertiary magmatic and structural evolution of the northern margin of the Xolapa Complex, Tierra Colorada area, southern Mexico: Geological Society of America Bulletin, 119(9-10), 1265-1279.

Talavera-Mendoza, O., Ruiz, J., Gehrels, G.E., Valencia, V.A., Centeno-García, E., 2007, Detrital zircon U/Pb geochronology of southern Guerrero and western Mixteca arc successions (southern Mexico): New insights for the tectonic evolution of the southwestern North America during the late Mesozoic: Geological Society of America Bulletin, 119, 1052-1065.

Zepeda-Martínez, M. del C., 2013, Estratigrafía y Sedimentología de la Sierra del Tentzo, Estado de Puebla, México: México, D. F., Universidad Nacional Autonoma de México, tesis de licenciatura, 127 pp.

Manuscrito recibido: Agosto 23, 2013
Manuscrito corregido recibido: Febrero 27, 2014
Manuscrito aceptado: Marzo 1, 2014

CAPÍTULO 3.

La Formación Atzompa (Cretácico Inferior): Registro de la evolución de una cuenca extensional de tras-arco hacia una plataforma de carbonatos.

Sierra-Rojas, M. I., Molina-Garza, R. S., y Lawton, T. F., 2016. The Lower Cretaceous Atzompa Formation in South-Central Mexico: Record of Evolution from Extensional Backarc Basin Margin to Carbonate Platform. Journal of Sedimentary Research, 86(6), 712-733.

Contribuciones individuales:

Maria Isabel Sierra-Rojas: Planteamiento del problema, revisión bibliográfica y análisis de sensores remotos. Trabajo de campo, levantamiento de columnas estratigráficas, toma de datos sedimentológicos y estructurales, toma de muestras. Preparación de muestras para análisis geocronológicos y obtención de datos geocronológicos, procesado de datos geocronológicos, petrografía de areniscas y análisis modales, análisis sedimentológico y de facies sedimentarias. Elaboración de mapas y figuras, redacción del manuscrito.

Roberto Molina-Garza: Planteamiento del problema y asesoría general del proyecto. Trabajo de campo, revisión y orientación en la interpretación de datos y revisión del manuscrito.

Timothy Lawton: Trabajo de campo y asesoría en toma de datos sedimentológicos, asesoría general en la interpretación sedimentológica y en la redacción y revisión del manuscrito.

Journal of Sedimentary Research

Journal of Sedimentary Research, 2016, v. 86, 712–733
Research Article
DOI: http://dx.doi.org/10.2110/jsr.2016.45

THE LOWER CRETACEOUS ATZOMPA FORMATION IN SOUTH-CENTRAL MEXICO: RECORD OF EVOLUTION FROM EXTENSIONAL BACKARC BASIN MARGIN TO CARBONATE PLATFORM

MARÍA I. SIERRA-ROJAS, ROBERTO S. MOLINA-GARZA, AND TIMOTHY F. LAWTON
Centro de Geociencias, Universidad Nacional Autónoma de México, Querétaro 76230, México
e-mail: misierra@geociencias.unam.mx

ABSTRACT: **Lower Cretaceous depositional systems of southwestern Oaxaquia, in south-central Mexico, were influenced by initiation of a continental arc on mainland Mexico and subsequent accretion of the Guerrero composite arc terrane to mainland Mexico. The Atzompa Formation, defined herein, which crops out in the Sierra de Tentzo, constitutes a succession of conglomerate, sandstone, siltstone, and limestone with Early Cretaceous fauna and detrital zircon maximum depositional ages that range 126–123 Ma (late Barremian to early Aptian). The lower part of the Atzompa records a transition from alluvial to deep lacustrine depositional environments, suggesting the early stages of an extensional basin; overlying deposits of anabranching axial fluvial systems that flowed to the NE–SE accumulated after a period of rapid subsidence in the Tentzo basin, also formerly undescribed. Fluvial facies grade up-section to tidal deposits overlain in turn by a carbonate ramp succession that contains late Barremian to early Aptian fossils. The ramp deposits of the uppermost Atzompa Formation are overlain on a sharp contact by basinal carbonates of early Albian age.**

The Tentzo basin, formed due to crustal extension of the overriding plate in a backarc setting, was characterized by very high rates of sedimentation (3.6 mm/yr) during the early stages of basin formation (rift initiation and rift climax), and slower rates during the development of tidal systems and the carbonate ramp (post-rift stage). Regional and local subsidence took place in the backarc region of the Zicapa magmatic arc, which was established in the western margin of Mexico by Hauterivian time. Abrupt deepening following Atzompa Formation deposition is attributed to flexural subsidence related to collision of the Guerrero composite volcanic terrane with the western margin of Mexico. Following late Aptian accretion of the Guerrero terrane to Oaxaquia, the carbonate basin eventually shallowed to become a carbonate platform that faced the Gulf of Mexico.

INTRODUCTION

Early Cretaceous sedimentary-basin development along the southern part of the North American Cordillera records essential data for insight into the relative importance of tectonic processes related to plate interactions along the paleo-Pacific margin versus processes associated with the opening of the Atlantic Ocean and the Gulf of Mexico. Plate interactions related to the opening of the Gulf of Mexico in particular may have potential relevance to basin development in Mexico, a relatively narrow strip of continental lithosphere whose eastern edge is the transform margin of the western Gulf of Mexico (e.g., Pindell and Dewey 1982; Pindell 1985) and whose western flank grew by terrane accretion and continental-arc magmatism (Campa and Coney 1983; Freydier et al. 1997; Sedlock et al. 1993; Dickinson and Lawton 2001a). The southern part of the North American Cordillera was truly a place where paleo-Pacific convergent-margin magmatism and accretionary tectonics might have interacted in space and time with Gulf of Mexico transform tectonics, and the challenge to basin analysts lies in deciphering the relative importance of contributions from the two plate-tectonic provinces.

Both temporal and geographic tectonic transitions characterize the Early Cretaceous Cordillera of the western United States and Mexico. Whereas crustal shortening had begun to create a retroarc foreland basin system east of a contemporary continental-margin arc in the Rocky Mountain region beginning sometime in Late Jurassic to Aptian time (compare Heller et al. 1986, Lawton 1994, DeCelles and Currie 1996 for differences of interpretation), Jurassic to Early Cretaceous basins of the southwestern United States and northern Mexico are universally interpreted as extensional basins. These basins include the Bisbee basin of southern Arizona and southern New Mexico (Bilodeau 1982; Klute 1991; Dickinson and Lawton 2001b), its southern counterpart in northern Sonora (Jacques-Ayala 1995; Peryam et al. 2011), the Chihuahua trough in Chihuahua (Haenggi 2001), and the Sabinas basin of northeastern Mexico (Eguiluz de Antuñano 2001) (Fig. 1). Although these basins have been extensively studied, proposed mechanisms for their origin vary. They include aulacogen formation associated with the breakup of Pangea or backarc extension related to variable slab dip along strike of a subduction zone (Bilodeau 1982), southwestward rollback of a subducted slab following Jurassic magmatism (Lawton and McMillan 1999; Dickinson and Lawton 2001a), extensional backarc basin formation (Jacques-Ayala 1995), and trans-tensional pull-apart during opening of the Gulf of Mexico (Anderson and Nourse 2005; Haenggi and Muehlberger 2005). In any of these scenarios, the contrast with contemporary retroarc shortening farther north is striking and suggests a fundamental along-strike change in active-margin processes such as plate convergence directions or plate-margin orientations.

Time-equivalent Early Cretaceous sedimentary basins, if they exist, along the margin of central Mexico are not available for study as a result of Cenozoic volcanic cover, but Early Cretaceous basins of southern Mexico

Published Online: June 2016
 1527-1404/16/086-712/$03.00

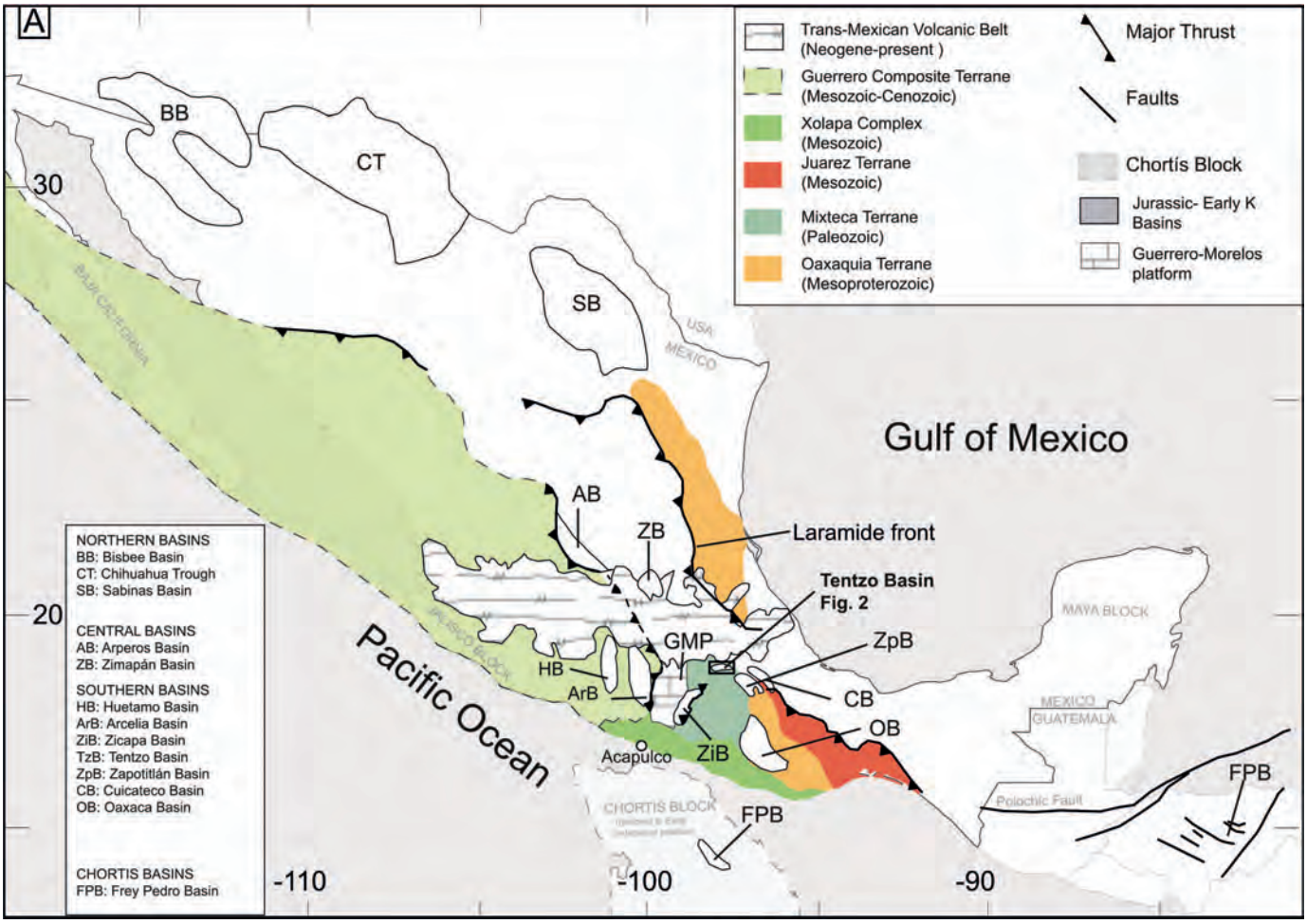

FIG. 1.—Tectonostratigraphic terranes of Mexico and major geological provinces. Major tectonic features, including the Oaxaquia block and its possible extensions, are from Ortega-Gutiérrez et al. (1995), Keppie (2004), and Centeno-García et al. (2011). Jurassic–Early Cretaceous basins are modified after the following sources: Bisbee basin from Dickinson and Lawton (2001b) and Peryam et al. (2011), Chihuahua trough from Haenggi (2001), Sabinas and Parras basins from Eguiluz de Antuñano (2001) and Lawton et al. (2001), Arperos basin from Martini et al. (2011), Zicapa basin from Sierra-Rojas and Molina-Garza (2014), Chivillas and Zapotitlán basins from Mendoza-Rosales (2010), Oaxacan basins from López-Ticha (1985),and the Guerrero–Morelos Platform from Hernandez-Romano et al. (1997).

offer great potential for improved contextual understanding of their counterparts in the north. Although these basins are comparatively understudied, deposition of the Barremian–Aptian basins in the eastern margin are interpreted to have taken place in a transtensional rift basin (e.g., Mendoza-Rosales et al. 2010); likewise western time-equivalent strata were deposited during coeval magmatism (Sierra-Rojas and Molina-Garza 2014). Improved understanding of the tectonic context of these basins will enhance assessment of the relative importance of Cordilleran versus Gulf of Mexico processes to the tectonic evolution of Mexico.

To contribute to general understanding of Early Cretaceous basin tectonics in southern Mexico, we describe a well-exposed succession, named here the Atzompa Formation, of Lower Cretaceous strata, which constitutes the fill of an extensive sedimentary basin directly south of the Trans-Mexican Volcanic Belt in the state of Puebla (Figs. 1, 2). We interpret provenance relations of the basin on the basis of sandstone petrography, conglomerate clast counts, and detrital-zircon U-Pb geochronology, and combine the compositional data with a depositional model and subsidence analysis to demonstrate that the Early Cretaceous history of south-central Mexico consisted of extensional basin development in a back-arc setting. We further infer that paleo-Pacific plate interactions drove basin subsidence, and therefore the opening of the Gulf of Mexico was irrelevant to that history.

REGIONAL TECTONIC SETTING

The Early Cretaceous paleogeography of Cordilleran Mexico consisted of a series of carbonate platforms bordering the Gulf of Mexico. The platforms lay east of an evolving convergent margin (e.g., Goldhammer and Johnson 2001) and were built on continental crust of Mesoproterozoic age, which Ortega-Gutiérrez et al. (1995) named Oaxaquia. The conventional view is that platform distribution was a response to basement architecture inherited from earlier Middle and Late Jurassic rifting and drifting episodes affecting the Gulf of Mexico (Wilson 1990); nevertheless, there is a significant hiatus between the end of the Gulf of Mexico drift phase in the Valanginian (~ 140 Ma; Pindell and Kennan 2009) and platform build-up in the Aptian (~ 120 Ma; Wilson and Ward 1993). Extensional basins predating carbonate platform deposition formed both near the Gulf in southern Mexico and well away from the Gulf across northern Mexico in Late Jurassic to Early Cretaceous time (Fig. 1), and they are the subject of this contribution.

There is a record of island-arc magmatism in the Guerrero superterrane of western Mexico (Fig. 1; Campa and Coney 1983; Talavera-Mendoza and

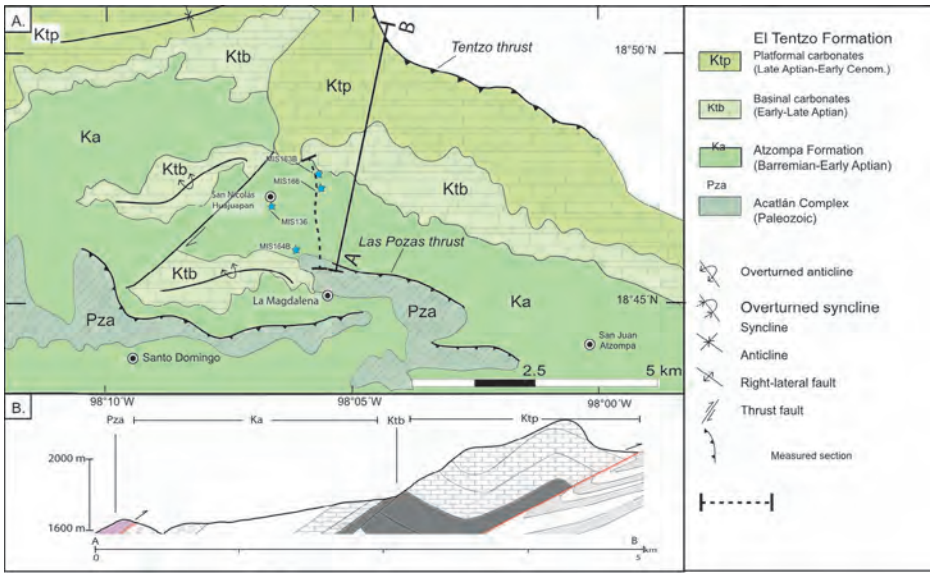

FIG. 2.—**A)** Geological map of Sierra de Tentzo in the state of Puebla. Dotted line shows the Pozo Grande section (Atzompa Formation stratotype). Sampling locations for U-Pb geochronology are plotted as blue stars. After (Monroy-Fernández and Sosa-Patrón 1984). **B)** Simplified S–N cross section with a vertical scale of 2 parallel to the measured section. Vertical exaggeration of 3.

Guerrero-Suástegui 2000; Centeno-García et al. 2008). The Guerrero superterrane has been interpreted according to different tectonic scenarios as a far-travelled intraoceanic arc (Lapierre et al. 1992; Tardy et al. 1994; Dickinson and Lawton 2001a), a multi-arc system (Talavera-Mendoza et al. 2007), and a long-lived extensional continental arc (Centeno-García et al. 2008; Pindell and Kennan 2001; Martini et al. 2011). In most interpretations of the above workers, the Guerrero superterrane was accreted to Oaxaquia in pre-Albian time to form the Arperos–Arcelia suture (Lapierre et al. 1992; Tardy et al. 1994; Dickinson and Lawton 2001a).

All models for the evolution of Guerrero incorporate oceanic elements to separate Guerrero from Oaxaquia, whether a back-arc basin or an oceanic plate. This oceanic element has been referred to as the Arperos–Arcelia basin (AAB). The oceanic nature of the AAB is documented by abundant deformed pillow basalts with flat rare-earth patterns and high positive εNd values and ultramafic rocks (Freydier et al. 2000, among others). It is also supported by widespread deposition of banded chert of the Arperos Formation. The width and paleogeography of the AAB remain uncertain, but some workers infer that it was a narrow basin (e.g., Pindell and Kennan 2001, Martini et al. 2011).

East of the Arcelia basin (Fig. 1), the Teloloapan sequence has been interpreted as the record of island-arc magmatism (Talavera-Mendoza and Guerrero-Suástegui 2000; Freydier et al. 2000). Cabral-Cano et al. (2000) argued for stratigraphic continuity between Teloloapan strata and the Guerrero-Morelos platform in the Oaxaquia margin; nevertheless, the Teloloapan succession has been restricted to the Guerrero superterrane (Centeno-García et al. 2008), and the Morelos and correlative strata may conform an overlap assemblage.

The relationship between Cretaceous arc magmatism in western Mexico and the Caribbean is also unclear. Early Cretaceous continental-arc magmatism has been reported from the part of the Chortis block (Fig. 1), which now lies in east-central Honduras, but has been linked to southern Mexico by similar basement rocks and Mesozoic stratigraphy (Rogers et al. 2007a). Tardy et al. (1994) and Pindell and Kennan (2001) inferred coeval east-dipping subduction beneath the Chortis block and Guerrero (western Mexico), but they link these separate trenches via a transform fault to the east-facing Great Arc of the Caribbean (GAC), which in contrast was constructed on oceanic crust. Evidence of the polarity of the GAC can be found in mantle tomography (van der Hilst and Mann 1994) and in structural relationships in Cretaceous strata in northern South America (Kroehler et al. 2011).

New clues to the Late Jurassic–Cretaceous evolution of the Oaxaquia margin and the Guerrero superterrane come from recent provenance studies of Lower Cretaceous sandstones (Talavera-Mendoza et al. 2007; Martini et al. 2011; Ortega-Flores et al. 2013; Sierra-Rojas and Molina-Garza 2014; Martini et al. 2014). In summary, these studies have demonstrated different sandstone provenance on opposite margins of the AAB. Sandstones are arc-derived in the west and mixed-sourced (continent- and arc-derived) in the east, with both margins having records of volcanism and similar Early Cretaceous detrital-zircon populations. These observations have been interpreted by Martini et al. (2011), among others, to indicate that backarc magmatism linked to subduction under Guerrero extended as far east as the Oaxaquia continent in the back-arc region. They thus argue for a small AAB. The same data have been interpreted to indicate that continental-arc magmatism occurred under Oaxaquia via east-dipping subduction in a different arc-trench system (Dickinson and Lawton 2001a; Talavera-Mendoza et al. 2007; Sierra-Rojas and Molina-Garza 2014). We support the latter interpretation.

The Atzompa Formation occupies the Tentzo Basin (TzB), one of several Early Cretaceous sedimentary basins in southern Mexico that developed on Oaxaquia and the adjacent Chortis block, which lies in Guatemala, Honduras, and Nicaragua (Figs. 1, 2). In the Early Cretaceous, sedimentary basins in eastern Oaxaquia (Cuicateco basin) and eastern Chortis (Frey Pedro Belt basin) filled with thick marine turbidites. In Chortis, volcaniclastic turbidites of the Aptian Tayaco Formation were deposited in an intra-arc extensional setting (Rogers et al. 2007a). In Oaxaca, Aptian turbidites are interbedded with volcanic rocks in the Chivillas and Xonamanca formations of the Cuicateco basin (Fig. 1; Carrasco et al. 1975; Mendoza-Rosales et al. 2010). The time-equivalent Atzompa Formation therefore offers the opportunity to shed light on the evolution of the Oaxaquia margin south of the Trans-Mexican Volcanic belt, and help discriminate among different subduction scenarios and tectonic models for this region.

The Atzompa Formation lies east of the Guerrero–Morelos Platform where the Taxco schist shows Early Cretaceous felsic calc-alkaline magmatism (Fig. 1). It lies west, however, of the regions of alkaline magmatism of the Cuicateco basin of eastern Oaxaquia. As the Zicapa Formation, it is part of the Mixteca terrane of the Oaxaquia margin and it was clearly deposited on continental crust (Fig. 1).

METHODS

One complete stratigraphic section of the Atzompa Formation (Fig. 3; Appendix B, see Supplemental Material) was measured from its basal unconformity to the base of the overlying Tentzo Formation along Pozo

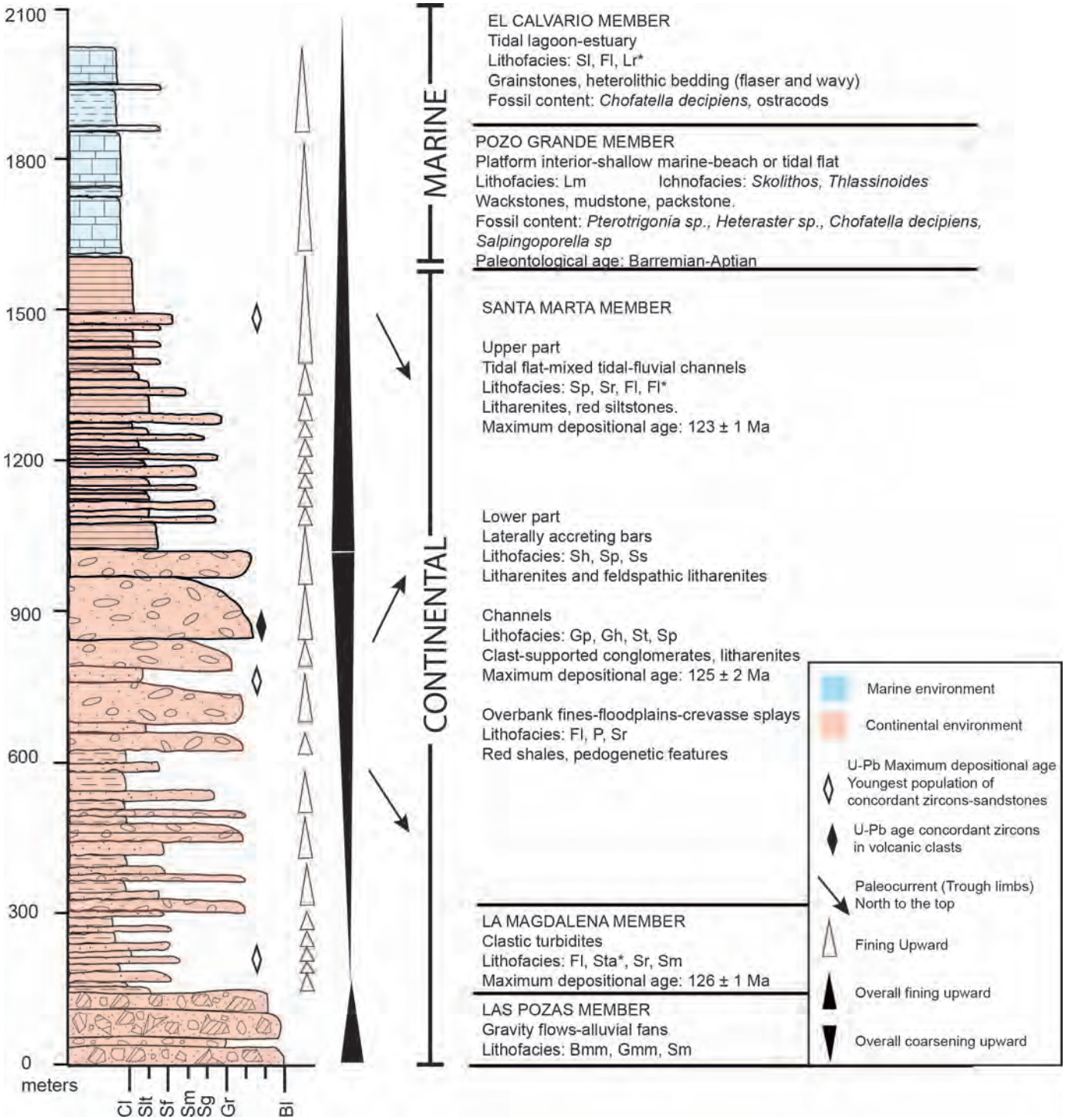

FIG. 3.—Generalized stratigraphic section of the Atzompa Formation, Pozo Grande arroyo shows lithological and sedimentological trends. Arrows show the paleocurrents of the axial channel belts; diamonds show the location of samples for geochronological analysis. The interpretation of the sedimentary environment is from the lithofacies analysis (Tables 1, 2). Detailed sections from each member of Atzompa Formation are in Appendix B.

Grande Arroyo (Appendix A). The entire section was measured at a scale of 1:100 using Jacob's Staff and the Abney level and described according to textural and lithological parameters (grain size, contacts, bed geometry, fossil content, and sedimentary structures). We collected paleocurrent data in trough cross-bed limbs of the Santa Marta Member using the methodology of DeCelles et al. (1983). Fifteen sandstone samples were collected along the section in prominent siliciclastic beds. Point-count analysis was made according to the Gazzi-Dickinson method (Ingersoll et al. 1984) with 400 framework grains counted for each thin section. Thin sections were half stained with sodium cobaltinitrite to readily identify K-feldspar. Six samples of medium-grained sandstone were selected for modal analysis to interpret provenance relations (e.g., Dickinson 1985). Criteria used for distinguishing

TABLE 1.—*Lithofacies codes and interpretation. Adapted from Miall (2006), Walker (1992), and Posamentier and Walker (2006).*

Lithofacies Code	Grain Size	Sedimentary Structures	Interpretation
Bmm	Cobbles and angular blocks	Massive breccias, matrix supported, no grading	Gravity flows, alluvial fan, debris flows
Gmm	Cobbles and blocks	Massive, matrix supported, imbrication	Deposits of hyperconcentrated flows
Gh	Pebbles and cobbles	Horizontal crossbeds, imbrication. Lenticular geometry	Lag deposits, longitudinal bars, sieve deposits
Gp	Pebbles and cobbles	Normal grading, planar cross-beds, lenticular geometry	Transverse bars, deltaic bars from remanent bars
St	Fine to very coarse sand	Normal grading, solitary or grouped trough crossbeds	3D dunes in fluvial to tidal environments
Sp	Fine to very coarse sand	Planar crossbeds	2D dunes, lower flow regime in fluvial to tidal environments
Sm	Fine to coarse sand	Massive lamination. Structureless sandstone	Gravity-flow deposits
Sh	Sand, very fine to very coarse, locally pebbly	Horizontal lamination, parting lineation	Plane-bed flow, upper-flow-regime deposition
Sr	Sand very fine to coarse	Ripple marks and ripples, cross-beds of all types	Lower flow regime in fluvial or tidal environments
STa*	Sand very fine to fine	Erosional, normal grading, ripple planar crossbeds	Beds deposited by traction
Slm*	Sand fine to calcareous sandstones	Massive, fossils and fossil fragments	Tidal flat to backshore, beach
P	Siltstones, mudstones, with carbonate	Massive to laminated, pedogenic features as carbonate nodules, some rootlets	Seat earth, paleosols of arid climates
Fl	Mudstone and siltstone	Thin lamination and very small ripples	Overbank or waning flood deposits
Fl*	Sand very fine, siltstone, and mudstone	Crossbeds, ripples, bioturbation (*Skolithos*)	Tidal flat
Lm	Grainstone–wackestone	Tabular limestone beds, fossils (bivalves, gastropods, echinoderms)	Inner platforms, carbonate ramp
Lr*	Wackestone–grainstone	Discontinuous wavy to crinkled laminae thinner than 5 cm, lenticular geometry, ostracods and gastropods	Tidal to estuarine

* Lithofacies code from this work.

lithic types, matrix types, and other components are those of Dickinson (1970) and Ingersoll and Suczek (1979). Recalculated petrographic modal data are presented in Table 3.

One to two hundred clasts were counted in selected cobble-conglomerate beds along the section; the clasts in a selected area were counted at each intersection point of a 5 cm × 5 cm grid. In addition to lithological clast composition, we noted textural parameters including roundness, angularity, shape, and size of the maximum diameter. In order to further define sediment sources, three sandstone samples and one sample of conglomerate clasts were collected for detrital-zircon U-Pb geochronology (Figs. 2, 3; Appendix B). One of the samples (MIS164b) belongs to the Magdalena Member and two (MIS166 and MIS163b) to the Santa Marta Member. For information about methods and data for U-Pb geochronology, see Appendix C.

STRATIGRAPHY AND SEDIMENTOLOGY OF THE ATZOMPA FORMATION

The Atzompa Formation is a thick succession of red beds composed of breccia, conglomerate, sandstone, and siltstone overlain by carbonate strata with Early Cretaceous fauna that crops out near San Juan Atzompa, in the Sierra de Tentzo (Fig. 2). The Atzompa Formation overlies the northernmost exposures of the extensive Acatlán Complex in the Sierra de Tentzo southeast of the city of Puebla. It was deposited on Paleozoic metasedimentary and igneous rocks of the Acatlán Complex that constitute the basement of the Mixteca terrane (Fig. 1). The minimum thickness of the formation at the type locality is 1990 m. The basal contact of the Atzompa Formation at the type locality is an angular unconformity with the Acatlán Complex, but elsewhere along the Mountain range it is a fault contact. The upper contact is transitional with the informal El Tentzo formation. The Atzompa Formation is herein divided into five members: Las Pozas, La Magdalena, Santa Marta, Pozo Grande, and El Calvario (Fig. 3). The formal stratigraphic definition, stratotype, and lithostratigraphic details are in Appendices A and B.

In order to interpret sedimentary environments, we defined 17 lithofacies (Table 1) and 8 lithofacies associations (Table 2) in the Atzompa Formation (Appendix B). This allowed us to distinguish alluvial, lacustrine, fluvial, shoreline, and tidal environments. The sedimentary facies were defined in relation to their contacts, lithology, and stratal geometry, as well as primary and secondary structures. The resulting architectural elements were defined according to Miall (1996) and Walker (1992) for fluvial deposits and by reference to Posamentier and Walker (2006) for the deposits of turbidity currents. On the basis of the facies associations, we define five main depositional environments, each one represented by one or more lithofacies associations. The resulting environmental interpretations demonstrate a transition from continental to marine settings from the base to top in the Atzompa Formation.

Las Pozas Member

The lowermost strata of the Atzompa Formation are assigned to the Las Pozas Member. The basal contact of the member is nonconformable upon schists and phyllites of the Acatlán Complex. To the west and east of the type locality, the contact of the Atzompa Formation and the basement rocks is a thrust fault (Fig. 2). Las Pozas Member is composed of 80 m of schist-clast breccia composed of boulders ~ 0.25 to 1.7 m in diameter (Fig. 4; Appendix B). The breccia is matrix-supported and occurs in beds of about 10 m in thickness (facies Bmm). It is interbedded with clast-supported reddish conglomerate 1 to 3 m thick, with crude bedding, and is overlain by tabular cross-stratified conglomerate beds interbedded with some massive sandstone intervals (facies Gmm and Sm).

The characteristics of these deposits indicate deposition by sediment gravity flows succeeded by ephemeral flow in shallow channels indicated by discontinuous layers of poorly sorted conglomerates interbedded with planar-bedded sandstones. These facies associations are characteristic of proximal alluvial fans dominated by fluid gravity flows (Blair and McPherson 1994); furthermore they indicate retrogradation of the fan recorded in the basal part of the section. These are source-proximal deposits typically related to nearby fault displacement. Clasts include chlorite schist (80%), milky quartz (10%), quartzite (5%), biotite-rich gneiss (2%), limestone (2%), and hematitic

TABLE 2.—*Lithofacies associations and interpretation of depositional environments for the members of the Atzompa Formation, Tentzo basin.*

Facies Association	Architectural Element	Description	Environmental Interpretation	Member
FA1	Gravity flow (SG)	Bmm, Gmm, Sm	Gravity-flow deposits near the source. Possible fault-associated deposits.	Las Pozas Lower Santa Marta
FA2	Clastic Turbidites (CT)	Tabular beds from 5 to 20 cm of sandstones with erosional base interbedded with siltstone with planar lamination. Fl, STa*, Sr, Sm	Turbidity-current deposits	La Magdalena
FA3	Channels (CH)	Lenticular; concave-up erosional base. scale varies from centimeters to meters. Gmm, Gh, Gp, St, Sp, Sm, and Sr	Channel-fill deposits	Lower Santa Marta
FA4	Overbank fines (OF)	Thin to thick blankets; tabular geometry. Locally associated with pedogenic features. Sr, Fl, P	Overbank deposits	Lower Santa Marta
FA5	Laterally accreting bars (LA)	Tabular beds of mature with parallel bedding. May contain parting lineation and tabular lamination. Sh, Sp, Ss	Plane-bed flows with increasing energy up-section	Lower Santa Marta
FA6	Tidal flat (TF)	Heterolithic inclined beds; common bioturbation, oscillation ripples. Fl*, Fl, Sp, Sr, Sh, Sl*, Lr*	Tidal flat	Upper Santa Marta Pozo Grande
FA7	Platform interior (IP*)	Tabular to wedge-shaped (limestone) beds from 1–1.5 m thickness, basal surfaces sharp. Lm, Lb*, Fl Fl*, Sl*	Platform-interior carbonate deposits	Pozo Grande
FA8	Tidal lagoon–estuary (TL*)	Lenticular beds. Heterolithic bedding (flaser and wavy). Sl, Fl, Lr*	Platform-interior carbonate deposits	El Calvario

* Lithofacies code from this work.

claystone (1%), all consistent with derivation from nearby metamorphic basement and overlying limestone strata of the Mixteca terrane (or Acatlán).

La Magdalena Member

The La Madgalena Member overlies the Las Pozas breccias on a sharp contact with a total minimum thickness of 197 m. This member is made of rhythmic bedding and interbedding of tabular beds from 5 to 20 cm of sandstones and siltstones with planar lamination (Facies Fl, STa*, Sr, and Sm) characteristic of clastic turbidites. The fine-grained sandstone beds show an erosional base, normal grading, as well as current ripples; the siltstones present plane-parallel lamination (Appendix B).

Facies of the La Madgdalena Member represent incomplete Bouma sequences (Ta, Tc, Td) deposited by turbidity currents. The absence of pelitic layers or carbonate rocks, as well as the absence of marine fossils, together with the facies association and the restricted lateral distribution of this unit, suggests a lacustrine environment for the development of the La Magdalena Member turbidites.

Santa Marta Member

This member, with a total thickness of 1260 m, gradationally overlies the La Magdalena Member; this contact lies at the base of a greenish-red clast-supported conglomerate bed (Appendix B). Cyclically distributed along the lower part of Santa Marta Member there are several finning-

TABLE 3.—*Recalculated modal point count data for Atzompa Formation, Tentzo basin.*

	QtFL%			QmFLt%			QpLvmLsm%			LmLvLs%		
	Qt	F	L	Qm	F	Lt	Qp	Lvm	Lsm	Lm	Lv	Ls
Santa Marta Member, Shallow marine facies												
MIS163B	45	31	24	26	31	42	43	43	14	20	65	15
Santa Marta Member, Continental facies												
MIS163C	45	11	44	33	11	56	22	19	59	45	23	32
MIS163D	52	10	38	38	10	51	26	27	47	26	35	39
MIS169A	19	6	74	8	6	85	13	44	43	33	50	17
MIS169B	31	23	46	21	23	56	19	28	54	59	32	9
La Magdalena Member												
MIS164	17	17	66	11	17	73	9	17	74	74	17	8

FIG. 4.—Outcrop photos of Atzompa Formation. **A)** Large block of chlorite schist in basal breccia of Las Pozas member. **B)** Cross-bedded conglomerate with normal grading. **C)** Channel conglomerates 8–20 m thick in Santa Marta member; this facies correlates with alluvial-fan facies west of the Pozo Grande section. **D)** Calcite nodules in a layer of red siltstone, Overbank facies. **E)** Silicified wood in massive sandstone bed. **F)** 15 cm sets of crossbeds in sandstones.

upward facies associations, characterized by conglomerates with scoured bases (Gh and Gp) in a transitional contact with coarse-grained immature conglomerates and sandstones with trough and planar cross-beds (Facies St, Sp). Massive reddish siltstones and claystones with pedogenic features such as micrite nodules (Facies P and Fl) are interbedded with thin lenticular beds of fine-grained sandstones with ripple marks (Facies Sr). Compositionally mature sandstone with tabular geometry and tabular cross-beds (Fig. 4F) usually alternate with flat-bedded sandstones with parting lineation and tabular lamination (Facies Sh, Sp, and Ss). Paleocurrents were measured in medium-grained sandstones with trough cross-bedding in the channel lithofacies association of the Santa Marta Member. The dominant structurally corrected directions are to the south, southeast, and northeast (Fig. 3; Appendix B).

The association described indicates fluvial channels (Fig. 4B, C) with vertical accretion in a stable floodplain with some crevasse-splay deposits (Fig. 4D); the pedogenic features in the overbank fines indicate an arid climate. The presence of intercalated mature sandstone facies with planar-bed flows indicates an increase in energy up-section over laterally accreting bars in a mixed-load river system. The low sinuosity of the channels can be assumed by the stable paleocurrent directions that indicate channels flowing from the NW or SW to the east in a WNW–SE-trending basin.

The upper part of the Santa Marta Member is dominated by sandstone beds with tabular cross-bedding (Facies Sp) and erosional bases, usually intercalated with red siltstones with plant impressions and silicified wood (Fig. 4E). These heterolithic inclined beds present ichnofacies and galleries of invertebrates as well as oscillation ripples in calcareous sandstones and flaser stratification (facies Sr, Fl, and Fl*), all of which are common in a tidal-flat setting.

This facies association records deposition in mixed tidal and fluvial channels in the transition between fluvial and estuarine environments. In the heterolithic bedding and flaser stratification the proportion of sand/mud is controlled by the dominance of the fluvial or the tidal system (Sisulak and Dashtgard 2012). The presence of small channels with intraclast conglomerates also indicates highly erosional and starved conditions for the depositional system. Common oscillation ripples and flaser stratification support the interpretation of tidal influence in this part of the section (Fig. 5).

Pozo Grande Member

This member overlies the Santa Marta Member on a sharp contact (Appendix B), and comprises 205 m of interbedded mudstone and wackestone. Calcareous mudstones and wackestones with Trigonia, oyster, gastropod, and echinoderm fossils (Facies Lm), as well as the development of bioherms associated with *Skolithos* and *Thalassinoides* Ichnofacies, are characteristics of the basal Pozo Grande Member (Fig. 5D, E).

These lithofacies and biofacies associations indicate a shallow-marine depositional environment such as beach or tidal flat with a sandy bottom (MacEachern et al. 2005). Fossils recovered from the member include *Pterotrigonia* sp. (with a wide chronostratigraphic range in the Cretaceous) and *Heteraster* sp., which indicates a Late Barremian to Aptian age (A.B. Villaseñor, written communication, 2013); this information together with the micropaleontological content of benthonic foraminifera *Chofatella decipiens* and *Salpingoporella* sp. algae confirm the Barremian to early Aptian age for the Pozo Grande Member.

El Calvario Member

The uppermost member of the Atzompa Formation is 303 m thick and overlies the Pozo Grande Member on a gradational contact (Appendix B). It consists of light green claystone, normally graded grainstone with bivalve fragments, and interbedded mudstone with ostracods. Some grainstone beds have discontinuous wavy to crinkled laminations thinner than 5 cm formed by mud drapes or siliciclastic red silt surrounding mudstones. The contact of the Atzompa Formation with the overlying "basinal carbonates" (Monroy-Fernandez and Sosa-Patron 1984) or the Tentzo Formation (Zepeda-Martinez 2013) is a sharp boundary marked by the lowermost occurrence of wackestone with scattered fragments of oysters and gastropods in a micritic matrix rich in planktonic *Globigerina* sp.

The alternation of grainstones and mudstones in wavy bedding indicates deposition in tidal flats where episodic tidal currents are separated by calm waters (Demicco and Hardie 1994). Also the presence of ostracods, abundant in grainstones, is an indicator of brackish waters, consistent with an estuarine or lagoonal environment.

PROVENANCE OF THE SEDIMENTS OF THE ATZOMPA FORMATION

Sandstone Petrology

Atzompa sandstones are litharenites and feldspathic litharenites (Folk 1974) composed of subangular to subrounded grains. The framework grains (Table 3) include monocrystalline and polycrystalline quartz, plagioclase, potassium feldspar, and a wide variety of polycrystalline lithic fragments, which range in QtFL abundance from 24 to 74% (Fig. 6). Polycrystalline quartz is represented by grains with crystallographic orientation and chert as a common component. Sedimentary lithic fragments represent 8 to 39% of the lithic population and include limestone, argillite, and siltstone; sedimentary grains generally decrease in abundance upsection (Table 3). Metamorphic lithic fragments, which range from 20 to 74% of the unstable lithic fraction, are represented by quartz-mica tectonites, foliated quartz aggregates, and microgranular quartz aggregates, and generally increases in abundance upsection. Volcanic lithic grains range from 17 to 65% of the lithic content and include a diverse population of felsitic, microlitic, and lathwork grains that are abundant near the base of the formation and display a moderate decrease upsection. Zircon, magnetite, hematite, and titanite are common accessory grains.

The sandstones of the La Magdalena Member classify as litharenites with a low abundance of feldspar (16%), a low quantity of volcanic fragments (12%), and very high amounts of metasedimentary fragments (46%). The metasedimentary rocks are almost exclusively schists and phyllites. Sandstones of the La Magdalena Member plot in the undissected, transitional, and dissected-arc provenance fields in the QmFL, QtFL, and QLvmLsm diagrams (Fig. 6).

The sandstones of the Santa Marta Member are litharenites and feldspar litarenites. These rocks are characterized by a very low abundance of feldspar (2 to 4%), a medium quantity of volcanic fragments (10 to 15%), and high amounts of monocrystalline quartz (20 to 38%) and metasedimentary fragments (18 to 25%). An outlier of this group is the sample MIS169A, located in the sandstones interbedded with the major conglomerates with high amounts of volcanic clasts; this sample has very low amounts of monocrystalline quartz (8%) and a very high amount of volcanic fragments (37%). The volcanic fragments are intermediate to felsitic. The metasedimentary fragments are almost exclusively schists and phyllites. The sandstones from the upper Santa Marta member plot in the undissected, transitional, and dissected arc provenance fields in the QmFL, QtFL, and QLvmLsm diagrams. The sandstones from the upper Santa Marta member plot in the recycled orogen field of the QtFL diagram (Fig. 6A). In the QmFLt diagram (Fig. 6B) the samples are distributed in the transitional recycled and lithic recycled provenance fields, with two samples from the Santa Marta Member in the arc field.

Conglomerate Clasts Counts

In order to compare the sediment sources in the conglomeratic beds of the Las Pozas and Santa Marta members, we analyzed composition and textural parameters of cobble-conglomerate clasts. We counted 5 beds in

FIG. 5.—Outcrop photos of Atzompa Formation. **A)** Ripple marks in overturned fine-grained sandstone bed, upper part of Santa Marta Member. **B)** Overturned heterolithic inclined beds of greenish sandstones and claystones, upper part of Santa Marta Member. **C)** Siltstone intraclast conglomerate. **D)** Wackestone beds with *Thalassinoides* burrows in oyster and gastropod carbonate mudstone, Pozo Grande Member. **E)** *Trigonia* bivalve in Pozo Grande Member. **F)** Oysters in boundstone, Pozo Grande Member.

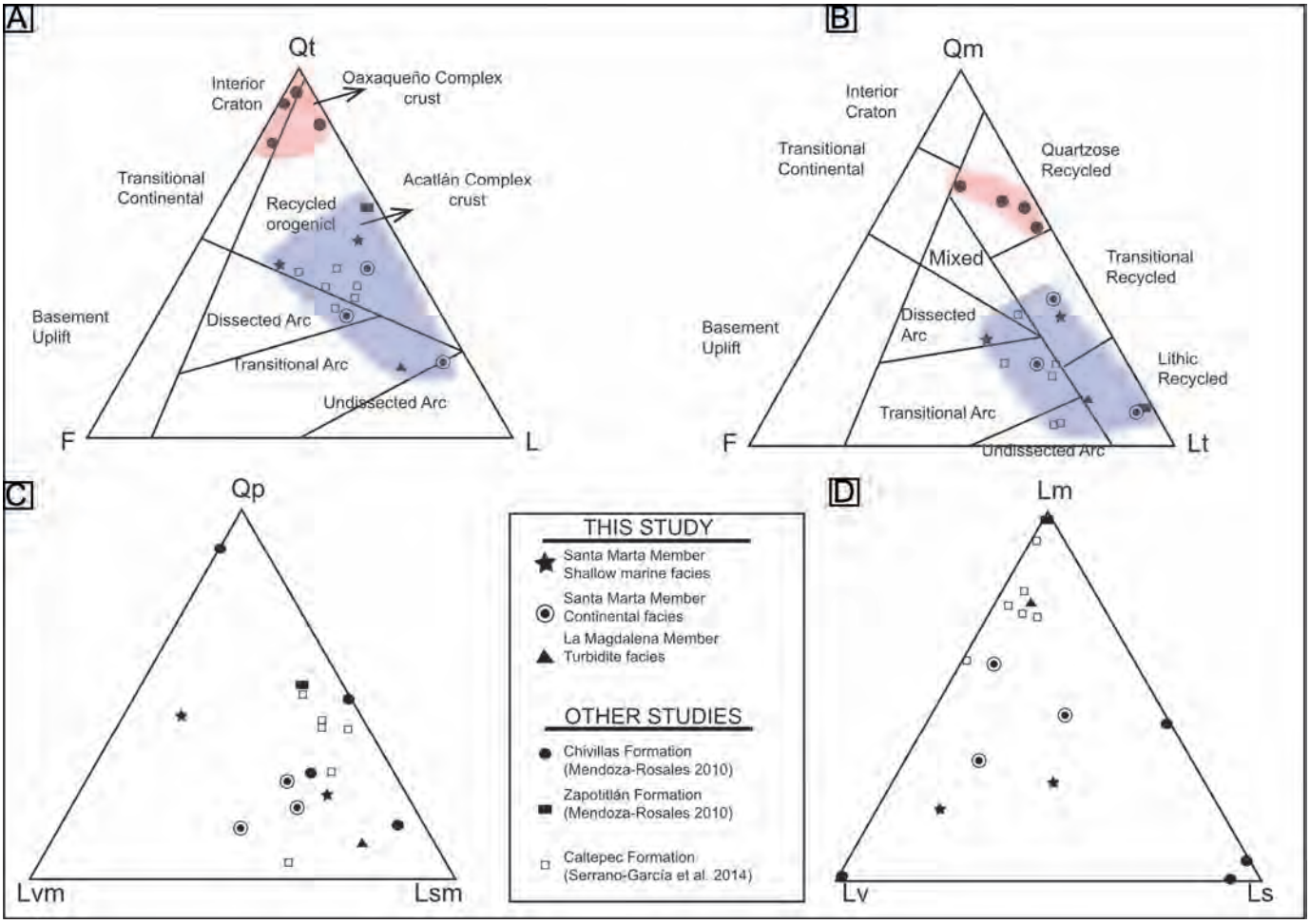

FIG. 6.—Ternary compositional plots for detrital modes of sandstones from Atzompa Formation and correlative units (Zapotitlán, Chivillas, and Caltepec formations). Data are listed in Table 3. **A)** QtFL plot (L = Lvm + Lsm). Provenance fields from Dickinson (1985). **B)** QmFlt plot (Lt = L + Qp). Provenance fields from Dickinson et al. (1983). **C)** QpLvmLsm plot. **D)** LmLvLs plot. Zapotitlán and Chivillas sample modes are from Mendoza-Rosales (2010), Caltepec Formation detrital modes are from Serrano-García et al. (2014).

the Las Pozas Member and 10 beds in lower Santa Marta Member. The conglomerates measured in the Las Pozas Member are in the upper part and consist mainly of metamorphic clasts (74 to 98%), some sedimentary (9 to 18%) and scarce volcanic clasts (3 to 9%). Metamorphic (38–68%) and sedimentary sources (2 to 27%) are still present in the Santa Marta Member; however, the incorporation of volcanic sources (21 to 61%) is remarkable.

Detrital-Zircon Geochronology

All the samples collected in the Atzompa Formation reveal zircon populations with wide age distributions from Archean to Early Cretaceous (Appendices C, D). The stratigraphically lowest geochronologic sample (MIS164b, n = 88) from the Atzompa Formation is a medium-grained litharenite collected in the La Magdalena Member. Pre-Mesozoic zircon age populations include an Archean to Mesoproterozoic population with an age range of 2968 to 1015 Ma (27%), a dominant Neoproterozoic to Cambrian population with a range of 939 to 486 Ma (42% of the grains) and subordinate populations of Ordovician to Silurian grains with an age range of 474 to 448 Ma (6%), and Carboniferous grains ranging in age from 347 to 328 Ma (2%). The youngest population is Early Cretaceous, with a range of concordant Valanginian to Albian ages centered at ~ 129–125 Ma (23%) indicating a maximum depositional age of 126 ± 1 Ma (MSWD = 1.02, n = 11). This sample lacks Permian to Jurassic zircon grains (Fig. 7).

A sample from the lower Santa Marta Member (MIS166, n = 95) contains Archean and Paleoproterozoic zircons ranging ~ 3000 to 2735 Ma (2%), a dominant Mesoproterozoic (~ 1600 to 940 Ma) zircon population (43%), Neoproterozoic to Cambrian grain ages of ~ 900 to 551 Ma (16%), subordinate Ordovician zircon grains at ~ 469 to 452 Ma (4%), and a Permian to Triassic population at ~ 296 to 234 Ma (9%). In contrast to the La Magdalena Member, the sandstones of the Santa Marta Member have a robust population of Early to Middle Jurassic zircons (10%) and a subordinate Late Jurassic population (3%). The youngest population ranges from Valanginian to early Aptian at ~ 138 to 127 Ma (13%) with a maximum depositional age of 129 ± 1 Ma (MSWD = 0.65, n = 5) (Fig. 7).

A sample near the top of the Santa Marta Member (MIS163, n = 96) has age populations similar to those of the lower sample. A Paleoproterozoic to Mesoproterozoic population ranging ~ 1920 to 944 (32%) dominates over the subordinate Neoproterozoic to Ordovician zircon population with and age range between 772 and 463 Ma (8%) and the Permian population (5%). There are only two Jurassic zircons, in contrast to a dominant Early Cretaceous population that ranges from Berriasian to Aptian (55%) and

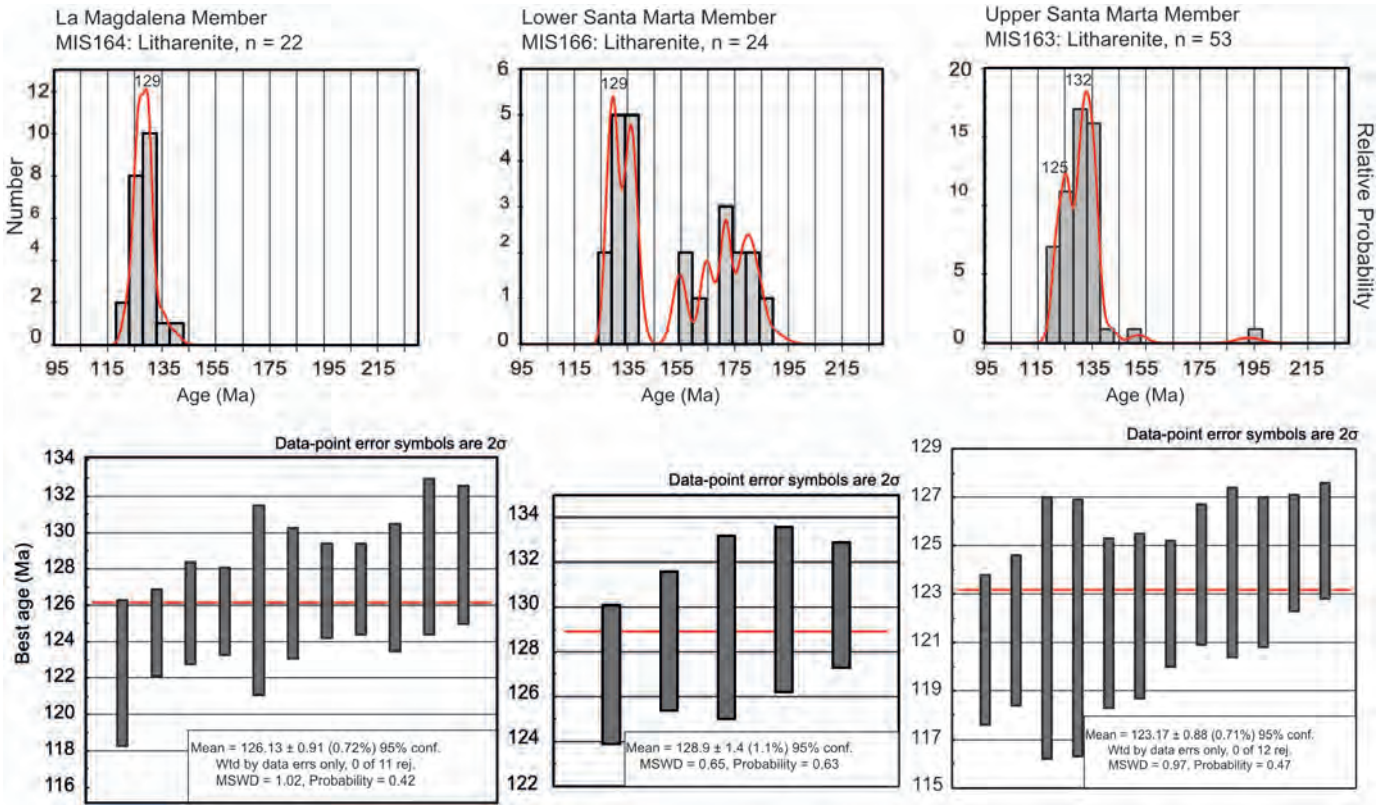

FIG. 7.—**A)** Probability density plots for detrital zircons of Mesozoic populations in sandstone samples MIS164, MIS166, and MIS163. Histogram bins are 5 Ma. Numbers indicate the approximate ages of the relative maximum of the probability function. **B)** Maximum depositional ages calculated as the weighted mean of the youngest population in each sample.

indicates a maximum depositional age of 123 ± 1 Ma (MSWD = 0.97, n = 12) (Fig. 7).

Volcanic clasts present in alluvial-fan breccias of the Santa Marta Member (MIS136) were also dated in order to interpret the maximum depositional age of sandstones (Fig. 8). Zircon grains obtained from 50 volcanic clasts (andesites, dacites, and a few basalts) of a conglomerate of the Santa Marta Member (MIS136, n = 30) constitute a population that ranges from latest Jurassic to Early Cretaceous age (~ 147 to 122 Ma) with a maximum depositional age of 125 ± 2 Ma (MSWD = 1.1, n = 6).

DISCUSSION

The Tentzo Extensional Basin: Depositional Style

Interpretation of the architectural elements observed in the Atzompa Formation indicates that a clear transition from proximal alluvial fans to a lacustrine depositional system took place in the Early Cretaceous in the Mixteca area. The size of the boulders in the basal breccias and the rapid transition from alluvial fan to deep lake with development of density currents suggests deposition in a fault-controlled basin. Alluvial-fan deposits in the basal member provide evidence of active faulting (e.g., Blair and McPherson 1994), as do the rapid subsidence rates implied by lake deposits (e.g., Gawthorpe and Leeder 2000).

The breccias and lacustrine facies are transitionally followed by fluvial facies, whose style reflects the development of anastomosing rivers. Anastomosing rivers are characterized by variable discharge, frequent and widespread overbank flooding, and high sediment load (Rust and Legun 1983). They can be defined by two principal factors: being a multichannel river with evidence of avulsion and by these channels being separated by vegetated or stable floodplains (Rust and Legun 1983; Smith and Smith 1980; Sinha et al. 2005).

Some of the evidence for depositional style of anastomosing rivers in arid climates in the Lower Santa Marta member are: (1) Cyclicity of coarsening-up and fining-up sequences in a general upward decrease in energy observed in the lower Santa Marta Member. (2) The low-sinuosity channels represented by the uniform paleocurrents. (3) The development of lateral-accretion bars. (4) The presence of extensive overbank fines with fining-up tendency. (5) The pedogenetic features as evidence of long periods of subaerial exposure of floodplains. (6) The overbank-fines lithofacies associated with the laterally accreted bars lithofacies represents episodic seasonal discharge affecting stable floodplains.

These fluvial lithofacies are followed by heterolithic and flaser bedding with evidence of bidirectional flow, interbedded with calcarenites and calcareous muds of brackish waters. These transitions in lithofacies are typical of fluvial and tidal-flat transitions in river-dominated estuaries (Greb and Martino 2005), and are observed at the limit between the Santa Marta and Pozo Grande members.

Other than the paleocurrent data found in this work, there is no direct evidence for the orientation of the Tentzo basin, but a NW–SE trend is inferred from the following evidence: (1) The structural grain in the region is defined by NW–NNW-trending faults such as the Pozo Hondo, Caltepec, and Oaxaca faults. These faults control the exposures of basement rocks in the region. (2) A prominent broad WNW-trending low can be identified in the regional total-magnetic-field map of the region across southern Puebla state (Servicio Geológico Mexicano 2008). (3) Coarse basement-clast-bearing conglomerate facies deposited in alluvial fans that include the Atzompa Formation and correlative strata of the Agua de Cordero and La Compañía formations in southern Puebla (Mendoza-Rosales 2010) are

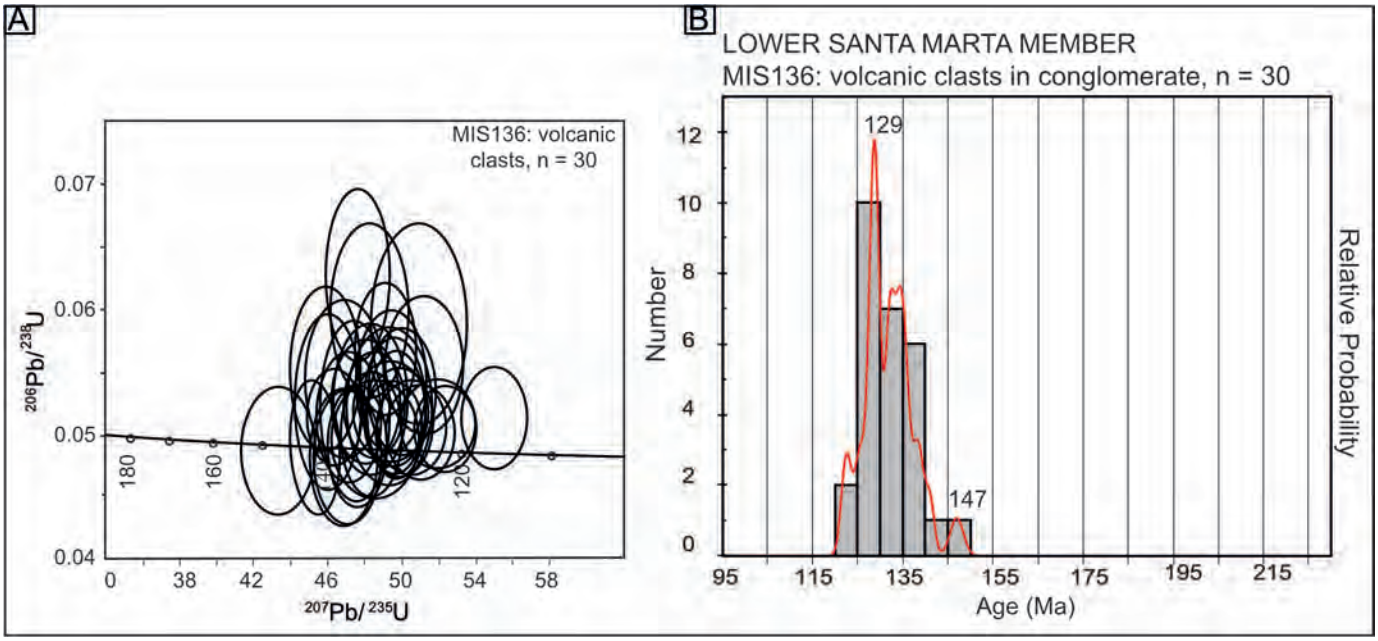

FIG. 8.—**A)** Wetherill U-Pb concordia diagram for zircon analysis of conglomerate volcanic clasts in alluvial-fan facies (sample MIS136), Atzompa Formation (data-point error ellipses are 2σ). **B)** Probability density plot of clast ages. Histogram bins are 5 Ma. Numbers indicate the approximate ages of the relative maximum of the probability function.

distributed along a NW-trending belt. An alternative view can be supported on the basis of correlation of the Atzompa Formation with the Zicapa Formation, for which exposures appear to be controlled by the NNE-trending Papalutla fault. However, on the basis of paleocurrents measured in the Atzompa Formation we prefer the interpretation of a WNW–SE-trending extensional basin.

Sandstone Provenance

The basement of the Atzompa Formation and the Mixteca terrane in general is composed of the poly-metamorphosed Acatlán Complex, which in its northern portion consists of greenschists and slates of the Cosoltepec Formation (Talavera-Mendoza et al. 2005). The sandstone composition of the La Magdalena Member reflects the composition of the basement affected by faulting, and also the superficial volcanic processes during deposition of the early stages of the Atzompa Formation. Pre-Cretaceous rocks involved in the faulting consist mostly of Paleozoic schist and phyllite, Permian intrusive rocks, and Jurassic migmatites and volcanic arc rocks. This assemblage is not the typical crust of cratonic basement uplift models, characteristic of continental rifts in the tectonic interpretation of ternary diagrams (Dickinson and Suczek 1979; Dickinson 1985). Litharenites in the Atzompa Formation are deficient in feldspar and volcaniclastic lithic fragments and enriched in metamorphic lithic fragments.

Some correlative units in the Zapotitlán Basin are the sandstones from the Caltepec and Zapotitlán formations, which despite their deposition in different environments than the Atzompa Formation, all of them are located over the Acatlán Complex. Otherwise, the Chivillas Formation was deposited in the Cuicateco Basin, and shows a different cluster in the QtFL and QmFLt diagrams (Fig. 6A, B), reflecting the different composition of the local source; this source corresponds to the Oaxaqueño Complex. The LmLvLs diagram (Fig. 6D) indicates that the basal units of the Atzompa Formation are similar in composition to samples of the Caltepec Formation, which also constitutes alluvial-fan deposits in an extensional environment (Serrano-García et al. 2014).

The Archean to Paleoproterozoic zircon ages in the Mixteca terrane are restricted to metasedimentary rocks of the Cosoltepec Formation of the Acatlán Complex (e.g., sample ACA55 from Talavera-Mendoza et al. 2005). Although the Mesoproterozoic age populations (1600 to 900 Ma), like those present in all samples of the Atzompa Formation, are generally attributed to Grenvillian sources in the Oaxaquia gneisses (Keppie et al. 2003), they could also be derived from metasedimentary units of the Acatlán Complex. Neoproterozoic to Cambrian age populations have been observed in the Acatlán Complex, mainly in rocks of the Cosoltepec, Magdalena, and Chazumba formations (Talavera-Mendoza et al. 2005). These units are thus a likely source of zircon populations of this age range in the Atzompa Formation. Small populations of Ordovician to Silurian zircons are present in all of the samples, and were most likely derived from megacrystic granitoids in the Acatlán Complex (Middleton et al. 2007) or recycled from the metasedimentary rocks of the Ayú Complex, located in the southeastern margin of the Mixteca terrane (Helbig et al. 2012).

Permian to Jurassic zircon ages are present only in samples of the Santa Marta Member, and were possibly sourced from either Permo-Triassic arc rocks represented in south-central Mexico by the Permian Totoltepec pluton or from clastic rocks of the Tecomate Formation; both units are located in the eastern part of the Acatlán Complex (Kirsch et al. 2013). The Jurassic zircons were likely derived from the Nazas Arc, with an age range of about 200 to 165 Ma, which extended the length of mainland Mexico in Early to Middle Jurassic time (Bartolini et al. 2003; Lawton and Molina-Garza 2014). Intermediate volcanic rocks attributed to the Nazas arc in south-central Mexico are not reported; only local units are located west and south of the study area (e.g., Las Lluvias Ignimbrite and Diquiyú Unit; Fig. 9). Sierra-Rojas et al. (2015), however, reported Jurassic ages for andesitic to dacitic clasts in conglomerates from the Caltepec Formation in the Zapotitlán basin. This indicates the presence of local volcanic rocks of this age in the Mixteca terrane, and a potential source of Jurassic zircons. Another possible source for the Jurassic zircons includes the migmatites of the Ayú Complex, with ages from Lower to Middle Jurassic (Helbig et al. 2012).

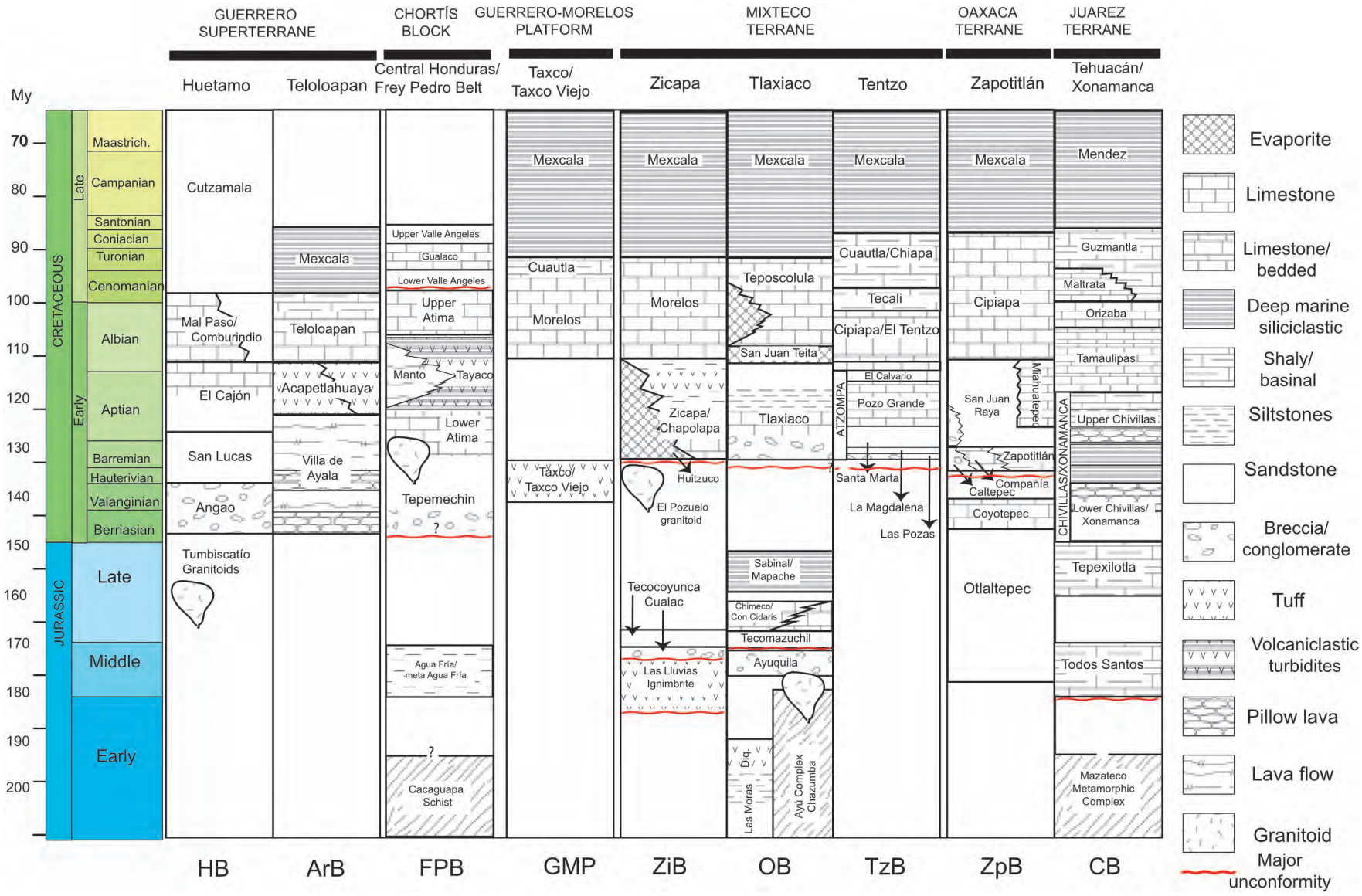

FIG. 9.—Southwest (left) to east (right) correlation of Mesozoic units in southern Mexico. The stratigraphic columns for each region are generalized from several authors. Guerrero superterrane (Centeno-García et al. 2008); Chortís Block (Rogers et al. 2007a); Guerrero–Morelos Platform (Hernández-Romano et al.1997; Campa et al. 2012); Mixteco Terrane–Zicapa basin (Sierra-Rojas and Molina-Garza 2014), Tlaxiaco (López-Ticha 1985; Helbig et al. 2012), Tentzo and Huajuapan (Monroy-Fernández and Sosa-Patrón 1984; Zepeda-Martinez 2013; this work), Zapotitlán (Mendoza-Rosales 2010) and Tehuacán and Xonamanca (Angeles-Moreno 2006; Mendoza-Rosales et al. 2010). Location of stratigraphic sections indicated by basins in Figure 1.

Zircons from large volcanic clasts in conglomerate of the Santa Marta Member constitute a latest Jurassic to Early Cretaceous age population (Fig. 9). Taking into account that the corresponding alluvial-fan facies indicates a local source of sediment, episodic events, and short transport distances, we interpret these facies with a maximum depositional age of ∼ 125 Ma to indicate that the volcanic clasts in the alluvial fans could be derived from a source of the same age as the youngest zircons in the sandstones. The volcanic grains in the sandstones of the Atzompa formation change from lathwork in La Magdalena petrofacies (14%) to microlithic, felsitic, and very rare lathwork in lower Santa Marta (6–10%, 3–5%, 1–0% respectively) and upper Santa Marta petrofacies (25%, 12%, 0% respectively) showing a shift in the source of volcanic fragments from mafic in the early deposition of turbidites in lacustrine environments to intermediate to felsitic sources in the fluvial to tidal environments. It is important to consider that the lithofacies in the lower members of the Atzompa Formation (Las Pozas and La Magdalena members) indicate a local source of sediments, and the fluvial Santa Marta Member may have more extensive and mixed sources. The volcanic-clast conglomerates in alluvial fans, the volcanic-derived sandstones, and the dominant younger populations of zircon grains with low evidence of transport and abrasion in the sandstones suggest that magmatism was closely contemporaneous with deposition.

The youngest age populations of all the samples of the Atzompa Formation indicate that the formation was deposited entirely in Early Cretaceous (> 126 to ∼ 123 Ma), with maximum depositional ages at ca. 126 Ma in the Magdalena Member to ca. 123 Ma in Upper Santa Marta Member. Detrital-zircon geochronology thus indicates that the Atzompa Formation is late Barremian to Aptian, or younger, according to the time scale of Gradstein et al. (2012).

Undecompacted Depositional Rate

The maximum depositional ages of the lower part of the La Magdalena Member (∼ 127 Ma) and the age of the top of Santa Marta Member (∼ 123 Ma) are consistent with the paleontological age of the boundary between Santa Marta and Pozo Grande members. Based upon the stratigraphic thickness between the sample from the La Magdalena Member (Fig. 3; Appendix B) and the position of the sample in the upper Santa Marta Member, we calculate an undecompacted accumulation rate for those siliciclastic members of the Atzompa Formation. The minimum thickness of 1440 m was deposited in ∼ 4 My, and yields a maximum undecompacted sedimentation rate of 3.6 mm/yr. Even if the error in the rate is considered, given that the ages are not absolute, we consider that it is an important first-order approximation to the accumulation rate; this estimate is necessary for the subsidence analysis of the basin.

We have calculated an accumulation rate in a long time span, which must be more complete than those measured in shorter timespans (Sadler 1981). Considering the stratigraphic completeness, we notice that in the 1400 meters of thickness considered for the sedimentation rate calculation there were no considerable surfaces or faults that may have reduced (or increased) the real thickness of the section. The times of nondeposition, if present, were not considered. In that case, the undecompacted sedimentation rate of 3.6 mm/yr that we calculated is a maximum sedimentation rate.

Tectonic Significance of the Tentzo Basin

Several authors have recognized different phases in the evolution of rift basins (Lambiase and Bosworth 1995; Nottvedt et al. 1995; Prosser 1993), in which an initial stage of rift initiation with low subsidence rate is followed by a stage of maximum displacement (rift climax), and a final stage in which active tectonism ceases and subsidence rate slows (post-rift stage). Rifts have been analyzed from the point of view of regional-scale structural features or local stratigraphic patterns, but regional-scale deformation strongly influences local stratigraphy.

The stratigraphic features of the Atzompa Formation, which overall fines upsection, include an assemblage of alluvial-fan to deep-lake deposits which evolved to anabranching rivers with a high depositional rate, followed by accumulation of terrigenous deposits in starved tide-influenced environments. Two dramatic stratigraphic transitions are observed in the Atzompa Formation. The first is the abrupt deepening of the basin recorded by the transition from alluvial and fluvial deposits to lacustrine turbidites between the Las Pozas and La Magdalena members. The second is the change from anabranching-river deposits to terrigenous platform and carbonate environments at the contact between the Santa Marta and Pozo Grande Members. We interpret the first change as the transition from "rift initiation" to "rift climax" observed in many continental rift basins (Gupta et al. 1998; Lambiase and Bosworth 1995; Prosser 1993), implying an association of basin deepening with the development of fault-controlled depocenters. The second change is interpreted as a decrease in the subsidence rate and accommodation-space creation, recorded by a decrease in terrigenous sedimentation rate and the starvation of the basin.

The very high rates of sedimentation (3.6 mm/yr) measured from the La Magdalena Member to upper the Santa Marta Member could be related to the total subsidence in the basin, representing a high rate with creation of accommodation space during the deposition in deep lakes, and a decrease in the subsidence rate during the establishment of the anastomosing river system. The high sediment supply continued during the low subsidence period, favoring the rapid aggradation and vertical accretion of channels. In this case, the establishment of an anabranching fluvial system was not controlled by subsidence or base level changes, as indicated by Smith and Smith (1980). Considering the presence of pedogenetic features in the floodplains typical of arid conditions, it could be considered that the morphology and dynamics of the fluvial system was the one of a dryland river system (Tooth and Nanson 2004).

The extremely high sedimentation rate in the siliciclastic members of the Atzompa Formation is comparable to syn-extensional units near border-fault systems in narrow Triassic rift basins of eastern North America (e.g., Richmond Basin; Schlische and Anders 1996). Some modern analogs for similar high sedimentation rates are the Tyrrhenian rift in western Italy for which sedimentation rates are as great as 4.6 mm/yr (Millia and Torrente 2015) and the basin of the Magdalena River, in northwest Colombia, in tectonically active Andean intermontane basins (Smith 1986).

The contact with the basinal limestones that overlie the Atzompa Formation marks an abrupt facies change. Sedimentary environments changed from tidal platform in the Aptian El Calvario Member to slope facies in the Tentzo Formation, which consists of muddy calcareous debris flows and contains planktonic foraminifera. This abrupt deepening event is post early-Aptian in age. The change is not associated with an obvious unconformity, and it may be correlative with tectonic events to the west of the basin. Here we submit that abrupt deepening is the response of the basin to Aptian–Albian accretion of the Guerrero terrane to mainland Mexico, as documented in central Mexico (Martini et al. 2011).

Correlation between the Studied Section and Other Stratigraphic Units

Sedimentation in an extensional environment has been postulated to the southwest for the Zicapa Formation (Sierra-Rojas and Molina-Garza 2014) and in the basal formations of the Zapotitlán and Cuicateco basins (Mendoza-Rosales 2010). Lower Cretaceous strata, widespread in southern Mexico, record deposition in extensional environments coeval with calc-alkaline magmatism (Figs. 9, 10, 11). The strata record mixed-source provenance, including metamorphic basement rocks and volcanic rocks. Volcanic clasts in these units are of Jurassic and Early Cretaceous age (e.g., Caltepec Formation in the Zapotitlán basin; Fig. 9).

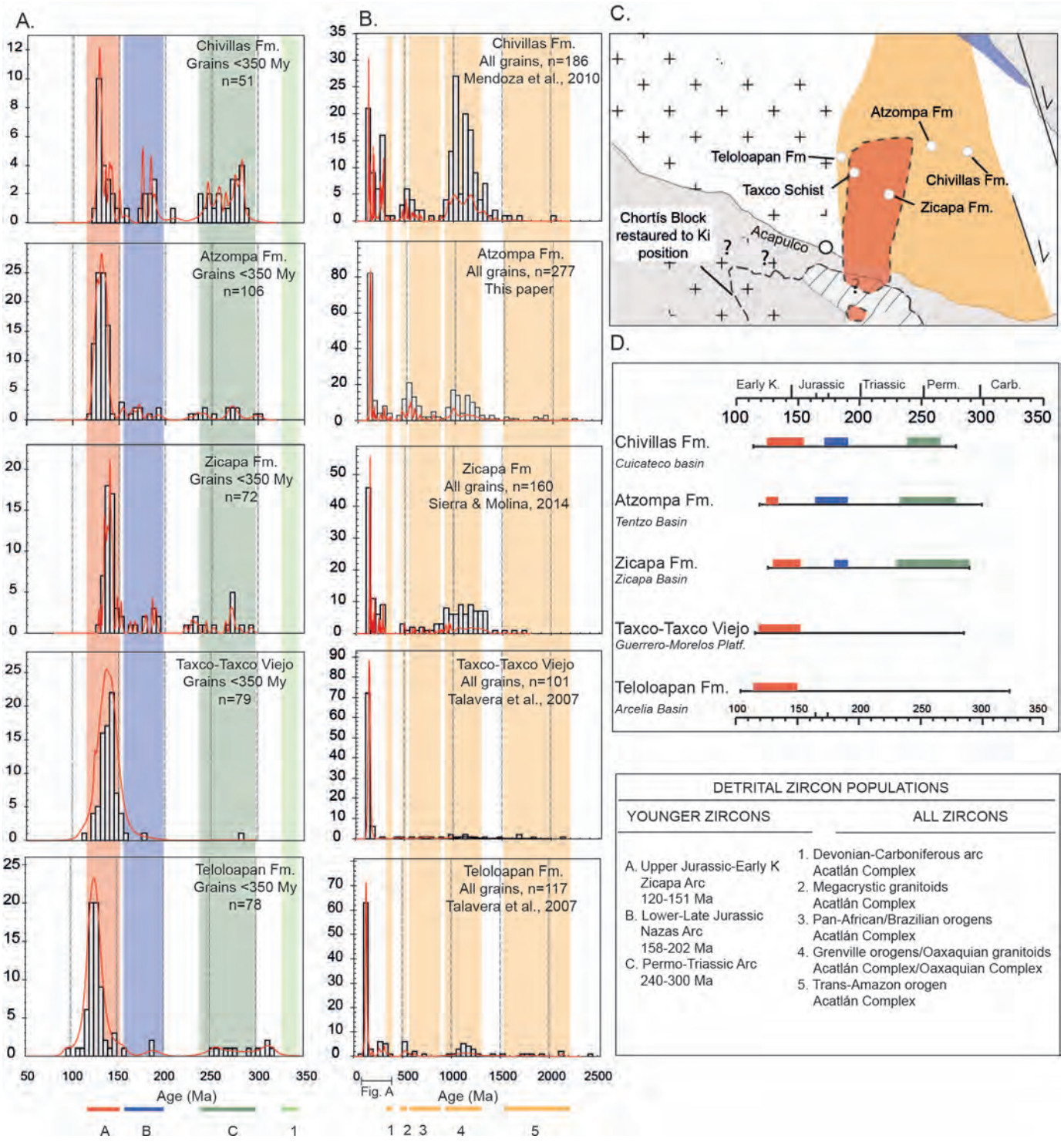

FIG. 10.—Detrital-zircon correlation for Lower Cretaceous Formations in Oaxaquia east to west (Chivillas, Atzompa, Zicapa, Taxco-Taxco Viejo, and Teloloapan formations). **A)** grains younger than 350 My. **B)** Probability density plots of all zircons. **C)** Actual geographic location of localities in the paleogeographic map of southern Mexico. Map keys are in Figure 11. Zicapa Formation data are from Sierra-Rojas and Molina-Garza (2014), Teloloapan Formations and Taxco-Taxco Viejo data are from Talavera-Mendoza et al. (2007), Chivillas Formation are from Mendoza-Rosales et al. (2010). **D)** Zircon populations related to magmatism in Oaxaquia from Permian to Jurassic discriminate central and eastern (Zicapa, Atzompa, and Cuicateco basins) from the western domain (Guerrero-Morelos Platform and Arcelia basin).

Basins located south of the Trans-Mexican Volcanic Belt (Figs. 1, 9) record deposition from Early Cretaceous to Paleogene. The similarity in the Early Cretaceous clastic deposits and the gradual facies change between the Tentzo basin, defined herein, and the Zapotitlán and Cuicateco basins (Mendoza-Rosales 2010) indicate a linkage between the three depocenters (Fig. 9). The Tentzo and Zapotitlán basins show a basal breccia made of basement-derived clasts like Las Pozas Member in the Tentzo basin and the Agua de Cordero and Caltepec formations in the

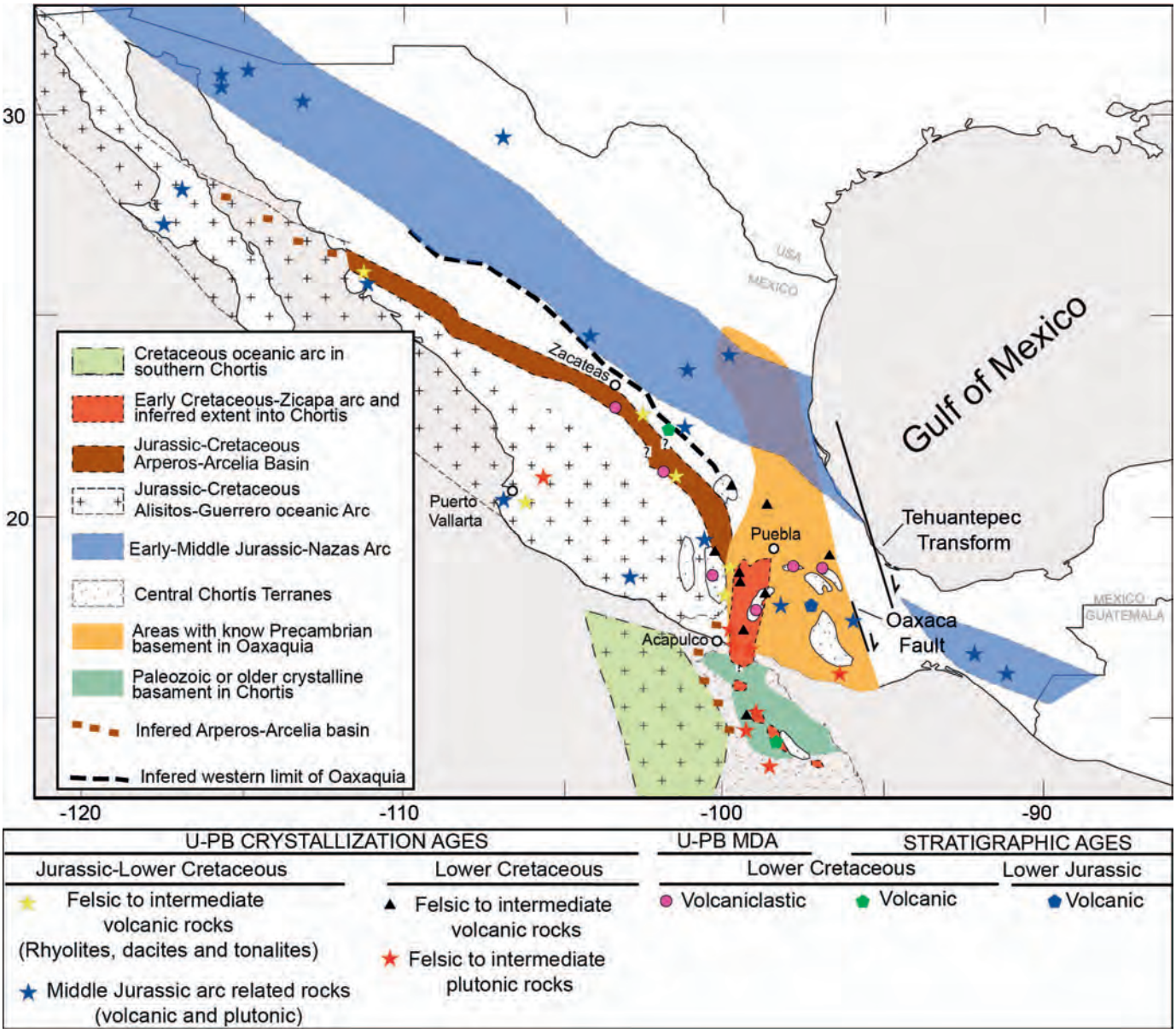

FIG. 11.—Location of Jurassic to Early Cretaceous magmatism in Western Mexico. Location of Precambrian basement of Oaxaquia are after Ortega-Gutierrez et al. (1995); the crystalline basement and the Cretaceous oceanic arc in southern Chortis are after Rogers et al. (2007a); the blue area with stars refers to the Nazas Arc rocks distribution after Bartolini et al. (2003) and Lawton and Molina (2014). Alisitos–Guerrero oceanic arc Centeno-García et al. (2008) and Keppie (2004); The Arperos–Arcelia basin from Freydier et al. (2000). Data of U-Pb crystallization ages, maximum depositional ages (MDA), and stratigraphic ages are in Table 4. The Early Cretaceous basins are the same as Figures 1 and 9.

Zapotitlán basin (Mendoza-Rosales 2010), which represents an opening stage of the basin. Although the lake facies have not been described in the Zapotitlán basin, a lateral facies variation is shown from the fluvial facies in the Tentzo basin to the deltaic facies in San Juan Raya Formation from the Zapotitlán basin; both formations record upsection an early Aptian carbonate ramp. The easternmost Cuicateco basin cannot be linked to the same opening mechanism as that of the Tentzo and Zapotitlán basins because of the inheritance of Gulf of Mexico paleogeographic features (Mendoza-Rosales et al. 2010), nevertheless it is possible to correlate the sediment supply with the processes in the westernmost basins (Fig. 10).

The Atzompa and Chivillas formations, located on eastern Oaxaquia, as well as the Zicapa Formation, and to a lesser extent the Taxco Schist and the San Juan de la Rosa Formation of western Oaxaquia, contain zircons derived from the Paleoproterozoic to Devonian basement associated with the Oaxaquia subcontinent represented by the Acatlán and Oaxacan complexes. Moreover, they contain a dominant contribution from coeval Early Cretaceous magmatic sources. There are also marked similarities in the detrital-zircon signatures of the Atzompa Formation reported here and the Chivillas Formation (Mendoza-Rosales et al. 2010) (Fig. 10). Sandstones from the Atzompa and Chivillas formations share similar proportions of Mesoproterozoic and Neoproterozoic to Cambrian zircons derived from the Acatlán and, perhaps, Oaxacan complexes as well as a similar proportion of Jurassic and Cretaceous zircons (Fig. 10).

The Zapotitlán and Tentzo basins in eastern Oaxaquia and the Zicapa basin in the west were separated by elevated areas in east-central Guerrero; those areas were subjected since the Jurassic to subaerial erosion and

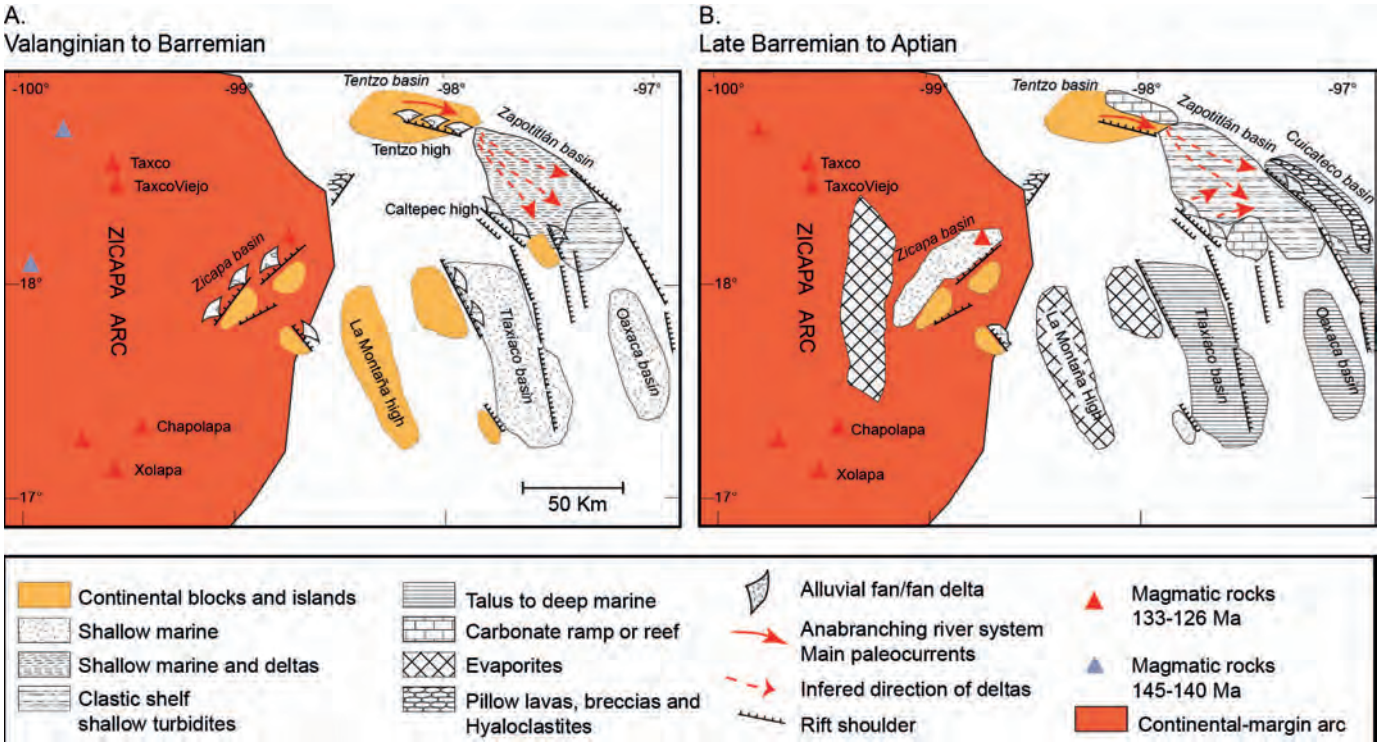

FIG. 12.—Paleogeographic map of Valanginian to Aptian Xolapa Zicapa arc and Tentzo, Zapotitlán, and Cuicateco back-arc basins of southern Mexico. Paleocurrent directions were measured in fluvial facies of the Atzompa Formation. The stratigraphy and facies from the Zicapa, Tlaxiaco, and Oaxaca basins are from the literature (see Fig. 9 for extended stratigraphy).

deposition in continental and shallow marine settings (Tlaxiaco and Oaxaca basins). The Early Cretaceous deposition in the western margin of the emerged area is recorded in the Zicapa basin by the Zicapa Formation with alluvial fans and littoral deposition with a maximum depositional age of Upper Jurassic followed by volcanic tuffs and volcaniclastic sandstones of Valanginian age (Sierra-Rojas and Molina Garza 2014).

Deposition in the Tentzo basin located north of a central emerged area in southern Mexico took place from the Barremian to the Aptian, and had a main source of volcanic clasts and zircons of near-Aptian age. This suggests contemporaneous deposition of the alluvial-fan facies of the Santa Marta Member with volcanism (Figs. 11, 12). The Cuicateco basin, located east of the emerged area, records an extensional submarine environment from the Late Jurassic to the Early Cretaceous; the volcanism of the Chivillas Formation took place after the Aptian, and was characterized by tuffs and pillow basalts (Carrasco et al. 1975, Mendoza-Rosales et al. 2010).

The sedimentological and chronological data suggest that the Zicapa basin may be somewhat older than the basins in the east (Sierra-Rojas and Molina-Garza 2014), indicating diachronous magmatism and extension from west to east (Figs. 9, 10). Zicapa and Chapolapa magmatism (Hernández-Treviño et al. 2004) took place in the Valanginian (~ 131 Ma), and sedimentation in these basins accompanied volcanism until Aptian time, when abrupt deepening of the Atzompa basin is recorded by the change from estuarine to slope marine facies at the lithostratigraphic contact between the Atzompa and El Tentzo formations.

We interpret the similarities in depositional environments (alluvial fan to shallow marine), stratigraphic relationships, and provenance to indicate that the Tentzo and Zapotitlán basins were connected at least during the later stages of deposition represented by the transition from continental to marine environments, with the Atzompa Formation containing more proximal continental sediments. In turn, Atzompa and Zapotitlán are the shallow marine equivalent of the Chivillas Formation, which is dominated by turbidites (Mendoza-Rosales et al. 2010). Underlying the Chivillas Formation is the Xonamanca Formation, which records calc-alkaline magmatism in the Cuicateco basin (H. Coombs, personal communication 2015). Thus, equivalent stratigraphic units in the Tentzo and Cuicateco basins record sedimentation associated with extension and mixed basement and volcanic sources for sediment. Furthermore, both basins record contemporaneous calcalkaline volcanism.

Early Cretaceous Magmatism and Back-Arc Position of Tentzo Cuicateco Basin

Nearly continuous intermediate to felsic magmatism from Valanginian to Aptian time is recorded in Oaxaquia basement from Zacatecas in northern Mexico to Acapulco on the southwestern coast of Mexico and in central Honduras, on the Chortis block (Fig. 11). Early Cretaceous magmatism in central and southern Mexico was recently summarized by Sierra-Rojas and Molina-Garza (2014), who describe a belt of calc-alkaline volcanic deposits that extend along the western Oaxaquia margin for about 1200 km (Fig. 11). The axis of the belt is located to the west of the Atzompa and Zicapa formations, perhaps in the Xolapa terrane, the Taxco area, and the Central Chortis block (Fig.11; Ratschbacher et al. 2009; Rogers et al. 2007b; Solari et al. 2007). Sierra-Rojas and Molina-Garza (2014) refer to this belt as the Zicapa continental arc. In an alternative view, other authors refer the calc-alkaline magmatism to a back-arc setting related to the Guerrero Terrane arc with eastward subduction in a single arc-trench system (Martini et al. 2011; Ortega-Flores et al. 2013; Escalona-Alcázar et al. 2009; Martini et al. 2014; Ortega-Flores et al. 2015).

We have shown that emplacement of plutonic and volcanic rocks was contemporaneous with sedimentation of the Zicapa, Atzompa, and Chivillas formations in southern Mexico. Aptian mafic rocks in the

TABLE 4.—*U-Pb crystallizations ages for some Jurassic to Early Cretaceous magmatic units, U-Pb maximum depositional ages for Early Cretaceous volcanosedimentary rocks, and stratigraphic ages of Jurassic to Early cretaceous formations.*

	Unit	Age (Ma)	Reference
U-Pb cristalization ages			
Lower Cretaceous felsic to intermediate granitoids			
	Xolapa Complex, Tonalitic Gneiss	140.9 ± 4.5	Ducea et al. 2004
	Teotitlán Migmatitic Complex	140 ± 1.5	Angeles-Moreno 2006
	Tingambato Batholith	129.6 ± 1.1	Martini et al. 2010
	Tuzantla Batholith	132.3 ± 1.4, 131.8 ± 1.1	Garza González 2007
	El Pozuelo Granite	129 ± 0.5	Solari et al. 2007
	Xolapa Complex, Tonalitic Gneiss	136.6 ± 4	Ducea et al. 2004
	Atenguillo Granitoids	133 ± 1.8	Valencia et al. 2013
	San Andres Dacite	124 ± 2	Drobe and Cann 2000
Lower Cretaceous volcanic and volcanoclastic formations			
	Palmar Chico Assemblage	129.5 ± 2.2	Martini et al. 2014
	San Juan de la Rosa Formation	137	Ortega-Flores et al. 2013
	Santuario Formation	129–125	Abascal and Murillo 2013
	Taxco Schist	130 ± 3,136.9 ± 1, 137 ± 1	Campa-Uranga et al. 2012
	Taxco Viejo	132 ± 1, 135 ± 1, 136 ± 1	Campa-Uranga et al. 2012
	Chapolapa Formation	126 ± 4, 133 ± 1, 130 ± 1	Hernández-Treviño et al. 2004; Campa-Uranga et al. 2004
	Zicapa Formation	126	Sierra-Rojas and Molina-Garza 2014
U-Pb Maximum depositional ages			
Lower Cretaceous clastic and volcanoclastic formations			
**	Los Pinos Volcanosedimentary Complex	135 ± 3	Escalona-Alcázar et al. 2009
	Zacatecas Formation	131 ± 2	
	Arperos Formation	131–133	Martini et al. 2011
	Peña Azul Formation	129.8 ± 0.6	Ortega-Flores et al. 2013
	Las Trancas Formation	127.2 ± 0.4	
**	Teloloapan Formation	124 ± 8	Talavera-Mendoza et al. 2007
	Esquisto Tejupilco	~ 142, 138	Elias-Herrera et al. 2000
	Atzompa Formation		This paper
	• La Magdalena	126 ± 1	
	• Lower Santa Marta Member	129 ± 1	
	• Upper Santa Marta Member	123 ± 1	
**	Zicapa Formation	134 ± 1	Sierra-Rojas and Molina-Garza 2014
**	Chivillas Formation	127 ± 2	Mendoza-Rosales et al. 2010
		127 ± 1	
Stratigraphic ages			
	Xonamanca Formation	Berriasian–Valanginian	Carrasco et al. 1975
	Taraises Formation	Berriasian–Valanginian	Cantú-Chapa 2009
	Diquiyú Unit	> 183 Ma	Morán-Zenteno et al. 1993

* Lithofacies code from this work.

** Recalculation from data of maximum depositional ages.

Early–Middle Jurassic boundary is 174.1 ± 1.0 Ma; Middle–Late Jurassic boundary is 163.5 ± 1.0 Ma; Late Jurassic–Early Cretaceous boundary ~ 145.0 Ma (Gradstein et al. 2012).

Cuicateco basin, represented by pillow basalts of the Chivillas Formation, have been interpreted as oceanic tholeiites from a ridge transform intersection (Mendoza-Rosales et al. 2010), but they also show a calc-alkaline component similar to that of the Barremian Xonamanca Formation in the northern Cuicateco basin (H. Coombs, personal communication 2015). Both geochemical compositions are possible in a marginal ensialic basin, as basalts erupted in back-arc basins can range from MORB-like basalts to arc-like basalts (e.g., Saunders and Tarney 1984; Keller et al. 2002). The submarine volcanism of the Chivillas Formation can be interpreted as the culmination of back-arc extension and associated asthenospheric melting. This interpretation contrasts with that of Mendoza-Rosales et al. (2010), who linked the Aptian magmatism of the Chivillas Formation in the Cuicateco basin to the opening of the Gulf of Mexico; however, the Early Cretaceous (Aptian) age of the Chivillas Formation is younger than the Late Jurassic to Valanginian (~ 140 Ma) opening of the gulf (e.g., Pindell and Kennan 2009). Westward propagation of seafloor spreading in the Gulf of Mexico may have contributed to extension, subsidence, and magmatism in the Cuicateco basin early in its history during Valanginian to Barresian time, but not during Aptian deposition of the Chivillas Formation as proposed by Mendoza-Rosales et al. (2010).

Paleogeography

Zircon populations and sandstone provenance support our interpretation for the integration of the Tenzo and Cuicateco basins (Fig. 10). We propose for southern Mexico a tectonic and sedimentary framework consisting of an arc axis, located between Taxco and Acapulco (Figs. 11, 12) and a series of extensional basins in the back-arc region: the Tentzo, Zapotitlán, and Cuicateco, which formed on Oaxaquian continental crust (Figs. 1, 12). From Valanginian to Barremian time, the northern Tentzo basin was dominated by alluvial, lacustrine, and fluvial sediments of the Atzompa Formation. At the same time, the southeastern Zapotitlán and Cauicateco basins were filled by siliciclastic sediments prograding from the Tentzo and

Caltepec highs to form a shallow marine environment consisting of fan-delta, deltaic, and clastic shelfal depositional systems (Fig. 12A). During Barremian to early Aptian time, the siliciclastic input from the Tentzo area decreased and a carbonate ramp was developed in the Tentzo, Zapotitlán, and Caltepec basins. In the early Aptian, the Cuicateco basin experienced rapid extension which led to transfer of high volumes of siliciclastic and carbonate sediment from the Zapotitlan platform to the basin by means of turbidity currents coeval with local basaltic submarine volcanism (Fig. 12B).

A back-arc tectonic setting for the Tentzo, Zapotitlán, and Cuicateco basins derives from facies distribution, sedimentation style, and provenance information from young detrital zircons and volcanic clasts in the alluvial-fan facies. While the basement was subjected to high rates of extension, as discussed above, the basin received sediment from a contemporary magmatic source. Following the episode of linked magmatism and extension, basin subsidence and sedimentation rate slowed, with the result that sedimentary environments changed to a carbonate ramp with no terrigenous influence (Fig. 12B). Sedimentation rates and provenance data indicate a transition from a back-arc extensional basin to a post-collisional assemblage of carbonate platforms and basins which characterize all of eastern Mexico (e.g., Wilson and Ward 1993). Thus, the extensional events of the Early Cretaceous in southwestern Mexico were succeeded by development of a stable Albian archipelago of isolated carbonate platforms and basins on the slowly subsiding former transcurrent Gulf margin (Fig. 9). We submit that renewed subduction in the Pacific margin, after terrane accretion, led to differential uplift of shallow basement blocks and development of Albian carbonate platforms.

CONCLUSIONS

The Tentzo basin of south-central Mexico is an extensional basin that contains deposits of alluvial fans, deep lakes characterized by turbidity-current deposits, and anabranching rivers. Detrital-zircon geochronology indicates that the Atzompa Formation is late Barremian to Aptian, or younger, according to the time scale of Gradstein et al. (2012), which indicates an age of 125 Ma for the Barremian to Aptian boundary.

Extremely high undecompacted sedimentation rates of 3.6 mm/yr are similar to the fastest subsiding rift basins reported in the literature, the modern Tyrrhenian back-arc basin west of Calabria (Millia and Torrente 2015). The very high supply of clastic sediment and the gradual facies changes in the Tentzo basin from alluvial, to lacustrine, to fluvial facies indicate that the rate of sediment supply was comparable to the rate of subsidence.

The general stratigraphy of the Tentzo basin compares well with the three main stages of the evolution in a rift basin: a rift initiation stage characterized by alluvial-fan facies, a rift climax with the development of deep lakes, and a post-rift stage with a decrease in tectonic subsidence and a fill of the basin. The last stage is recorded by the vertical aggradation of channels in an axial fluvial system followed by estuarine and platform facies. The time between the rift initiation and the post-rift stages in the Tentzo basin is as short as 4 My or as long as 10 My given the age uncertainty, corresponding to a short-lived rift basin. This rapid evolution of the basin could be related to the interaction between tectonic dynamics of an east-dipping slab to the west and the inheritance of an extensional province to the east (the Gulf of Mexico).

The main axial fluvial system of the Tentzo basin that flowed during Barremian to early Aptian from the northwest and southwest over Mixteca basement to the southeast deltaic systems developed in a clastic platform. The input of clastic sediments from the west decrease in the late early Aptian when a carbonate ramp was instituted. The change in sediment supply is recorded in the composition of turbidites deposited in the easternmost part of the Mixteca in the Cuicateco basin.

The presence of syndepositional magmatic zircon grains in the sandstones of the Atzompa Formation, as well as alluvial fan deposits containing 80% volcanic clasts of early Aptian age, is consistent with the existence of contemporary regional magmatism west of the Tentzo and neighboring Zapotitlán and Cuicateco basins, and indicates a back-arc position of those basins in Barremian to early Aptian time.

The upper contact of the Atzompa Formation with the Tentzo Formation, early Aptian in age, is marked by an abrupt change of estuarine and tidal facies in El Calvario Member to deep marine and talud facies in the lowest Tentzo formation. This change could be correlated with a fluxural response of the basin to the accretion of oceanic terranes from the west dated in central Mexico as Aptian to Albian.

SUPPLEMENTAL MATERIAL

Appendices A–D are available from JSR's Data Archive: http://sepm.org/pages.aspx?pageid=229.

ACKNOWLEDGMENTS

We acknowledge the Programa de Apoyo a Proyectos de Investigación e Innovación Tecnológica (PAPIIT: IN104511-3) for funds to support the fieldwork and geochronological analyses. We also acknowledge partial support from CONACYT gran 129862 to RSMG. We thank Ana Bertha Villaseñor for the fossil identification, Carlos Ortega-Obregón for the technical assistance provided in the Laboratorio de Estudios Isotópicos, Centro de Geociencias, UNAM, Juan Tomás Vázquez for preparation of thin sections, and Rosario Adriana Rodríguez for assistance in the field. The authors also want to thank to Paul Mann and an anonymous reviewer for their reviews that clearly improved the manuscript.

REFERENCES

Abascal, G., and Murillo, G., 2013, Preliminary Sequence stratigraphy framework of the SW part of the Actopan platform, Lower Cretaceous, Hidalgo, Mexico [Abstract]: American Geophysical Union, Meeting of the Americas, Abstracts with Programs.

Anderson, T.H., and Nours, J.A., 2005, Pull-apart basins at releasing bends of the sinistral Late Jurassic Mojave–Sonora fault system, *in* Anderson, T.H., Nourse, J.A., McKee, J.W., and Steiner, M., The Mojave–Sonora megashear hypothesis: development, assessment, and alternatives: Geological Society of America, Special Paper 393, p. 97–122.

Ángeles-Moreno, E., 2006, Petrografía, geología estructural y geocronología del borde noroccidental del terreno Cuicateco, Sierra Mazateca, estado de Oaxaca, México [M.S. Thesis]: Universidad Nacional Autónoma de México, 194 p.

Bartolini, C., Lang, H., and Spell, T., 2003, Geochronology, geochemistry, and tectonic setting of the Mesozoic Nazas arc in north-central Mexico, and its continuation to northern South America, *in* Bartolini, C., Buffler, R., and Blickwede, J.F., eds., Circum-Gulf of Mexico and the Caribbean: Hydrocarbon Habitats, Basin Formation, and Plate Tectonics: America Association of Petroleum Geologists, Memoir 79, p. 427–461.

Bilodeau, W.L., 1982, Tectonic models for Early Cretaceous rifting in southeastern Arizona: Geology, v. 10, p. 466–470.

Blair, T.C., and McPherson, J.G., 1994, Alluvial fans and their natural distinction from rivers based on morphology, hydraulic processes, sedimentary processes, and facies assemblages: Journal of Sedimentary Research, v. 64, p. 450–489.

Cabral-Cano, E., Lang, H.R., and Harrison, C.G.A., 2000, Stratigraphic assessment of the Arcelia–Teloloapan area, southern Mexico: implication for southern Mexico's post-Neocomian tectonic evolution: Journal of South American Earth Sciences, v. 13, p. 443–457.

Campa, M.F., and Coney, P.J., 1983, Tectono-stratigraphic terranes and mineral distributions in Mexico: Canadian Journal of Earth Sciences, v. 20, p. 1040–1051.

Campa-Uranga, M.F., García-Díaz, J.L., and Iriondo, A., 2004, El arco volcánico–sedimentario del Jurásico Medio (Grupo Tecocoyunca y Las Lluvias) de Olinalá, Guerrero [Abstract]: IV Reunión Nacional de Ciencias de la Tierra, Abstracts with Programs, p. 76

Campa-Uranga, M.F., Torres de León, R., Iriondo, A., and Premo, W.R., 2012, Caracterización geológica de los ensambles metamórficos de Taxco y Taxco el Viejo, Guerrero, México: Sociedad Geológica Mexicana, Boletín, v. 64, p. 369–385.

Cantú-Chapa, A., 2009, Ammonites of the Cretaceous Taraises and lower Tamaulipas formations in Eastern Mexico, *in* Bartolini, C., and Román-Ramos, J.R., eds., Petroleum Systems in the Southern Gulf of Mexico: American Association of Petroleum Geologists, Memoir 90, p. 191–216.

Carrasco, B., Flores, V., and Godoy, D., 1975, Tobas del Cretácico Inferior del área de Fortín–Zongolica, estado de Veracruz: Instituto Mexicano del Petróleo, Revista, p. 7–27.

Centeno-García, E., Guerrero-Suástegui, M., and Talavera-Mendoza, O., 2008, The Guerrero Composite Terrane of western Mexico: collision and subsequent rifting in a supra-subduction zone, *in* Draut, A., Clift, P.D., and Scholl, D.W., eds., Formation and Application of the Sedimentary Record in Arc Collision Zones: Geological Society of America, Special Paper 436, p. 279–308.

Centeno-García, E., Busby, C., Busby, M., and Gehrels, G.E., 2011, Evolution of the Guerrero composite terrane along the Mexican margin, from extensional fringing arc to contractional continental arc: Geological Society of America, Bulletin, v. 123, p. 1776–1797.

DeCelles, P.G., Langford, R.P., and Schwartz, R.K., 1983, Two new methods of paleocurrent determination from trough cross-stratification: Journal of Sedimentary Petrology, v. 53, p. 629–642.

DeCelles, P.G., and Currie, B.S., 1996, Long-term sediment accumulation in the Middle Jurassic–early Eocene Cordilleran retroarc foreland-basin system: Geology, v. 24, p. 591–594.

DeCserna, Z., Ortega G.F., and Palacios, N.M., 1980, Reconocimiento geológico de la parte central de la cuenca del alto Río Balsas, estados de Guerrero y Puebla, *in* Sociedad Geológica Mexicana, Libro Guía de la Excursión Geológica a la Parte Central de la Cuenca del Alto Rio Balsas: V Convención Geológica Nacional, p. 1–33.

Demicco, R.V., and Hardie, L.A., 1994, Sedimentary structures and early diagenetic features of shallow marine carbonate deposits: SEPM, Atlas 1, 265 p.

Dickinson, W.R., 1970, Interpreting detrital modes of greywacke and arkose: Journal of Sedimentary Petrology, v. 40, p. 695–707.

Dickinson, W.R., 1985, Interpreting provenance relations from detrital modes of sandstones, *in* Zuffa, G.G., ed., Provenance of Arenites: NATO, ASI Series, p. 333–363.

Dickinson, W.R., and Gehrels, G.E., 2009, U-Pb ages of detrital zircons in Jurassic eolian and associated sandstones of the Colorado Plateau: evidence for transcontinental dispersal and intraregional recycling of sediment: Geological Society of America, Bulletin, v. 121, p. 408–433.

Dickinson, W.R., and Lawton, T.F., 2001a, Carboniferous to Cretaceous assembly and fragmentation of Mexico: Geological Society of America, Bulletin, v. 113, p. 1142–1160.

Dickinson, W.R., and Lawton, T.F., 2001b, Tectonic setting and sandstone petrofacies of the Bisbee basin (USA–Mexico): Journal of South American Earth Sciences, v. 14, p. 475–504.

Dickinson, W.R., and Suczek, C.A., 1979, Plate tectonics and sandstone compositions: American Association of Petroleum Geologists, Bulletin, v. 63, p. 2164–2182.

Drobe, J., and Cann, R., 2000, Cu-Au Skarn Mineralization, Minas de Oro District, Honduras, Central America: Exploration and Mining Geology, v. 9, p. 51–63.

Ducea, M., Gehrels, G.E., Shoemaker, S., Ruíz, J., and Valencia, V.A., 2004, Geologic evolution of the Xolapa Complex, southern Mexico: evidence from U-Pb zircon geochronology: Geological Society of America, Bulletin, v. 116, p. 1016–1025.

Eguiluz de Antuñano, S., 2001, Geologic evolution and gas resources of the Sabinas basin in northeastern Mexico, *in* Bartolini, C., Buffler, R.T., and Cantú-Chapa, A., eds., The Western Gulf of Mexico Basin: Tectonics, Sedimentary Basins, and Petroleum Systems: American Association of Petroleum Geologists, Memoir 75, p. 241–270.

Elías-Herrera, M., Sánchez-Zavala, J.L., and Macías-Romo, C., 2000, Geologic and geochronologic data from the Guerrero terrane in the Tejupilco area, southern Mexico: new constraints on its tectonic interpretation: Journal of South American Earth Sciences, v. 13, p. 355–375.

Escalona-Alcázar, F.J., Delgado-Argote, L.A., Weber, B., Núñez-Peña, E.P., Valencia, V.A., and Ortiz-Acevedo, O., 2009, Kinematics and U-Pb dating of detrital zircons from the Sierra de Zacatecas, Mexico: Revista Mexicana de Ciencias Geológicas, v. 26, p. 48–64.

Fitz-Diaz, E., 2001, Evolución estructural del sinclinorio de Zacango en el límite oriental de la Plataforma Guerrero Morelos: Guerrero, México [Undergraduate Thesis]: Mexico, Instituto Politécnico Nacional, 103 p.

Folk, R.L., 1974, Petrology of Sedimentary Rocks: Austin, Texas, Hemphill Publishing Company, 182 p.

Freydier, C., Lapierre, H., Briqueu, L., Tardy, M., Coulon, C., and Martinez-Reyes, J., 1997, Volcaniclastic sequences with continental affinities within the Late Jurassic–Early Cretaceous Guerrero intra-oceanic arc terrane (Western Mexico): The Journal of Geology, v. 105, p. 483–502.

Freydier, C., Lapierre, H., Ruiz, J., Tardy, M., Martinez, R.J., and Coulon, C., 2000, The Early Cretaceous Arperos basin: an oceanic domain dividing the Guerrero arc from nuclear Mexico evidenced by the geochemistry of the lavas and sediments: Journal of South American Earth Sciences, v. 13, p. 325–336.

Garza-González-Vélez, C.E., 2007, Metalogenia del pórfido de cobre de Tiámaro, estado de Michoacán, México [Ph.D. Thesis]: Universidad Nacional Autónoma de México, 258 p.

Gawthorpe, R.L., and Leeder, M.R., 2000, Tectono-sedimentary evolution of active extensional basins: Basin Research, v. 12, p. 195–218.

Goldhammer, R.K., and Johnson, C.A., 2001, Middle Jurassic–Upper Cretaceous paleogeographic evolution and sequence-stratigraphic framework of the northwest Gulf of Mexico rim, *in* Bartolini, C., Buffler, R.T., and Cantu-Chapa, A., eds., The Western Gulf of Mexico Basin: Tectonics, Sedimentary Basins, and Petroleum Systems: American Association of Petroleum Geologists, Memoir 75, p. 45–81.

Gradstein, F.M., Ogg, J.G., Schmitz, M.D., and Ogg, G.M., 2012, The Geologic Time Scale 2012: Boston, Elsevier, 1144 p.

Greb, S.F., and Martino, R.L., 2005 Fluvial–estuarine transitions in fluvial dominated successions: examples from the Lower Pennsylvanian of the Central Appalachian Basin *in* Blum, M., Marriot, S.B., and Leclair, S.F., Fluvial Sedimentology VI: International Association of Sedimentologists, Special Publication 35, p. 425–452.

Gupta, S., Cowie, P.A., Dawers, N.H., and Underhill, J.R., 1998, A mechanism to explain rift-basin subsidence and stratigraphic patterns through fault-array evolution: Geology, v. 26, p. 595–598.

Haenggi, W.T., 2001, Tectonic history of the Chihuahua trough, Mexico and adjacent USA, Part I: the pre-Mesozoic setting: Sociedad Geológica Mexicana, Boletín, v. 54, p. 28–66.

Haenggi, W.T., and Müehlberger, W.R., 2005, Chihuahua trough: a Jurassic pull-apart basin, *in* Anderson, T.H., Nourse, J.A., McKee, J.W., and Steiner, M., eds., The Mojave–Sonora Megashear Hypothesis: Development, Assessment, and Alternatives: Geological Society of America, Special Paper 393, p. 619–630.

Helbig, M., Keppie, J.D., Murphy, J.B., and Solari, L., 2012, U–Pb geochronological constraints on the Triassic–Jurassic Ayú Complex, southern Mexico: derivation from the western margin of Pangea-A: Gondwana Research, v. 22, p. 910–927.

Heller, P.L., Bowdler, S.S., Chambers, H.P., Coogan, J.C., Hagen, E.S., Shuster, M.W., Winslow, N.S., and Lawton, T.F., 1986, Time of initial thrusting in the Sevier orogenic belt, Idaho–Wyoming and Utah: Geology, v. 14, p. 388–391.

Hernández-Romano, U., Aguilera-Franco, N., Martínez-Medrano, M., and Barceló-Duarte, J., 1997, Guerrero–Morelos Platform drowning at the Cenomanian–Turonian boundary, Huitziltepec area, Guerrero State, southern Mexico: Cretaceous Research, v. 18, p. 661–86.

Hernández-Treviño, T., Torres de León, R., Solís-Pichardo, G., Schaaf, P., Hernández-Bernal, M., and Morales-Contreras, J., 2004, Edad de la Formación Chapolapa en la localidad de río Cochoapa, al oeste del Ocotito, estado de Guerrero: Unión Geofísica Mexicana, Reunión Anual, Abstracts with Programs, v. 24, p. 179.

Ingersoll, R.V., and Suczek, C.A., 1979, Petrology and Provenance of Neogene sand from Nicobar and Bengal fans, DSDP sites 211 and 218: Journal of Sedimentary Petrology, v. 49, p. 1217–1228.

Ingersoll, R.V., Bullard, T.F., Ford, R.L., Grimm, J.P., Pickle, J.D., and Sares, S.W., 1984, The effect of grain size on detrital modes: a test of the Gazzi–Dickinson point-counting method: Journal of Sedimentary Petrology, v. 54, p. 103–116.

Jacques-Ayala, C., 1995, Paleogeography and provenance of the Lower Cretaceous Bisbee Group in the Caborca–Santa Ana area, northwestern Sonora, *in* Jacques-Ayala, C., González-León, C.M., and Roldan-Quintana, J., eds., Studies on the Mesozoic of Sonora and Adjacent Areas: Geological Society of America, Special Paper 301, p. 79–98.

Keller, R.A., Fisk, M.R., Smellie, J.L., Strelin, J.A., Lawver, L.A., and White, W.M., 2002, Geochemistry of back arc basin volcanism in Bransfield Strait, Antarctica: subducted contributions and along-axis variations: Journal of Geophysical Research, v. 17, p. 1–17.

Keppie, J.D., 2004, Terranes of Mexico revisited: a 1.3-billion-year odyssey: International Geology Review, v. 46, p. 765–794.

Keppie, J.D., Dostal, J., Cameron, K.L., and Solari, L.A., 2003, Geochronology and geochemistry of Grenvillian igneous suites in the northern Oaxacan Complex, southern Mexico: tectonic implications: Precambrian Research, v. 120, p. 356–389.

Kirsch, M., Keppie, D., Murphy, B., and Lee, J., 2013, Arc plutonism in a transtensional regime: the late Palaeozoic Totoltepec pluton, Acatlán Complex, southern Mexico: International Geology Review, v. 55, p. 263–286.

Klute, M.A., 1991, Sedimentology, sandstone petrofacies, and tectonic setting of the Mesozoic Bisbee basin, southeastern Arizona [Unpublished PhD Thesis]: University of Arizona, 268 p.

Kroehler, M.E., Mann, P., Escalona, A., and Christeson, G., 2011, Late Cretaceous–Miocene diachronous onset of back thrusting along the south Caribbean deformed belt and its importance for understanding processes of arc collision and crustal growth: Tectonics, v. 30, no. TC6003.

Lambiase, J.J., and Bosworth, W., 1995, Structural controls on sedimentation in continental rifts, *in* Lambiase, J.J., ed., Hydrocarbon Habitat in Rift Basins: Geological Society of London, Special Publication 80, p. 117–144.

Lapierre, H., Ortiz, L.E., Abouchami, W., Monod, O., Coulon, C., and Zimmermann, J.L., 1992, A crustal section of an intra-oceanic island arc: the Late Jurassic–Early Cretaceous Guanajuato magmatic sequence, central Mexico: Earth and Planetary Science Letters, v. 108, p. 61–77.

Lawton, T.F., 1994, Tectonic setting of Mesozoic sedimentary basins, Rocky Mountain region, United States, *in* Caputo, M.V., Peterson, J.A., and Franczyk, K.J., eds., Mesozoic Systems of the Rocky Mountain Region, USA: SEPM, Special Publication, p. 1–25.

Lawton, T.F., and McMillan, N.J., 1999, Arc abandonment as a cause for passive continental rifting: comparison of the Jurassic Mexican Borderland rift and the Cenozoic Rio Grande rift: Geology, v. 27, p. 779–782.

Lawton, T.F., and Molina-Garza, R.S., 2014, U-Pb geochronology of the type Nazas Formation and superjacent strata, northeastern Durango, Mexico: implications of a Jurassic age for continental-arc magmatism in north-central Mexico: Geological Society of America, Bulletin, v. 126, p. 1–19.

Lawton, T., Vega, F.J., Giles, K.A., and Rosales-Domínguez, M.C., 2001, Stratigraphy and origin of the La Popa Basin, Nuevo León and Coahuila, Mexico, *in* Bartolini, C., Buffler, R.T., and Cantu-Chapa, A., eds., The Western Gulf of Mexico Basin: Tectonics,

Sedimentary Basins, and Petroleum Systems: American Association of Petroleum Geologists, Memoir 75, p. 219–240.

López-Ticha, D., 1985, Revisión de la estratigrafía y potencial petrolero de la Cuenca de Tlaxiaco: Asociación Mexicana de Geólogos y Petroleros, Boletín, v. 37, p. 49–92.

MacEachern, J.A., Bann, K.L., Bhattacharya, J.P., and Howell, C.D., 2005, Ichnology of deltas: organism responses to the dynamic interplay of rivers, waves, storms and tides, *in* Giosan, L., and Bhattacharya, J.P., eds., River Deltas: Concepts, Models, and Examples: SEPM, Special Publication 83, p. 49–85.

Martini, M., Ferrari, L., López-Martínez, M., and Valencia, V.A., 2010, Stratigraphic redefinition of the Zihuatanejo area, southwestern Mexico: Revista Mexicana de Ciencias Geológicas, v. 27, p. 412–430.

Martini, M., Mori, L., Solari, L.A., and Centeno-García, E., 2011, Sandstone provenance of the Arperos Basin (Sierra de Guanajuato, Central Mexico): Late Jurassic–Early Cretaceous back-arc spreading as the foundation of the Guerrero terrane: Journal of Geology, v. 119, p. 597–617.

Martini, M., Solari, L., and Martínez-López, M., 2014, Correlating the Arperos Basin from Guanajuato, central Mexico, to Santo Tomás, southern Mexico: implications for the paleogeography and origin of the Guerrero terrane: Geosphere, v. 10, p. 1–17.

Mendoza-Rosales, C., 2010, Estratigrafía y facies de las cuencas cretácicas de Puebla y su significado tectónico [Ph.D. Thesis]: Universidad Nacional Autónoma de México, 190 p.

Mendoza-Rosales, C.C., Centeno-García, E., Silva-Romo, G., Campos-Madrigal, E., and Bernal, J.P., 2010, Barremian rift-related turbidites and alkaline volcanism in southern Mexico and their role in the opening of the Gulf of Mexico: Earth and Planetary Science Letters, v. 295, p. 419–434.

Miall, A.D., 1996, The Geology of Fluvial Deposits: New York, Springer-Verlag, 582 p.

Middleton, M., Keppie, J.D., and Murphy, J.B., 2007, PTt constraints on exhumation following subduction in the Rheic Ocean from eclogitic rocks in the Acatlán Complex of southern México, *in* Linnemann, U., Nance, R.D., Kraft, P., and Zulauf, G., eds., The evolution of the Rheic Ocean: From Avalonian–Cadomian Active Margin to Alleghenian–Variscan Collision: Geological Society of America, Special Paper 423, p. 489–509.

Millia, A., and Torrente, M.M., 2015, Tectono-stratigraphic signature of a rapid multistage subsiding rift basin in the Tyrrhenian–Apennine hinge zone (Italy): a possible interaction of upper plate with subducting slab: Journal of Geodynamics, v. 86, p. 42–60.

Monroy-Fernández, M.G., and Sosa-Patrón, A.A., 1984, Geología de la Sierra del Tentzo, Puebla, borde Norte del terreno Mixteca: Sociedad Geológica Mexicana, Boletín, v. 45, p. 43–71.

Morán-Zenteno, D.J., Caballero-Miranda, C.I., Silva-Romo, G., Ortega-Guerrero, B., and González-Torres, E., 1993, Jurassic–Cretaceous paleogeographic evolution of the northern Mixteca terrane, southern Mexico: Geofísica Internacional, v. 32, p. 453–473.

NACSN, 2005, North American Stratigraphic Code: American Association of Petroleum Geology, Bulletin, v. 89, p. 1547–1591.

Nottvedt, A., Gabrielsen, R.H., and Steel, R.J., 1995, Tectonostratigraphy and sedimentary architecture of rift basins, with reference to the northern North Sea: Marine and Petroleum Geology, v. 12, p. 881–901.

Ortega-Flores, B., Solari, L., Lawton, T.F., and Ortega-Obregón, C., 2013, Detrital-zircon record of major Middle Triassic–Early Cretaceous provenance shift, central Mexico: demise of Gondwanan continental fluvial systems and onset of back-arc volcanism and sedimentation: International Geology Review, v. 56, p. 237–261.

Ortega-Flores, B., Solari, L.A., and Escalona-Alcázar, F., 2015, The Mesozoic successions of western Sierra de Zacatecas, Central Mexico: provenance and tectonic implications: Geological Magazine, p. 1–22.

Ortega-González, J.V., and Lambarria-Silva, C., 1991, Informe geológico del prospecto Hoja Oaxaca, compilación geológica I.G.R.S. 1129: PEMEX, Coordinación Divisional de Exploración, Gerencia de Exploración Región Sur, Subgerencia de Geología Superficial y Geoquímica, Unedited file, 190 p.

Ortega-Gutiérrez, F., Ruiz, J., and Centeno-García, E., 1995, Oaxaquia, a Proterozoic microcontinent accreted to North America during the late Paleozoic: Geology, v. 23, p. 1127–1130.

Peryam, T.C., Lawton, T.F., Amato, J.M., Gonzalez-Leon, C.M., and Mauel, D.J., 2011, Lower Cretaceous strata of the Sonora Bisbee Basin: a record of the tectonomagmatic evolution of northwestern Mexico: Geological Society of America, Bulletin, v. 124, p. 532–548.

Pindell, J.L., 1985, Alleghanian reconstruction and subsequent evolution of the Gulf of Mexico, Bahamas, and Proto-Caribbean: Tectonics, v. 4, p. 1–39.

Pindell, J.L., and Dewey, J., 1982, Permo-Triassic reconstruction of western Pangea and the evolution of the Gulf of Mexico/Caribbean region: Tectonics, v. 1, p. 179–211.

Pindell, J.L., and Kennan, L., 2001, Kinematic evolution of the Gulf of Mexico and Caribbean, *in* Petroleum Systems of Deep-Water Basins: Global and Gulf of Mexico Experience: SEPM, Gulf Coast Section, 21st Annual Research Conference, Houston, Texas, Proceedings, p. 193–220.

Pindell, J., and Kennan, L., 2009, Tectonic evolution of the Gulf of Mexico, Caribbean and northern South America in the mantle reference frame: an update, *in* James, K., Lorente, M.A., and Pindell, J., eds., The Geology and Evolution of the Region between North and South America: Geological Society of London, Special Publication 328, p. 1–55.

Posamentier, H.W., and Walker, R.G., 2006, Deep-water turbidites and submarine fans, *in* Posamentier, H.W., and Walker, R.G., eds., Facies Models Revisited: SEPM, Special Publication 84, p. 399–520.

Prosser, S., 1993, Rift-related linked depositional systems and their seismic expression, *in* Williams, G.D., and Dobb, A., eds., Tectonics and Seismic Sequence Stratigraphy: Geological Society of London, Special Publication 71, p. 35–66.

Ratschbacher, L., Franz, L., Min, M., Bachmann, R., Martens, U., Stanek, K., Stubner, K., Nelson, B.K., Herrmann, U.R., Weber, B., López-Martínez, M., Jonckheere, R., Sperner, B., Tichomirowa, M., McWilliams, M.O., Gordon, M.B., Meschede, M., and Bock, P., 2009, The North American–Caribbean Plate boundary in Mexico–Guatemala–Honduras, *in* James, K., Lorente, M.A., and Pindell, J., eds., The Origin and Evolution of the Caribbean Plate: Geological Society of London, Special Publication 328, p. 219–293.

Rogers, R.D., Mann, P., Scott, R.W., and Patino, L., 2007a, Cretaceous intra-arc rifting, *in* Mann, P., ed., Geologic and Tectonic Development of the Caribbean Plate in Northern Central America: Geological Society of America, Special Paper 428, p. 89–128.

Rogers, R.D., Mann, P., and Emmet, P.A., 2007b, Tectonic terranes of the Chortis block based on integration of regional aeromagnetic and geologic data, *in* Mann, P., ed., Geologic and Tectonic Development of the Caribbean Plate in Northern Central America: Geological Society of America, Special Paper 428, p. 65–88.

Rust, B.R., and Legun, A.S., 1983, Modern anastomosing-fluvial deposits in arid Central Australia, and a Carboniferous analogue in New Brunswick, Canada *in* Collinston, J., and Lewin, J., eds., Modern and Ancient Fluvial Systems: International Association of Sedimentologists, Special Publication 6, p. 385–392.

Sadler, P.M., 1981, Sediment accumulation rates and the completeness of stratigraphic sections: Journal of Geology, v. 89, p. 569–584.

Saunders, A.D., and Tarney, J., 1984, Geochemical characteristics of basaltic volcanism within back-arc basins, *in* Kokelaar, B.P., and Howells, M.F., eds., Marginal Basin Geology: Volcanic and Associated Sedimentary and Tectonic Processes in Modern and Ancient Marginal Basins: Geological Society of America, Special Publication 16, p. 59–76.

Schlische, R.W., and Anders, M.H., 1996, Stratigraphic effects and tectonic implications of the growth of normal faults and extensional basins, *in* Beratan, K.K., ed.., Reconstructing the History of Basin and Range Extension Using Sedimentology and Stratigraphy: Geological Society of America, Special Paper 303, p. 183–203.

Sedlock, R.L., Ortega-Gutiérrez, F., and Speed, R.C., 1993, Tectonostratigraphic terranes and tectonic evolution of Mexico: Geological Society of America, Special Paper 278, 153 p.

Serrano-García, D., Sierra-Rojas, M.I., and Molina-Garza, R.S., 2014, Paleomagnetismo, magnetoestratigrafía y análisis de procedencia de la Formación Caltepec, Sur de Puebla [Abstract]: Unión Geofísica Mexicana, Reunión Anual, Abstracts with Programs, v. 34, p. 131–132.

Servicio Geológico Mexicano, 2008, Mapa campo magnético total.

Sierra-Rojas, M.I., and Molina-Garza, R.S., 2014, La Formación Zicapa del sur de México: revisión estratigráfica, sedimentología y ambientes sedimentarios: Revista Mexicana de Ciencias Geológicas, v. 3, p. 1174–189.

Sierra-Rojas, M.I., Molina, R., and Serrano-García, D., 2015, La Formación Caltepec y las evidencias del arco Jurásico en Puebla, México [Abstract]: Tectónica Jurásica en la Parte Noroccidental de Sur América y Bloques Adyacentes, Simposio, Abstracts with Programs.

Silva-Romo, G., 2010, Origen tectónico y evolución de la Cuenca Tehuitzngo–Tepexi Estado de Puebla [Ph.D. thesis]: Querétaro, Universidad Nacional Autónoma de México, 196 p.

Sinha, R., Gibling, M.R., Jain, V., and Tandon, S.K., 2005, Sedimentology and avulsion patterns of the anabranching Baghmati River in the Himalayan foreland basin, India *in* Blum, M., Marriot, S.B., and Leclair, S.F., eds., Fluvial Sedimentology VI: International Association of Sedimentologists, Special Publication 35, p. 181–196.

Sisulak, C.F., and Dashtgard, S.E., 2012, Seasonal controls on the development and character of inclined heterolithic stratification in a tide-influenced, fluvially dominated channel: Fraser River, Canada: Journal of Sedimentary Research, v. 82, p. 244–257.

Smith, D.G., 1986, Anastomosing river deposits, sedimentary rates and basin subsidence, Magdalena River, Northwestern Colombia, South America: Sedimentary Geology, v. 46, p. 177–196.

Smith, D.G., and Smith, N.D., 1980, Sedimentation in anastomosed river systems: examples from alluvial valleys near Banff, Alberta: Journal of Sedimentary Petrology, v. 50, p. 157–164.

Solari, L.A., Torres de León, R., Hernández-Pineda, G., Solé, J., Solís-Pichardo, G., and Hernández-Treviño, T., 2007, Tectonic significance of Cretaceous–Tertiary magmatic and structural evolution of the northern margin of the Xolapa Complex, Tierra Colorada area, southern Mexico: Geological Society of America, Bulletin, v. 119, p. 1265–1279.

Talavera-Mendoza, O., and Guerrero-Suastegui, M., 2000, Geochemistry and isotopic composition of the Guerrero Terrane (western Mexico): implications for the tectono-magmatic evolution of southwestern North America during the late Mesozoic: Journal of South American Earth Sciences, v. 13, p. 297–324.

Talavera-Mendoza, O., Ruiz, J., Gehrels, G.E., Meza-Figueroa, D.M., Vega-Granillo, R., and Campa-Uranga, M.F., 2005, U–Pb geochronology of the Acatlán Complex and implications for the Paleozoic paleogeography and tectonic evolution of southern Mexico: Earth and Planetary Science Letters, v. 235, p. 682–699.

Talavera-Mendoza, O., Ruiz, J., Gehrels, G.E., Valencia, V.A., and Centeno-García, E., 2007, Detrital zircon U/Pb geochronology of southern Guerrero and western Mixteca arc successions (southern Mexico): new insights for the tectonic evolution of southwestern North America during the late Mesozoic: Geological Society of America, Bulletin, v. 119, p. 1052–1065.

Tardy, M., Lapierre, H., Freydier, C., Coulon, C., Gill, J.-B., Mercier de Lepinay, B., Beck, C., Martíne R.J., Talavera M.O., Ortiz H.E., Stein, G., Bourdier, J.L., and Yta, M., 1994, The Guerrero suspect terrane (western Mexico) and coeval arc terranes (the Greater Antilles and the Western Cordillera of Colombia): a late Mesozoic intraoceanic arc accreted to cratonal America during the Cretaceous: Tectonophysics, v. 230, p. 49–73.

Tooth, S., and Nanson, G., 2004, Forms and processes of two highly contrasting rivers in arid central Australia, and the implications for channel-pattern discrimination and prediction: Geological Society of America, Bulletin, v. 116, p. 802–816.

Valencia, V.A., Righter, K., Rosas-Elguera, J., López-Martínez, M., and Grove, M., 2013, The age and composition of the pre-Cenozoic basement of the Jalisco Block: implications for and relation to the Guerrero composite terrane: Contributions to Mineralogy and Petrology, v. 166, p. 801–824.

van der Hilst, R., and Mann, P., 1994, Tectonic implications of tomographic images of subducted lithosphere beneath northwestern South America: Geology, v. 22, p. 451–454.

Walker, R.G., 1992, Facies Models: The Geological Association of Canada, 317 p.

Wilson, J.L., 1990, Basement structural controls on Mesozoic carbonate facies *in* northeastern Mexico: a review, *in* Tucker, M., Wilson, J.L., Crevello, D., Sarg, R., and Read, J.F., eds., Carbonate Platforms: Facies, Sequences and Evolution: International Association of Sedimentologists, Special Publication 9, p. 235–255.

Wilson, J.L., and Ward, W.C., 1993, Early Cretaceous carbonate platforms of northeastern and east-central Mexico, *in* Simo, J.A., Scott, R.W., and Masse, J.P., eds., Cretaceous Carbonate Platforms: American Association of Petroleum Geologists, Memoir 56, p. 35–50.

Zepeda-Martinez, M.C., 2013, Estratigrafía y sedimentología de la Sierra del Tentzo, Estado de Puebla, México [Undergraduate thesis]: Universidad Nacional Autónoma de México, Facultad de Ingeniería, 127 p.

Received 13 May 2015; accepted 19 January 2016.

CAPÍTULO 4.

Adquisición temprana de la magnetización detrítica remanente y tardía de la magnetización química en capas rojas: un ejemplo en la Formación Zicapa en el sur de México.

Sierra-Rojas, M. I. and Molina-Garza, R. S, 2017, Detrital and Early Chemical Remanent Magnetization in redbeds and their rock magnetic signature: Zicapa Formation, southern Mexico, Geophysical Journal International, Accepted manuscript.

Contribuciones individuales:

Maria Isabel Sierra-Rojas: Revisión bibliográfica. Trabajo de campo, levantamiento de columnas estratigráficas, toma de datos estructurales, toma de muestras paleomagnéticas, orientación de nucleos paleomagnéticos. Preparación de muestras y obtención de datos paleomagnéticos y de magnetismo de roca en el laboratorio, desmagnetización por campos alternos y térmica, obtención de curvas termomagnéticas, determinación de parámetros de histéresis. Procesado e interpretación de datos paleomagnéticos, procesado e interpretación de datos de magnetismo de rocas, análisis petrográficos. Escritura del manuscrito.

Roberto Molina-Garza: Planteamiento del problema, trabajo de campo, toma de muestras paleomagneticas y asesoría en obtención de datos de campo. Asesoría en procesado de datos paleomagnéticos y de magnetismo de rocas. Interpretación de datos paleomagnéticos y magnetismo de rocas, asesoría en la escritura del manuscrito y elaboración de figuras.

Geophysical Journal International

Geophys. J. Int. (2018) **213,** 1701–1719
Advance Access publication 2018 February 23
GJI Geomagnetism, rock magnetism and palaeomagnetism

doi: 10.1093/gji/ggy076

Detrital and early chemical remanent magnetization in redbeds and their rock magnetic signature: Zicapa Formation, southern Mexico

Maria Isabel Sierra-Rojas and Roberto Stanley Molina-Garza

Centro de Geociencias, Universidad Nacional Autónoma de México, Campus Juriquilla, Boulevard Juriquilla 3001*, Querétaro* 76230*, Mexico.*
E-mail: misierra@geociencias.unam.mx

Accepted 2018 February 22. Received 2018 February 6; in original form 2017 June 5

SUMMARY

Poles from continental redbeds are a large fraction of the world's palaeomagnetic database. Nonetheless, the time of acquisition and origin of the remanent magnetization of redbeds has been long debated. We report palaeomagnetic data, rock magnetic data and microscope observations for Lower Cretaceous redbeds in southern Mexico. These data allow us to discriminate between the hysteresis properties of remanent magnetizations of detrital and chemical origin, and to establish the early origin of a chemical remanence. Red sandstones of the Zicapa Formation contain a multicomponent remanence revealed by thermal demagnetization, and consisting of three stable components with partially overlapping laboratory unblocking temperatures of $<250\ ^{\circ}$C, $\sim$300 to $\sim$500 $^{\circ}$C and $>600\ ^{\circ}$C, (low, intermediate and high temperature, respectively). They are interpreted as a viscous remanence residing in detrital magnetite, a chemical remanence residing in authigenic hematite and a depositional remanence residing in detrital hematite, respectively. The low-temperature component is nearly parallel to the recent dipole field. The tilt-corrected overall site means of the intermediate (chemical) and high temperature (depositional) components are indistinguishable (Dec $= 282.0^{\circ}$, Inc $= 12.4^{\circ}$, $k = 13.33$, $\alpha 95 = 10.1^{\circ}$, $N = 17$, for the intermediate temperature; and Dec $= 272.5^{\circ}$, Inc $= 16.5^{\circ}$, $k = 14.04$, $\alpha 95 = 11$, $N = 14$, for the high temperature). Elongation/inclination analysis suggests that depositional and chemical components require applying an $f =$ factor of approximately 0.4. Both of these components define a magnetic polarity zonation, but the polarity of the chemical and detrital components may or may not be the same. The chemical remanence coincides, more often than not, with the polarity of the depositional remanence of the overlying (younger) strata, suggesting a delay in remanence acquisition of tens to a few hundred ka for the chemical component. Pigmentary and detrital haematite were recognized with microscopic observations. The particle size of haematite ranges from approximately 10 to 300 μm for detrital haematite (martite, specularite and laterite), and from *ca.* 0.2 to 1 μm for pigmentary haematite flakes. The IRM of these rocks can be modelled with components of low coercivity ($H_{1/2}$ between 5 and 10 mT interpreted as detrital magnetite), and components of a wide coercivity range (prevailing $H_{1/2}$ from $\sim$400 to 600 mT interpreted as haematite). Hysteresis ratios show a systematic correlation with demagnetization behaviour, with lower Hcr/Hc values and higher Mrs/Ms values for samples with a dominant chemical component, than form samples with a significant (>40 per cent) depositional component.

Key words: Magnetic mineralogy and petrology; Magnetostratigraphy; Palaeomagnetism; Rock and mineral magnetism.

INTRODUCTION

In the case of redbeds (haematite cemented siliciclastic rocks), controversy exists as to the origin and timing of acquisition of its remanent magnetization. Some authors consider that the natural remanence in redbeds corresponds to a chemical remanent magnetization (CRM) acquired by long-lasting diagenetic processes (Roy & Park 1972; Larson & Walker 1975; Walker *et al*. 1981; Larson *et al*. 1982; Molina-Garza *et al*. 2003). Other authors suggest that the magnetization is provided by ferromagnetic particles, which are oriented with a small bias to the magnetic field during the deposition creating a detrital remanent magnetization (DRM; Elston & Purucker 1979; Tauxe *et al*. 1980; Steiner 1983; Tauxe & Kent 1984; Maillol & Evans 1993; Garces *et al*. 1996; Kruiver *et al*. 2001;

Kodama & Dekkers 2004). Recognizing the mechanism is important because a DRM may be affected by inclination shallowing, while in principle, a CRM will not. Evidence for a primary magnetization residing in detrital specularite in redbeds is supported by particles with high-temperature exsolution textures, and the observation of inclination shallowing error in thin laminations of tabular grains of specularite (Elston & Purucker 1979). Also, the instability of the magnetization that resides in pigmentary haematite compared to magnetization residing in detrital haematite supports the hypothesis that the redbeds characteristic magnetization (ChRM) may be of primary or detrital origin (Collinson 1974; Tauxe *et al*. 1980; Tauxe & Kent 1984).

There are strong arguments, however, that favour a secondary mechanism of acquisition of magnetization in redbeds (Walker *et al*. 1981). By far the most convincing evidence is found in petrographic observations, where a significant fraction of the iron oxides is authigenic. Textural observations suggest they formed by alteration of primary specularite, magnetite, and other Fe-bearing mineral phases; based on these observations and other palaeomagnetic analyses, it has been proposed that remanence acquisition occurs long after deposition (Walker *et al*. 1981; Larson *et al*. 1982; Whidden *et al*. 1998; Beck *et al*. 2003).

Conglomerate and other field tests, as well as magnetostratigraphy in redbeds (Liebes & Shive 1982; Steiner 1983; Molina-Garza *et al*. 1989, 1991, 2003; Tan *et al*. 2007), have shown that the ChRM of redbeds can be both chemical and depositional in origin. The diagenetic processes responsible for the growth of haematite as an authigenic magnetic mineral, however, may be early and sandstones can be magnetized shortly after deposition. In his summary of the redbed controversy, Butler (1998) suggests that the reliability of the magnetization record in redbeds must be considered in a case-by-case basis evaluating, for instance, the relative contributions to the remanence from pigmentary and specular haematite.

The study of the delay in acquisition of magnetization in sedimentary rocks is of importance for magnetostratigraphy and reversal transition studies, as well as investigation of short geomagnetic field events within longer chrons. The delayed magnetization can be considered in some cases a remagnetization, and it depends on whether an earlier magnetization is being replaced by a new one or whether it is the ChRM of the sediment not corresponding to the stratigraphic age (Van der Voo & Torsvik 2012).

The aim of this study is to present palaeomagnetic and rock magnetic data for a Lower Cretaceous redbeds sequence in southern Mexico, in which the natural remanence is interpreted as a combination of a DRM and an 'early acquired' CRM, both residing in haematite. For that purpose, detailed step-wise thermal demagnetization, as well as rock magnetic experiments, were performed. The results suggest that the relative contributions from DRM and CRM vary within a sandstone bed and between beds. A magnetostratigraphic record also suggests that acquisition of a CRM is delayed by tens to hundreds of ka.

It is known that changes in polarity can be recorded by different magnetic phases with variations in the lock-in depth for pDRM or time of precipitation for CRM, indicating that different magnetic phases located in the same stratigraphic level did not acquire their magnetization simultaneously because they did not form at the same time. In the case of the record across transitions of magnetic polarity, the different phases may record two different polarities in the same specimen. An explanation for the presence of both normal and reverse polarities in one specimen is that a polarity is locked-in prior to the transition, being recorded by an early detrital phase, and this is followed by an early chemical magnetization in an authigenic phase formed after the transition. Here we present such a case, where two polarities are recorded in the same stratigraphic level in redbeds. One magnetization corresponds to a DRM that resides in specular haematite of high unblocking temperature (>600 °C), and the other to a CRM residing in pigmentary haematite of intermediate unblocking temperature (250–500 °C).

GEOLOGIC FRAMEWORK

The lower Cretaceous of southwestern Mexico is characterized by a record of magmatism and sedimentation in a volcanic setting, interpreted as allochthonous island arc (s) (Talavera-Mendoza *et al*. 2007), a para-autochthonous arc system (Cabral-Cano *et al*. 2000, Martini *et al*. 2010), or a continental arc (Sierra-Rojas & Molina-Garza 2014). The Lower Cretaceous Zicapa Formation is characterized by the presence of fine- to coarse-grained siliciclastic rocks interbedded with intervals of limestone and calcareous sandstone, deposited in continental to marine transitional environments. The Zicapa Formation contains a record of contemporaneous intermediate calc-alkaline volcanism (Sierra-Rojas & Molina-Garza 2014).

Sedimentology

The data presented here correspond to the Zicapa Formation near its type locality in San Juan de las Joyas, Guerrero State, Mexico (Fig. 1b). The section studied is on the western flank of a latest Cretaceous antiform with a Palaeozoic schist as the oldest unit (Fig. 1b). Here, the Zicapa Formation overlies Middle Jurassic quartz-rich siliciclastic strata of the Tecocoyunca Group, which together with volcanogenic sediments and basement rocks, are the primary source of its detritus. The Zicapa Formation has been divided among five members (Sierra-Rojas & Molina-Garza 2014), but sampling was concentrated in the middle Ajuatetla Member (Fig. 2).

The Ajuatetla Member overlies shallow marine packstone and grainstone beds of the San Juan de las Joyas Member in a transitional contact, and it is characterized by a coarsening-upward section with fine-grained heterolithic beds with ripple cross-laminations. The lack of erosional contacts suggests a continuous and homogeneous sedimentation rate. The siltstones are red to purple in tabular beds with *Thalassinoides*; some conglomeratic beds at the top of this member show trough cross-beds, and are associated with coarse-grained sandstone. A shallow siliciclastic shelf with foreshore deposits is interpreted as the sedimentary environment for this member (Sierra-Rojas & Molina-Garza 2014).

The sandstones of the Ajuatetla Member are litharenites and lithic arkoses, with abundant clasts of metamorphic polycrystalline quartz, monocrystalline quartz, feldspar, albite, metamorphic and felsitic grains. The age range of the deposition for the Ajuatetla Member is determined by the maximum depositional age of a lithic sandstone near the base of the Zicapa Formation of 149 ± 1 Ma (youngest concordant zircon), and the near-depositional age of the volcaniclastic sandstone in the overlying San Andres Member of 133 ± 3 Ma (Sierra-Rojas & Molina-Garza 2014).

SAMPLING AND METHODS

For this study, we sampled a sequence of coarse to very fine lithic sandstones tinted purple to reddish brown. A sequence 190 m thick was described and sampled in the eastern flank of an anticline with an axial plane oriented N20°E (Fig. 1b) and sampled at a

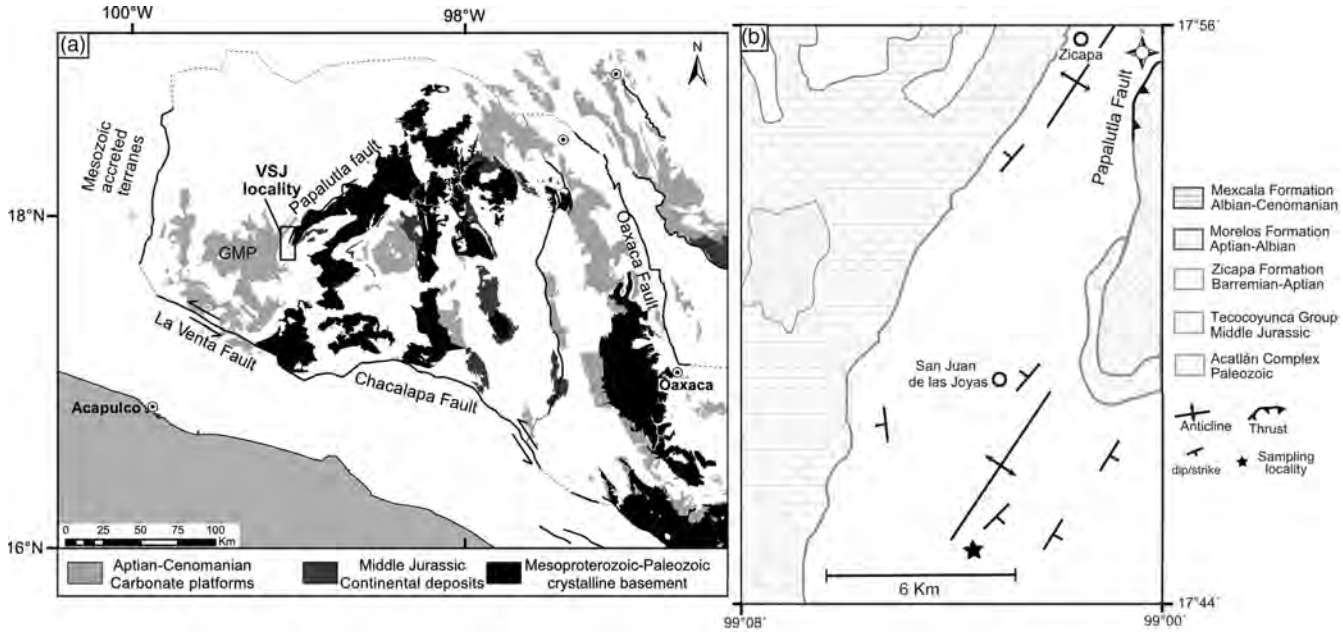

Figure 1. (a) Localization of the San Juan de las Joyas (VSJ) area and sampling sites in a map showing the distribution of Cretaceous strata in southern Mexico. GMP: Guerrero-Morelos platform. (b) Geologic map of the area of the San Juan de las Joyas locality.

total of 19 sites (Fig. 2b). Six to eight samples were drilled with a gasoline portable drill obtaining 2.5 cm diameter cores 6–12 cm deep; the samples were oriented in the field with magnetic and solar compasses, as well as an inclinometer. Each site was collected from a single bed, and site spacing depended on the availability of suitable material in the section. In the laboratory, the cores, 117 in total, were cut into 2 cm long specimens, obtaining two to four specimens for sample. All magnetic measurements were made at the palaeomagnetic laboratory of the Centro de Geociencias, UNAM, at the Juriquilla campus.

The natural remanent magnetization (NRM) was measured using a JR-5 spinner magnetometer housed in a shielded room. A set of samples, one for each site, were subjected to progressive alternating field (AF) pilot demagnetization tests, using an LDA-3A Demagnetizer (AGICO), exposing the samples to inductions from 1 to 100 mT in steps not larger than 10 mT. After the AF pilot test, the samples were subjected to thermal demagnetization in air in a thermal demagnetizer TD-48 SC (ASC-Scientific). The specimens were progressively heated from room temperature to 500 °C every 50 °C and from 500 to 650 °C in 25 °C steps. After every heating step the NRM and magnetic susceptibility were measured for each one of the specimens. For the visualization and analysis of the results of the demagnetization experiments, we used orthogonal demagnetization diagrams (Zijderveld 1967) and equal-area stereographic projections (Figs 3 and 4). The remanence vector directions were determined in each specimen using principal components analysis (Kirschvink 1980), and then the mean for each site was calculated; the site means were calculated assuming the distribution of directions of Fisher statistics. The data-set was further examined to evaluate the fit to a Fisher distribution.

Rock magnetic experiments were used to characterize magnetic carriers (a minimum of one specimen per site). Hysteresis parameters (Ms, Mrs, Hc and Hcr), isothermal remanent magnetization (IRM) and backfield curves of saturation of IRM were determined with a Princeton Measurements Corp. MicroMag 2900 vibrating sample magnetometer. The IRM acquisition curves were modelled by the first derivative method, allowing one to infer the magnetic mineralogy of a sample based on its coercivity spectra (Kruiver *et al*. 2001). Thermomagnetic curves were obtained in a custom-made Curie balance using approximately 3.5 g of pulverized sandstones in a DC field of 0.4 T in air, with heating-cooling rates of 30–40 °C min^{-1}. A Lowrie test was performed applying fields of 3, 0.5 and 0.15 T along three orthogonal directions. Then the samples where thermally demagnetized up to 660 °C in 50 and 20 °C steps. The petrography of samples was studied in thin sections with a petrographic microscope of polarized light (Olympus Bx-51), and textures of magnetic oxides were studied with a scanning electron microscope (SEM).

RESULTS

Palaeomagnetism

AF demagnetization caused a small change in the NRM, except in very few sites, leading one to conclude that most of the magnetization resides in phases of high coercivity such as haematite. In 80 per cent of sites, AF demagnetization resulted in the removal of a north-directed remanence. Thermal demagnetization revealed that the remanent magnetization in the rocks of the Zicapa Formation is relatively complex, with a multivectorial behaviour. Some of the rocks show two-components (Figs 3a and b); the component removed at low temperatures is designated as low-temperature component (LTC). It has a north to northwest-directed declination and is of moderate positive inclination. This component is generally completely removed after heating to 200 °C. An abrupt decay upon heating to 100 °C was observed at two sites (Fig. 3b) where this component is prominent. A univectorial decay is observed after removing the LTC, showing distributed laboratory unblocking temperatures between 250 °C and >650 °C (Fig. 3); most of the specimens show a linear trend to the origin. The magnetization component defined in this interval of demagnetization is northwest to west-northwest directed with moderate positive inclination, or its antipode of negative inclination and southeast declination (Figs 3d and e; VSJ9A2, VSJ13B). Upon further examination of the unblocking temperatures is evident that in some cases

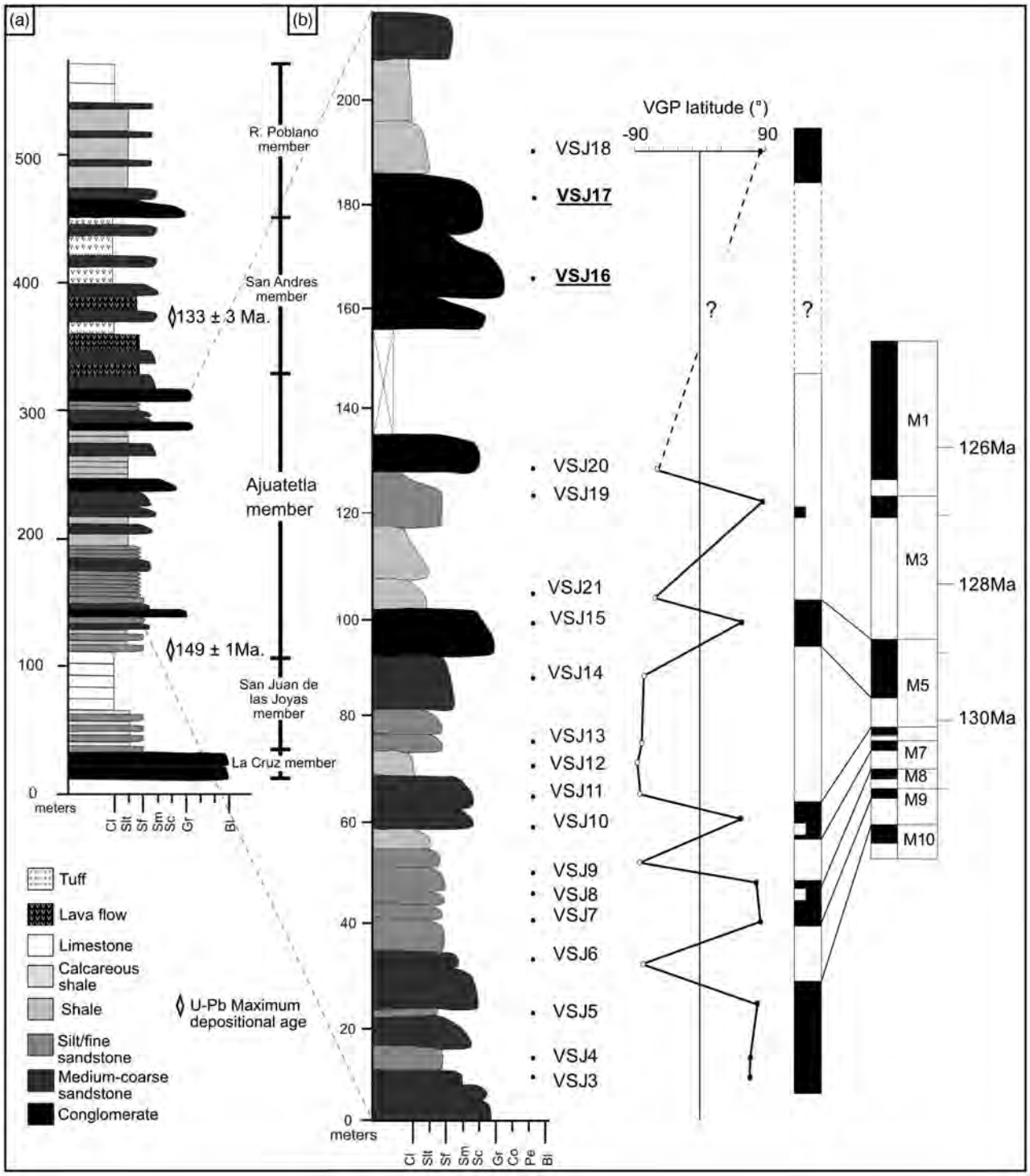

Figure 2. (a) A generalized column of the Zicapa Formation. (b) Stratigraphic section and magnetostratigraphy of the Ajuatetla Member, Zicapa Formation (base: 17.77457, −99.0813; top: 17.76489, −99.08405). The location of the sampling sites is shown in each stratigraphic level. We also include a plot of virtual geomagnetic pole (VGP) latitude versus stratigraphic level. The black bars represent normal polarity intervals and the white bars reverse polarity intervals. The magnetic polarity zonation is correlated with the geomagnetic scale for the Early Cretaceous (Ogg 2012).

the remanence decays primarily between approximately 300 and 600 °C (Fig. 3b), while others show greater decay at higher temperatures above 600 °C (Figs 3d and e).

Some of the samples show more complex magnetization records, wherein at least three magnetizations components contribute to the NRM (Fig. 4). An LTC is again north to north-west directed and of moderate positive inclination, of obout 40 °C; again, this is removed by heating to 200 °C. A second component is of intermediate laboratory unblocking temperature (intermediate-temperature component, ITC), and is defined between 250 °C and approximately 500 °C; this component is northwest directed and moderate positive inclination, or its antipode. The high-temperature component

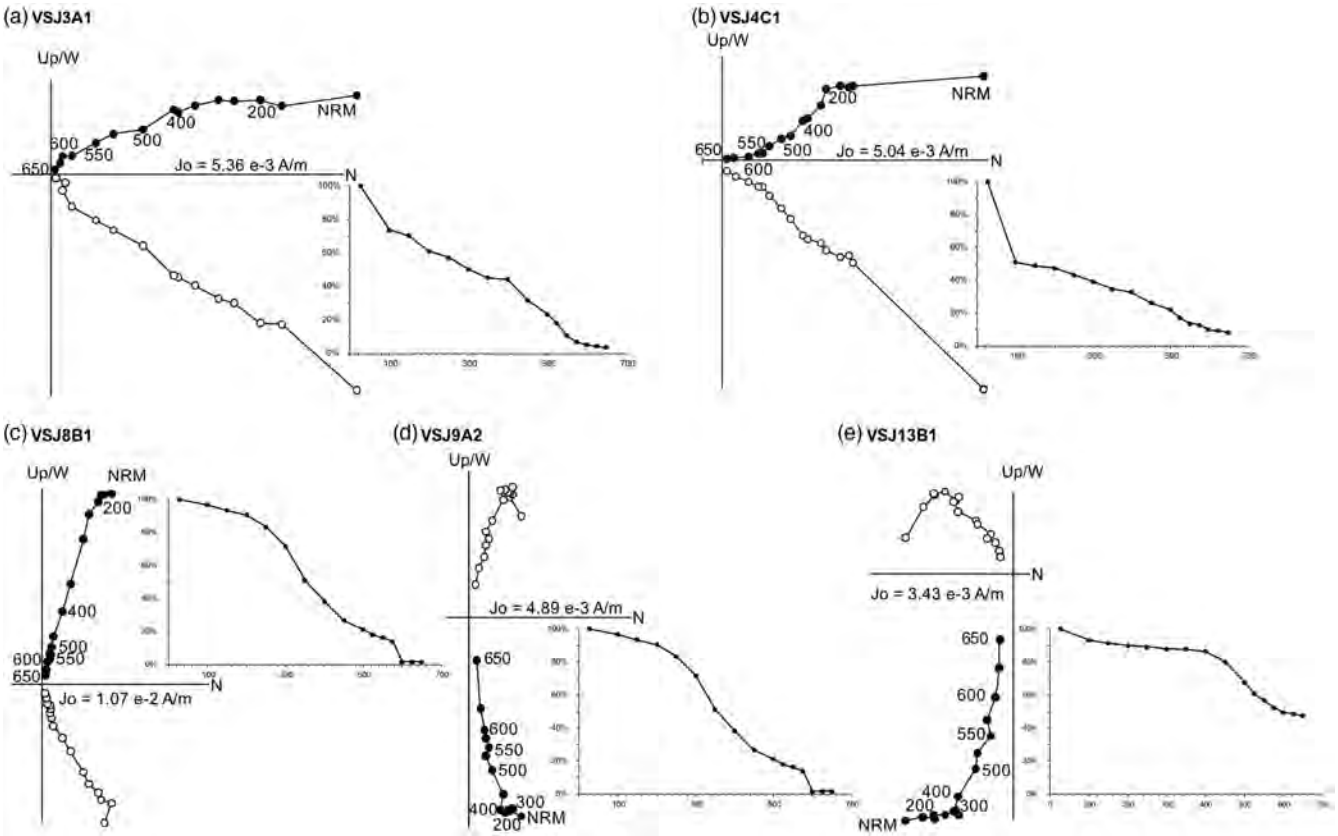

Figure 3. (a–e) Representative examples of orthogonal demagnetization diagrams and evolution of the remanence intensity (normalized with respect to the maximum J0) during thermal demagnetization. The samples show apparent univectorial or two NRM components. The characteristic magnetization, defined in the range 250 to over 650 °C, is overprinted by a small secondary component, which is mostly north-directed and of positive inclination (a and b). Closed (open) circles correspond to the projection of the NRM vector onto the horizontal (vertical) plane.

(HTC) is defined in temperatures over 600 °C, and it is west to west-northwest directed with a positive moderate inclination (or its antipode). Thus two near parallel components were recorded in some specimens, and two antipodal components were recorded in others. Occasionally the demagnetization diagrams show curved trajectories (Fig. 4c), suggesting that unblocking temperature spectra of the three components overlap to some degree.

Mixed polarities are observed within a single site for the ITC, such as at VSJ5, VSJ6, VSJ12, VSJ13, VSJ19 and VSJ20; HTCs, in contrast, are of uniform polarity within a site. When samples are analysed in a stratigraphic context, important details are observed, as follows. If adjacent sites are of opposite polarity, the ITC more often than not corresponds to the direction of the HTC of the overlying site. This behaviour is observed, for instance, at siteVSJ6 where the ITC is of mixed but predominantly normal polarity, HTC is of reverse polarity, while HTC is normal at the overlying site VSJ7. Similarly, the polarity of the HTC of VSJ14 is of reverse polarity, while the ITC is a normal polarity corresponding to the polarity of the HTC of overlying site VSJ15 (Fig. 5). Yet another example is VSJ19, where the ITC is of mixed but mostly reverse polarity, the HTC is of normal polarity, and the ITC corresponds to the reversed polarity of the HTC of VSJ20 above. After these observations were made, we calculated the directions of vectors corresponding to unblocking temperatures of the ITC and the HTC at each stratigraphic level. We made this calculation even if the components appear colinear (as in Fig. 3). When mixed polarities occur in the ITC we inverted directions to the dominant polarity in the site to report a single polarity. Results of these calculations are in Tables 1 and 2.

The polarity zonation in all the Ahuejutla Member sites was determined from end-point directions for the HTC, and occasionally demagnetization trajectories. For the mean direction, four sites were excluded due to large within-site dispersion, an insufficient number of samples, or an unstable behaviour during demagnetization. Nine magnetic polarity zones were recognized in the locality (Fig. 2b).

Overall means were calculated using Fisher's statistics (Fisher 1953) inverting reverse polarity magnetizations. The low-temperature component of magnetization in all sites is close to the present-day field direction at the sampling location, so it is interpreted as viscous remanent magnetization and will not be further discussed. The ITC and HTC of magnetization form two indistinguishable populations, both with bipolar distributions (Tables 1 and 2). The ITC and the HTC group means are, *in situ*, west-directed and of moderate positive inclination (Fig. 6) that become moderately shallow after tilt correction. The tilt corrected means of the ITC and HTC components are: Dec = 282°, Inc = 12.4° ($k = 13.33$, $\alpha 95 = 10.1°$, $N = 17$) and Dec = 272.5°, Inc = 16.5° ($k = 14.04$, $\alpha 95 = 11$, $N = 16$), respectively. In tilt corrected coordinates both groups pass the reversal test of McFadden & McElhinny (1990) with a positive reversal test classification or 'Rb' (Tables 1 and 2). The ITC and HTC means are statistically indistinguishable.

Elongation–inclination correction

A flattened directional distribution of sample directions suggests the possibility of an effect of sedimentary shallowing of the inclination. We performed an elongation–inclination (*E*/*I*) correction in

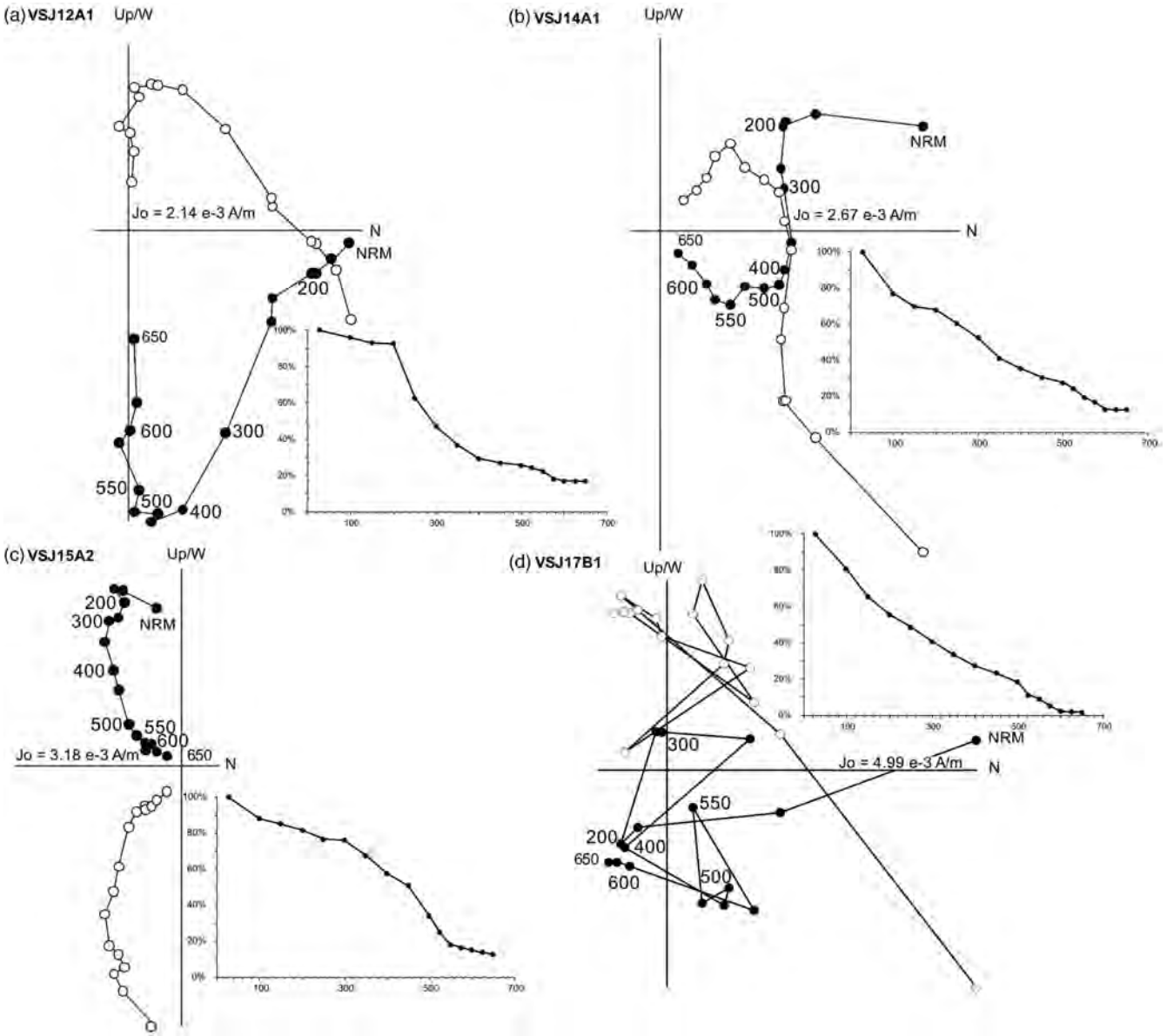

Figure 4. Examples of orthogonal demagnetization diagrams and evolution of the remanence intensity (normalized with respect to the maximum J0) during thermal demagnetization for samples with multivectorial behaviour. (a–c) Samples with three components showing a near present-day field magnetization (NRM-200 °C), an intermediate laboratory unblocking temperature magnetization (250–400 °C), and a high-temperature magnetization component (>575 °C). (d) VSJ17B shows a well-defined low unblocking temperature component and an erratic behaviour after 250 °C. Symbols as in Fig 3.

both ITC and HTC to evaluate the effect of inclination shallowing (Tauxe & Kent 2004). For the analysis, we used 114 sample directions for the ITC and 110 for the HTC (Figs 7a and d). The *E*/*I* technique can give inaccurate results if there are vertical axis rotations between sites, but these rotations are considered unlikely because a continuous section of near uniformly dipping strata was sampled. For the ITC the original distribution of samples directions shows a mean principal eigenvector of $D = 283.1^{\circ}$, $I = 13.5^{\circ}$ with an initial eccentricity of $E = 1.816$ and an elongation to the NW or SW. The *E*/*I* analysis determined a crossing-point model for the data (Figs 7b and c) predicting inclination of $I = 28^{\circ}$, which represents the inclination versus elongation pair more consistent with the geomagnetic model; this indicates a flattening factor of $f = 0.41 + 0.34/-0.49$ and an eccentricity of $E = 2.3272$. The HTC original distribution is also elongated to the NW and SW and shows mean eigenvector direction of $D = 277.8^{\circ}$, $I = 14.7^{\circ}$ and an initial eccentricity of $E = 1.617$. The model predicts an inclination $I = 34.6^{\circ}$ (Figs 7e and f), eccentricity $E = 2.1412$, and a flattening factor $f = 0.4 + 0.32/-0.55$. In both cases there is a greater dispersion in declination than inclination, as observed when flattening is suspected. The overall means of the ITC and HTC sample directions after correcting for inclination shallowing with an *f*-factor of 0.4 are $D = 282.0$, $I = 28.2^{\circ}$, and $D = 272.5$, $I = 36.5^{\circ}$, respectively.

When the overall means are compared with the expected direction, assuming stability with respect to the North America craton and using the reference pole of Torsvik *et al.* (2012), they are discordant; the discordance is primarily in declination. Using the directional-space approach to analyse the vertical-axis rotations and the latitudinal motions from palaeomagnetic directions (Beck 1980; Demarest 1983), the ITC indicates R and F (rotation and flattening

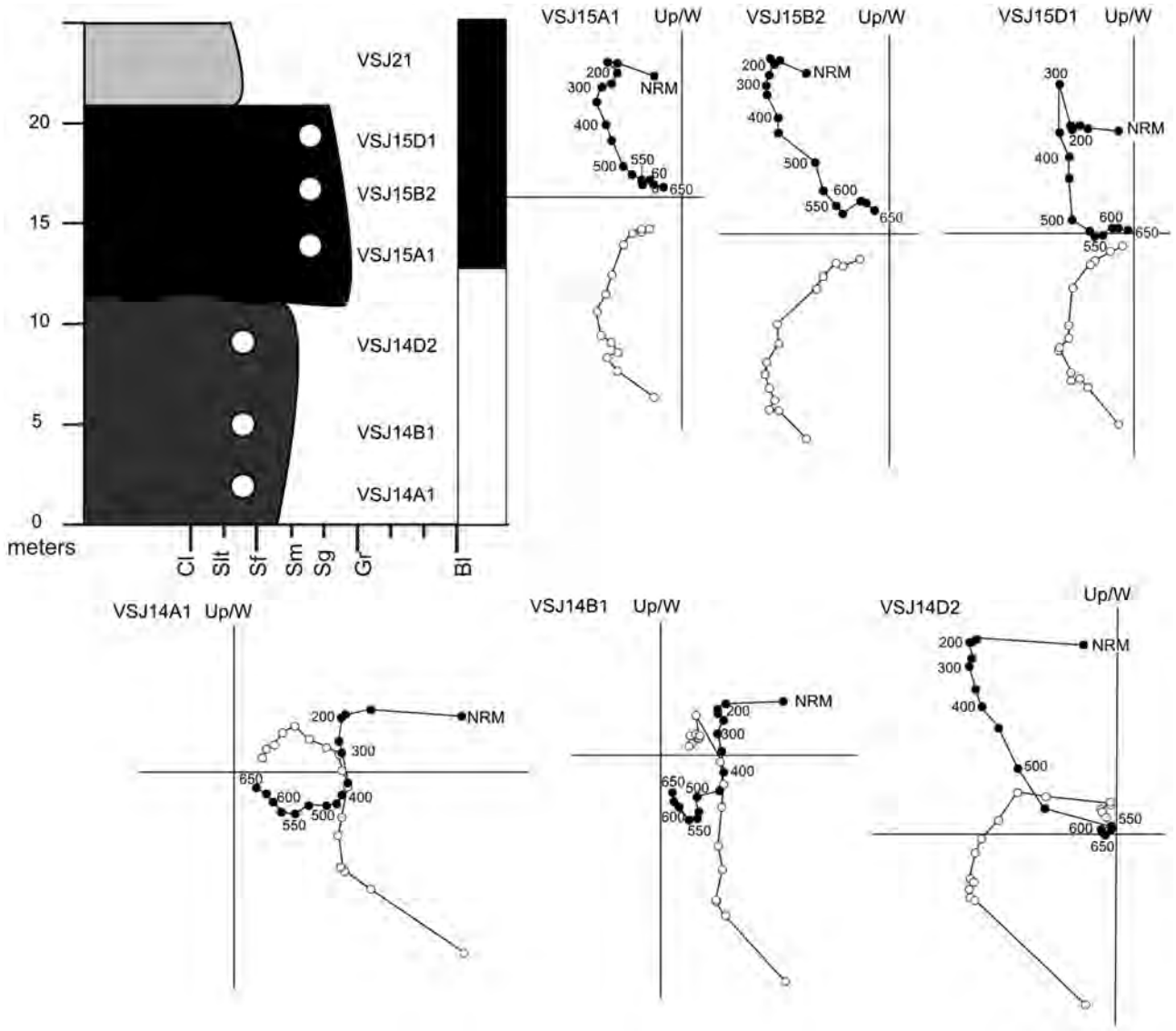

Figure 5. Interval with polarity transition from reverse to normal of the high-temperature component. In the lower site (VSJ14) the HTC (DRM) is reverse in all three samples and the ITC (CRM) is normal, as the HTC of the overlying site.

parameters) of -58.6 ± 10.1 and -16.8 ± 12.7. The HTC indicates values of R and F of -69.2 ± 10.1 and -7.7 ± 13.0. The F value for HTC is not discordant in inclination.

Rock magnetism

The results of AF and thermal demagnetization experiments suggest that the remanence resides in one or more magnetic phases. For instance, resistance to AF demagnetization and the observation of components that reside in intermediate (250–500 °C) and high maximum unblocking temperatures (600–650 °C) suggest that there are varying contributions to the remanence from possibly fine-grained authigenic and coarser detrital haematite (Collinson 1974). This hypothesis is further explored in rock magnetic experiments.

Representative thermomagnetic curves for samples of pulverized sandstones are shown in Fig. 8. The cooling cycle shows that there are mineralogical changes caused by laboratory heating of the samples, possibly oxidation because the curves are not reversible and decrease their magnetic moment upon cooling. In the heating cycle, the inflection at ∼580 °C confirms the presence of magnetite in some samples. All the samples are characterized by a change in the slope above 620 °C associated with the Neel/Curie temperature of haematite with a small degree of cation substitution (assumed to be both pigmentary and detrital hematite). In the sample of Fig. 8(b) the intensity of magnetization increases upon cooling, but very slightly. There are no signs of maghemite inversion, we, therefore, conclude that magnetite and haematite are present in varying proportions, but magnetite may be absent (e.g. VSJ3). Again, considering the low saturation magnetization of haematite compared to magnetite, it is evident that, when present, by volume magnetite occurs in significantly smaller proportion.

Examples of hysteresis acquisition curves are shown in Fig. 9. The loops show a variety of shapes, but almost all of them are constricted in the middle section of the loop and widen in the lower and upper sections; this morphology has been defined as a 'wasp-waisted' hysteresis loop (Roberts *et al*. 1995; Tauxe 1996). We distinguish three types of curves in terms of the geometry of the

Table 1. Palaeomagnetic data for intermediate-temperature component (ITC) obtained from 350 to 600 °C. Inclination before *E/I* correction.

		In situ					Tilt corrected				
Samples	*n/N*	Dec(°)	Inc(°)	*k*	α_{95}	Dip/Strike	Dec(°)	Inc(°)			
VSJ18	7/7	275.8	27.4	79.2	6.8	175, 5	275.6	22.4			
VSJ17*	2/2	102.2	−21.6	–	–	156, 17	109	66.2			
VSJ20	3/10	58.6	−52.8	25.9	24.7	145, 16	59.2	−37.8			
VSJ19	6/8	87	−30	39.6	10.8	145, 15	84.3	−16.4			
VSJ21	3/3	289.8	21.2	38.4	2.9	85, 20	281.2	26.3			
VSJ15	3/3	253.4	40.1	58.1	16.3	221, 30	267.3	20.7			
VSJ14	4/6	263.2	44.8	83.5	10.1	221, 30	276.5	21.8			
VSJ13	3/4	110.1	−28.6	39.8	19.8	221, 30	112.7	−0.3			
VSJ12	11/11	101.2	−32.3	13.9	12.7	221, 30	106	−5.5			
VSJ11	6/8	86.2	−26.4	15.7	17.4	221, 30	91.8	−3.9			
VSJ10	5/5	298	15.4	42.4	11.9	191, 30	297.8	−13.4			
VSJ9	8/9	92.5	−33.5	42.1	8.6	191, 30	93.9	−3.8			
VSJ8	8/8	289.7	26.7	75.3	6.4	191, 30	288.8	−3			
VSJ7	4/4	287.3	27.4	400.1	4.6	191, 30	286.6	−2.4			
VSJ6	6/9	119.8	−42.4	26	13.4	231, 15	123.4	−28.2			
VSJ5	4/4	257.2	39.1	7.3	36.4	201, 30	264.7	12.9			
VSJ4	9/9	295	29.2	49.6	7.4	201, 30	294.5	−0.7			
VSJ3	6/8	336.1	44.9	47.3	9.8	201, 30	323.6	21.2	**k**	α_{95}	**n**
Mean normal	10	284.5	33.5	14.46	13.1		285.5	11.1	14.09	13.3	10
Mean reverse	7	94.8	−36.3	21.84	13.2		96.8	−14.3	11.69	18.4	7
Overall mean	**17**	**276.9**	**37.3**	**8.38**	**13.1**		**282**	**12.4**	**13.33**	**10.1**	**17**

Table 2. Palaeomagnetic data for high-temperature component (HTC) obtained from 600–650 °C. Inclination before E/I correction.

			In situ				Tilt corrected				
Samples	n/N	Dec(°)	Inc(°)	k	α_{95}	Dip/Strike	Dec(°)	Inc(°)			
VSJ18	4/6	278.6	28.5	95.4	9.5	175,5	278.3	23.5			
VSJ20	8/10	65.5	−50.2	56	7.5	145,16	64.5	−35.2			
VSJ19	4/6	276.1	29.6	7.8	35.2	145,15	272.5	17			
VSJ21	3/4	83.3	−41.1	6.9	46	85,20	67.8	−35.7			
VSJ15	3/3	209.7	48.9	17.9	30	221,30	243.4	45.8			
VSJ14	3/5	65.6	−39.5	11.1	5.8	221,30	81.4	−23			
VSJ13	5/5	94.8	−21.1	25.3	15.5	221,30	97.5	3.7			
VSJ12	9/9	88.4	−32.7	147.9	4.2	221,30	95.8	−9.1			
VSJ11	4/8	89.6	−21.3	166	7.2	221,30	92.9	2			
VSJ10	2/3	129.5	−26.7	–	–	191,30	126.2	0.2			
VSJ9	8/8	95.6	−31.8	62.6	7.1	191,30	96.4	−1.9			
VSJ8	7/7	281.1	37.3	15.4	17.6	191,30	281.1	7.4			
VSJ7	4/4	274.6	42.5	28.8	17	191,30	276.2	12.6			
VSJ6	8/9	98.2	−30.2	21.3	12.6	231,15	102.7	−18.8			
VSJ5∗	1/5	256	37	–	–	201,30	263.2	11.2			
VSJ3∗	2/8	294	48	–	–	201,30	293.1	18	**k**	α_{95}	**n**
Mean normal	5	267.8	40	12.22	22.8		272	21.6	17.18	19	5
Mean reverse	9	91.2	−34	19.82	11.9		92.8	−13.6	12.06	15.5	9
Overall mean	**14**	**90.1**	**−36.1**	**17.3**	**9.8**		**92.5**	**−16.5**	**14.04**	**11**	**14**

loops as well as hysteresis parameters (Özdemir & Dunlop 2014). The first type is represented by only one sample, VSJ17 (Fig. 9c), with low bulk coercive force, Hc (0.013 T), low remanent coercive force, Hcr (0.0039 T), and an incipient 'wasp-waisted' loop. This sample is near saturation at inductions of approximately 1 T, thus the low coercivity is not solely caused by a cubic phase such as magnetite; magnetite is, however, evidently present. Sample VSJ17 shows a rather steep IRM acquisition curve with up to 70 per cent of the remanence acquired below 0.1 T, but the sample does not reach saturation until it is exposed to inductions of approximately 1 T (see the discussion of IRM below). Therefore, the low coercivity observed in the hysteresis loop does not indicate the presence of a single cubic phase such as magnetite of varying grain-sizes; the hysteresis loop suggests that magnetite overwhelms the signal from hematite. The second and more common curve type is the typical 'wasp-waisted' hysteresis loops, with coercive force values ranging from 0.105 to 0.319 T, and ratios of remanent saturation to saturation magnetization (Mrs/Ms) of up to 0.53 (Figs 9d–f). The third curve type corresponds to the 'goose-neck' hysteresis loops (VSJ4, Fig. 9a) with the high Hc value (0.3 T). Type 2 and 3 curves are far from saturation even at inductions of 2 T; these curves also show high Mrs/Ms values between 0.27 to 0.58 and Hcr/Hc ratios of approximately 1.5 to 3.5 (Fig. 10), which are consistent with SD haematite behaviour (Özdemir & Dunlop 2014).

As we considered the ChRM to reside primarily in hard magnetic phases with different grain-size (and inherently different coercivity), a components analysis of the IRM is necessary to properly identify and quantify the contributions from different magnetic carriers. We modelled the IRM acquisition curves (Kruiver *et al.* 2001) for the sandstones of the Zicapa Formation. In all samples, IRM

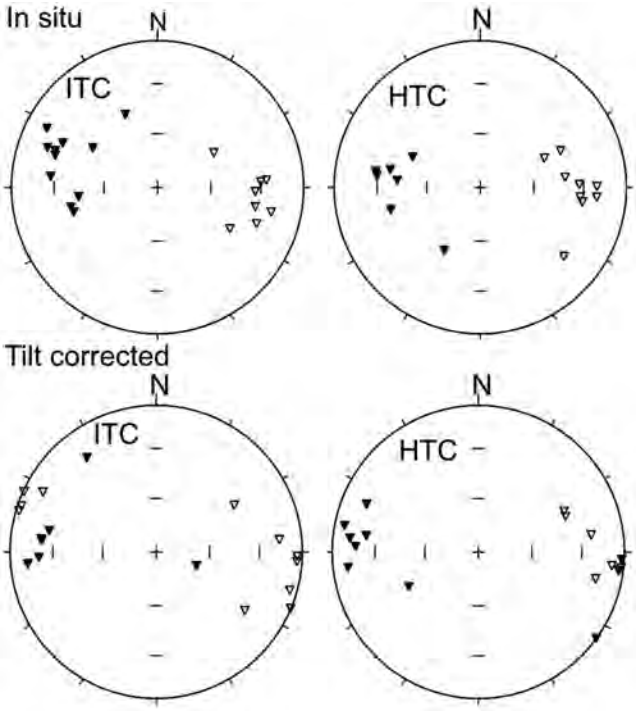

Figure 6. Site means *in situ* (above) and tilt corrected (below) directions isolated components of the VSJ locality. Left: site means of the intermediate-temperature component (ITC). Right: site means for the characteristic remanent magnetization (ChRM) of the high-temperature component (HTC). Close triangles for normal polarity and open triangles for reverse polarities.

acquisition curves were modelled with more than one component (Fig. 11). Generally, the dominant mineral phase shows high coercivities (H1/2 = ∼500–600 mT), this phase makes generally ∼85 to 90 per cent of the total IRM. In the sample from site VSJ4 (Fig. 11d), the dominant coercivity phase exceeds 800 mT, in agreement with very high Hc values observed in hysteresis experiments.

A very low coercivity phase (<10 mT) is necessary to model some of the curves (Fig 11a). This component may contribute to the IRM as much as 10 per cent, and it most likely contributes to the NRM because it is associated with sites where a large north-directed and positive inclination component was observed. A very small component (<5 per cent of the IRM) with maximum coercivities of approximately 1 and 1.5 T was used to fit the IRM curve in some samples (Figs 11a and c). Finally, a moderately high coercivity component was required to fit most of the curves; it makes generally approximately 10 per cent of the IRM and has a mean coercivity of *ca.* 30–100 mT. This component is present in small proportion at nearly all sites. The low coercivity values of about 30 are consistent with a magnetite-like phase, but coercivities above 50 mT are too high to indicate that they are solely in magnetite (e.g. Dunlop 1986; Sagnotti *et al*. 2006), even uniaxial single-domain magnetite, and it is probably associated with some forms of very fine pigmentary haematite or perhaps maghemite.

The samples modelled with a dominant contribution of the high coercivities (i.e. >400 mT; Fig. 11) are consistent with the results from the thermomagnetic curves and the hysteresis loops, indicating the predominance of haematite. Sample VSJ17 is interesting in that the coercivity values used to model the curve are significantly lower than at other sites (Fig 11a). The high coercivity component of

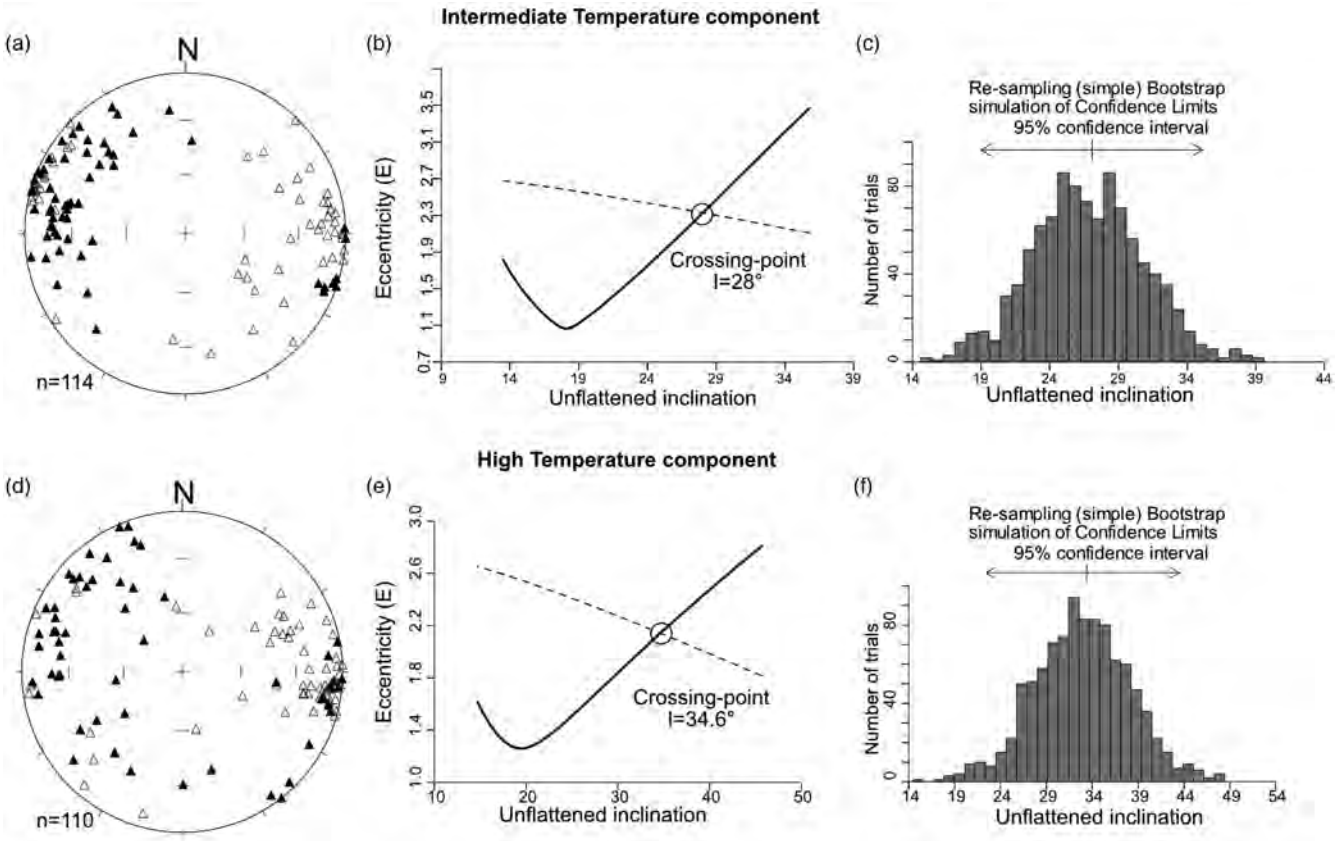

Figure 7. Elongation–inclination correction (Tauxe & Kent 2004) performed at all sites with lithologies that vary from fine-grained to coarse-grained clean sandstones. (a and d). Equal-area projections of the sample directions for the ITC and HTC, respectively. (b and e) Plots of elongation versus inclination of the data in (a) and (d), respectively. (c and f) Histogram of crossing point from 1000 bootstrap simulations of confidence limits.

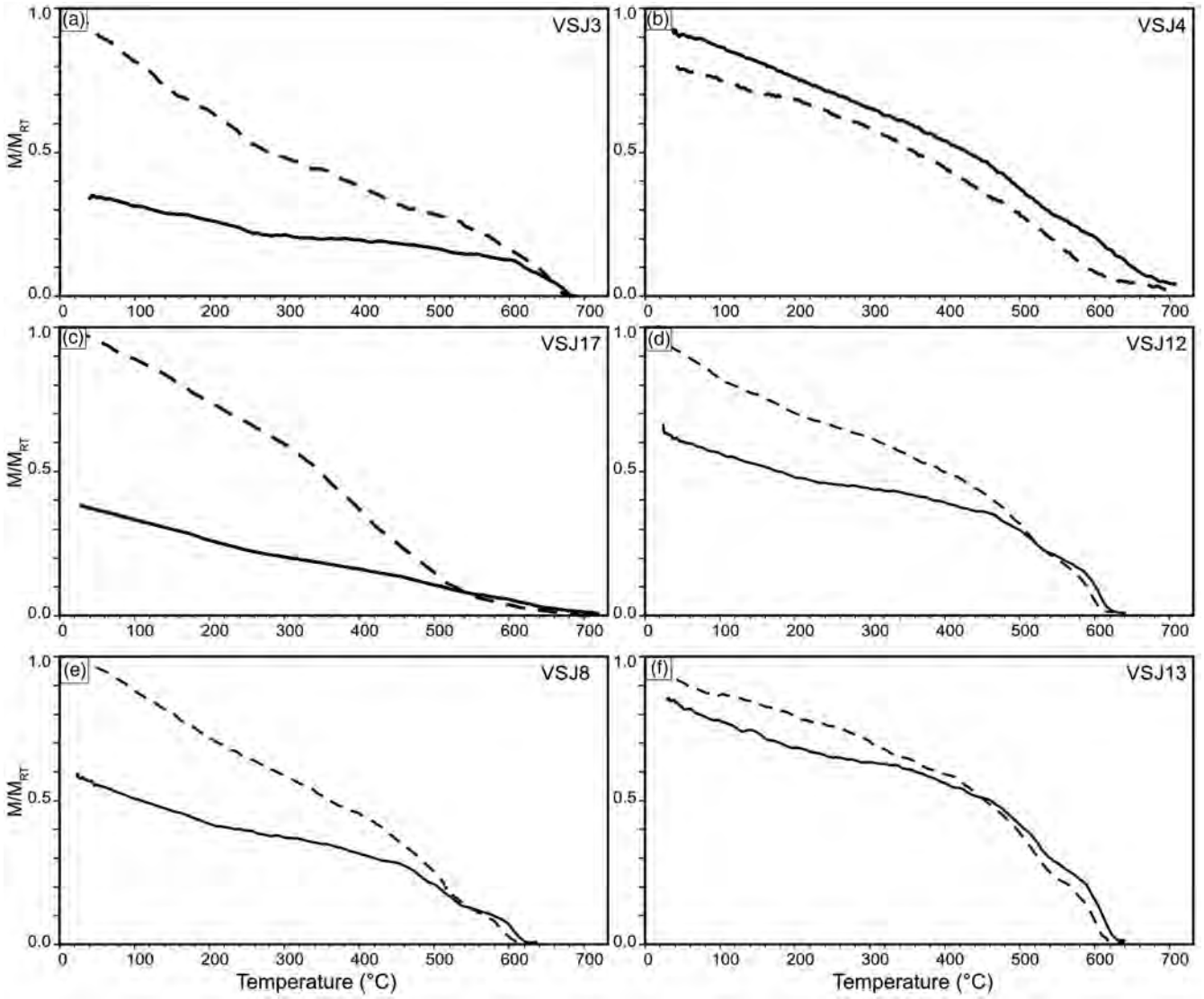

Figure 8. Representative thermomagnetic curves showing the heating cycle in dotted line and the cooling cycle in solid line. All the samples are heated in air from room temperature up to 700 °C. Samples VSJ3, VSJ4 with haematite (a,b), VSJ17, VSJ12, VSJ8, VSJ13 with both magnetite and haematite (c–f).

approximately 500 mT is not required to model the VSJ17 IRM acquisition curve, we used instead of a component with H1/2 = 200 mT. Also, the hysteresis loop is narrower than for other sites (Fig. 9c); despite having a loop associated with a mixture between different coercivities or grain sizes, it presents the lowest Hc and the narrowest loop, and haematite is barely visible in the thermomagnetic curve (Fig. 8c). This sample is also associated with unstable demagnetization behaviour (Fig. 4d), and we failed to isolate a HTC at this site.

Lowrie test

The rock magnetic experiments previously described indicate the presence of a mixture of low and high coercivity magnetic minerals, and suggest the presence of goethite in some samples. In order to better understand the remanence carriers, we performed a Lowrie test to evaluate the presence of goethite, haematite, and magnetite (Lowrie 1990). A subset of nine samples was used to perform the test, applying inductions of 3, 0.5, and 0.150 T in three orthogonal directions using a pulse magnetizer. The specimens were subsequently demagnetized up to 660 °C in 50–20 °C steps. Thermal demagnetization of IRM components reveals that the dominant magnetic phases are of coercivity greater than 150 mT, making (combined) 85 to 98 per cent of the remanence (Fig. 12). In all the samples the IRM components induced at 0.5 and 3 T have distributed laboratory unblocking temperatures between about 200 and 600 °C and a maximum unblocking temperature near 660 °C (Fig. 12). Both the hard and intermediate components (3 and 0.5 T respectively) thus reside in haematite. We observed a hint of goethite in one of the samples analysed (VSJ6, Fig. 12d), with a small decrease of about 15 per cent in the hard IRM component. Goethite is however absent in the other samples analysed. Magnetite is present in most samples but in low concentration. We observed decay of the soft IRM component (<150 mT) at temperatures near 580 °C (it was observed in five of the samples used for the test, Samples VSJ5, and VSJ8, Fig. 12), but clear inflections in the decay curve are not observed in the 550–590 °C range; furthermore, as little as 5 per cent or as much as 30 per cent of the soft component unblocks at temperatures of about 650 °C, and thus resides in haematite. In sample VSJ12 the soft component is less than about 2 per cent of

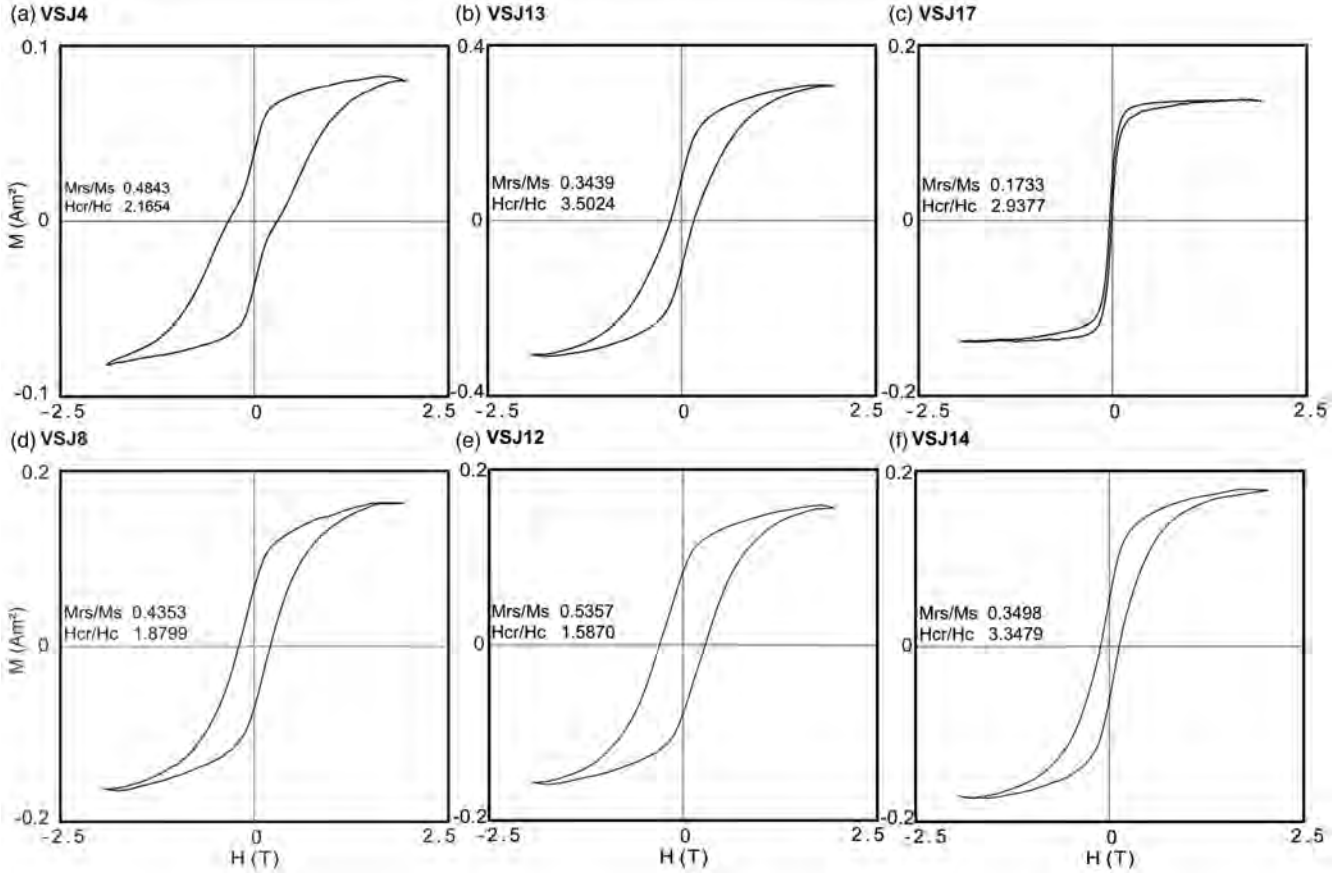

Figure 9. Representative hysteresis loops showing characteristic parameters ratios, saturation remanence (Mrs), saturation magnetization (Ms), and bulk coercive field (Hc). The loops are displayed after paramagnetic slope correction.

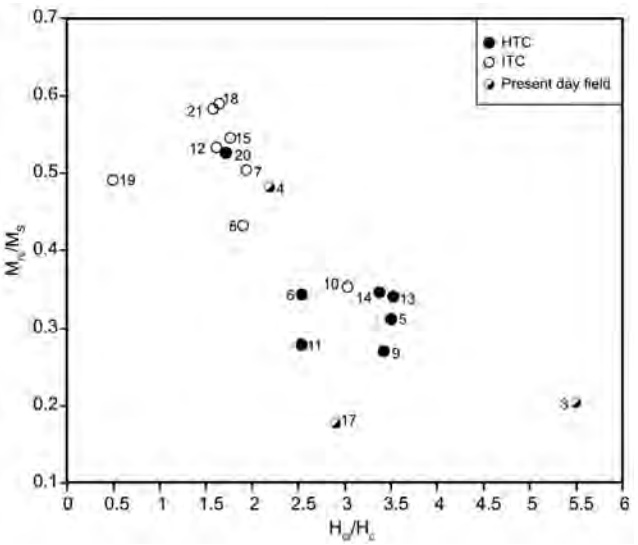

Figure 10. Modified Day plot (Day *et al.* 1977)) of the hysteresis ratios Mrs/Ms and Hcr/Hc for the samples of VSJ locality. The sites with a large recent component are indicated under 'Present-day field'. Samples with a larger HTC are indicated in closed circles, while samples with a larger ITC component are shown in open circles.

the total IRM. We thus conclude the following: goethite is not common and is generally absent; both the HTC and ITC observed in demagnetization of the NRM can be associated with IRM components of Hc > 150 mT consistent with their high resistance to AF demagnetization, the HTC, and the ITC thus reside in haematite; magnetite in small proportions is present in most samples.

Petrographic observations

Examples of the texture, shape, and size of the magnetic minerals carrying the magnetization in sandstones of the Zicapa Formation are shown in the SEM images (Fig. 13). Titanomagnetite pseudomorphs with exsolution textures replaced by haematite (Figs 13a and b), and with haematite substituting trellis texture (Fig. 13c) with sizes from 50 to 75 μm were found in most samples (examples shown are for VSJ4a and VSJ12). The trellis texture can be indicative of martite from former Ti-poor magnetite grains. Authigenic 'flakes' of haematite as cement with a size <5 μm are found in most of the samples (Fig. 13d).

Detrital grains and cement with cross-cutting relations are shown in the SEM backscattered images and in the reflected light images of the sandstones in the VSJ locality (Figs 13 and 14). Under transmitted light, at least three cement generations were observed. One primary cement was found in all samples, anisotropic red-coloured, and coating the framework grains. It was attributed to haematite; a secondary cement cuts across the primary clasts and cement, filling microfractures and it is constituted by calcite. The third type of cement is made of quartz and is found in the interpore space of the coarser sandstones as secondary after haematite. Detrital grains of martite with trellis texture (Figs 13c and 14a) were identified as a persistent and abundant phase in the samples. Laterite grains were observed as a lithic component in sandstones

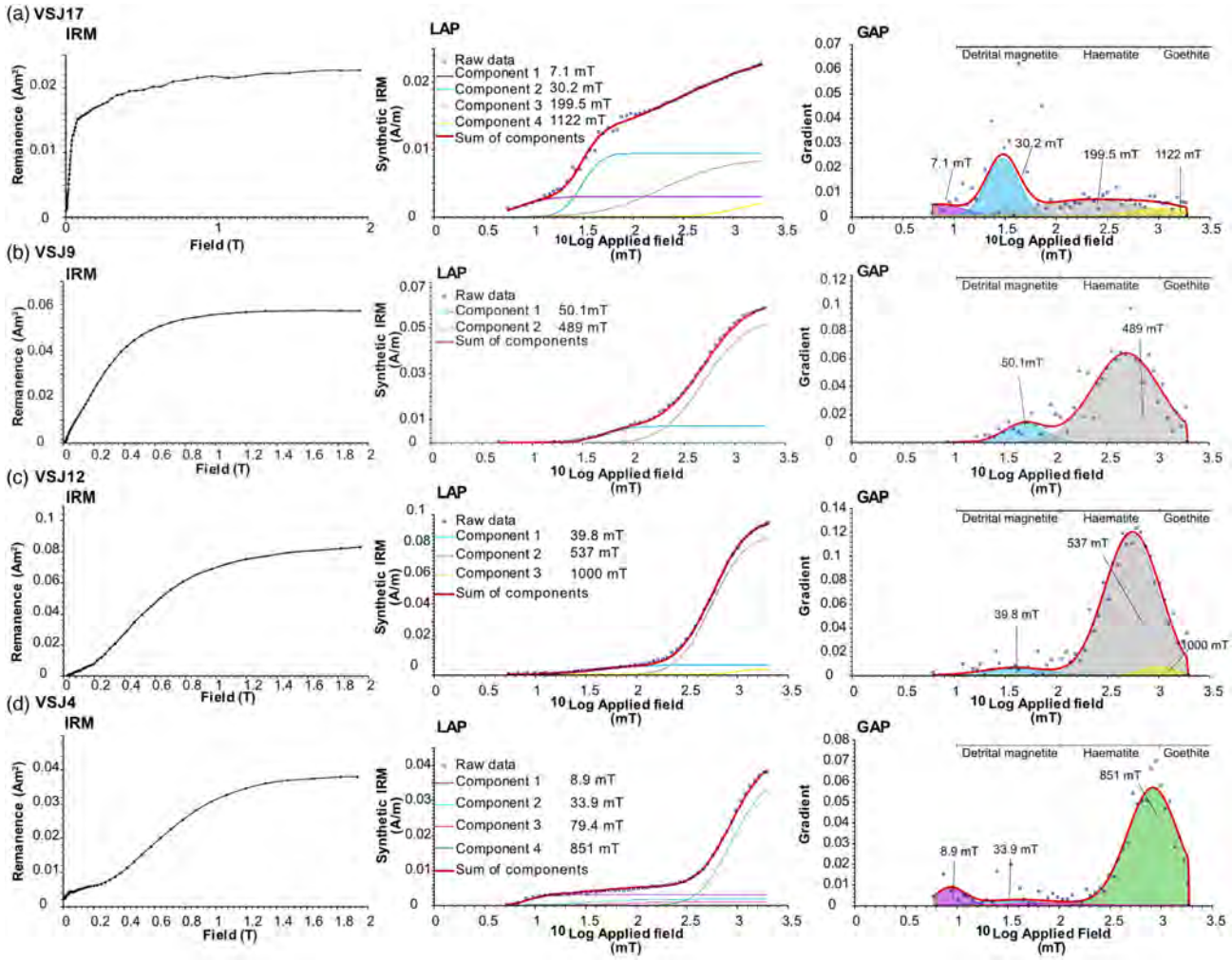

Figure 11. Representative samples of the IRM component analysis (Kruiver *et al.* 2001). From left to right the isothermal remanent magnetization plot (IRM), the linear acquisition plot (LAP) and the gradient acquisition plot (GAP) after Kruiver *et al.* (2001). In the LAP and GAP plots, open squares represent raw data points. The different components obtained are marked with different line colour (LAP) and fill colours (GAP). In the GAP the components with the major contribution to the magnetization are shown. IRM is in $Am^2\ kg^{-1}$, log10 (H1/2) and DP are in log10 mT. Values of H1/2 are displayed with the colour code in the LAP. Identification of components in GAP after Abrajevitch *et al.* (2009) and reference therein.

ca. 10–20 mm (Fig. 14d) and were also observed as pebbles in conglomerates. Fig 13(c) shows textures of haematite grains with rutile inclusions. Haematite cement is also observed in pore spaces with euhedral habits, which indicate an authigenic origin. Euhedral haematite flakes occur in pore spaces perpendicular to detrital grain boundaries. Finally, branching textures of secondary haematite of relatively large grain-size were also found (Fig. 14f).

DISCUSSION

Magnetic carriers

Redbeds may include different magnetic minerals with different grain sizes ranging from MD to SD, resulting in contrasting coercivities and demagnetization behaviour. Defining the magnetic carriers is thus crucial for the interpretation of the results in terms of early or late acquisition of the magnetization, inclination shallowing correction, and/or remagnetization.

The NRM of samples of the Zicapa Formation at the VSJ locality is multicomponent. The decrease in NRM intensity during thermal demagnetization between approximately 250 and 500 °C is generally attributed to fine-grained pigmentary haematite, and a narrow unblocking temperature distribution attributed to detrital haematite (Kodama 2012). We observed mainly univectorial behaviour in samples such as VSJ8B1, VSJ9A2, and VSJ13B above 200 °C (Fig. 3). These samples show unblocking of the remanence between 350 and 600 °C, and a narrow range of unblocking-temperatures at temperatures over 650 °C (Figs 3 and 4). This suggests that the magnetization may be carried by both detrital and pigmentary haematite; in these samples both haematite forms record a field direction of the same polarity. It is evident, however, that the proportion of the remanence residing in detrital or pigmentary haematite varies along the section, and may even vary within a single bed. In other cases, the component that may be attributed to detrital haematite carries a nearly antipodal magnetization to that of the pigmentary haematite (e.g. VSJ12 and VSJ14; Fig. 4).

The thermomagnetic curves show either a single magnetic phase with a Curie/Neel temperature of approximately 650 °C (Fig. 8a), a dominant magnetic phase with a Curie temperature of approximately 580 °C (Figs 8b and c), or inflections that suggest similar contributions to the magnetization form these two phases (Figs 8d–f). Because of the larger saturation magnetization of magnetite relative to haematite, the haematite signal is overwhelmed and hardly recognizable in samples such as Figs 8(b) and (c). Also, the Neel

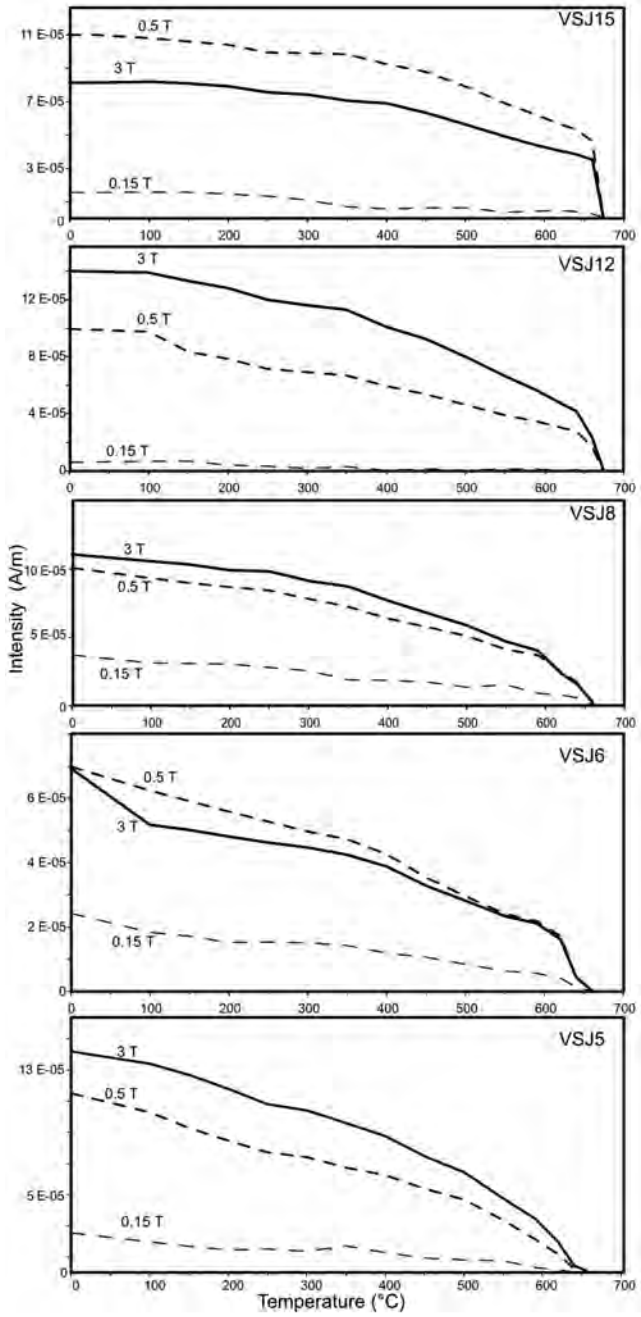

Figure 12. Thermal demagnetization of three orthogonal IRM components (Lowrie test). The hard and intermediate components reside in haematite, except in VSJ6 where there is a small contribution from goethite. The soft component (<150 mT) resides partly in magnetite and partly of low coercivity haematite.

temperature of haematite in samples such as Figs 8(d) and (e) are calculated at approximately 620 °C. Although this could be attributed to poor calibration of the thermocouple in the balance system, lower Neel temperatures have been observed when there is Al or Ti substitution in the haematite structure; this is our preferred interpretation. Thermomagnetic curves indicate the presence of low Ti-magnetite with a Curie temperature of approximately 570 °C, and haematite with a Neel temperature of 620 to 650 °C. On the other hand, the shape of the hysteresis loops and modelling of the IRM acquisition curves show that the magnetization in the VSJ locality cannot be solved by a single ferromagnetic phase. Rather, a mixture of particles with different coercivities is necessary to fit IRM curves and explain hysterresis loops.

Magnetic hysteresis properties and IRM curves

Rock magnetism results indicate that several magnetic phases are present in the red sandstones of the Zicapa Formations. Hysteresis loops indicate mixtures of different magnetic minerals, or particles with different grain-size, and thus coercivity. Thermomagnetic curves indicate the presence of nearly pure magnetite as well as haematite. The natural remanence is multivectorial, with three magnetization components. Unmixing the signal from different magnetic phases recognized in the rock magnetic experiments, and assigning each component to a particular magnetization component is a challenge. We attribute the LT component to MD magnetite, or occasionally goethite. The ITC and HTC reside in haematite.

From modelling of IRM acquisition curves (Fig. 11) we can identify at least two different components in terms of coercivities, but more commonly three or four components are necessary to get acceptable fits in the model (Kruiver *et al*. 2001). The dominant component is characterized by coercivities ($H_{1/2}$) between 400 and 600 mT, with somewhat narrow distributions (Figs 11b and c). This component of the IRM is likely to represent haematite particles that record the intermediate and the high unblocking temperature components of the NRM.

The weakest representative component in the IRM curves (generally contributing about 5 per cent to the total IRM) has an $H_{1/2}$ between 5 and 10 mT and is found in most samples in a small proportion. The weight in the IRM of this component relates to samples that carry a relatively large north-directed recent component (e.g. Fig 3b), supporting the viscous origin of this NRM component. Usually, the peak for this component is wide, which can be interpreted as a wide distribution of MD particles of low Ti-magnetite (according to thermomagnetic curves) of detrital origin (Fig. 13f). The maximum induction used in the IRM acquisition may be insufficient to fully detect goethite in the models. Although Lowrie tests show that goethite is not common, it may carry an LT component in some sites.

Samples such as VSJ4 illustrate an LT component as dominant in the NRM. This sample exhibits a remanence made of two components: a very low-unblocking-temperature recent magnetization in the direction of the modern geomagnetic field, and the intermediate magnetization of distributed unblocking temperature (Fig. 3b). The north-directed component is prominent (62 per cent of the NRM intensity; Table 3), and there is only very small or nearly insignificant component with high unblocking temperature. The sharp drop of the NRM intensity at <100 °C (Fig. 3b) may reside in a hard phase such as goethite. A Lowrie test is not available for this site to confirm this and no clear indication of goethite was observed in thermomagnetic curves, but at site VSJ6 with similar demagnetization behaviour we recognized goethite in the Lowrie test. MD magnetite also contributes significantly to this NRM component in VSJ4 because the north directed overprint is only completely removed upon heating to 200 °C. The presence of MD magnetite in VSJ4 is supported by IRM modelling and thermomagnetic curves (Fig. 11d). This sample is also characterized by a square hysteresis loop with very high coercivity (Fig. 9a). The magnetization of distributed unblocking temperatures is carried, most likely, by high coercivity authigenic haematite.

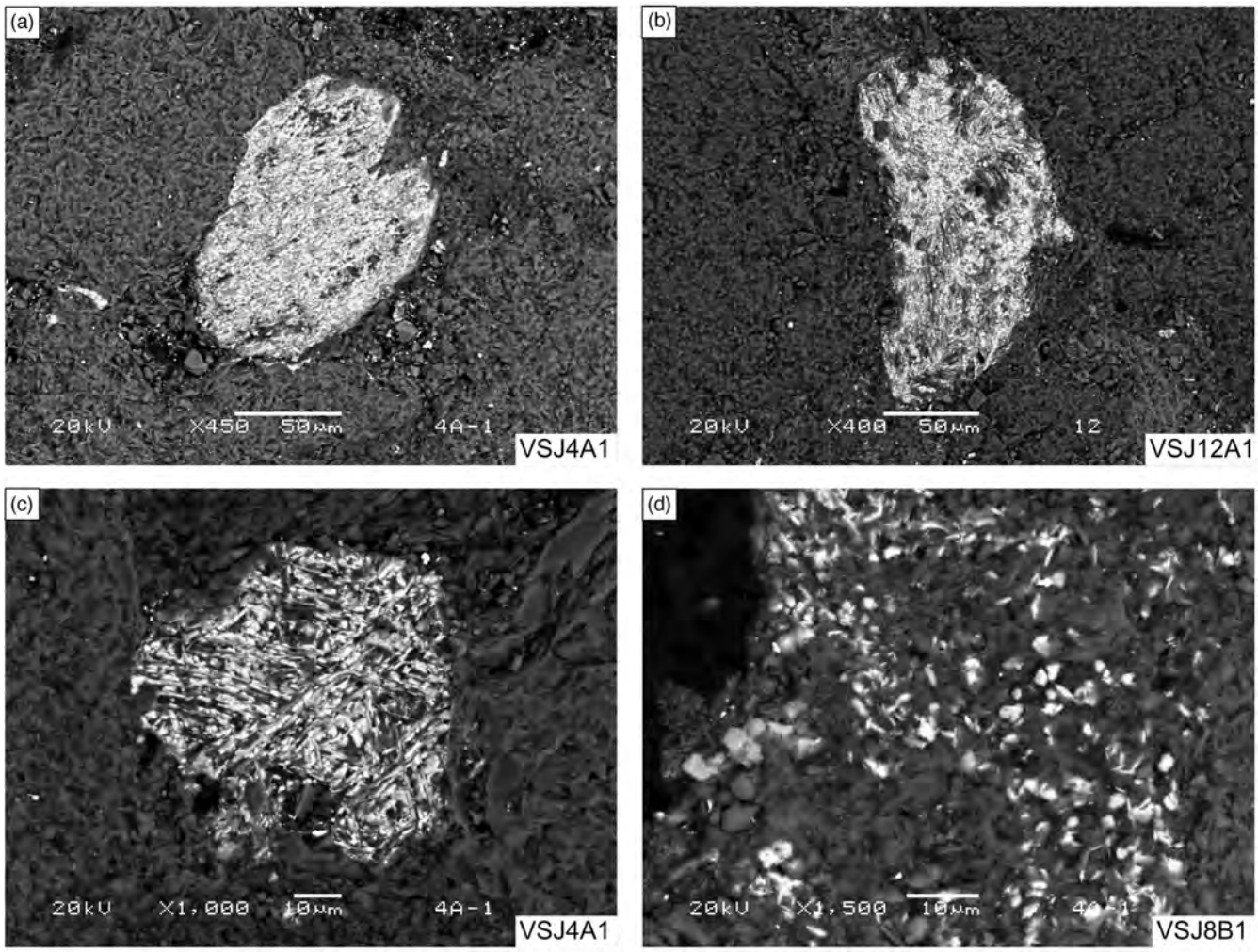

Figure 13. SEM back-scattered electron image of sandstone samples from the VSJ locality. (a and b) Large specularite grains. (c) Magnetite pseudo-morph complete altered to haematite. The haematite grows in three different directions (martite). (d) Secondary pigmentary haematite as cement in the sandstones from VSJ4.

Samples such as VSJ17, from a site where no stable remanence was observed, lack the IRM component with $H_{1/2}$ of 400–600 mT commonly observed at other sites (Table 3; Figs 4d and 11a). Instead, the dominant IRM signal is from a phase with a coercivity similar to that reported for MD magnetite (Abrajevitch *et al.* 2009). This example, for which the IRM is solved with four components, 80 per cent of the total contribution is from particles with $H_{1/2} < 200$ mT. This sample is also characterized by a narrow hysteresis loop (Fig. 9c), and a thermomagnetic curve with only one clear inflection point around 580 °C (Fig. 8c). According to the magnetic properties of the sample, the main carrier of the magnetization is interpreted as low Ti-magnetite. This sample carries a relatively large north-directed magnetization with a maximum unblocking temperature of *ca.* 200 °C and maximum coercivities of 20 mT (as seen in the AF pilot tests) but carries no stable magnetization residing in haematite (Fig 4d).

All the observations thus point to the nearly ubiquitous presence of a soft magnetic phase with the lowest coercivity, which is the most likely carrier of a viscous remanence. This component of the IRM will not be considered further, as demagnetization experiments suggest that the viscous component it carries is completely removed by heating to approximately 200 °C (Figs 3 and 4). The Lowrie tests also indicate that a magnetization in the direction of the recent dipole field resides in magnetite, and that one residing in goethite is observed only at very few sites.

For sample VSJ9, the modelled IRM shows a total contribution to the IRM of 94 per cent for particles with $H_{1/2}$ *ca.* 500 mT, with one component (6 per cent contribution) of $H_{1/2}$ of *ca.* 50 mT (Fig. 11b). The LTC component in this site is insignificant (Fig. 3d). The component with coercivities around 500 mT is characterized by an ample peak in the GAP diagram, which indicates that the corresponding population of ferromagnetic grains has a wide coercivity range as a response to a distribution grain-size and/or composition (Abrajevitch *et al.* 2009). This sample is characterized by a relatively large magnetization component residing in particles with unblocking temperatures >650 °C (Fig. 3); this magnetization of high unblocking temperature and high resistance to AF demagnetization is likely carried by specular or detrital haematite with an IRM signal of high $H_{1/2}$, but not greater than about 500 mT (Table 3).

Laboratory unblocking temperatures (Figs 3 and 4) and thermomagnetic curves (Fig. 8) suggest that the remanence resides primarily in the fine-grained haematite fraction, which is consistent with Collinson (1974) who attributes this behaviour to pigmentary haematite. In most of the samples less than 30 per cent of the remanence remains after heating to 600 °C, but with some exceptions

Table 3. Summary of the palaeomagnetism and rock magnetism results for the VSJ locality. The results are in stratigraphic order, and the main lithology for each site is indicated.

			NRM relative intensity			Magnetic properties					
Site	Depht (m)	Lithology	LTC (%)	ITC (%)	HTC (%)	*T* Curie (° C)	Hc (mT)	IRM components (mT)			
VSJ18A1	0	Very fine-grained sandstone	16.7	53.3	30.0	540, 640	178.6636				
VSJ17A1	10	Coarse-grained sandstone				580	12.8782	7.1	30.2	199.5	1122
VSJ20C1	60	Medium-grained lithic sandstone	30.8	15.4	53.8	580, 620	213.2925				
VSJ19B2	65	very fine-grained sandstone	8.3	47.3	44.5	670	194.3647				
VSJ21A1	85	Very fine-grained sandstone	39.6	47.2	13.2	No data	146.3372				
VSJ15A2	90	Medium-grained lithic sandstone	19.7	54.4	26.0	580, 640	177.8711	10	70	446	
VSJ14A1	100	Medium-grained lithic sandstone	20.1	39.4	40.5	560, 640	92.60009	25	100	446.7	1000
VSJ13B1	105	Fine-grained sandstone	25.8	35.9	38.4	560, 640	104.5236	17.8	100	660.7	
VSJ12A1	110	Fine-grained sandstone	12.8	46.1	41.1	560, 640	165.3917		39.8	537	1000
VSJ11E1	125	Coarse-grained sandstone	28.5	26.3	45.3	540, 620	175.8687				
VSJ10C1	130	Medium-grained lithic sandstone	25.9	63.0	11.1	No data	87.89395	5.6	50.1	190.5	501.2
VSJ9A2	140	Very fine-grained sandstone	11.6	25.6	62.8	No data	90.84353		50.1	489	
VSJ8B1	145	Very fine-grained sandstone	7.9	77.3	14.9	580, 620	141.8717				
VSJ7C1	150	Very, red to purple	12.2	70.7	17.1	540, 620	162.8903				
VSJ6A2	160	Medium-grained lithic sandstone	23.8	36.6	39.7	No data	129.4849		31.6	631	
VSJ5B1	168	Very fine-grained sandstone	20.2	37.1	42.7	540, 620	89.81049		31.6	251	
VSJ4C1	178	Fine-grained sandstone	62.2	21.1	16.8	640	236.4715	8.9	33.9	79.4	851
VSJ3A1	182	Medium-grained lithic sandstone	37.7	32.9	29.5	580, 630	38.09765		31.6	251.2	631	1258

(Figs 3 and 4; Table 3). The fraction remaining after heating to 600 °C represents a maximum of approximately 63 per cent of the remanence in samples such as VSJ9 (Figs 3d, Table 3); this fraction is very small in samples such as VSJ4 and VSJ8 (Figs 3b and c, Table 3). This fraction of the NRM is attributed to detrital (specular haematite).

As mentioned above, IRM acquisition curves were modelled components with coercivity components around 500 mT. We note, however, that some samples suggest that slightly higher coercivities ($H_{1/2} > \sim$600 mT) are required to model the curves for the samples where the HTC is large or dominant. For instance, lower coercivities ($H_{1/2} < \sim$500 mT) are required to model IRM curves for samples VSJ14 and VSJ15 where the distributed unblocking temperature component of the NRM (ITC) is more important (Table 3). This observation is tentative because throughout the study we observed, as has been pointed out before, that different techniques (hysteresis, IRM, and median destructive fields of AF demagnetization) result in different estimates of coercivity. It is thus difficult to show a consistent correspondence between coercivities of the ITC and the HT component, but there is a hint of higher coercivity for specular haematite. Hysteresis, however, appears to discriminate between a dominant authigenic component and a dominant detrital component.

There is a good correlation between hysteresis ratios and the nature of the remanence carriers inferred from demagnetization behaviour (Fig. 10). Higher Hcr/Hc ratios (between *ca.* 2.5 and 3.7) and lower Mrs/Ms ratios (between *ca.* 0.28 and 0.35) are observed for samples where the high-temperature remanence component is significant: making more than approximately 40 to 63 per cent of the NRM (Table 3). Lower Hcr/Hc ratios (between *ca.* 1.5 and 2) and higher Mrs/Ms ratios (between *ca.* 0.43 and 0.58) are observed for samples where the high-temperature remanence is small: making less than approximately 15 per cent of the NRM. This correlation breaks down when there is a large viscous remanence or where there is evidence of goethite, which probably indicates that the magnetite affects the hysteresis ratios, as is evident by the anomalous position of samples 3 and 17 in Fig. 10. The Hcr/Hc and Mrs/Ms ratios of the group of samples where the remanence is dominated by the component of distributed unblocking temperature (ITC) are consistent with ratios reported by Özdemir & Dunlop (2014) for SD haematite grains, perhaps suggesting that internal strain induced coercivity or crystal lattice defects may be reduced in the large (>10 μm) SD particles of detrital origin such as laterite fragments.

Particle grain size

Mixtures of different mineral grain-sizes are evident in the rock magnetic experiments (thermomagnetic curves, hysteresis loops and IRM acquisition curves), and the microscope observations indicate the presence of (generally) >10 μm detrital particles and <1 μm authigenic particles. The presence of components with different coercivities is well supported by hysteresis loops and IRM acquisition curves (Figs 9 and 11).

Laboratory determined median particle sizes of the single domain (SD) haematite range from 0.1 to 0.6 μm (Dunlop & Özdemir 2002), but SD behaviour is observed over a wide range of grain-sizes up to tens of μm. MD behaviour is observed in larger particles in the grain size range from ∼200 to 5 mm (Özdemir & Dunlop 2006). Values of magnetization saturation from the hysteresis experiments in both SD and MD particles show a great variation in the values from 270 $Am^2 kg^{-1}$ in SD particles and near 9 Am^2Kg^{-1} in MD particles (Özdemir & Dunlop 2014). From SEM and petrographic observations, the particle size in the VSJ samples ranges from 10 to 300 μm in the detrital haematite (martite, specularite) and from approximately 0.2 to 1 μm in the pigmentary haematite flakes (Figs 13 and 14). We also determined values of magnetization saturation from 80 to 306 $Am^2 kg^{-1}$ and Hc values from 131 to 350 mT. Our data have Hc and Mrs values comparable with those obtained for the fraction between 0.1 μm and 2 mm by other authors (e.g. Dankers 1981; Bao *et al*. 2011; Özdemir & Dunlop 2014). We thus consider that despite having large grains of haematite in the detrital fraction, the main contribution to the bulk magnetization is given by the small fraction (pigmentary haematite), which are single domain particles of relatively low laboratory unblocking temperature.

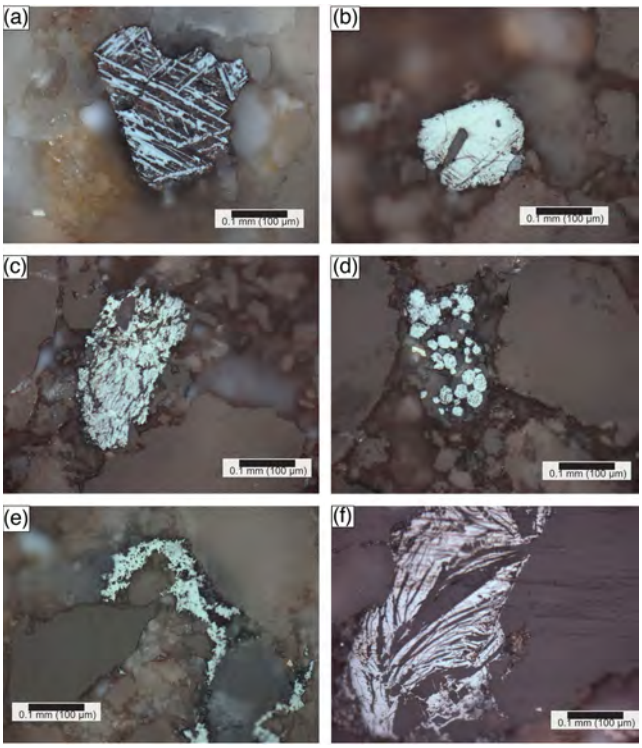

Figure 14. Petrographic characteristics of some magnetic carriers under reflected light. (a) Sample VSJ4, *in situ* alterations of ilmenite grain to leucoxene (rutile and anatase) in a trellis texture. (b) Sample VSJ12, anisotropic specularite grain with internal reflections. (c) Sample VSJ12, detrital haematite (specularite grain). (d) Sample VSJ12, oolithic haematite in a laterite grains. (e) Sample VSJ8, pigmentary haematite as a coating of quartz grains. (f) Sample VSJ4, haematite in lamellas as a product of alteration of a larger grain.

Magnetostratigraphy

The high temperature (600 to >650 °C) component or characteristic remanent magnetization of the sites in the VSJ locality was used to determine the polarity at the time of deposition, and with this, we propose a magnetic polarity zonation consisting of eight magnetozones defined on the basis of VGP latitudes. At sites VSJ8 and VSJ10, the polarity of the HTC is reverse in two samples, with a normal polarity in the rest. We assume that samples in the lower part of each bed record a reverse polarity. The reversal sequence can be correlated with the M10n to M3r chrons, from 132 to 129 Ma in the geomagnetic polarity time scale (Ogg 2012; Fig 2). The correlation is supported by geochronological constraints, with maximum depositional ages between *ca.* 149 ± 1 Ma (for the underlying San Juan de la Joya Member) and 133 ± 3 Ma for the overlying San Andrés Member (Sierra-Rojas & Molina-Garza 2014). Available palaeontological data of the overlying Morelos Formation also constraint the age of deposition of the Zicapa Formation as pre-Albian (Hernández-Romano *et al*. 1997).

Climate

Redbeds have been related to climatic conditions over the geologic time (Walker 1967a; Walker 1967b; Van Houten 1973; Besly & Turner 1983), indicating prolonged arid climatic conditions or strong seasonality. Sedimentological and depositional environment observations in continental redbeds show that alternations between wet and dry seasons in a monsoonal climate can favour the formation of redbeds (Dubiel & Smoot 1994; Parrish *et al*. 1998). On the other hand, early diagenesis has been proposed to be the origin of the haematite carrying the magnetization in redbeds in continental (as well as shallow marine) environments, locking the remanence in periods of $<10^2$ ka after deposition (Whidden *et al*. 1998). Also, hydrological conditions in palaeosols have been suggested as the mechanism responsible for the precipitation of haematite, and not a long seasonal or climatic condition (Sheldon 2005); but this also translates into the acquisition of an early chemical magnetization after the deposition.

Evidence of an arid and monsoonal climate during the Early Cretaceous is found in the continental deposits in southern Mexico (Sierra-Rojas *et al*. 2016), where anabranching river systems were formed under arid conditions allowing the generation of calcareous concretions in palaeosols. The Early Cretaceous climatic conditions in southern Mexico have also been considered arid because of the deposition of evaporitic units (e.g. Huitzuco Anhydrite) and the association of limestones and gypsum in the Guerrero Morelos platform (Gonzalez-Pacheco 1991; Hernández-Romano *et al*. 1997; Sierra-Rojas & Molina-Garza 2014).

In the San Juan de la Joyas locality, the presence of laterite pebbles is common in conglomerates. We show the presence of laterite grains in the sandstones of the VSJ locality, consisting of oolite of 5– 20 µm (Fig. 14d). Reflected light petrography shows as well the presence of goethite that may indicate the association haematite-goethite found in oolithic laterites in nickeliferous ores (Katzagiannakis *et al*. 2014), in ferruginous concretions in shallow marine sediments (Nejbert & Jurewicz 2004), in ferruginous oolithic laterites in tropical environment, and oolithic haematite-bearing ironstones (Hodych *et al*. 1985). Rather than indicating an Early Cretaceous tropical environment, the laterite grains observed in the Zicapa Formation were probably derived from Jurassic floodplain deposits of the Tecocoyunca Group and later transported to the fluvial systems of the Zicapa basin.

CRM as early diagenetic process

As we demonstrated above, the sediments in the VSJ locality acquired both CRM and DRM which are represented by ITC and HTC respectively. The fact that the chemical magnetization was affected by burial compaction as demonstrated by the inclination shallowing in the site means indicate that the chemical magnetization, despite being secondary in origin, must have been acquired soon after deposition. Previous work has shown that acquisition of chemical magnetization can occur even before compaction (Liebes & Shive 1982; Tan *et al*. 2007; Kodama 2012 and references therein).

The sedimentological trends of the Ajuatetla Member of the Zicapa Formation suggest continuous deposition, without evident erosional contacts or long-lasting periods of no deposition. Based on the magnetostratigraphy and the geochronological constraints, we estimate for the Ajuatetla Member an undecompacted sedimentation rate of ∼36 m my^{-1}, which is comparable with the average sedimentation rates calculated for intra-arc extensional basins of 43 m my^{-1} (Stern 2010) and for near-shore marine deposits of 100–1000 m my^{-1} (Kodama 2012).

The magnetization component with high narrow unblocking-temperatures in the >600 °C temperature range is interpreted to be carried by detrital haematite. In intervals that contain polarity transitions (e.g. VSJ14 to VSJ15, Figs 2 and 5) in the sites with clear multicomponent behaviour (e.g. VSJ14), while the high-temperature component or ChRM records a DRM like the

underlying site (VSJ13), the intermediate temperature components (350–500 °C) records the polarity of the site above it (VSJ15). This component is usually attributed to pigmentary haematite. It thus seems that while a sediment acquired a DRM at the time that it was deposited, the underlying layer is already acquiring a CRM.

At the VSJ locality the acquisition of a delayed CRM occurs not only at the transition R-N polarity between sites VSJ14 and VSJ15, it is also observed in sites below VSJ14 such as VSJ12 and VSJ13 about 12 and 10 m below the transition, respectively (Fig. 2). In site VSJ10 although the record is complex, the ITC is of reverse polarity and the HTC is normal in two specimens. A delayed CRM of opposite polarity to the HTC is observed at seven stratigraphic levels, with the ITC generally recording a normal polarity magnetization. Both the high and intermediate temperature magnetizations record normal and reverse polarities, indicating the prevalence of the phenomenon of early magnetization in pigmentary haematite in the Zicapa red beds. We consider a continuous minimum undecompacted sedimentation at a rate of ∼35 m my^{-1}, calculated from the magnetostratigraphic correlation. Using this value we can roughly estimate a maximum time of precipitation of the pigmentary haematite carrying the ITC. For instance, site VSJ12 records the ITC about 300 kyr (12 m) after deposition.

Yet another way to approximate the time of CRM acquisition is by the thickness of the interval of strata of opposite polarity to that of the DRM, but similar to the CRM. For instance, approximately 7 m of strata of normal polarity and 15 of reverse polarity overlie site VSJ14, where the DRM is reverse but the CRM is normal. For a sedimentation rate of 35 m my^{-1}, this suggests that the CRM is locked-in less than about 200 kyr after deposition. These results are congruent with estimates previously presented in literature, in similar depositional and climatic environments as the ones at the time of deposition of the Zicapa Formation (Whidden *et al*. 1998).

Tectonic implications

The tilt corrected directions show nearly the same dispersion as in-situ directions because the entire locality was sampled in a single anticline limb and dip directions vary only slightly (Fig. 1). However, the mean direction obtained before *E*/*I* correction in the VSJ locality (Dec = 272.5°, Inc = 16.5°) does not resemble the Early Cretaceous to Cenozoic expected direction for the North America craton (McElhinny & McFadden 2000), nor the directions observed in Upper Cretaceous strata (Dec = 323.1, Inc = 36.5; Molina-Garza *et al*. 2003) or Cenozoic strata (Dec = 340.8°, Inc = 34.3°; Molina-Garza & Ortega-Rivera 2006) in the Guerrero-Morelos platform in nearby sites. This suggests that a regional remagnetization has not affected Zicapa strata, as it appears to have affected shallow marine limestones of the Morelos Formation (Molina-Garza *et al*. 2003). Furthermore, the record of both polarities suggests that the magnetization is of primary, or near primary origin. The HTC is interpreted as the ChRM of the Zicapa Formation redbeds. We argue that both the intermediate and high-temperature components predate compressional Laramide age (latest Cretaceous) deformation of the Sierra Madre del Sur. The age of the magnetization can be constrained by the maximum depositional age of the Zicapa Formation of Hauterivian-Barremian age (Sierra-Rojas & Molina-Garza 2014), and correlation with the geomagnetic polarity time scale (Fig. 2).

The ChRM is rotated counter-clockwise with respect to the North American reference direction (Torsvik *et al*. 2012). Both the ITC and the HTC indicate a counter-clockwise rotation of approximately 60°; latitudinal displacement is uncertain, however. The ITC inclination indicates statistically significant inclination anomaly ($F = -16.8 \pm 12.7$), but there is not flattening ($F = -7.7 \pm 13.0$) for the HTC. Because of the possibility of unremoved overprints in the ITC, we lend more credibility to the flattening estimate of the HTC. It is unclear if the rotation is a regional or a local phenomenon, but we tend to support rotation about a local vertical axis. Counter-clockwise rotation about a local vertical axis has been previously reported for localities in the Guerrero-Morelos platform (Molina Garza *et al*. 2003), and it is thought to be related to strike-slip tectonics along the southwest Mexican margin.

CONCLUSIONS

Samples from the Ajuejutla Member of the Zicapa Formation have a multivectorial NRM. Widespread, there is a north-directed magnetization of low unblocking temperature (<200 °C). Rock magnetic experiments suggest that this is carried by a magnetic phase with a Curie temperature near 580 °C, and IRM curves suggest has coercivities ∼10 mT. It is interpreted as a viscous component, for which rock magnetism and petrography strongly suggest the carrier is MD detrital magnetite. In general, however, the NRM is mostly dominated by an intermediate laboratory unblocking temperature component. This component shows distributed laboratory unblocking-temperatures between *ca.* 300–500 °C. An additional component is of high, discrete, laboratory unblocking-temperatures (600 to >650 °C). Curie–Neel temperatures ∼620 to 670 °C, and relatively high coercivity (>∼450–650 mT) indicate that the principal remanence carrier of the intermediate and high-temperature components is haematite. The ITC and HTC may be near parallel to each other or anti-parallel, which indicates that both polarities may be recorded in some samples. In some sites (beds) the intermediate unblocking temperature component is of both normal and reverse polarity, but the high temperature is of uniform polarity. Often, the polarity of the intermediate component corresponds to the polarity of the overlying strata.

The intermediate temperature component is interpreted as a CRM obtained early after deposition, and is carried by authigenic haematite. The high-temperature component is interpreted as a DRM. Magnetic carriers, inferred from observations in SEM as well as petrographic inspection of thin sections, are laterite grains and specularite with high-temperature textures (trellis texture).

Hysteresis parameters of the samples of the VSJ locality show evidence of a mixture of magnetic minerals with contrasting coercivities, or different grain size distributions (single-domain and multidomain). IRM acquisition curves require modelling with a minimum of two, but more often three or four components. Also, lower Hcr/Hc ratios (between *ca.* 1.5 and 2) and higher Mrs/Ms ratios (between *ca.* 0.43 and 0.58), comparable to those of SD haematite (Özdemir & Dunlop 2014), are observed for samples where the high-temperature remanence (DRM) is small and the remanence is interpreted as a CRM. Hcr/Hc ratios are higher (between 2.5 and 3.7) for samples with a substantial DRM (Fig. 10).

In the Zicapa Formation, a large fraction of the remanence resides in fine-grained authigenic SD haematite (Fig. 9). This suggests, in turn, that as little as 36 per cent (e.g. sample VSJ12) and as much as 77 per cent of the remanence (e.g. sample VSJ8) is of chemical origin. Authigenic haematite (<1 μm in size) was identified as fine-grained early cement in pore spaces with euhedral habits, euhedral haematite flakes occur in pore spaces perpendicular to detrital

grain boundaries, and branching textures of secondary haematite of relatively large grain-size (>100 μm in size) were also found.

Early CRM in redbeds can be inferred from demagnetization behaviour, magnetostratigraphy, SEM observations, and rock magnetism. We emphasize the VSJ14 to VSJ15 transition of polarity, where an early acquisition of chemical magnetization was determined to be acquired in a maximum of approximately 0.5 Ma.

Even with an important amount of the magnetization residing in pigmentary haematite, corrections for inclination shallowing of the palaeomagnetic data were necessary according to elongation/inclination analysis. However, the fact that the inclination of chemical magnetization was affected by compaction, is considered as evidence of an early chemical magnetization. The overall means of the intermediate and high-temperature components are $D = 282.0$, $I = 12.4^\circ$, $k = 13.33$, $n = 17$ and $D = 272.5$, $I = 16.5^\circ$, $k = 14.04$, $n = 11$; after correction for inclination shallowing with an f factor of 0.41 and 0.4 the corresponding inclination are 28.2° and 36.5°, respectively. The ChRM is rotated counter-clockwise with respect to the North American reference direction approximately 60°.

ACKNOWLEDGEMENTS

We acknowledge the Programa de Apoyo a Proyectos de Investigación e Innovación Tecnológica (PAPIIT: IN104511–3) for funds to support the fieldwork. We also acknowledge partial support from CONACYT grant 129862 to RSMG. We thank Jorge Escalante for the technical assistance provided in the Laboratorio de Paleomagnetismo y Magnetismo de Rocas, Centro de Geociencias, UNAM, Juan Tomás Vázquez for preparation of thin sections and Dr Marina Vega for assistance with the SEM images.

REFERENCES

Abrajevitch, A., Van der Voo, R. & Rea, D.K., 2009. Variations in relative abundances of goethite and hematite in Bengal Fan sediments: Climatic vs diagenetic signals, *Mar. Geol.,* **267**(3–4), 191–206.

Bao, L., Yang, H., Wang, X., Zhang, F., Shi, R., Liu, B., Wang, L. & Zhao, H., 2011. Synthesis and size-dependent magnetic properties of single-crystalline hematite nanodiscs, *J. Cryst. Growth,* **328**(1), 62–69.

Beck, M.E., Jr., 1980. Paleomagnetic record of plate-margin tectonic processes along the western edge of North America, *J. geophys. Res.,* **85**(B12), 7115–7131.

Beck, M.E., Burmester, R.F. & Housen, B.A., 2003. The red bed controversy revisited: shape analysis of Colorado Plateau units suggests long magnetization times, *Tectonophysics,* **362**(1-4), 335–344.

Besly, B.M. & Turner, P., 1983. Origin of red beds in a moist tropical climate (Etruria Formation, Upper Carboniferous, UK), *Geol. Soc. London Spec. Publ.*, **11**(1), 131–147.

Butler, R.F., 1998. *Paleomagnetism: Magnetic Domains to Geologic Terranes*, Blackwell Scientific Publications, p. 319.

Cabral-Cano, E., Lang, H.R. & Harrison, C.G.A., 2000. Stratigraphic assessment of the Arcelia–Teloloapan area, southern Mexico: implications for southern Mexico's post-Neocomian tectonic evolution, *J. South Am. Earth Sci.,* **13**(4–5), 443–457.

Collinson, D.W., 1974. The role of pigment and specularite in the remanent magnetism of red sandstones, *Geophys. J. Int.,* **38**(2), 253–264.

Dankers, P.H.M, 1981. Relationship between median destructive field and remanent coercive forces for dispersed natural magnetite, titanomagnetite and hematite, *Geophys. J. Int.,* **64**(2), 447–461.

Day, R., Fuller, M.D. & Schmidt, V.A., 1977. Hysteresis properties of titanomagnetites: Grain size and composition dependence, *Phys. Earth Planet. Inter.,* **13**, 260–267.

Demarest, H.H., 1983. Error analysis for the determination of tectonic rotation from paleomagnetic data, *J. geophys. Res.,* **88**(B5), 4321–4328.

Dubiel, R.F. & Smoot, J.P., 1994. Criteria for interpreting paleoclimate from red beds-a tool for Pangean reconstructions, in *Pangea: Global Environment and Resources*, pp. 295–310, eds Embry, A.F., Beauchamp, B. & Glass, D.J., Canadian Society of Petroleum Geologist.

Dunlop, D.J., 1986. Hysteresis properties of magnetite and their dependence on particle size: a test of pseudo-single-domain remanence models, *J. geophys. Res.,* **91**(B9), 9569–9584.

Elston, D.P. & Purucker, M.E., 1979. Detrital magnetization in red beds of the Moenkopi formation (Triassic), Gray Mountain, Arizona, *J. geophys. Res.,* **84**(B4), 1653–1665.

Fisher, R.A., 1953. Dispersion on a sphere, *Proc. R. Soc. A,* **217,** 295–305.

Garcés, M., Parés, J.M. & Cabrera, L., 1996. Further evidence for inclination shallowing in red beds, *Geophys. Res. Lett.,* **23**(16), 2065–2068.

Gonzalez-Pacheco, V.V. 1991. *Evolución sedimentológica y diagénesis del Cretácico de la porción norte del Estado de Guerrero, MSc Thesis*, UNAM, México.

Hernández-Romano, U., Aguilera-Franco, N., Martínez-Medrano, M. & Barceló-Duarte, J., 1997. Guerrero-Morelos Platform drowning at the Cenomanian–Turonian boundary, Huitziltepec area, Guerrero State, southern Mexico, *Cretaceous Res.,* **18**(5), 661–686.

Hodych, J.P., Paetzold, R.R. & Buchan, K.L., 1985. Chemical remanent magnetization due to deep-burial diagenesis in oolitic hematite-bearing ironstones of Alabama, *Phys. Earth planet. Inter.,* **37**(4), 261–284.

Katzagiannakis, N., Alevizos, G., Stamboliadis, E., Stratakis, A. & Petrakis, E., 2014. Mineralogical investigation and washability treatment of the nickeliferous lateritic deposit of nome (Albania), *Geomaterials,* **4**(03), 105–115.

Kirschvink, L, 1980. The least-squares line and plane and the analysis of palaeomagnetic data, *Geophys. J. Int.,* **62**(3), 699–718.

Kodama, K.P. 2012. *Paleomagnetism of Sedimentary Rocks: Process and Interpretation*, John Wiley & Sons.

Kodama, K.P. & Dekkers, M.J. 2004. Magnetic anisotropy as an aid to identifying CRM and DRM in red sedimentary rocks, *Stud. Geophys. Geod.,* **48**(4), 747–766.

Kruiver, P.P., Dekkers, M.J. & Heslop, D., 2001. Quantification of magnetic coercivity components by the analysis of acquisition curves of isothermal remanent magnetisation, *Earth planet. Sci. Lett.,* **189**(3–4), 269–276.

Larson, E.E. & Walker, T.R., 1975. Development of chemical remanent magnetization during early stages of Red-Bed formation in Late Cenozoic Sediments, Baja California, *Bull. geol. Soc. Am.,* **86**(5), 639–650.

Larson, E.E., Walker, T.R., Patterson, P.E., Hoblitt, R.P. & Rosenbaum, J.G., 1982. Paleomagnetism of the Moenkopi Formation, Colorado Plateau: basis for long-term model of acquisition of chemical remanent magnetism in red beds, *J. geophys. Res.,* **87**(B2), 1081–1106.

Liebes, E. & Shive, P.N., 1982. Magnetization acquisition in two Mesozoic red sandstones, *Phys. Earth planet. Inter.,* **30**(4), 396–404.

Lowrie, W., 1990. Identification of ferromagnetic minerals in a rock by coercivity and unblocking temperature properties, *Geophys. Res. Lett.,* **17**(2), 159–162.

Maillol, J.M. & Evans, M.E., 1993. Permian palaeosecular variation as recorded in the Lodève redbeds, southern France, *Geol. Carpath.* **44,** 281–287.

Martini, M., Ferrari, L., López-Martínez, M. & Valencia, V.A., 2010. Stratigraphic redefinition of the Zihuatanejo area, southwestern Mexico, *Rev. Mex. Cienc. Geol.*, **27,** 412–430.

McElhinny, M.W. & McFadden, P.L., 2000. In *Paleomagnetism: continents and oceans*, Vol. 73, p. 1, eds Dmowska, R., Holton, J.R. & Rossby, H.T., Academic Press, San Diego.

McFadden, P.L. & McElhinny, M.W. 1990. Classification of the reversal test in palaeomagnetism, *Geophys. J. Int.,* **103**(3), 725–729.

Molina-Garza, R.S. & Ortega-Rivera, A., 2006. Chronostratigraphy and paleomagnetism of the Balsas Group in the Tuzantlán-Copalillo basin, northern Guerrero state, Mexico, *Rev. Mex. Cienc. Geol.*, **23**(2), 215–232.

Molina-Garza, R.S., Geissman, J.W. & Van der Voo, R., 1989. Paleomagnetism of the Dewey Lake Formation (Late Permian), northwest Texas:

end of the Kiaman superchron in North America, *J. geophys. Res.,* **94**(B12), 17 881–17 888.
Molina-Garza, R.S., Böhnel, H.N. & Hernández, T., 2003. Paleomagnetism of the Cretaceous Morelos and Mezcala formations, southern Mexico, *Tectonophysics,* **361**(3–4), 301–317.
Molina-Garza, R.S., Geissman, J.W., Van der Voo, R., Lucas, S.G. & Hayden, S.N., 1991. Paleomagnetism of the Moenkopi and Chinle Formations in central New Mexico: implications for the North American apparent polar wander path and Triassic magnetostratigraphy, *J. geophys. Res.,* **96**(B9), 14 239–14 262.
Nejbert, K. & Jurewicz, E., 2004. Mineralogy and petrography of the ferruginous concretions from siliciclastic Rhaetian deposit, Tatra Mountains, *Mineral. Soc. Poland-Spec. Pap.,* **24,** 299–302.
Ogg, J.G., 2012. Geomagnetic polarity time scale, in *The Geologic Time Scale 2012*, pp. 85–113, eds Gradstein, F.M., Ogg, J.G, Schmitz, M. & Ogg, G., Elsevier.
Özdemir, Ö. & Dunlop, D.J., 2002. Thermoremanence and stable memory of single-domain hematites, *Geophys. Res. Lett.*, **29**(18).
Özdemir, Ö. & Dunlop, D.J., 2006. Magnetic memory and coupling between spin-canted and defect magnetism in hematite, *J. geophys. Res.,* **111**(B12), doi:10.1029/2006JB004555.
Özdemir, Ö. & Dunlop, D.J., 2014. Hysteresis and coercivity of hematite, *J. geophys. Res.,* **119**(4), 2582–2594.
Parrish, J.T., Daniel, I.L., Kennedy, E.M. & Spicer, R.A., 1998. Paleoclimatic significance of mid-Cretaceous floras from the middle Clarence Valley, New Zealand, Palaios, **13**(2), 149–159.
Roberts, A.P., Cui, Y. & Verosub, K.L., 1995. Wasp-waisted hysteresis loops: mineral magnetic characteristics and discrimination of components in mixed magnetic systems, *J. geophys. Res.,* **100**(B9), 17 909–17 924.
Roy, J.L. & Park, J.K., 1972. Red beds: DRM or CRM?, *Earth Planet. Sci. Lett.*, **17**, 211
Sagnotti, L., Macrì, P., Egli, R. & Mondino, M., 2006. Magnetic properties of atmospheric particulate matter from automatic air sampler stations in Latium (Italy): toward a definition of magnetic fingerprints for natural and anthropogenic PM 10 sources, *J. geophys. Res.,* **111**(B12), doi:10.1029/2006JB004508.
Sheldon, N.D., 2005. Do red beds indicate paleoclimatic conditions?: a Permian case study, *Palaeogeogr. Palaeoclimatol. Palaeoecol.,* **228**(3–4), 305–319.
Sierra-Rojas, M.I. & Molina-Garza, R.S., 2014. La Formación Zicapa del sur de México: revisión estratigráfica, sedimentología y ambientes sedimentarios, *Rev. Mex. Cienc. Geol.,* **31**(2), 174–189.
Sierra-Rojas, M.I., Molina-Garza, R.S. & Lawton, T.F., 2016. The lower Cretaceous Atzompa Formation in South-Central Mexico: record of evolution from extensional backarc basin margin to carbonate platform, *J. Sediment Res.,* **86**(6), 712–733.
Steiner, M.B., 1983. Detrital remanent magnetization in hematite, *J. geophys. Res.,* **88**(B8), 6523–6539.
Stern, B., 2010, The anatomy and ontogeny of modern intra-oceanic arc systems, in *The Evolving Continents: Understanding Processes of Continental Growth*, pp. 7–34, eds Kusky, T.M., Zhai, M.G. & Xiao, W., Geological Society, London, Special Publications, 338, doi:10.1144/SP338.2.
Talavera-Mendoza, O., Ruiz, J., Gehrels, G.E., Valencia, V.A. & Centeno-García, E., 2007. Detrital zircon U/Pb geochronology of southern Guerrero and western Mixteca arc successions (southern Mexico): new insights for the tectonic evolution of southwestern North America during the late Mesozoic/, *Bull. geol. Soc. Am.,* **119,** 1052–1065.
Tan, X., Kodama, K.P., Gilder, S. & Courtillot, V. 2007. Rock magnetic evidence for inclination shallowing in the Passaic Formation red beds from the Newark basin and a systematic bias of the Late Triassic apparent polar wander path for North America, *Earth planet. Sci. Lett.,* **254**(3–4), 345–357.
Tauxe, L. & Kent, D.V., 1984. Properties of a detrital remanence carried by haematite from study of modern river deposits and laboratory redeposition experiments, *Geophys. J. Int.,* **76**(3), 543–561.
Tauxe, L. & Kent, D.V., 2004. A simplified statistical model for the geomagnetic field and the detection of shallow bias in paleomagnetic inclinations: was the ancient magnetic field dipolar?, in *Timescales of the Paleomagnetic Field*, pp. 101–115, eds Channell, J.E.T., Kent, D.V., Lowrie, W. & Meert, J.G., American Geophysical Union.
Tauxe, L., Kent, D.V. & Opdyke, N.D., 1980. Magnetic components contributing to the NRM of Middle Siwalik red beds, *Earth planet. Sci. Lett.,* **47**(2), 279–284.
Tauxe, L., Mullender, T.A.T. & Pick, T., 1996. Potbellies, wasp-waists, and superparamagnetism in magnetic hysteresis, *J. geophys. Res.,* **101**(B1), 571–583
Torsvik, T.H. *et al.*, 2012. Phanerozoic polar wander, palaeogeography and dynamics, *Earth Sci. Rev.,* **114**(3–4), 325–368.
Van der Voo, R. & Torsvik, T.H., 2012. The history of remagnetization of sedimentary rocks: deceptions, developments and discoveries, *Geol. Soc. London Spec. Publ.,* **371**(1), 23–53.
Van Houten, F.B., 1973. Origin of Red Beds a Review-1961–1972. *Annu. Rev. Earth Planet. Sci.,* **1**(1), 39–61.
Walker, T.R., 1967a. Formation of red beds in modern and ancient deserts, *Bull. geol. Soc. Am.,* **78**(3), 353–368.
Walker, T.R., 1967b. Color of recent sediments in tropical Mexico: a contribution to the origin of red beds, *Bull. geol. Soc. Am.,* **78**(7), 917–920.
Walker, T.R., Larson, E.E. & Hoblitt, R.P., 1981. Nature and origin of hematite in the Moenkopi Formation (Triassic), Colorado Plateau: a contribution to the origin of magnetism in red beds, *J. geophys. Res.,* **86**(B1), 317–333.
Whidden, K.J., Lund, S.P., Bottjer, D.J., Champion, D. & Howell, D.G., 1998. Paleomagnetic evidence that the central block of Salinia (California) is not a far-traveled terrane, *Tectonics,* **17**(3), 329–343.
Zijderveld, J.D.A., 1967. A.C. demagnetization of rocks: analysis of results, in *Methods in Paleomagnetism*, pp. 254–286, eds Collinson, D., Creer, K. & Runcorn, S., Elsevier Science B.V.

CAPITULO 5. DISCUSIÓN Y CONCLUSIONES

Oaxaquia según la definición de Ortega-Gutiérrez et al. (1995) corresponde a un bloque de corteza continental con similaridades litológicas, estructurales y de edad que se extiende desde Tamaulipas hasta Oaxaca. En el desarrollo de la tesis no es utilizado el término *Sensu Stricto*, sino que se usa el concepto de "margen occidental de Oaxaquia" como referencia al bloque de corteza continental del sur de México, que integra tanto Oaxaquia como terrenos aledaños con corteza continental, el cual fue afectado durante el Mesozoico por eventos de acreción de terrenos, extensión y magmatismo.

En el trabajo de tesis la evolución del margen occidental de Oaxaquia es evaluado desde dos puntos de vista:

Proveniencia de Sedimentos: La composición de granos detríticos y minerales densos de afinidad Oaxaquia en lo que refiere a su composición y edad.

Corteza continental sujeta a procesos de extensión: Con base en los resultados de proveniencia de sedimentos, inferimos que el bloque continental siendo erosionado y que proporciona sedimentos a las cuencas activas durante el Mesozoico, eran derivados directamente de la corteza continental del Mesoproterozoico-Paleozoico (Bloque Oaxaquia).

Depositación directa de unidades del Cretácico Inferior sobre el Basamento del Complejo Acatlán (el cual es parte del microcontiente de Oaxaquia), unidades de brechas con bloques mayores a 1 metro de igual composición que el basamento circundante, predominio en la señasl de edad en circones detríticos en areniscas.

Durante el Proyecto de doctorado se recolectaron datos con el fin de determinar el ambiente tectónico en el cual se desarrollaron las cuencas sedimentarias y el magmatismo en el sur occidente de México durante el Cretácico Temprano. En los capítulos presentados previamente, se mostraron evidencias sedimentológicas que confirman la apertura de cuencas en un ambiente tectónico de un arco extensional.

Estudios paleomagnéticos y magnetoestratigráficos en capas rojas permiten además de conocer la paleolatitud de la cuenca de depósito, constreñir las edades de depósito. Sin embargo, para mayor confiabilidad de los resultados magnéticos obtenidos en capas rojas, en especial con lo que respecta a tiempo, es necesario conocer a fondo las características de los minerales portadores de la magnetización y los tiempo de adquisición de ésta. Para tal propósito, se realizó un estudio detallado de paleomagnetismo, magnetoestratigrafía y magnetismo de rocas (Capítulo 4) en la Formación Zicapa.

Finalmente, con los datos y observaciones obtenidos se puede concluir que:

Durante el Cretácico Temprano el núcleo continental del sur de México (bloque Mixteco-Oaxaca) fue afectado por magmatismo intermedio, correspondiente a un arco continental. Dicho magmatismo es evidenciado en una serie de granitoides félsicos a intermedios, derrames de lava, y depósitos volcanoclásticos de edad entre 140-126 Ma (Tabla 4 y Figura 11, capítulo 3). En la Formación Zicapa los derrames de lava y las rocas volcano-sedimentarias hacen parte primordial del miembro San Andrés, con edades máxima de depósito de 133 ± 1 Ma, interpretado con una edad cercana a la edad de depósito. Facies sedimentarias correlacionables se observaron en la Formación Chapolapa al sur de la zona de estudio, las cuales presentan edades entre 133 y 126 Ma (Hernández et al., 2004; Campa e Iriondo, 2004). Los elementos correspondientes a las raíces del arco magmático se atribuyen a migmatitas e intrusivos calci-alcalinos del Complejo Xolapa (e.g. Granito el Pozuelo; Solari et al., 2007). Dicho arco continental es denominado como arco arco Zicapa-Xolapa (Sierra-Rojas y Molina-Garza, 2014).

Análisis sedimentológicos y de arquitectura de facies permitieron determinar los ambientes de depósito para la Formación Zicapa en la región de la plataforma Guerrero-Morelos (Figura 1, Capitulo 2). Las unidades basales de la Formación Zicapa se caracterizan por brechas, conglomerados y areniscas correspondientes a depósitos de gravedad con fuentes locales. La fuente de dichos sedimentos corresponde al basamento metamórfico que subyace a la Formación Zicapa, los cuales son interpretados como contemporáneos con la apertura de la cuenca.

Posteriormente se dan las condiciones propicias para que en algunas localidades se desarrollen depocentros continentales lacustres, mientras que en otras localidades se presenta invasión marina con depósitos de calizas marinas someras. La depositación de calizas continentales y marinas (miembro cerro La Cruz), es intepretado como un periodo de calma tectónica previo al desarrollo del volcanismo explosivo (Miembro San Andrés). La arquitectura de facies permitió establecer que la Formación Zicapa fue depositada en una cuenca extensional ubicada en un ambiente transicional, el cuál permitió la incursión marina y la depositación de gruesas sucesiones de sedimentos contemporáneas con vulcanismo.

Durante el Cretácico Temprano un régimen extensional favoreció la apertura de cuencas a lo largo del bloque Mixteco-Oaxaca. Dichas cuencas localizadas al oriente del arco Zicapa-Xolapa reciben sedimentos provenientes de el basamento ígneo-metamórfico (Bloque Oaxaquia) y el arco (Arco Zicapa-Xolapa), tal es el caso de la cuenca del Tentzo (Figura 12, Capítulo 3). Por su posición con respecto al arco, la distribución de facies sedimentarias y la proveniencia de sedimentos, la cuenca de Tentzo es interpretada como una cuenca de tras arco.

La cuenca del Tentzo, al igual que la cuenca de Zicapa, es una cuenca de carácter extensional con deposición continental a marina, cuya evolución sedimentológica está directamente relacionada a las tasas de sedimentación y extensión. Las altas tasas de sedimentación en la cuenca del Tentzo (3.6 mm/año) durante las etapas de inicio y climax de la extensión, permitieron el depósito de abanicos aluviales, turbiditas lacustres y ríos anastomosados. Tasas de sedimentación menores se presentan posteriormente durante el depósito en ambientes mareales y marinos someros, dónde el aporte de sedimetos terrígenos disminuye notablemente y se propicia la sedimentación carbonatada. El estimado del tiempo transcurrido entre las etapas de apertura de la cuenca y la calma tectónica con depósito de carbonatos oscila entre 4 y 10 Ma. La rápida evolución de la cuenca puede estar relacionada con la interacción entre la dinámica tectónica de una slab localizado al occidente de la cuenca y la tectónica extensional heredada desde el Jurásico en el Golfo de México.

Una característica predominante en las rocas de las formaciones Zicapa y Atzompa, es la presencia de capas rojas, la cuales se caracterizan por su coloración rojiza como respuesta a la presencia de hematita pigmentaria como cemento. Experimentos de desmagnetización térmica y magnetismo de rocas en la Formación Zicapa sugieren que las capas rojas poseen una mezcla de partículas responsables por la magnetización remanente natural (MRN). La magnetización característica (ChM) en las capas rojas de la Formación Zicapa reside en hematita detrítica, es caracterizada por una componente con altas temperaturas de bloqueo (CAT) >550°C, relaciones ente parámetros de histéresis H_{cr}/H_c entre 2.5 y 3.7 y M_{rs}/M_s entre 0.25 y 0.35 (Figura 10, capítulo 4), y tamaño de partícula > 10 μm correspondiente a partículas de dominio sencillo. Una magnetización sobreimpuesta es encontrada en todas los sitios analizados de una componente de temperatura de bloqueo intermedia (CTI) (250°C-500°C) es atribuida a hematita pigmentaria, presenta relaciones ente parámetros de histéresis H_{cr}/H_c bajos entre 0.5 y 2 y M_{rs}/M_s altos entre 0.4 y 0.6, y tamaño de partícula < 1 μm. Finalmente, una magnetización viscosa fue encontrada en varios sitios con temperaturas de bloqueo baja menores a 250°C, y coercitividades bajas ~10 mT, por lo cual se atribuye a magnetita.

Las direcciones paleomagnéticas obtenidas para la magnetización detrítica (CAT) y pigmentaria (CTI) tras aplicar la corrección de elongación e inclinación (E/I) son de D=272.5, I=36.5° y D=282.0, I=28.2° respectivamente. Al comparar las direcciones obtenidas con las direcciones esperadas para el cratón de Norteamérica (McElhinny & McFadden, 2000) se observa que son discordantes, especialmente en la declinación; se determinaron rotaciones en el eje vertical antihorarias entre 69° y 59°. Sin embargo, al comparar inclinaciones esperadas con obtenidas no fue posible determinar un movimiento latitudinal preciso, ya que la componente de temperatura intermedia muestra una anomalía significativa en inclinación (F=-16.8±12.7), mientras que la componente de alta temperatura no presenta anomalía (F=-7.7 ± 13.0). Debido a la posibilidad de que existan magnetizaciones sobreimpuestas en la componente de temperatura intermedia que no fueron removidas, le damos mayor credibilidad a los valores de inclinación obtenidos en la componente de alta temperatura.

Con base en las dirección media de la componente de alta temperatura obtenida después de la corrección estructural, corregida por el método de Elongation/Inclination (E/I), es posible estimar la paleolatitud al tiempo de depósito. La inclinación media de la Formación Zicapa es de 36.5º+/-12.8º, con lo cual se obtiene una paleolatitud para la región de la Plataforma Guerrero-Morelos de 20.3º/-5.1. La edad de la magnetización está constreñida entre la edad máxima de depósito de 133+/-3 Ma y la edad determinada por la correlación magnetoestratigráfica de 126 a 131 Ma.

La paleolatitud esperada a partir del polo de referencia para Norte América es de 26º+/- 2º. Los resultados paleomagnéticos reportados para la Formación Morelos en la región de Huajuapan de León (345.5,39.5 – α95=3.6º) indica una paleolatitud comparable con la obtenida en este estudio. El hecho de que el paleopolo para la Formación Morelos por Bohnel et al. (1999) es concordante, sugiere que la discordancia en declinación observada en la Formación Zicapa puede ser explicada por la cercanía de la localidad San Juan de las Joyas con los sistemas de fallas laterales izquierdas La Venta-Tierra Colorada.

En los trabajos de Rodriguez-Rodriguez et al. (2013) y Serrano-García et al. (2013) realizados en el marco del proyecto doctoral, se reportan las paleo latitudes para las formaciones Atzompa y Caltepec respectivamente. Las direcciones paleomagnéticas obtenidas para la formación Atzompa de D=334.8, I=24.3 (α95=14.2, k=14.1, n=9) y para la Formación Caltepec de D=352.6, I=24.3 (α95=8.4, k=33.8, n=10) son ambas discordantes con las direcciones esperadas para el cratón de Norteamérica en el Cretácico Temprano, lo cual indica una rotación moderada en sentido horario.

Las rotaciones antihorarias en el eje vertical observadas en la Formación Zicapa ya habían sido reportadas en localidades de la plataforma Guererro-Morelos (Molina-Garza et al., 2003). Estas rotaciones son explicadas como consecuencia de rotación de bloques asociados a la actividad lateral izquierda del sistema Chacalapa-La Venta y La Venta-Tierra Colorada (Ratschbacher et al., 1991; Riller et al., 1992; Tolson, 2005; Solari et al., 2007) ocurrida entre el Cretácico Superior y Eoceno.

Dicha deformación ha sido reportada afectando unidades correlacionables genéticamente con la Formación Zicapa, las cuales hemos agrupado dentro del Arco de Zicapa-Xolapa, como son la Formación Chapolapa y el granito Las Piñas (Solari et al., 2007).

Datos paleomagnéticos previos en el Bloque Chortís (Gose, 1985; Molina-Garza et al., 2017), modelos geodinámicos basados en similitudes estratigráficas, estructurales y anomalías magnéticas (Rogers et al., 2007; Harlow et al., 2004, Molina-Garza et al., 2017) ubican al bloque Chortís adyacente al sur de México. El movimiento del bloque Chortís con dirección lateral izquierda desde el sur de México a partir del Cretácico Superior fue el mecanismo geodinámico responsable de la deformación en la región de Tierra Colorada y La venta y de la rotación de bloques en la plataforma Guerrero-Morelos.

REFERENCIAS

Alaniz-Alvarez, S.A., van der Heyden, P., Samaniego-Nieto, A.F., y Ortega-Gutiérrez, F.,1996, Radiometric and kinematic evidence for Middle Jurassic strike-slip faulting in southern Mexico related to the opening of the Gulf of Mexico. Geology, 24(5), 443-446.

Anderson, T.H., McKee, J.W., y Jones, N.W., 1991, Anorthwest-trending, Jurassic fold nappe, northernmost Zacatecas, Mexico: Tectonics, v. 10, p. 383–401.

Ángeles-Moreno, E., 2006, Petrografía, geología estructural y geocronología del borde noroccidental del terreno Cuicateco, Sierra Mazateca, estado de Oaxaca, México [M.S. Thesis]: México, D.F., Universidad Nacional Autónoma de México, 194 p.

Barboza-Gudiño, J.R., Hoppe, M., Gómez-Anguiano, M., y Martínez-Macías, P.R., 2004, Aportaciones para la interpretación estratigráfi ca y estructural de la porción noroccidental de la Sierra de Catorce, San Luis Potosí, México: Revista Mexicana de Ciencias Geológicas, v. 21, p. 299–319.

Barboza-Gudiño, J.R., Orozco-Esquivel, M.T., Gomez-Anguiano, M., y Zavala-Monsiváis, A., 2008, The early Mesozoic volcanic arc of western North America in northeastern Mexico: Journal of South American Earth Sciences, v. 25, p. 49–63.

Barboza-Gudiño, J.R., Tristán-González, M., y Torres-Hernández, J.R., 1998, The Late Triassic–Early Jurassicactive continental margin of western North America in northeastern Mexico: Geofísica Internacional, v. 37,p. 283–292.

Barboza-Gudiño, J.R., Tristán-González, M., y Torres-Hernández, J.R., 1999, Tectonic setting of pre-Oxfordian units from central and northeastern Mexico: A review, in Bartolini, C., Wilson, J.L., and Lawton,T.F., eds., Mesozoic Sedimentary and Tectonic History of North-Central Mexico: Geological Society ofAmerica Special Paper 340, p. 197–210.

Bartolini, C., Lang, H., y Spell, T., 2003, Geochronology, geochemistry, and tectonic setting of the Mesozoic Nazas arc in north-central Mexico, and its continuation to northern South America: America Association of Petroleum Geologists Memoir 79, p. 427–461.

Blickwede, J.F., 2001, The Nazas Formation: A detailed look at the early Mesozoic convergent margin along the western rim of the Gulf of Mexico Basin, in Bartolini, C., Buffl er, R.T., and Cantú-Chapa, A., eds., The Western Gulf of Mexico Basin:

Tectonics, Sedimentary Basins, and Petroleum Systems: American Association of Petroleum Geologists Memoir 75, p. 317–342.

Busby, C. ,2004, Continental growth at convergent margins facing large ocean basins: a case study from Mesozoic convergent-margin basins of Baja California, Mexico. Tectonophysics, 392(1-4), p. 241-277.

Campa-Uranga, M. F., García-Díaz, J. L. e Iriondo, A., 2004, El arco volcánico-sedimentario del Jurásico Medio (Grupo Tecocoyunca y Las Lluvias) de Olinalá, Guerrero: IV Reunión de Nacional de Ciencias de la Tierra, Abstracts with Programs, Juriquilla, Qro., p. 76

Campa-Uranga, M.F., e Iriondo A., 2004, Significado de dataciones cretácicas de los arcos volcánicos de Taxco, Taxco el Viejo y Chapolapa, en la evolución de la Plataforma Guerrero Morelos: IV Reunión Nacional de Ciencias de la Tierra, Juriquilla, Querétaro, Sociedad Geológica Mexicana, Libro de Resúmenes, 76.

Campa-Uranga, M.F., Torres de León, R., Iriondo, A. y Premo, W.R., 2012, Caracterización geológica de los ensambles metamórficos de Taxco y Taxco el Viejo, Guerrero, México: Boletín la Sociedad Geológica Mexicana, v. 64, p. 369–385.

Campos-Madrigal, E., Centeno-García, E., Mendoza-Rosales, C.C., y Silva-Romo, G., 2013, Sedimentología, reconstrucción paleoambiental y significado tectónico de las sucesiones clásticas del Jurásico Medio en el área de Texcalapa, Puebla-Huajuapan de León, Oaxaca: Revisión de las formaciones Ayuquila y Tecomazúchil: Revista Mexicana de Ciencias Geológicas, 30, p. 34–50.

Carfantan, J. C.,1981, Evolución estructural del sureste de México, Paleogeografía e historia tectónica de las zonas internas mesozoicas. Revista mexicana de ciencias geológicas, 5(2), 207-216.

Centeno-García, E., Corona-Chávez, P., Talavera-Mendoza, O., e Iriondo, A., 2003, Geologic and tectonic evolution of the western Guerrero terrane-a transect from Puerto Vallarta to Zihuatanejo, Mexico, en Geologic transects across Cordilleran Mexico, Guidebook for the field trips of the 99th Geological Society of America Cordilleran Section Annual Meeting, Puerto Vallarta, Jalisco, Mexico: Universidad Nacional Autónoma de México, Instituto de Geología, Publicación Especial, 1, 201-228.

Coombs, H.E., 2016, Geochemical and geochronological constraints on terrane definition in Mexico [Ph.D. Thesis]: Cardiff University, 349 p.

Delgado-Argote, L.A., López-Martínez, M., York, D., y Hall, C.M., 1992, Geologic framework and geochronology of ultramafic complexes of southern Mexico: Canadian Journal of Earth Sciences, v. 29, p. 1590-1604.

Dickinson, W. R., 2004, Evolution of the North American cordillera. Annu. Rev. Earth Planet. Sci., 32, 13-45. Dickinson, W.R., and Lawton, T.F., 2001a, Carboniferous to Cretaceous assembly and fragmentation of Mexico: Geological Society of America Bulletin, v. 113, p. 1142–1160.

Dickinson, W.R., y Lawton, T.F., 2001, Tectonic setting and sandstone petrofacies of the Bisbee basin (USA–Mexico): Journal of South American Earth Sciences, v. 14, p. 475–504.

Elías-Herrera, M., Sánchez-Zavala, J.L. y Macías-Romo, C., 2000, Geologic and geochronologic data from the Guerrero terrane in the Tejupilco area, southern Mexico: New constraints on its tectonic interpretation: Journal of South American Earth Sciences, v. 13, p. 355–375.

Ferrari, L., López-Martínez, M., Orozco-Esquivel, T., Bryan, S. E., Duque-Trujillo, J., Lonsdale, P., y Solari, L.,2013, Late Oligocene to Middle Miocene rifting and synextensional magmatism in the southwestern Sierra Madre Occidental, Mexico: The beginning of the Gulf of California rift. Geosphere, 9(5), 1161-1200.

Freydier, C., Lapierre, H., Briqueu, L., Tardy, M., Coulon, C. and Martinez-Reyes, J., 1997, Volcaniclastic Sequences with Continental Affinities within the Late Jurassic-Early Cretaceous Guerrero Intra-oceanic Arc Terrane (Western Mexico): The Journal of Geology, V. 105, p. 483-502.

Ferrusquia-Villafranca, I., 1976, Estudios geológico-paleontológicos en la región Mixteca, pt.1: Geología del área Tamazulapan, Teposcolula, Yanhuitlan, Mixteca Alta, Estado de Oaxaca, México: Boletín del Instituto de Geología, v. 97, 160 p.

Fitz-Díaz, E., Campa-Uranga, M.F., López-Martínez, M., 2002, Fechamiento de las lavas andesíticas de la Formación Zicapa, en el límite oriental de la Plataforma Guerrero-Morelos, en III Reunión Nacional de Ciencias de la Tierra (Resumen): GEOS, 22(2), 178-179.

Freydier, C., Lapierre, H., Ruiz, J., Tardy, M., Martinez-R, J. y Coulon, C., 2000, The Early Cretaceous Arperos basin: an oceanic domain dividing the Guerrero arc from nuclear Mexico evidenced by the geochemistry of the lavas and sediments: Journal of South American Earth Sciences, v 13, 325–336.

Gabrielse, H., y Yorath, C. J., 1989, DNAG# 4. The Cordilleran Orogen in Canada, Geoscience Canada, 16(2).

Gose, W., 1985. Paleomagnetic results from Honduras and their bearing on Caribbean tectonics. Tectonics 4, p. 565–585.

Haenggi, W.T., 2001, Tectonic history of the Chihuahua trough, Mexico and adjacent USA, Part I: the pre-Mesozoic setting: Boletín la Sociedad Geológica Mexicana, v. LIV, p. 28–66.

Harlow, G., Hemming, S., Avé Lallemant, H., Sisson, V., y Sorensen, S., 2004, Two high-pressure-low-temperature serpentinite-matrix mélange belts, Motagua fault zone, Guatemala; a record of Aptian and Maastrichtian collisions: Geology, v. 32, p. 17–20.

Helbig, M., Keppie, J.D., Murphy, J.B. y Solari, L., 2012, U–Pb geochronological constraints on the Triassic–Jurassic Ayú Complex, southern Mexico: Derivation from the western margin of Pangea-A: Gondwana Research, v. 22, p. 910–927.

Hernández-Treviño, T., Torres de León, R., Solís-Pichardo, G., Schaaf, P., Hernández-Bernal, M. y Morales-Contreras, J., 2004, Edad de la Formación Chapolapa en la localidad de río Cochoapa, al oeste del Ocotito, estado de Guerrero: Reunión Anual de la Unión Geofísica Mexicana, Abstracts with Programs, v. 24, p. 179.

Johnson, S.E., Fletcher, J.M., Fanning, C.M., Vernon, R.H.,Paterson, S.R., y Tate, M.C., 2003, Structure, emplacement and lateral expansion of the San José tonalite pluton, Peninsular ranges batholith, Baja California, México: Journal of Structural Geology, v. 25, p. 1933–1957.

Jones, N.W., McKee, J.W., Anderson, T.H., y Silver, L.T., 1995, Jurassic volcanic rocks in northeastern Mexico: A possible remnant of a Cordilleran magmatic arc, in Jacques-Ayala, C., Gonzalez-Leon, C.M., and Roldan-Quintana, J., eds., Studies on the Mesozoic of Sonora and Adjacent Areas: Geological Society of America Special Paper 301, p. 179–190.

Kimbrough, D.L., Grove, M., y Morton, D.M., 2014, Timing and significance of gabbro emplacement within two distinct plutonic domains of the Peninsular Ranges batholith, southern and Baja California: Geological Society of America Bulletin, B30914–1.

Kimbrough, D.L., y Moore, T.E., 2003, Ophiolite and volcanic arc assemblages on the Vizcaino Peninsula and Cedros Island, Baja California Sur, Mexico: Mesozoic forearc lithosphere of the Cordilleran magmatic arc, en Johnson, S.E., Paterson, S.R., Fletcher, J., Girty, G.H., Kimbrough, D.L., y Martin-Barajas, A., eds., Tectonic evolution of northwestern Mexico and the southwestern USA: Boulder, Colorado, Geological Society of America Special Paper 374, p. 43–72.

Kirsch, M., Keppie, J.D., Murphy, J.B. y Solari, L.,2012, Permian–Carboniferous arc magmatism basin evolution along the western margin of Pangea: geochemical and geochronological evidence from the eastern Acatla´n Complex, southern Mexico. GSA Bull 124(9–10):1607–1628

Lawton, T.F. y Molina-Garza, R.S., 2014, U-Pb geochronology of the type Nazas Formation and superjacent strata, northeastern Durango, Mexico: Implications of a Jurassic age for continental-arc magmatism in north-central Mexico: Geological Society of America Bulletin, v. 126, p. 1–19.

López-Doncel, R.,2003, La Formación Tamabra del Cretácico medio en la porción central del margen occidental de la Plataforma Valles-San Luis Potosí, centro-noreste de México. Revista Mexicana de Ciencias Geológicas, 20(1).

López-Ticha, D., 1985, Revisión de la estratigrafía y potencial petrolero de la cuenca de Tlaxiaco: Boletín de la Asociación Mexicana de Geólogos Petroleros, v, 37, p. 49-92.

Martini, M., Ferrari, L., López-Martínez, M., Cerca-Martínez, M., Valencia, V., Serrano-Durán, L., y Dickinson, W. R., 2009, Cretaceous–Eocene magmatism and Laramide deformation in southwestern Mexico: No role for terrane accretion. Backbone of the Americas: Shallow subduction, plateau uplift, and ridge and terrane collision: Geological Society of America Memoir, 204, 151-182.

Martini, M., Mori, L., Solari, L.A. y Centeno-García, E., 2011, Sandstone provenance of the Arperos Basin (Sierra de Guanajuato, Central Mexico): Late Jurassic–Early Cretaceous backarc spreading as the foundation of the Guerrero terrane: Journal of Geology, v. 119, p. 597–617.

Martini, M., Solari, L. y Martínez-López, M., 2014, Correlating the Arperos Basin from Guanajuato, central Mexico, to Santo Tomás, southern Mexico: Implications for the paleogeography and origin of the Guerrero terrane: Geosphere, v. 10, p. 1-17.

Martini, M., y Ortega-Gutiérrez, F.,2016, Tectono-stratigraphic evolution of eastern Mexico during the break-up of Pangea: A review. Earth-Science Reviews.

Molina-Garza, R. S., van Hinsbergen, D. J., Boschman, L. M., Rogers, R. D., y Ganerød, M., 2017, Large-scale rotations of the Chortis Block (Honduras) at the southern termination of the Laramide flat slab. Tectonophysics. Ortega-Flores, B., Solari, L., Lawton, T.F., and Ortega-Obregón, C., 2013, Detrital-zircon record of major Middle Triassic–Early Cretaceous provenance shift, central Mexico: demise of Gondwanan continental fluvial systems and onset of backarc volcanism and sedimentation: International Geology Review, v. 56, p. 237–261.

Molina-Garza, R.S., Böhnel, H.N., y Hernández, T., 2003, Paleomagnetism of the Cretaceous Morelos and Mexcala formations, southern Mexico. Tectonophysics 361 (3), p. 301–317.

Molina-Garza, R.S., Delgado-Argote, L.A., Böhnel, H., Ramírez, E., Ortega, A., y Contreras Flores, R., 2014, A palaeomagnetic transect of the mid-Cretaceous Peninsular ranges batholith, Baja California, Mexico, in Morton, D.M., y Miller, F.K., eds., Peninsular Ranges batholith, Baja and Southern California: Geological Society of America Special Paper 211, p. 713–737.

Monger, J.W.H., Price, R.A. y Tempelman-Kluit, D.J., 1982, Tectonic accretion and the origin of the two major metamorphic and plutonic welts in the Canadian Cordillera, Geology, 10, 70–75.

Monroy-Fernández, M.G., Sosa-Patrón, A.A., 1984, Geología de la Sierra de Tentzo, Pue., borde norte del Terreno Mixteco: Boletín de la Sociedad Geológica Mexicana, 45(1-2), 43-71.

Mortensen, J. K., Hall, B. V., Bissig, T., Friedman, R. M., Danielson, T., Oliver, J., y Gabites, J. E.,2008, Age and paleotectonic setting of volcanogenic massive sulfide deposits in the Guerrero Terrane of central Mexico: Constraints from U-Pb age and Pb isotope studies. Economic Geology, 103(1), 117-140.

Ortega-Flores, B., Solari, L., Lawton, T. F., y Ortega-Obregón, C.,2014, Detrital-zircon record of major Middle Triassic–Early Cretaceous provenance shift, central Mexico: Demise of Gondwanan continental fluvial systems and onset of back-arc volcanism and sedimentation. International Geology Review, 56(2), 237-261.

Ortega-González, J. V., Lambarria-Silva, C., 1991 Informe geológico del prospecto Hoja Oaxaca, compilación geológica I. G. R. S. 1129: PEMEX, Coordinación Divisional de Exploración, Gerencia de Exploración Región Sur, Subgerencia de Geología superficial y Geoquímica, Inédito, 190 p.

Ortega-Gutiérrez, F., Elías-Herrera, M., Reyes-Salas, M., Macías-Romo, C., y López, R., 1999, Late Ordovician–Early Silurian continental collisional orogeny in southern Mexico and its bearing on Gondwana-Laurentia connections: Geology, v. 27, p. 719-722.

Ortega-Obregón, C., Solari, L., Gómez-Tuena, A., Elías-Herrera, M., Ortega-Gutiérrez, F., y Macías-Romo, C., 2013, Permian–Carboniferous arc magmatism in southern Mexico: U–Pb dating, trace element and Hf isotopic evidence on zircon grains of earliest subduction beneath the western margin of Gondwana: International Journal of Earth Sciences, v. 103, p. 1287-1300.

Ortuño-Arzate, S., Ferket, H., Cacas,M.C., Swennen, R., y Roure, F., 2003. Late cretaceous arbonate reservoirs in the Cordoba platform and Veracruz Basin, Eastern Mexico, En: Bartolini, C., Buffler, R.T., Blickwede, J. Eds., The Circum-Gulf of Mexico and the Caribbean: Hydrocarbon Habitats, Basin Formation, and Plate Tectonics: American Association of Petroleum Geologists Memoir, v. 79, pp. 476–514.

Pantoja-Alor, J., 1972, La formación Nazas del levantamiento de Villa Juárez, Estado de Durango: México, D.F., Sociedad Geológica Mexicana, Memorias de la Segunda Convención Nacional, p. 25-31.

Pindell, J. L., Cande, S. C., Pitman III, W. C., Rowley, D. B., Dewey, J. F., LaBrecque, J., y Haxby, W.,1988, A plate-kinematic framework for models of Caribbean evolution. Tectonophysics, 155(1-4), 121-138.

Pindell, J., y Kennan, L., 2009, Tectonic evolution of the Gulf of Mexico, Caribbean and northern South America in the mantle reference frame : an update: Geological Society of London Special Publication, v. 328, p. 1–55.

Ratschbacher, L., Franz, L., Min, M., Bachmann, R., Martens, U., Stanek, K., Stubner, K., Nelson, B.K., Herrmann, U.R., Weber, B., López-Martínez, M., Jonckheere, R., Sperner, B., Tichomirowa, M., Mcwilliams, M.O., Gordon, M.B., Meschede, M., y Bock, P., 2009, The North American-Caribbean Plate boundary in Mexico-Guatemala-Honduras: Geological Society of London, Special Publication 328, p. 219–293.

Riller, U., Ratschbacher, L., Frisch, W., 1992, Left-lateral transtension along the Tierra Colorada deformation zone, northern margin of the Xolapa magmatic arc of southern Mexico. J. S. Am. Earth Sci. 5, p. 237–249.

Rodríguez-Rodríguez, R., Molina-Garza, R.S., y Sierra-Rojas, M.I., 2013, Paleomagnetismo y Magnetoestratigrafía de la Formación Atzompa, Cretácico Inferior, Puebla, [Resumen]: Unión Geofísica Mexicana, Reunión Anual, Libro de Resumenes, v. 31, p. 91.

Rogers, R.D., Mann, P., y Emmet, P.A., 2007, Tectonic terranes of the Chortis block based on integration of regional aeromagnetic and geologic data. En: Mann, P., eds, Geologic and tectonic development of the Caribbean plate in northern Central America: Geological Society of America Special Paper 428, p. 65–88

Schmidt, K.L., Wetmore, P.H., Alsleben, H., y Paterson, S.R., 2014, Mesozoic tectonic evolution of the southern Peninsular ranges batholith, Baja California, Mexico: Longlived history of a collisional segment in the Mesozoic Cordilleran arc: Geological Society of America Memoirs, v. 211, p. 645–668.

Serrano-García, D., Sierra-Rojas, M.I., y Molina-Garza, R.S., 2014, Paleomagnetismo, magnetoestratigrafía y análisis de procedencia de la Formación Caltepec, Sur de Puebla [Resumen]: Unión Geofísica Mexicana, Reunión Anual, Libro de Resumenes, v. 34, p. 131–132.

Sierra-Rojas, M.I., and Molina-Garza, R.S., 2014, La Formación Zicapa del sur de México: revisión estratigráfica, sedimentología y ambientes sedimentarios: Revista Mexicana de Ciencias Geológicas, v. 3, p. 1174–189.

Sierra-Rojas, M.I., Molina-Garza, R.S., Lawton, T.F., 2016. The Aptian Atzompa formation in south central Mexico: record of evolution from extensional back-arc basin margin to carbonate platform. J. Sediment. Res. 86, p. 712–733.

Sigloch, K., & Mihalynuk, M. G., 2013, Intra-oceanic subduction shaped the assembly of Cordilleran North America. Nature, 496(7443), 50.

Solari, L.A., Dostal, J., Ortega-Gutiérrez, F. y Keppie, J.D., 2001, The 275 Ma arc-related La Carbonera stock in the northern Oaxacan Complex of southern Mexico: U–Pb geochronology and geochemistry. Rev Mex Cienc Geol 18(2):149–161.

Solari, L.A., Torres de León, R., Hernández-Pineda, G., Solé, J., Solís-Pichardo, G., and Hernández-Treviño, T., 2007, Tectonic significance of Cretaceous-Tertiary magmatic and structural evolution of the northern margin of the Xolapa Complex, Tierra Colorada area, southern Mexico: Geological Society of America Bulletin, v. 119, p. 1265–1279.

Stern, R. J., y Dickinson, W. R. (2010). The Gulf of Mexico is a Jurassic backarc basin. Geosphere, 6(6), 739-754.

Talavera-Mendoza, O., Ruiz, J., Gehrels, G.E., Valencia, V.A., and Centeno-García, E., 2007, Detrital zircon U/Pb geochronology of southern Guerrero and western Mixteca arc successions (southern Mexico): New insights for the tectonic evolution of southwestern North America during the late Mesozoic Geological Society of America Bulletin, v. 119, p. 1052–1065.

Tolson, G., 2005, La falla Chacalapa en el sur de Oaxaca. Boletín de la Sociedad Geológica Mexicana, 57(1), p. 111-122.

Torres, R., Ruiz, J., Patchett, P.J. y Grajales-Nishimura, J.M., 1999, Permo–Triassic continental arc in Eastern Mexico; tectonic implications for reconstructions of southern North America. En: Bartolini C, Wilson JL, Lawton TF (eds) Mesozoic sedimentary and tectonic history of north–central Mexico. Geological Society of America Special Paper 340, pp 191–196

Torres-Carrillo, X. G., Delgado-Argote, L. A., Böhnel, H., Molina-Garza, R. S., & Weber, B., 2016, Palaeomagnetic assessment of plutons from the southern Peninsular Ranges batholith and the Jurassic Vizcaíno igneous suites, Baja California, México. International Geology Review, 58(4), p. 489-509.

Valencia, V.A., Righter, K., Rosas-Elguera, J., López-Martínez, M., y Grove, M., 2013, The age and composition of the pre-Cenozoic basement of the Jalisco Block: implications for and relation to the Guerrero composite terrane: Contributions to Mineralogy and Petrology, v. 166, p. 801–824.

Vega-Granillo, R., Salgado-Souto, S., Herrera-Urbina, S., Valencia, V., Ruiz, J., Meza-Figueroa, D., y Talavera-Mendoza, O., 2008. U–Pb detrital zircon data of the Rio Fuerte Formation (NW Mexico): Its peri-Gondwanan provenance and exotic nature in relation to southwestern North America. Journal of South American Earth Sciences, 26(4), 343-354.

Wilson, J.L., y Ward, W.C., 1993, Early Cretaceous carbonate platforms of northeastern and east-central Mexico, En: Simo, J.A., Scott, R.W., and Masse, J.P., eds., Cretaceous carbonate platforms: American Association of Petroleum Geologists Memoir 56, p. 35-49.

ANEXO 1

GEOCRONOLOGÍA DE U-PB PARA LAS MUESTRAS DE LA FORMACIÓN ZICAPA (CAPÍTULO 2)

Formación Zicapa, Miembro Ajuatetla MIS055

17°45'35.50"N		99° 5'10.65"W				CORRECTED RATIOS								CORRECTED AGES (Ma)							
	U (ppm)	Th (ppm)	Th/U	207Pb/ 206Pb	±1s	207Pb/ 235U	±1s	206Pb/ 238U	±1s	208Pb/ 232Th	±1s	Rho	206Pb/ 238U	±1s	207Pb/ 235U	±1s	207Pb/ 206Pb	±1s	Best age (Ma)	±1s
Zircon_10_018	273	56	0.17	0.0801 6	0.0016	1.9275	0.04496	0.17413	0.00209	0.04697	0.00136	0.52	110	2	141	8	766	103	110	2.0
Zircon_100_126	461	88	0.16	0.0829 7	0.00149	2.1482	0.05033	0.18669	0.0028	0.05332	0.00128	0.64	128	1	144	5	417	73	128	1.0
Zircon_12_021	226	54	0.20	0.0598 6	0.0018	0.76319	0.02411	0.09246	0.00092	0.02608	0.00083	0.31	149	3	207	16	932	147	149	3.0
Zircon_13_022	195	137	0.59	0.1043 6	0.00167	4.0611	0.07885	0.28157	0.0031	0.07764	0.00171	0.57	152	1	160	5	269	72	152	1.0
Zircon_14_023	156	72	0.39	0.0769 3	0.00162	2.0915	0.04865	0.1975	0.00198	0.05866	0.00141	0.42	178	3	193	12	413	133	178	3.0
Zircon_15_024	129	72	0.47	0.0795 1	0.00191	1.9532	0.05157	0.17873	0.00197	0.05038	0.00131	0.41	179	2	196	8	410	92	179	2.0
Zircon_16_026	382	311	0.68	0.0605 9	0.00115	0.82125	0.01745	0.09849	0.00094	0.02965	0.00065	0.45	191	3	241	6	827	47	191	3.0
Zircon_18_028	400	132	0.28	0.0733 7	0.00154	1.5455	0.03588	0.1528	0.00151	0.04362	0.00122	0.43	222	3	287	14	865	101	222	3.0
Zircon_2_009	69	45	0.55	0.0748 5	0.00232	1.3721	0.04561	0.13357	0.0016	0.0371	0.00152	0.36	228	3	248	11	446	91	228	3.0
Zircon_20_030	83	88	0.89	0.0838 1	0.00344	1.278	0.05672	0.11679	0.00199	0.0163	0.00057	0.38	230	4	250	17	444	145	230	4.0
Zircon_21_032	306	210	0.58	0.0724 1	0.00206	1.63819	0.05881	0.16409	0.00197	0.0496	0.00054	0.55	232	4	264	19	555	156	232	4.0
Zircon_22_033	345	118	0.29	0.0809 8	0.00146	2.1037	0.04215	0.18853	0.00166	0.05325	0.00122	0.44	235	3	253	11	444	91	235	3.0
Zircon_24_035	322	107	0.28	0.0724 3	0.00109	1.5826	0.02752	0.15863	0.0014	0.04676	0.00103	0.5	252	4	260	11	341	92	252	4.0
Zircon_25_036	-5489	-1514	0.23	0.0858 8	0.00617	1.80284	0.13284	0.15225	0.00206	0.04518	0.00071	0.18	270	2	289	6	456	50	270	2.0
Zircon_27_039	1582	503	0.27	0.0784 5	0.00118	1.8426	0.03177	0.17024	0.00145	0.03931	0.00094	0.49	271	3	284	9	404	77	271	3.0
Zircon_28_040	564	722	1.08	0.0602 3	0.00096	0.80138	0.01448	0.09654	0.00081	0.02953	0.00059	0.47	272	3	283	9	374	70	272	3.0
Zircon_29_041	150	91	0.51	0.0777 6	0.00202	1.3245	0.0364	0.124	0.0011	0.01562	0.00062	0.33	273	3	277	9	326	78	273	3.0
Zircon_3_010	204	76	0.31	0.0727 5	0.00153	1.5209	0.04307	0.15125	0.00287	0.04546	0.00132	0.67	274	4	290	20	421	145	274	4.0
Zircon_30_042	-1061	-662	0.53	0.0558 3	0.00231	0.27676	0.01343	0.03595	0.00051	0.0112	0.00015	0.34	280	4	288	13	366	113	280	4.0
Zircon_31_044	1374	459	0.28	0.0777 7	0.00109	1.9188	0.0329	0.17844	0.00177	0.05606	0.00129	0.58	293	4	317	8	572	58	293	4.0
Zircon_32_045	27	15	0.47	0.0817	0.00301	2.02984	0.08535	0.1802	0.00234	0.05376	0.00068	0.34	490	6	521	10	667	42	490	6.0
Zircon_33_046	156	61	0.33	0.0529 4	0.00185	0.3142	0.01163	0.04319	0.00052	0.0155	0.00053	0.33	496	6	537	12	712	56	496	6.0
Zircon_34_047	235	88	0.31	0.0549 5	0.00229	0.21349	0.00984	0.02818	0.00036	0.00879	0.00011	0.29	500	7	326	20	-89	148	500	7.0
Zircon_35_048	103	44	0.36	0.0826 2	0.0024	2.2209	0.07058	0.19502	0.00254	0.05274	0.00158	0.41	570	5	576	14	599	61	570	5.0
Zircon_38_052	477	178	0.31	0.0560 9	0.00129	0.32915	0.008	0.04277	0.00034	0.01376	0.00032	0.32	594	5	598	8	612	34	594	5.0
Zircon_39_053	191	66	0.29	0.0734 2	0.00132	1.6377	0.03303	0.16208	0.00147	0.04828	0.00111	0.45	606	6	609	10	625	38	606	6.0
Zircon_4_011	708	184	0.22	0.0591 4	0.0016	0.36695	0.011	0.04656	0.00061	0.01322	0.00082	0.43	678	19	747	21	865	57	678	19.0

Zircon_40_054	347	165	0.40	0.07665	0.00115	1.9009	0.03406	0.17794	0.00174	0.05142	0.00113	0.55	712	11	836	25	1288	75	712	11.0
Zircon_41_056	241	71	0.25	0.07108	0.00135	1.5481	0.03275	0.15836	0.00147	0.04827	0.00106	0.44	754	6	856	16	1141	51	754	6.0
Zircon_42_057	126	45	0.30	0.07336	0.00285	1.40398	0.06386	0.13881	0.00206	0.0419	0.00061	0.47	808	9	877	20	1064	58	808	9.0
Zircon_43_058	166	66	0.34	0.05481	0.00192	0.32242	0.01183	0.04289	0.00047	0.01336	0.00043	0.3	838	12	891	27	1024	78	838	12.0
Zircon_44_059	182	49	0.23	0.07369	0.00177	1.6895	0.04361	0.1661	0.00158	0.04878	0.00112	0.37	848	8	927	15	1132	39	848	8.0
Zircon_45_060	458	93	0.17	0.07475	0.0012	1.8051	0.03323	0.17499	0.00159	0.04811	0.00135	0.49	867	8	885	16	929	47	867	8.0
Zircon_46_062	801	154	0.16	0.07909	0.00127	1.9972	0.03727	0.18277	0.00175	0.05299	0.00122	0.51	878	7	923	10	1039	30	878	7.0
Zircon_47_063	483	62	0.11	0.07923	0.00127	2.0821	0.03782	0.19052	0.00164	0.06008	0.00144	0.47	894	8	929	12	1021	36	894	8.0
Zircon_48_064	328	86	0.22	0.07773	0.00117	1.8625	0.03268	0.17349	0.00158	0.0503	0.00131	0.51	908	16	939	17	1007	42	908	16.0
Zircon_49_065	300	127	0.35	0.0792	0.00198	1.8979	0.05348	0.17507	0.00228	0.05057	0.00177	0.46	913	8	955	15	1058	43	913	8.0
Zircon_5_012	1128	1183	0.88	0.06666	0.00153	0.26808	0.00736	0.03005	0.00045	0.00958	0.00021	0.55	917	8	949	14	1024	40	917	8.0
Zircon_50_066	1024	331	0.27	0.0819	0.00115	2.1428	0.03815	0.19	0.00209	0.0551	0.00121	0.61	923	8	937	15	980	42	923	8.0
Zircon_51_068	197	73	0.31	0.07001	0.00163	1.38961	0.03689	0.14396	0.0014	0.04368	0.00042	0.43	923	9	931	20	957	57	923	9.0
Zircon_52_069	172	24	0.12	0.07586	0.00144	1.805	0.03954	0.17257	0.00179	0.0519	0.00055	0.52	948	8	950	13	960	38	948	8.0
Zircon_53_070	153	59	0.32	0.074	0.00148	1.6757	0.03682	0.16489	0.0015	0.04976	0.00119	0.41	949	8	963	11	998	29	949	8.0
Zircon_55_072	731	84	0.10	0.05162	0.00166	0.17011	0.00573	0.0239	0.00023	0.00751	0.00009	0.35	964	7	981	15	1017	43	964	7.0
Zircon_56_074	195	48	0.21	0.08334	0.00142	2.4771	0.05301	0.21436	0.00279	0.06299	0.00157	0.61	968	8	985	13	1026	36	968	8.0
Zircon_57_075	446	181	0.34	0.09103	0.00137	2.7455	0.0495	0.2189	0.00219	0.05018	0.00151	0.55	971	9	982	17	1011	49	971	9.0
Zircon_59_077	153	61	0.33	0.05388	0.00275	0.32738	0.01731	0.04444	0.00062	0.01345	0.0005	0.26	979	11	985	23	997	54	979	11.0
Zircon_6_014	257	220	0.72	0.07605	0.00183	1.7843	0.0505	0.16903	0.00254	0.05075	0.00147	0.53	991	13	995	15	1000	40	991	13.0
Zircon_60_078	236	134	0.48	0.07874	0.00157	2.0153	0.04395	0.18516	0.00161	0.0542	0.00119	0.41	998	8	1005	13	1023	37	1023	37.0
Zircon_61_080	169	58	0.29	0.07462	0.00164	1.5615	0.03718	0.15213	0.00138	0.04579	0.00114	0.38	991	9	1005	16	1033	48	1033	48.0
Zircon_62_081	545	205	0.32	0.07989	0.00136	1.8732	0.03695	0.17122	0.00171	0.04684	0.00108	0.51	1006	8	1016	14	1037	39	1037	39.0
Zircon_65_084	554	169	0.26	0.0739	0.00111	1.4825	0.02556	0.14598	0.00124	0.03449	0.001	0.49	984	8	999	14	1041	40	1041	40.0
Zircon_66_086	451	151	0.28	0.05408	0.00171	0.32158	0.01121	0.04313	0.00046	0.01348	0.00015	0.36	958	8	984	13	1046	37	1046	37.0
Zircon_67_087	132	62	0.40	0.08249	0.0019	2.0682	0.05273	0.1822	0.002	0.04976	0.00159	0.43	983	7	1006	12	1056	33	1056	33.0
Zircon_68_088	223	83	0.31	0.08477	0.00144	2.1454	0.04591	0.1837	0.00239	0.03453	0.00104	0.61	1040	9	1047	12	1062	32	1062	32.0
Zircon_69_089	233	62	0.22	0.07418	0.00141	1.6353	0.03467	0.16031	0.00151	0.04894	0.00122	0.44	962	9	999	19	1080	51	1080	51.0
Zircon_7_015	101	45	0.37	0.07288	0.00182	1.6302	0.04366	0.16248	0.00156	0.04606	0.00115	0.36	1026	10	1047	14	1091	37	1091	37.0
Zircon_71_092	108	62	0.49	0.08555	0.0018	2.6005	0.06049	0.22118	0.00221	0.06616	0.00185	0.43	978	7	1015	11	1093	29	1093	29.0

Zircon_72_093	523	104	0.17	0.07453	0.00127	1.6944	0.03169	0.1648	0.00129	0.04899	0.00108	0.41	1007	14	1040	18	1096	47	1096	47.0
Zircon_73_094	405	151	0.31	0.06787	0.0019	1.0871	0.04382	0.11097	0.00322	0.0312	0.001	0.72	1056	10	1081	12	1112	29	1112	29.0
Zircon_74_095	69	29	0.35	0.07886	0.00229	1.5455	0.04794	0.14305	0.00157	0.04523	0.00335	0.35	1162	11	1146	16	1119	39	1119	39.0
Zircon_75_096	110	100	0.76	0.0731	0.00161	1.6271	0.03826	0.16134	0.00134	0.04832	0.00101	0.35	1031	9	1068	12	1140	29	1140	29.0
Zircon_76_098	198	53	0.23	0.08325	0.00167	2.5641	0.05592	0.22329	0.00194	0.06538	0.00177	0.39	1058	10	1088	11	1141	27	1141	27.0
Zircon_77_099	467	126	0.23	0.07594	0.00114	1.7177	0.02936	0.16379	0.00134	0.04666	0.00126	0.48	996	9	1050	13	1149	35	1149	35.0
Zircon_78_100	89	84	0.79	0.06311	0.0017	0.69666	0.02088	0.08006	0.00104	0.02383	0.00057	0.44	1013	8	1061	11	1158	29	1158	29.0
Zircon_79_101	308	59	0.16	0.07324	0.00132	1.4963	0.03011	0.14868	0.00134	0.04347	0.00122	0.44	1095	9	1121	15	1166	39	1166	39.0
Zircon_80_102	359	79	0.18	0.07249	0.00145	1.6644	0.04063	0.16626	0.00233	0.04738	0.00142	0.57	862	9	949	19	1169	56	1169	56.0
Zircon_81_104	250	58	0.20	0.07384	0.00148	1.7208	0.03713	0.1689	0.00137	0.05	0.00125	0.37	1082	10	1115	13	1174	31	1174	31.0
Zircon_82_105	107	65	0.51	0.08476	0.00178	2.6636	0.06442	0.22792	0.00274	0.0651	0.0015	0.5	1040	13	1080	19	1177	49	1177	49.0
Zircon_83_106	764	157	0.17	0.0618	0.00124	0.66997	0.01598	0.07896	0.00103	0.02041	0.00082	0.54	1124	9	1143	12	1178	31	1178	31.0
Zircon_85_108	26	7	0.24	0.0819	0.00369	1.8255	0.08603	0.16306	0.00228	0.05054	0.00227	0.29	1060	11	1100	18	1185	44	1185	44.0
Zircon_86_110	377	83	0.18	0.07333	0.00139	1.6912	0.035	0.16749	0.00137	0.05021	0.00121	0.4	1019	9	1072	13	1194	33	1194	33.0
Zircon_88_112	503	134	0.22	0.08619	0.00121	2.6299	0.04254	0.22135	0.00179	0.06359	0.00134	0.5	1180	10	1186	13	1194	29	1194	29.0
Zircon_89_113	273	324	1.00	0.07807	0.00141	1.8131	0.03699	0.167	0.0016	0.0434	0.00122	0.47	1035	11	1091	16	1201	37	1201	37.0
Zircon_9_017	173	61	0.30	0.07178	0.00165	1.5153	0.03765	0.15386	0.00145	0.04512	0.00117	0.38	1113	9	1150	14	1221	33	1221	33.0
Zircon_90_114	290	87	0.25	0.07988	0.00128	2.2145	0.04132	0.20089	0.00193	0.05377	0.00129	0.51	1068	13	1126	29	1238	71	1238	71.0
Zircon_91_116	537	175	0.27	0.05512	0.00198	0.15187	0.00567	0.02006	0.0002	0.00657	0.00021	0.27	1121	11	1163	12	1243	27	1243	27.0
Zircon_92_117	1676	742	0.37	0.0865	0.0013	2.2402	0.05423	0.18802	0.00357	0.04515	0.00113	0.78	974	13	1055	31	1243	86	1243	86.0
Zircon_94_119	368	217	0.50	0.05578	0.00251	0.28267	0.01341	0.03714	0.00056	0.01112	0.00033	0.32	1079	11	1138	17	1257	44	1257	44.0
Zircon_95_120	301	62	0.17	0.08407	0.00135	2.5479	0.04754	0.21975	0.00211	0.06241	0.00206	0.51	1149	14	1188	22	1260	56	1260	56.0
Zircon_96_122	59	28	0.40	0.05501	0.00358	0.20981	0.01415	0.02801	0.0005	0.00921	0.00041	0.26	1103	15	1164	16	1269	33	1269	33.0
Zircon_98_124	-328	-147	0.38	0.07742	0.0017	1.4913	0.03604	0.14065	0.00141	0.04365	0.00297	0.42	1299	10	1290	16	1275	38	1275	38.0
Zircon_99_125	154	56	0.31	0.05328	0.0024	0.29129	0.01382	0.03983	0.0006	0.01228	0.00053	0.31	1252	15	1265	15	1277	33	1277	33.0
Zircon_1_MIS055_008	124	43	0.29	0.05579	0.00399	0.27896	0.02161	0.03626	0.00059	0.0113	0.00019	0.33	1281	11	1286	14	1294	28	1294	28.0
Zircon_17_027	-72	-25	0.29	0.03462	0.00246	0.37809	0.02744	0.08065	0.00121	0.01118	0.00067	0.2	1087	13	1164	15	1310	32	1310	32.0
Zircon_19_029	-257	-276	0.90	0.08476	0.00305	1.4676	0.05724	0.12514	0.00188	0.01794	0.00068	0.39	1324	14	1318	18	1310	40	1310	40.0
Zircon_36_050	102	27	0.22	0.06789	0.00365	0.32727	0.01895	0.03496	0.0005	0.01065	0.00016	0.31	760	11	917	24	1310	63	1310	63.0
Zircon_37_051	51	23	0.38	0.05868	0.00458	0.29655	0.02381	0.03672	0.0007	0.01271	0.00074	0.23	1288	12	1301	17	1328	40	1328	40.0

Zircon_58_076	132	69	0.44	0.05522	0.00393	0.33056	0.02585	0.04342	0.00073	0.01354	0.00022	0.32	914	12	1046	48	1335	138	1335	138.0
Zircon_63_082	67	17	0.21	0.07544	0.00211	1.6752	0.04981	0.16094	0.00161	0.05365	0.00199	0.34	1289	9	1309	12	1342	26	1342	26.0
Zircon_84_107	331	170	0.43	0.06474	0.0035	0.14924	0.00849	0.01716	0.00031	0.00548	0.0002	0.31	1111	19	1194	17	1349	26	1349	26.0
Zircon_87_111	114	6	0.05	0.07099	0.0022	1.5019	0.0494	0.1539	0.00169	0.05153	0.00304	0.34	1276	12	1341	13	1447	28	1447	28.0
Zircon_93_118	170	103	0.51	0.07013	0.00551	0.2262	0.01966	0.02339	0.00045	0.0071	0.00013	0.33	1599	16	1647	16	1703	28	1703	28.0

Formación Zicapa, Miembro San Andrés 0118-3c

18°12'16.77"N **98°42'24.04"W** **CORRECTED RATIOS** **CORRECTED AGES (Ma)**

	U (ppm)	Th (ppm)	Th/U	207Pb/ 206Pb	±1s	207Pb/ 235U	±1s	206Pb/ 238U	±1s	208Pb/ 232Th	±1s	Rho	206Pb/ 238U	±1 s	207Pb/ 235U	±1 s	207Pb/ 206Pb	±1s	Best age (Ma)	±1s
Zircon_11_020	768	355	0.44	0.04988	0.0012	0.15054	0.0039	0.02191	0.00021	0.00671	0.00015	0.37	130.6	0.8	142	4	340	63	130.6	0.8
Zircon_12_021	313	21	0.06	0.06331	0.00114	0.97809	0.02014	0.11155	0.00112	0.03949	0.00209	0.49	132.3	0.9	133	3	147	43	132.3	0.9
Zircon_13_022	485	190	0.37	0.05893	0.00212	0.17479	0.00658	0.02153	0.00024	0.00698	0.00019	0.29	133	1	141	3	287	51	133	1.0
Zircon_14_023	145	91	0.59	0.06759	0.00445	0.20887	0.01501	0.02241	0.00036	0.00683	0.00011	0.26	133.8	0.9	132	2	95	41	133.8	0.9
Zircon_16_026	3016	1137	0.36	0.04912	0.00088	0.14274	0.00274	0.02102	0.00014	0.00662	0.00013	0.36	134	1	141	3	245	49	134	1.0
Zircon_15_024	114	55	0.46	0.07454	0.00157	1.8049	0.04037	0.17553	0.00135	0.05088	0.00107	0.34	134	1	144	3	298	50	134	1.0
Zircon_17_027	995	355	0.34	0.05163	0.00124	0.16036	0.00407	0.02246	0.00019	0.00699	0.00015	0.32	134.1	0.9	135	2	154	40	134.1	0.9
Zircon_21_032	304	112	0.35	0.05762	0.0019	0.23224	0.00801	0.02926	0.00029	0.00881	0.0003	0.29	135	1	149	4	374	62	135	1.0
Zircon_19_029	391	128	0.31	0.05555	0.00217	0.16718	0.00673	0.02187	0.00022	0.00683	0.00018	0.24	135	1	143	4	270	67	135	1.0
Zircon_18_028	1171	316	0.25	0.07071	0.00099	1.5502	0.02406	0.15844	0.00106	0.03985	0.00072	0.43	135	2	158	14	513	197	135	2.0
Zircon_20_030	383	108	0.27	0.0953	0.00133	3.6822	0.06556	0.28016	0.00308	0.07606	0.00152	0.62	135	1	139	4	210	68	135	1.0
Zircon_23_034	1649	1173	0.67	0.05756	0.00524	0.16802	0.01647	0.02117	0.00027	0.00657	0.00009	0.33	136	2	145	4	302	59	136	2.0
Zircon_24_035	862	339	0.37	0.04929	0.00162	0.15094	0.00548	0.02221	0.00019	0.00702	0.00006	0.33	136	1	153	5	419	84	136	1.0
Zircon_22_033	424	189	0.42	0.08178	0.00123	2.5479	0.04579	0.22503	0.00223	0.06726	0.00128	0.55	136	1	147	5	334	75	136	1.0
Zircon_26_038	614	304	0.47	0.05355	0.00139	0.16219	0.00446	0.02204	0.0002	0.00678	0.00015	0.33	137	1	153	6	406	86	137	1.0
Zircon_28_040	649	349	0.51	0.05312	0.00181	0.15558	0.00551	0.02128	0.00021	0.00651	0.00016	0.27	137	1	136	3	129	48	137	1.0
Zircon_25_036	1309	308	0.22	0.10132	0.00132	3.9885	0.05694	0.28468	0.00168	0.08235	0.00148	0.41	137	2	164	6	565	76	137	2.0
Zircon_27_039	489	14	0.03	0.05691	0.00114	0.61777	0.0132	0.07861	0.00059	0.03031	0.00142	0.35	137	1	142	3	225	59	137	1.0
Zircon_31_044	877	417	0.45	0.05374	0.00208	0.16213	0.00698	0.02188	0.00022	0.00685	0.00006	0.29	138	1	144	6	246	94	138	1.0
Zircon_29_041	1400	947	0.64	0.05238	0.00141	0.15346	0.00453	0.02128	0.00026	0.00649	0.00013	0.41	138	1	147	3	292	53	138	1.0
Zircon_3_010	809	420	0.49	0.05166	0.00155	0.15071	0.00474	0.02109	0.0002	0.00661	0.00015	0.3	138	2	178	11	745	135	138	2.0
Zircon_30_042	2681	171	0.06	0.07665	0.001	1.8468	0.0266	0.17411	0.00108	0.02037	0.00081	0.42	138	1	142	4	211	59	138	1.0
Zircon_32_045	546	238	0.41	0.05517	0.00204	0.16233	0.0062	0.02138	0.0002	0.00692	0.00016	0.25	139	1	157	6	434	84	139	1.0
Zircon_35_048	1188	465	0.37	0.05222	0.00125	0.1613	0.0041	0.02238	0.00019	0.00714	0.00016	0.34	139	1	135	4	83	65	139	1.0
Zircon_34_047	653	253	0.37	0.05094	0.00153	0.15451	0.00487	0.0219	0.00021	0.00679	0.00016	0.3	139	1	147	6	285	100	139	1.0
Zircon_33_046	2090	653	0.29	0.04932	0.00109	0.15099	0.00346	0.02215	0.00014	0.00684	0.00014	0.26	139	2	155	5	404	66	139	2.0
Zircon_39_053	519	172	0.31	0.0838	0.00325	1.09531	0.05703	0.0948	0.00206	0.0282	0.0006	0.69	140	1	149	5	290	80	140	1.0

Zircon_4_011	474	233	0.46	0.0548 5	0.00208	0.16311	0.00641	0.02152	0.00022	0.00651	0.00019	0.2 6	140	1	144	3	208	54	140	1.0
Zircon_37_051	890	471	0.50	0.0548	0.00159	0.16488	0.00517	0.02179	0.00026	0.00686	0.00019	0.3 8	140	1	153	6	360	89	140	1.0
Zircon_40_054	968	397	0.39	0.0521 6	0.0012	0.15615	0.00381	0.02166	0.00018	0.00639	0.00013	0.3 3	140	1	149	4	306	64	140	1.0
Zircon_38_052	1456	581	0.38	0.0492 3	0.00113	0.15898	0.00388	0.02328	0.00019	0.00711	0.00016	0.3 4	140	1	146	4	238	70	140	1.0
Zircon_36_050	2561	759	0.28	0.0751 9	0.00098	2.0158	0.03046	0.19394	0.00149	0.05396	0.00097	0.5 1	140	1	142	3	189	54	140	1.0
Zircon_41_056	967	667	0.65	0.0641	0.00401	0.19154	0.01304	0.02167	0.00024	0.00664	0.00007	0.2 7	141	1	153	4	352	57	141	1.0
Zircon_42_057	2228	1360	0.58	0.0520 3	0.00114	0.14928	0.00347	0.02084	0.00016	0.00643	0.00013	0.3 3	141	2	158	8	417	103	141	2.0
Zircon_43_058	1033	535	0.49	0.0503 3	0.00146	0.14724	0.00446	0.0212	0.00019	0.00631	0.00014	0.2 9	141	1	142	3	145	52	141	1.0
Zircon_44_059	1337	821	0.58	0.0506 5	0.00127	0.15001	0.00391	0.0215	0.00016	0.00645	0.00013	0.2 7	141.2	0.9	143	3	163	52	141.2	0.9
Zircon_48_064	1265	262	0.20	0.0599 7	0.00276	0.21649	0.01052	0.02618	0.00026	0.00809	0.00009	0.2 5	142	2	148	5	248	73	142	2.0
Zircon_47_063	1916	536	0.26	0.0540 7	0.00146	0.15807	0.00481	0.0212	0.00019	0.00663	0.00006	0.3 3	142	2	170	7	580	86	142	2.0
Zircon_46_062	1342	543	0.38	0.0518 9	0.00467	0.16538	0.01576	0.02311	0.00032	0.00726	0.00026	0.2 2	142	1	139	3	94	58	142	1.0
Zircon_45_060	1843	736	0.38	0.0479	0.0012	0.14677	0.00385	0.02222	0.00018	0.00654	0.00014	0.3	142	1	143	5	162	73	142	1.0
Zircon_5_012	383	215	0.53	0.0577 8	0.00185	0.18956	0.00641	0.02397	0.00026	0.0077	0.00018	0.3 2	143	1	151	4	269	53	143	1.0
Zircon_50_066	7087	3625	0.48	0.0532 7	0.00153	0.15037	0.00481	0.02047	0.00013	0.00641	0.00004	0.3	143	1	152	4	295	55	143	1.0
Zircon_51_068	1716	627	0.35	0.0494 4	0.00114	0.15307	0.0039	0.02242	0.00025	0.00737	0.00015	0.4 3	143	2	145	3	169	52	143	2.0
Zircon_49_065	1676	393	0.22	0.0743 4	0.00097	1.8186	0.02677	0.17691	0.00122	0.04659	0.00089	0.4 6	143	2	193	13	856	134	143	2.0
Zircon_52_069	326	221	0.64	0.0539 2	0.00194	0.28709	0.0107	0.03854	0.00037	0.01384	0.00032	0.2 6	147	2	155	14	281	201	147	2.0
Zircon_53_070	3529	1685	0.45	0.0479 2	0.00086	0.13869	0.00266	0.02097	0.00014	0.00646	0.00013	0.3 5	148	1	150	3	159	54	148	1.0
Zircon_54_071	367	249	0.64	0.0573 1	0.00166	0.33098	0.01001	0.04191	0.00036	0.01257	0.00028	0.2 9	153	2	176	5	521	71	153	2.0
Zircon_55_072	1110	838	0.71	0.0522 9	0.0012	0.152	0.00373	0.02104	0.00018	0.00629	0.00013	0.3 5	162	2	175	5	347	63	162	2.0
Zircon_56_074	2589	994	0.36	0.0489 8	0.00093	0.14036	0.00284	0.02073	0.00014	0.00636	0.00012	0.3 5	167	2	199	9	602	101	167	2.0
Zircon_57_075	661	389	0.56	0.0521	0.00188	0.15831	0.00591	0.02195	0.00022	0.00649	0.00017	0.2 6	186	2	212	7	515	70	186	2.0
Zircon_58_076	484	123	0.24	0.0805 7	0.00113	2.3871	0.03715	0.21406	0.00146	0.06242	0.00119	0.4 3	186	1	191	5	252	62	186	1.0
Zircon_59_077	423	301	0.67	0.0730 3	0.00124	1.8262	0.03305	0.18096	0.00112	0.05182	0.00093	0.3 5	189	2	198	7	302	77	189	2.0
Zircon_6_014	416	148	0.34	0.052	0.00234	0.15554	0.00717	0.02177	0.00022	0.00691	0.00017	0.2 2	190	2	201	7	339	86	190	2.0
Zircon_60_078	254	77	0.29	0.0593 6	0.00243	0.18276	0.00781	0.02228	0.00027	0.0078	0.00047	0.2 9	244	2	256	8	368	78	244	2.0
Zircon_61_080	1761	837	0.45	0.0486 1	0.00102	0.14358	0.00324	0.02142	0.00018	0.00667	0.00013	0.3 7	265	2	290	8	504	61	265	2.0
Zircon_62_081	505	182	0.34	0.0523 9	0.00183	0.21506	0.00781	0.02975	0.00029	0.00884	0.00023	0.2 7	488	4	488	8	488	43	488	4.0
Zircon_63_082	479	128	0.25	0.0532 3	0.00208	0.21882	0.00887	0.02984	0.00033	0.00945	0.00032	0.2 7	584	12	751	28	1288	77	584	12. 0

Zircon_64_083	1510	888	0.56	0.0502 9	0.00121	0.15261	0.00386	0.02203	0.00018	0.00676	0.00015	0.3 1	682	6	693	10	719	37	682	6.0
Zircon_65_084	1033	448	0.41	0.0476 7	0.00143	0.14265	0.00444	0.02173	0.00018	0.00678	0.00016	0.2 7	948	6	951	10	949	28	948	6.0
Zircon_1_118c3_008	225	90	0.38	0.0726 8	0.00167	1.60865	0.04407	0.16053	0.00143	0.04851	0.00041	0.4 4	960	8	974	17	1005	43	960	8.0
Zircon_66_086	470	159	0.32	0.0511 6	0.00169	0.15741	0.00548	0.02235	0.00025	0.00708	0.00023	0.3 2	1072	6	1055	12	1015	33	1015	33. 0
Zircon_67_087	737	438	0.56	0.0551 2	0.00263	0.16851	0.00904	0.02217	0.00024	0.00692	0.00007	0.3 2	1050	7	1052	10	1051	26	1051	26. 0
Zircon_68_088	1245	407	0.31	0.0489 5	0.00113	0.14995	0.00372	0.02213	0.00021	0.00689	0.00017	0.3 7	1043	7	1047	15	1056	41	1056	41. 0
Zircon_69_089	1201	781	0.61	0.0524 6	0.00152	0.15841	0.00477	0.02191	0.00018	0.0067	0.00014	0.2 7	1143	8	1121	10	1074	26	1074	26. 0
Zircon_7_015	479	153	0.30	0.0534 3	0.00155	0.18757	0.00582	0.02542	0.00028	0.0071	0.0002	0.3 5	1035	6	1062	9	1112	25	1112	25. 0
Zircon_70_090	804	189	0.22	0.0512 5	0.00144	0.20668	0.00601	0.02924	0.00023	0.00916	0.00024	0.2 6	1250	8	1239	11	1211	27	1211	27. 0
Zircon_71_091	3207	159	0.05	0.0824	0.00115	2.5545	0.03842	0.22272	0.00122	0.06571	0.00125	0.3 7	1308	12	1286	13	1240	28	1240	28. 0
Zircon_72_092	1586	951	0.57	0.0511	0.00112	0.14884	0.00347	0.02108	0.00016	0.00642	0.00014	0.3 4	1296	6	1288	11	1255	26	1255	26. 0
Zircon_8_016	712	231	0.31	0.0503 5	0.00131	0.14985	0.00406	0.02158	0.00016	0.00684	0.00017	0.2 8	1592	16	1568	14	1534	25	1534	25. 0
Zircon_9_017	321	189	0.56	0.0511 2	0.00215	0.15233	0.00658	0.02169	0.00022	0.00672	0.00018	0.2 3	1615	8	1632	12	1648	23	1648	23. 0

ANEXO 2

REPOSITORIO DE DATOS CAPÍTULO 3

A. Definición estratigráfica formal de la Formación Atzompa
B. Secciones estratigráficas medidas, Formación Atzompa
C. Metodología U-Pb
D. Datos U-Pb

APPENDIX A. FORMAL STRATIGRAPHIC DEFINITION

The Atzompa Formation, defined formally herein, overlies the northernmost exposures of the Acatlán Complex in the Sierra de Tentzo area southeast of the city of Puebla. Paleozoic metasedimentary and igneous rocks of the Acatlán Complex belong to the basement of the Mixteco terrane (Fig 2. 1, 2). Strata of Pozo Grande measured section crop out along the arroyo of the same name near the village of Santa Marta Yancuitlalpan (Fig. 2), and constitute a unique continuous exposure of the Lower Cretaceous succession of the Mixteco terrane.

Historical Background

The Atzompa Formation was originally defined by Tarango (1968, in Monroy-Fernández and Sosa-Patrón 1984) to describe a succession of conglomerates, sandstones and siltstones with limestone lenses with Early Cretaceous fauna that crops out near San Juan Atzompa, in the Sierra de Tentzo area. This unit was correlated with the Zicapa Formation (DeCserna et al. 1980), exposed south of Sierra de Tentzo in the Mixteco terrane. Monroy-Fernández and Sosa-Patrón (1984) referred to siliciclastic rocks underlying Cretaceous limestone in the central and western part of Sierra de Tentzo as Neocomian red beds. Those authors subdivided the strata into two units: a conglomeratic unit A and a unit B consisting of red siltstones and limestones with Barremian-Aptian fauna. Despite producing a detailed description of the lithology, Monroy-Fernández and Sosa-Patrón (1984) did not define a stratotype and type locality. Rocks included in the Atzompa Formation in the Tentzo area were assigned to the Agua de Cordero Formation by Silva-Romo (2010) and Zepeda-Martinez (2013) by correlation with conglomerates and sandstones that crop out east of the Tentzo area in the Zapotitlán basin (Fig. 1). This correlation does not incorporate the

limestones interbedded with the red beds; instead, Zepeda-Martinez (2013) informally termed carbonate rocks overlying the Atzompa Formation in Sierra de Tentzo as El Tentzo formation.

Stratotype

The Pozo Grande section is the stratotype of the Atzompa Formation. It is located between the villages of Santa Marta Yancuitlaltan and San Nicolás Huajuapan (initial coordinates: 18°46'8"N, 98°6'0.0"W, final coordinates 18°47'14"N, 98°5'50.0"W, Fig. 2) along Pozo Grande Arroyo. The section has a minimum thickness of 1990 m. We define the Lower Cretaceous Atzompa Formation as a formal lithostratigraphic unit according to the North American Commission on Stratigraphic Nomenclature (NACSN, 2005). As this name was applied formerly to these strata, we preserve its priority. We divide it in five members: Las Pozas, La Magdalena, Santa Marta, Pozo Grande and El Calvario. These members are described in text-section sedimentology.

Age

The Atzompa Formation was assigned to the Neocomian-early Aptian by Monroy-Fernández and Sosa-Patrón (1984) based on the presence of the benthonic foraminifera *Chofatella decipiens* and *Salpingoporella sp*. algae of Barremian-Aptian age. In this study we confirm the late Barremian-Aptian age for the Pozo Grande Member by the occurrence of bivalve *Pterotrigonia sp*. and the echinoid *Heteraster sp* and the Maximum depositional ages of the members La Magdalena and Santa Marta (see section Detrital Zircon Geochronology).

Stratigraphic Correlation

The Atzompa Formation has been correlated with the Zicapa Formation (De Cserna et al. 1980, Monroy-Fernández and Sosa-Patrón 1984, Fitz-Diaz 2001, Sierra-Rojas and Molina-Garza 2014), which is composed of conglomerates, limestones, continental red beds, tuffs and lava flows upper muddy marine unit in transitional contact with the overlying Morelos Formation (Sierra-Rojas and Molina-Garza 2014). The upper part of the Santa Marta Member of the Atzompa Formation can be correlated with the tidal platform facies of the Jaltepetongo Fomation (Ortega and Lambarria 1991) in the Tlaxiaco basin (Fig. 9). East of the type locality of the Atzompa Formation, similarities in lithology, age, and sedimentary facies indicate correlation of the Atzompa Formation with formations deposited in the Zapotitlán basin, including the Agua de Cordero, Caltepec, San Juan Raya, La Compañía, and Miahuatepec formations (Mendoza-Rosales . 2010).

APPENDIX B. DETAILED MEASURED SECTION

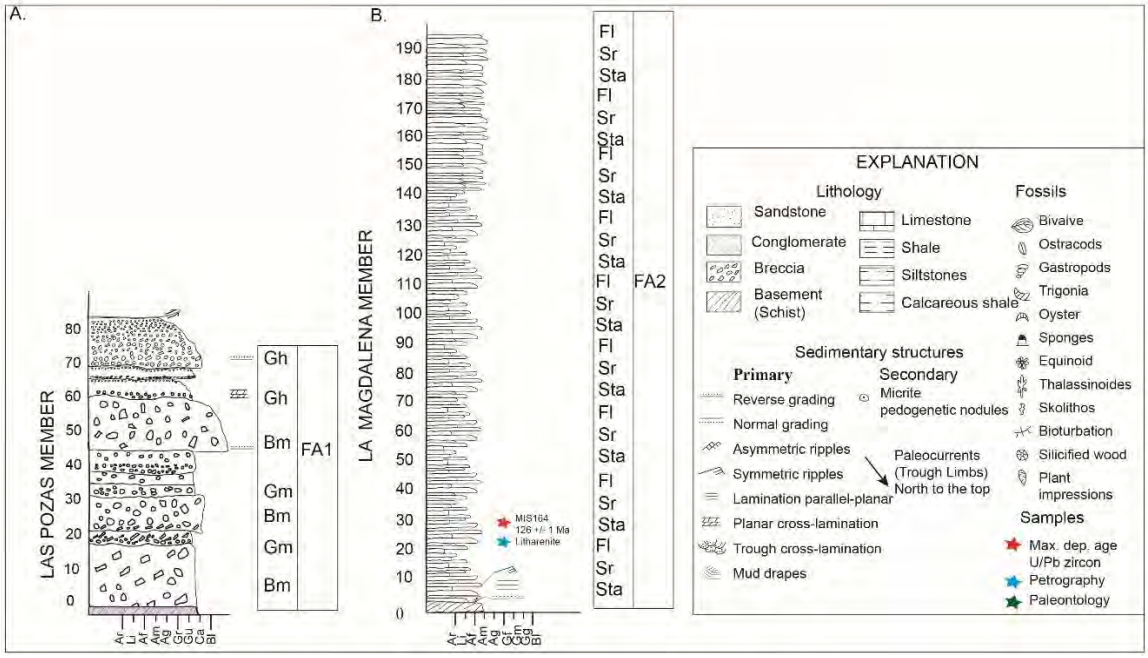

B1. Stratigraphic sections of the Atzompa Formation. a) Las Pozas member, b) La Magdalena Member, c) explanation of lithofacies codes, which correspond to facies and facies association codes in Tables 2 and 3. The numbers in the left side of the stratigraphic columns corresponds to meters.

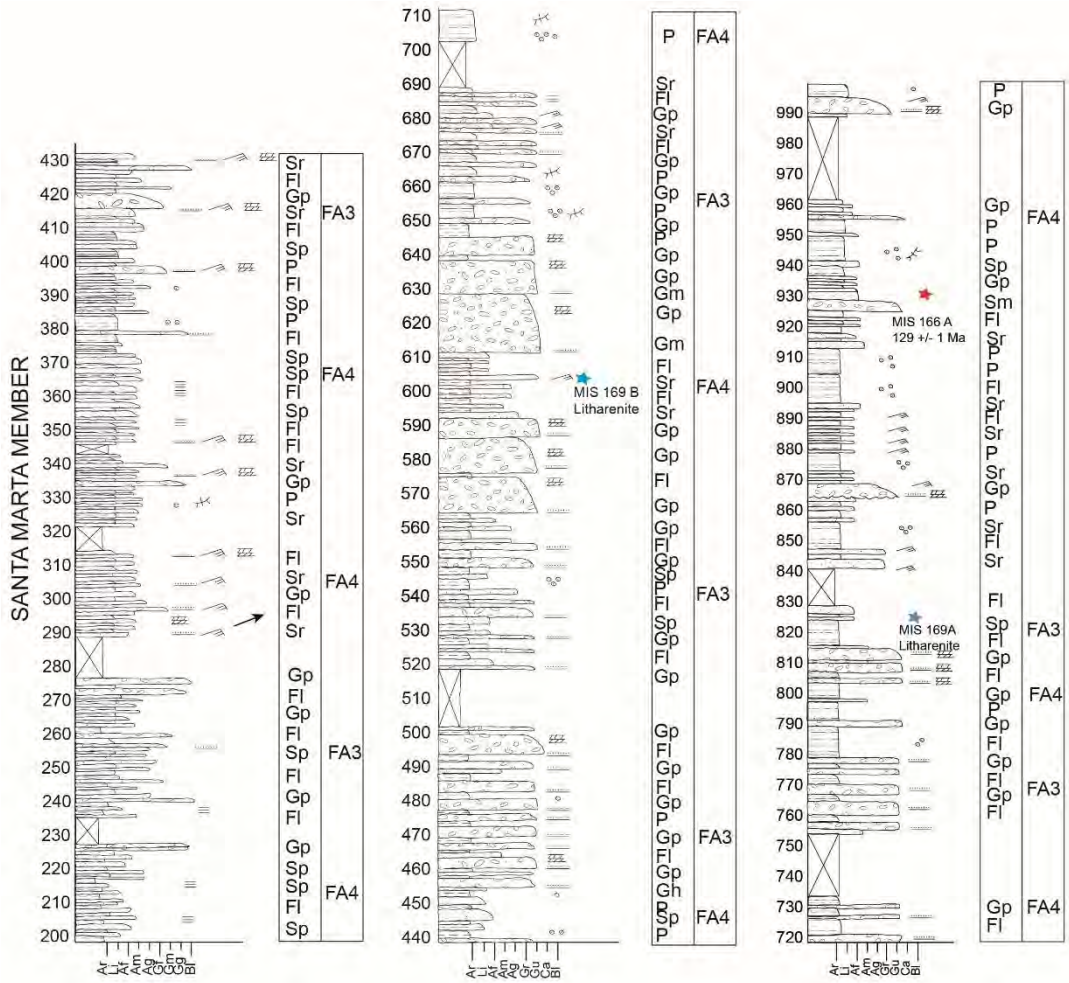

B2. Stratigraphic section of Santa Marta member. The codes correspond to facies and facies association code en Table 2 and Table 3. Facies codes and symbols as in Figure 3. The numbers in the left side of the stratigraphic columns corresponds to meters.

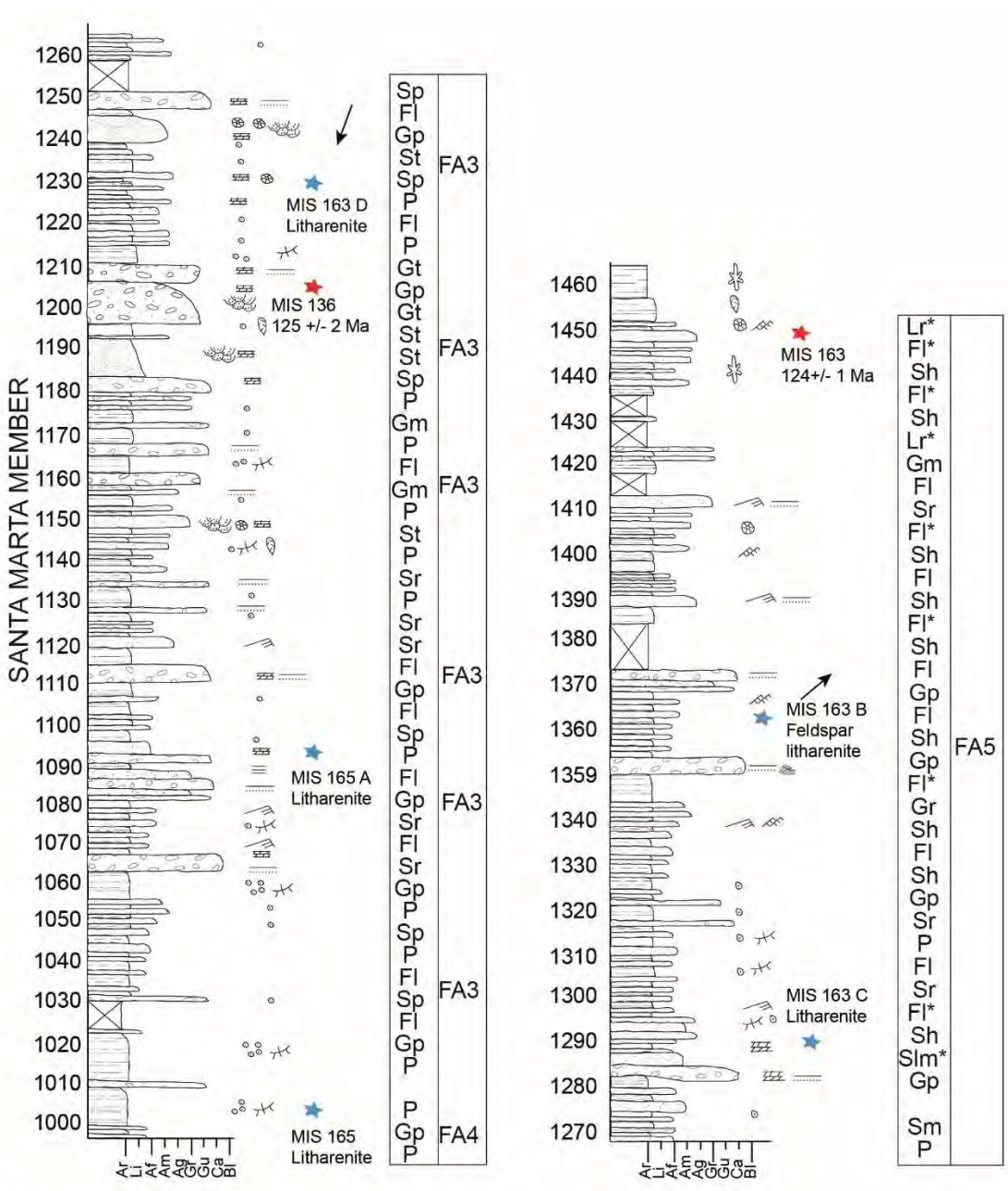

B3. Stratigraphic section of Santa Marta member. The codes correspond to facies and facies association code en Table 2 and Table 3. Facies codes and symbols as in Figure 3. The numbers in the left side of the stratigraphic columns corresponds to meters.

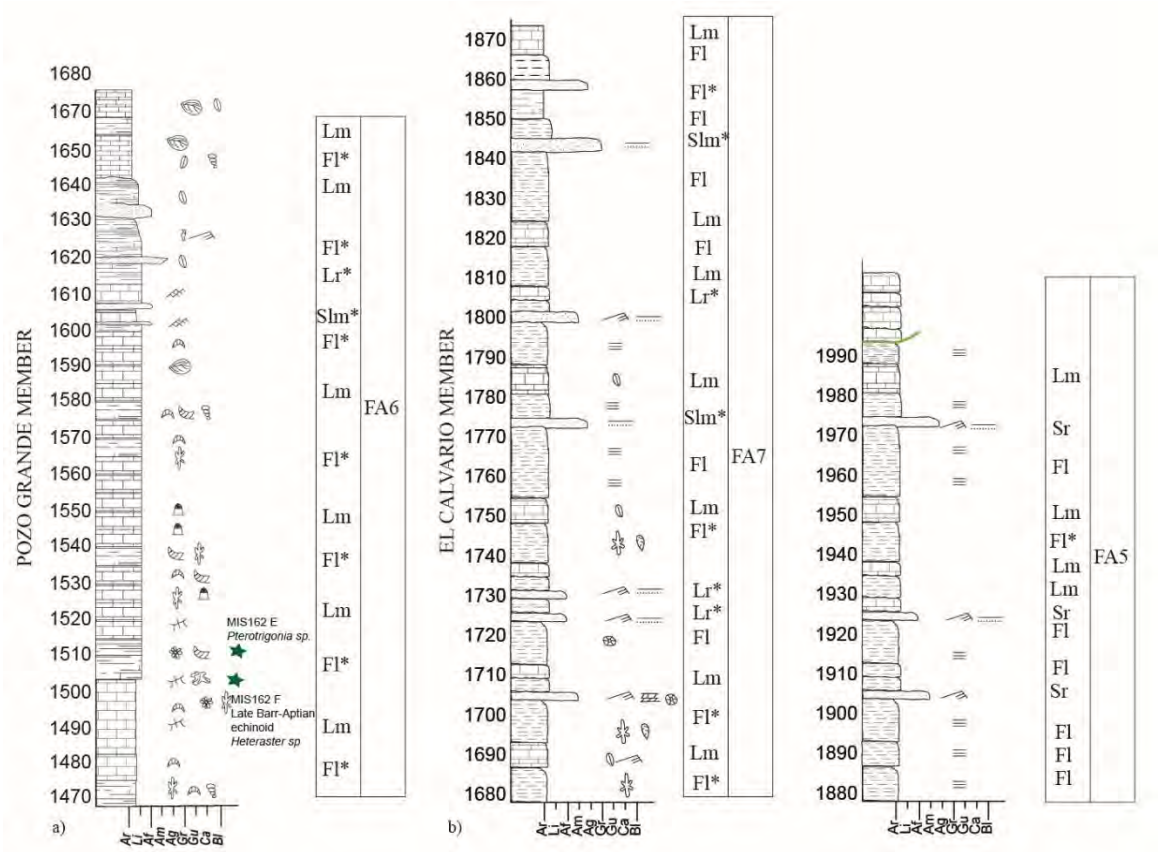

B4. a). Stratigraphic section of Pozo Grande Member. b). Stratigraphic section for El Calvario Member. The codes and symbols correspond to facies and facies association codes en Tables 2 and 3 and Figure B1. The numbers in the left side of the stratigraphic columns corresponds to meters.

APPENDIX C. DETRITAL ZIRCON GEOCHRONOLOGY

Methods

Medium- to fine-grained sandstone samples were collected for detrital zircon analysis. The sample preparation for zircon analysis included crushing, sieving, Wilfley density separation, and Frantz magnetic separation. A grain mount of about 120 zircons per sample was made by random picking using a binocular microscope. After polishing the mount to expose the zircon walls, every sample was scanned by binocular microscope to evaluate the external structure (shape, roundness, color) and by cathodoluminiscence to obtain details of the interior structure (zonation, inherited cores, inclusions). We analyzed cores and rims of the zircon grains by laser ablation inductively coupled mass spectrometry (LAICP-MS) with a laser beam spot of 23 μm on a target fluence of 6 J/cm. The maximum depositional age was estimated using a weighted mean of the youngest zircon cluster, following the method of Dickinson and Gehrels (2009). All the analyses were made at the Laboratorio de Estudios Isotópicos (LEI) of the Centro de Geociencias-UNAM.

FORMACIÓN ATZOMPA, MIEMBRO LA MAGDALENA, MIS164B

18°46´6.3´´N **98°6´33.35´´W** **CORRECTED RATIOS** **CORRECTED AGES (Ma)**

	U (ppm)	Th (ppm)	Th/U	207Pb/ 206Pb	±1s	207Pb/ 235U	±1s	206Pb/ 238U	±1s	208Pb/ 232Th	±1s	Rho	206Pb/ 238U	±1s	207Pb/ 235U	±1s	207Pb/ 206Pb	±1s	Best age (Ma)	±1s
Zircon_066	580	250.8	0.43	0.0494	0.0072	0.13	0.017	0.0192	0.0006	0.00614	0.00088	0.2554	122.3	4	124	16	390	150	122.3	4
Zircon_096	426	269	0.63	0.0602	0.0078	0.16	0.019	0.0192	0.0006	0.00776	0.00054	0.2759	122.8	4	150	17	670	130	122.8	4
Zircon_100	214.1	137.5	0.64	0.078	0.015	0.208	0.039	0.0193	0.0004	0.00707	0.00058	0.1217	123.1	2.8	190	33	1050	240	123.1	2.8
Zircon_099	1054	450.2	0.43	0.0504	0.0048	0.135	0.012	0.0195	0.0004	0.00633	0.00037	0.2193	124.5	2.4	129	11	300	110	124.5	2.4
Zircon_050	494	255	0.52	0.0498	0.0057	0.137	0.014	0.0197	0.0004	0.00638	0.00042	0.2188	125.6	2.8	130	13	217	86	125.6	2.8
Zircon_075	1825	888	0.49	0.0527	0.0047	0.141	0.012	0.0197	0.0004	0.00664	0.00039	0.2327	125.7	2.4	135	10	330	120	125.7	2.4
Zircon_033	418.1	223.3	0.53	0.072	0.01	0.19	0.028	0.0197	0.0008	0.0071	0.00065	0.2650	125.9	4.9	176	24	970	190	125.9	4.9
Zircon_013	320	197.3	0.62	0.0521	0.0054	0.145	0.017	0.0198	0.0008	0.00642	0.00057	0.3534	126.3	5.2	137	15	400	260	126.3	5.2
Zircon_042	519	304	0.59	0.0532	0.0075	0.147	0.019	0.0198	0.0006	0.00621	0.00053	0.2223	126.7	3.6	139	17	480	150	126.7	3.6
Zircon_094	839	226	0.27	0.0493	0.005	0.13	0.013	0.0199	0.0004	0.00682	0.00045	0.2063	126.8	2.6	125	11	243	83	126.8	2.6
Zircon_098	587	315.8	0.54	0.0497	0.005	0.134	0.013	0.0199	0.0004	0.00649	0.00041	0.2022	126.9	2.5	128	12	340	150	126.9	2.5
Zircon_062	383.7	170.1	0.44	0.0561	0.0074	0.153	0.019	0.0199	0.0006	0.00701	0.00051	0.2227	127	3.5	144	17	450	140	127	3.5
Zircon_028	585	335.1	0.57	0.056	0.01	0.153	0.026	0.0202	0.0007	0.0063	0.00089	0.1984	128.7	4.3	144	23	480	110	128.7	4.3
Zircon_084	241	125	0.52	0.0572	0.0085	0.159	0.024	0.0202	0.0006	0.00683	0.00055	0.1969	128.8	3.8	148	20	700	190	128.8	3.8
Zircon_022	300	147.4	0.49	0.0566	0.0075	0.157	0.02	0.0202	0.0007	0.00643	0.00049	0.2601	129	4.3	147	17	670	200	129	4.3
Zircon_083	265	188	0.71	0.0545	0.0065	0.152	0.018	0.0203	0.0005	0.00645	0.00056	0.2208	129.3	3.3	143	16	470	130	129.3	3.3
Zircon_003	405.5	187.6	0.46	0.0538	0.0056	0.153	0.016	0.0203	0.0005	0.00756	0.0005	0.2121	129.5	2.8	144	14	380	170	129.5	2.8
Zircon_010	512	252.3	0.49	0.0525	0.0083	0.14	0.019	0.0203	0.0005	0.00708	0.00072	0.1851	129.5	3.2	132	17	400	110	129.5	3.2
Zircon_041	370.1	189.2	0.51	0.0561	0.0068	0.156	0.018	0.0203	0.0005	0.00729	0.00052	0.1962	129.7	2.9	146	16	500	150	129.7	2.9
Zircon_059	369.3	188.1	0.51	0.061	0.012	0.159	0.028	0.0203	0.0006	0.0079	0.00067	0.1759	129.8	4	149	24	720	170	129.8	4
Zircon_080	403.3	211.2	0.52	0.0507	0.0054	0.139	0.014	0.0204	0.0004	0.00719	0.00049	0.1947	130.2	2.5	131	13	350	130	130.2	2.5
Zircon_052	547	266	0.49	0.0642	0.007	0.185	0.02	0.0205	0.0006	0.00768	0.00065	0.2529	130.7	3.5	172	17	730	170	130.7	3.5
Zircon_055	245	119	0.49	0.065	0.01	0.186	0.029	0.0206	0.0006	0.00865	0.00092	0.1717	131.1	3.5	171	25	1000	210	131.1	3.5
Zircon_018	456	229.4	0.50	0.0498	0.0055	0.141	0.015	0.0207	0.0004	0.00677	0.00047	0.1866	131.8	2.6	133	14	249	93	131.8	2.6
Zircon_097	776	384	0.49	0.075	0.01	0.215	0.032	0.021	0.0007	0.0093	0.001	0.2085	133.6	4.1	197	27	1060	240	133.6	4.1
Zircon_009	459.6	229	0.50	0.108	0.026	0.311	0.085	0.0211	0.0008	0.0125	0.0037	0.1408	134.3	5.1	270	60	1720	290	134.3	5.1
Zircon_070	430	223	0.52	0.0529	0.0064	0.151	0.017	0.0212	0.0005	0.00797	0.00056	0.2184	134.9	3.3	142	15	410	130	134.9	3.3
Zircon_053	218.1	99.1	0.45	0.066	0.011	0.182	0.026	0.0217	0.0009	0.00852	0.00071	0.2996	138.5	5.9	169	23	710	170	138.5	5.9
Zircon_046	325.5	359.7	1.11	0.0592	0.0061	0.423	0.044	0.0522	0.001	0.018	0.001	0.1806	327.8	6	357	32	550	110	327.8	6
Zircon_063	620	490	0.79	0.0532	0.0048	0.405	0.036	0.0553	0.0014	0.0182	0.0013	0.2848	346.7	8.8	345	26	350	120	346.7	8.8
Zircon_036	809	67.1	0.08	0.0596	0.005	0.599	0.05	0.072	0.0013	0.0312	0.0026	0.2163	447.9	8.1	476	32	620	100	447.9	8.1
Zircon_002	559	63.7	0.11	0.0609	0.0069	0.619	0.069	0.0727	0.0018	0.017	0.0034	0.2221	452	11	489	43	630	140	452	11
Zircon_056	443.3	32.9	0.07	0.0612	0.0053	0.634	0.053	0.0739	0.0016	0.037	0.0059	0.2590	459.6	9.8	498	33	647	93	459.6	9.8
Zircon_048	411	48.1	0.12	0.0608	0.0055	0.627	0.055	0.0753	0.0014	0.0278	0.003	0.2120	468.3	8.3	499	39	640	140	468.3	8.3

Zircon_082	1114	347.1	0.31	0.0597	0.0051	0.617	0.051	0.0763	0.0013	0.024	0.0014	0.2061	473.7	7.9	487	32	590	100	473.7	7.9
Zircon_085	369.4	7.01	0.02	0.0627	0.0056	0.679	0.06	0.0783	0.0015	0.0441	0.0075	0.2168	486	8.9	525	36	684	88	486	8.9
Zircon_006	277	162	0.58	0.0593	0.0053	0.672	0.058	0.0809	0.0015	0.0251	0.0014	0.2148	501.4	9.2	521	35	590	110	501.4	9.2
Zircon_088	389	117.6	0.30	0.0586	0.0052	0.659	0.058	0.0812	0.0015	0.0262	0.0015	0.2099	503.5	8.9	513	35	560	130	503.5	8.9
Zircon_026	407.6	170.4	0.42	0.0581	0.0056	0.651	0.061	0.0819	0.0017	0.0267	0.0016	0.2215	508	10	514	34	580	140	508	10
Zircon_004	119.3	107.1	0.90	0.0663	0.0068	0.774	0.077	0.0838	0.0017	0.0281	0.0017	0.2039	519	10	584	42	850	110	519	10
Zircon_025	120.8	7.47	0.06	0.0675	0.0077	0.75	0.082	0.084	0.0018	0.063	0.01	0.1960	520	11	572	44	840	150	520	11
Zircon_086	685	166	0.24	0.0582	0.0049	0.67	0.055	0.0849	0.0015	0.0271	0.0015	0.2152	525.4	8.8	520	34	531	93	525.4	8.8
Zircon_072	392.7	13.6	0.03	0.0626	0.0055	0.741	0.063	0.0852	0.0015	0.0528	0.0071	0.2071	527.2	8.6	562	37	700	140	527.2	8.6
Zircon_067	797.4	65.5	0.08	0.0586	0.0049	0.683	0.056	0.0853	0.0017	0.0312	0.0024	0.2431	527.5	9.8	528	34	566	94	527.5	9.8
Zircon_038	346	128.1	0.37	0.0612	0.0059	0.726	0.065	0.0853	0.0022	0.0286	0.0021	0.2881	528	13	554	39	662	99	528	13
Zircon_058	549	270.3	0.49	0.0602	0.0053	0.699	0.062	0.0862	0.0017	0.026	0.0015	0.2223	533	10	542	40	600	170	533	10
Zircon_030	512	18.3	0.04	0.0602	0.0056	0.694	0.073	0.087	0.0023	0.0609	0.0066	0.2513	538	13	534	44	560	130	538	13
Zircon_021	137.4	30.3	0.22	0.0666	0.007	0.788	0.081	0.0874	0.0021	0.0313	0.0037	0.2337	540	12	587	47	840	120	540	12
Zircon_007	163.6	157.6	0.96	0.0595	0.006	0.718	0.072	0.0875	0.0016	0.0266	0.0015	0.1823	540.6	9.6	546	43	601	88	540.6	9.6
Zircon_081	197	251	1.27	0.0601	0.007	0.704	0.077	0.0878	0.0024	0.0271	0.0016	0.2499	542	14	540	46	720	140	542	14
Zircon_054	652	117	0.18	0.0604	0.0051	0.724	0.061	0.0879	0.0019	0.0288	0.0018	0.2566	543	11	553	36	609	83	543	11
Zircon_044	786	99.9	0.13	0.0624	0.0056	0.752	0.067	0.0882	0.002	0.0288	0.0023	0.2545	545	12	569	39	675	93	545	12
Zircon_092	173.6	172	0.99	0.0618	0.0058	0.748	0.067	0.0882	0.0018	0.0284	0.0016	0.2278	545	10	566	39	660	100	545	10
Zircon_037	485	175.4	0.36	0.0626	0.0053	0.754	0.063	0.0885	0.0017	0.0284	0.0017	0.2299	546	10	570	37	683	97	546	10
Zircon_014	214	135.5	0.63	0.06	0.0061	0.728	0.072	0.0885	0.0019	0.028	0.0019	0.2171	547	11	560	45	650	150	547	11
Zircon_074	193	81.8	0.42	0.0592	0.0059	0.777	0.075	0.0945	0.002	0.0313	0.002	0.2193	582	12	585	42	590	140	582	12
Zircon_093	74.4	62.5	0.84	0.0641	0.0081	0.828	0.097	0.0945	0.0032	0.0308	0.0025	0.2891	582	19	607	54	870	200	582	19
Zircon_019	342	2.93	0.01	0.0652	0.0061	0.842	0.074	0.095	0.0018	0.149	0.029	0.2156	585	11	619	41	795	86	585	11
Zircon_024	733	59.2	0.08	0.0605	0.0053	0.777	0.066	0.0959	0.0022	0.0427	0.0029	0.2701	591	13	583	37	619	96	591	13
Zircon_071	152	55.2	0.36	0.062	0.0064	0.839	0.081	0.0973	0.0031	0.0303	0.0021	0.3300	599	18	617	45	660	100	599	18
Zircon_069	1008	106.3	0.11	0.0604	0.0052	0.8	0.068	0.0978	0.0017	0.0313	0.0023	0.2045	602	10	596	39	620	120	602	10
Zircon_047	144.8	179.7	1.24	0.066	0.006	0.897	0.083	0.0982	0.002	0.0317	0.0017	0.2201	604	12	652	43	817	93	604	12
Zircon_078	277	199.4	0.72	0.06	0.0052	0.804	0.067	0.0985	0.0016	0.0288	0.0017	0.1949	605.5	9.5	600	39	600	130	605.5	9.5
Zircon_077	122.8	43.4	0.35	0.0644	0.0066	0.875	0.085	0.102	0.0022	0.0336	0.0022	0.2220	626	13	640	48	807	97	626	13
Zircon_011	183.6	108	0.59	0.0604	0.0056	0.886	0.078	0.1052	0.002	0.0318	0.0019	0.2160	645	11	643	41	650	100	645	11
Zircon_065	515	13.75	0.03	0.0615	0.0051	0.881	0.071	0.1053	0.0018	0.0408	0.0045	0.2121	645	10	643	40	650	130	645	10
Zircon_091	140.3	109.91	0.78	0.062	0.0057	0.933	0.083	0.1094	0.0025	0.036	0.0021	0.2569	669	14	672	39	630	140	669	14
Zircon_095	226	169	0.75	0.0661	0.0065	1.017	0.097	0.1134	0.0024	0.0362	0.0025	0.2219	692	14	711	49	830	110	692	14
Zircon_008	131	7.6	0.06	0.0601	0.007	1.03	0.11	0.1226	0.0041	0.134	0.038	0.3131	745	23	714	57	590	140	745	23
Zircon_043	307.8	79.3	0.26	0.067	0.0056	1.191	0.097	0.1286	0.0021	0.0399	0.0024	0.2005	780	12	796	45	822	59	780	12
Zircon_023	659	211	0.32	0.067	0.0057	1.18	0.1	0.129	0.0025	0.039	0.0022	0.2287	782	14	788	47	830	130	782	14
Zircon_015	173.9	36.4	0.21	0.0754	0.0069	1.6	0.14	0.1511	0.0029	0.0656	0.0051	0.2193	907	16	977	50	1080	120	907	16

Zircon_017	124	99	0.80	0.0691	0.0065	1.46	0.13	0.1527	0.0032	0.0489	0.0029	0.2354	916	18	915	53	940	110	916	18
Zircon_034	161.8	45.17	0.28	0.0716	0.0067	1.57	0.13	0.1568	0.004	0.0512	0.0037	0.3081	939	22	956	53	980	130	939	22
Zircon_001	181	100.5	0.56	0.0719	0.0064	1.63	0.14	0.1635	0.0033	0.0484	0.0028	0.2350	976	18	981	56	960	100	976	18
Zircon_057	250	172	0.69	0.0722	0.0062	1.64	0.13	0.1656	0.0029	0.0505	0.0027	0.2209	988	16	985	52	1000	110	988	16
Zircon_076	356	130	0.37	0.073	0.0061	1.66	0.14	0.1675	0.0027	0.0519	0.0029	0.1911	998	15	994	52	1015	83	1015	83
Zircon_049	657	32.8	0.05	0.0727	0.006	1.7	0.14	0.1691	0.0028	0.0585	0.0036	0.2011	1007	16	1009	51	1019	95	1019	95
Zircon_031	459	167.1	0.36	0.073	0.0061	1.71	0.14	0.1708	0.0028	0.0523	0.0028	0.2002	1017	15	1013	52	1021	77	1021	77
Zircon_035	544	154.8	0.28	0.0757	0.0063	1.67	0.14	0.1607	0.0029	0.047	0.0027	0.2153	960	16	995	54	1075	87	1075	87
Zircon_045	278	192	0.69	0.0759	0.0065	1.92	0.16	0.1834	0.0031	0.0557	0.003	0.2028	1086	17	1087	55	1103	79	1103	79
Zircon_012	233.4	72.8	0.31	0.0778	0.0068	1.73	0.15	0.1611	0.0027	0.0523	0.0031	0.1933	963	15	1018	54	1140	100	1140	100
Zircon_087	462	115	0.25	0.0789	0.0065	2.14	0.17	0.1972	0.0041	0.0619	0.0036	0.2617	1160	22	1160	56	1166	94	1166	94
Zircon_073	214.6	309.4	1.44	0.0785	0.0066	1.85	0.15	0.1715	0.003	0.0547	0.0029	0.2157	1020	17	1067	50	1180	150	1180	150
Zircon_016	170	83.4	0.49	0.0816	0.0073	1.98	0.2	0.178	0.0061	0.0622	0.004	0.3393	1055	33	1103	65	1230	130	1230	130
Zircon_061	62.1	77.8	1.25	0.0832	0.0086	1.82	0.18	0.158	0.0047	0.0519	0.0033	0.3008	946	26	1048	66	1286	93	1286	93
Zircon_068	470	66.2	0.14	0.0835	0.008	2.36	0.23	0.204	0.013	0.0744	0.0067	0.6539	1194	68	1229	71	1287	98	1287	98
Zircon_090	185.4	112.7	0.61	0.0857	0.0077	2.28	0.2	0.1932	0.0044	0.0376	0.0025	0.2596	1138	24	1202	63	1355	76	1355	76
Zircon_005	100	79.4	0.79	0.0945	0.0079	3.4	0.28	0.2625	0.0047	0.0788	0.0043	0.2174	1503	24	1504	63	1515	73	1515	73
Zircon_079	30.8	18	0.58	0.098	0.015	1.35	0.22	0.1026	0.0038	0.0464	0.0047	0.2273	629	22	839	96	1630	150	1630	150
Zircon_060	244	120.7	0.49	0.11	0.0091	4.74	0.38	0.3157	0.0053	0.0922	0.0049	0.2094	1768	26	1774	67	1801	84	1801	84
Zircon_040	73.8	58.1	0.79	0.1145	0.0096	5.13	0.42	0.3281	0.0072	0.0963	0.0053	0.2680	1829	35	1839	70	1866	96	1866	96
Zircon_029	193.1	183	0.95	0.1188	0.0099	5.53	0.45	0.3465	0.0059	0.0977	0.0051	0.2092	1918	28	1908	72	1936	91	1936	91
Zircon_064	117.1	44.48	0.38	0.136	0.016	3.59	0.44	0.1926	0.0042	0.143	0.02	0.1779	1135	23	1532	99	2140	200	2140	200
Zircon_027	1139	106	0.09	0.137	0.011	5.92	0.48	0.3146	0.006	0.0916	0.0051	0.2352	1763	29	1963	70	2200	120	2200	120
Zircon_051	382	249	0.65	0.182	0.015	12.11	0.97	0.48	0.018	0.1345	0.0072	0.4682	2525	77	2613	76	2680	100	2680	100
Zircon_039	332	200.2	0.60	0.184	0.015	12.7	1	0.5037	0.0092	0.1367	0.0074	0.2320	2630	39	2654	74	2687	93	2687	93
Zircon_089	325.6	167	0.51	0.188	0.015	12.7	1	0.4956	0.0085	0.1358	0.0078	0.2178	2595	37	2654	74	2726	58	2726	58
Zircon_020	230	116.5	0.51	0.189	0.015	12.24	0.97	0.4744	0.0078	0.1083	0.0058	0.2075	2503	34	2622	74	2734	75	2734	75
Zircon_032	131.1	30.6	0.23	0.219	0.018	15.8	1.3	0.532	0.01	0.1445	0.0089	0.2285	2748	44	2865	78	2968	71	2968	71

FORMACIÓN ATZOMPA, MIEMBRO SANTA MARTA, MIS166

98°6´1.4´´W

18°46´46.55´´N

				CORRECTED RATIOS									CORRECTED AGES (Ma)							
	U (ppm)	Th (ppm)	Th/U	207Pb/ 206Pb	±1s	207Pb/ 235U	±1s	206Pb/ 238U	±1s	208Pb/ 232Th	±1s	Rho	206Pb/ 238U	±1s	207Pb/ 235U	±1s	207Pb/ 206Pb	±1s	Best age (Ma)	±1s
Zircon_026	274.9	96.3	0.35	0.0514	0.0068	0.141	0.021	0.0199	0.0005	0.16	0.00682	0.00092	127	3.1	133	19	430	130	127	3.1
Zircon_013	342.5	125.5	0.37	0.0478	0.0067	0.131	0.02	0.0201	0.0005	0.16	0.0078	0.0011	128.5	3.1	125	18	370	110	128.5	3.1
Zircon_033	284	118.5	0.42	0.0591	0.0072	0.164	0.022	0.0202	0.0007	0.24	0.00675	0.00089	129.1	4.1	154	19	660	100	129.1	4.1
Zircon_060	320.4	152	0.47	0.0507	0.0062	0.143	0.018	0.0204	0.0006	0.23	0.00725	0.00094	129.9	3.7	136	16	320	120	129.9	3.7
Zircon_052	397	105.9	0.27	0.0515	0.0049	0.141	0.015	0.0204	0.0005	0.21	0.00574	0.00077	130.1	2.8	134	14	350	130	130.1	2.8
Zircon_002	429	174	0.41	0.0568	0.0099	0.16	0.028	0.0206	0.001	0.27	0.0066	0.0012	131.4	6.2	150	24	534	79	131.4	6.2
Zircon_043	259.4	130.9	0.50	0.0532	0.0054	0.144	0.018	0.0209	0.0006	0.21	0.00615	0.0008	133.3	3.5	139	15	440	120	133.3	3.5
Zircon_075	447.8	235.9	0.53	0.0516	0.0055	0.15	0.018	0.0213	0.0005	0.21	0.0072	0.0011	135.7	3.3	141	16	420	130	135.7	3.3
Zircon_071	261	145	0.56	0.0528	0.0093	0.155	0.029	0.0214	0.001	0.24	0.0062	0.0011	136.6	6	145	25	560	190	136.6	6
Zircon_099	519	181.6	0.35	0.0543	0.0078	0.159	0.024	0.0214	0.0006	0.18	0.0075	0.0011	136.6	3.6	149	21	600	160	136.6	3.6
Zircon_061	238.1	74	0.31	0.0521	0.0082	0.159	0.026	0.0214	0.0009	0.24	0.0078	0.0014	136.8	5.4	149	23	620	160	136.8	5.4
Zircon_065	499.9	161.8	0.32	0.0635	0.0076	0.187	0.028	0.0214	0.0007	0.20	0.0078	0.0017	136.8	4.1	174	24	770	280	136.8	4.1
Zircon_014	274.9	92.3	0.34	0.061	0.013	0.18	0.04	0.0216	0.0007	0.14	0.0119	0.0019	137.9	4.1	167	34	730	160	137.9	4.1
Zircon_096	217	121	0.56	0.0515	0.0074	0.172	0.027	0.0242	0.0008	0.21	0.0084	0.0012	154.1	5	160	23	610	150	154.1	5
Zircon_053	2740	287	0.10	0.0511	0.0045	0.167	0.016	0.0243	0.0009	0.37	0.0097	0.0011	154.6	5.5	157	14	287	73	154.6	5.5
Zircon_058	282	235	0.83	0.0515	0.0054	0.179	0.02	0.0258	0.0007	0.24	0.00791	0.00087	163.9	4.2	167	17	470	120	163.9	4.2
Zircon_034	224	97	0.43	0.056	0.01	0.201	0.038	0.0259	0.0009	0.19	0.0098	0.0022	165	5.9	185	32	550	100	165	5.9
Zircon_098	496	48.43	0.10	0.0538	0.0075	0.199	0.037	0.0267	0.0014	0.28	0.02	0.0054	169.6	9	184	31	374	48	169.6	9
Zircon_027	437	58.9	0.13	0.0506	0.0043	0.187	0.018	0.0269	0.0006	0.24	0.0107	0.0013	171.1	3.9	174	16	366	89	171.1	3.9
Zircon_097	210.3	216.8	1.03	0.0515	0.0097	0.194	0.037	0.027	0.0006	0.11	0.0088	0.0011	171.8	3.6	180	31	530	300	171.8	3.6
Zircon_055	479	186.4	0.39	0.0519	0.0076	0.199	0.031	0.0278	0.0009	0.21	0.00734	0.00093	176.6	5.6	184	26	350	120	176.6	5.6
Zircon_076	293	95.9	0.33	0.0511	0.0052	0.198	0.022	0.028	0.0007	0.21	0.0081	0.00097	178.1	4.1	183	18	380	110	178.1	4.1
Zircon_089	597	326.1	0.55	0.0494	0.0036	0.194	0.017	0.0284	0.0006	0.24	0.00893	0.00097	180.8	3.7	180	14	270	110	180.8	3.7
Zircon_077	235	94.3	0.40	0.0529	0.0056	0.206	0.023	0.0289	0.0007	0.22	0.0091	0.0012	183.8	4.4	192	21	520	120	183.8	4.4
Zircon_078	32.9	19.12	0.58	0.057	0.025	0.24	0.1	0.0293	0.0017	0.14	0.0085	0.0022	186	11	182	85	1460	300	186	11
Zircon_059	131.3	63.5	0.48	0.067	0.015	0.281	0.068	0.0302	0.0013	0.18	0.013	0.0018	191.5	8.4	247	54	980	230	191.5	8.4
Zircon_080	130.4	169.3	1.30	0.093	0.013	0.447	0.061	0.0357	0.0013	0.27	0.0095	0.0012	226.3	8.3	371	43	1480	140	226.3	8.3
Zircon_028	343	336	0.98	0.0529	0.0044	0.271	0.025	0.037	0.0008	0.22	0.0113	0.0012	234.4	4.7	243	20	390	91	234.4	4.7
Zircon_031	334	347	1.04	0.0614	0.0053	0.314	0.03	0.0383	0.0011	0.30	0.0118	0.0013	242.2	6.6	277	23	649	91	242.2	6.6
Zircon_079	164.3	106.1	0.65	0.0541	0.0095	0.314	0.061	0.0422	0.0011	0.13	0.0137	0.0017	266.6	6.7	275	47	700	250	266.6	6.7
Zircon_064	660	232	0.35	0.0523	0.004	0.306	0.027	0.0427	0.0009	0.23	0.0125	0.0015	269.7	5.5	271	21	390	130	269.7	5.5
Zircon_008	163	135	0.83	0.0503	0.006	0.313	0.039	0.0433	0.0011	0.20	0.0128	0.0015	273.2	6.9	275	30	360	130	273.2	6.9
Zircon_042	367	154	0.42	0.0533	0.0044	0.317	0.03	0.0433	0.0009	0.21	0.0137	0.0016	273.2	5.5	279	23	340	100	273.2	5.5

Zircon_011	205.3	202.5	0.99	0.0472	0.007	0.286	0.045	0.0439	0.0012	0.17	0.014	0.0015	277.2	7.4	254	36	360	140	277.2	7.4
Zircon_009	113.9	44.5	0.39	0.0541	0.0076	0.353	0.053	0.0469	0.0014	0.20	0.0171	0.0025	295.7	8.9	304	40	760	180	295.7	8.9
Zircon_085	226	84.2	0.37	0.0529	0.0048	0.398	0.04	0.0542	0.0012	0.22	0.0147	0.0017	340.4	7.2	339	28	410	130	340.4	7.2
Zircon_068	90.1	124.9	1.39	0.064	0.01	0.62	0.13	0.0643	0.0023	0.17	0.0186	0.0026	402	14	485	78	910	210	402	14
Zircon_046	222.6	214	0.96	0.0581	0.0044	0.57	0.052	0.0727	0.0018	0.27	0.0208	0.0022	452	11	463	33	508	92	452	11
Zircon_015	257	247	0.96	0.0585	0.0073	0.587	0.077	0.0733	0.0018	0.19	0.024	0.0027	456	11	477	44	634	85	456	11
Zircon_045	192	152.7	0.80	0.0654	0.0059	0.628	0.066	0.0733	0.0024	0.31	0.0177	0.0021	456	15	494	41	760	100	456	15
Zircon_037	104.1	59.4	0.57	0.0737	0.0077	0.768	0.088	0.0755	0.0026	0.30	0.0267	0.0034	469	16	575	50	1030	140	469	16
Zircon_044	244.5	197.1	0.81	0.0586	0.0043	0.7	0.06	0.0859	0.0016	0.22	0.0264	0.0028	531.4	9.4	538	36	565	80	531.4	9.4
Zircon_024	217.6	243.6	1.12	0.0602	0.0056	0.724	0.07	0.0892	0.002	0.23	0.0278	0.003	551	12	564	41	610	110	551	12
Zircon_019	182.8	60.4	0.33	0.069	0.0059	0.855	0.081	0.0902	0.0022	0.26	0.0328	0.0036	557	13	626	44	920	130	557	13
Zircon_100	72.6	26.6	0.37	0.0861	0.0077	1.12	0.12	0.0912	0.0036	0.37	0.0414	0.005	562	21	760	58	1410	110	562	21
Zircon_051	890	118	0.13	0.0608	0.004	0.78	0.065	0.0937	0.0019	0.24	0.0449	0.005	578	11	591	32	640	100	578	11
Zircon_094	326	123.6	0.38	0.0579	0.0043	0.755	0.066	0.0942	0.0017	0.21	0.0278	0.0031	580	10	570	38	526	98	580	10
Zircon_036	306	161.9	0.53	0.0663	0.0052	0.853	0.08	0.0942	0.0017	0.19	0.0307	0.0035	580.3	9.9	628	45	810	130	580.3	9.9
Zircon_067	874	42.5	0.05	0.059	0.0039	0.781	0.063	0.0958	0.0016	0.21	0.0275	0.0032	589.6	9.2	586	36	590	76	589.6	9.2
Zircon_016	606	123.3	0.20	0.0602	0.0041	0.858	0.071	0.1041	0.0026	0.30	0.0347	0.0038	638	15	628	39	599	78	638	15
Zircon_062	102.3	44.87	0.44	0.0651	0.0056	1.04	0.1	0.1178	0.0027	0.24	0.0339	0.0039	718	15	722	50	760	100	718	15
Zircon_032	132.1	58.3	0.44	0.0702	0.0066	1.26	0.12	0.1289	0.003	0.24	0.0194	0.0024	781	17	828	56	1010	140	781	17
Zircon_056	235.3	71.3	0.30	0.0709	0.0076	1.29	0.15	0.1309	0.0031	0.20	0.0155	0.0035	793	18	839	68	950	140	793	18
Zircon_020	153.4	92	0.60	0.0736	0.0052	1.41	0.12	0.1401	0.0036	0.30	0.0234	0.0033	845	20	891	50	1040	100	845	20
Zircon_012	189.8	42.3	0.22	0.0701	0.005	1.34	0.11	0.1405	0.0043	0.37	0.0662	0.0089	847	25	863	48	968	86	847	25
Zircon_040	203	38	0.19	0.0766	0.0053	1.51	0.12	0.1462	0.0033	0.28	0.037	0.0054	880	19	934	50	1119	74	880	19
Zircon_039	555	96	0.17	0.0697	0.0045	1.42	0.12	0.1498	0.0026	0.21	0.0472	0.0051	900	15	897	48	910	77	900	15
Zircon_004	140.2	76.5	0.55	0.0706	0.005	1.49	0.13	0.1532	0.0031	0.23	0.0467	0.0054	919	17	926	52	1000	100	919	17
Zircon_050	230	59.3	0.26	0.0704	0.0046	1.52	0.12	0.1574	0.0026	0.21	0.0457	0.005	942	15	936	50	917	80	942	15
Zircon_017	405	185	0.46	0.0707	0.0045	1.55	0.12	0.1609	0.003	0.24	0.0477	0.0052	962	17	949	50	943	73	962	17
Zircon_035	259	53.3	0.21	0.0725	0.0047	1.63	0.13	0.1643	0.0028	0.21	0.048	0.0053	980	16	980	51	1000	72	980	16
Zircon_021	202.7	101.6	0.50	0.0715	0.0051	1.78	0.15	0.1789	0.0033	0.22	0.0536	0.0059	1061	18	1037	55	982	67	982	67
Zircon_007	435	123.6	0.28	0.0716	0.0048	1.78	0.15	0.1785	0.0039	0.26	0.055	0.006	1058	21	1038	54	983	53	983	53
Zircon_084	447	199.3	0.45	0.072	0.0047	1.64	0.13	0.1655	0.0027	0.21	0.0484	0.0052	987	15	985	51	985	76	987	15
Zircon_063	104.7	88.6	0.85	0.0724	0.0053	1.72	0.15	0.17	0.0041	0.28	0.0469	0.0051	1012	23	1014	55	996	87	996	87
Zircon_010	208.2	57.1	0.27	0.0698	0.0049	1.64	0.14	0.1693	0.0033	0.23	0.0513	0.0057	1008	18	983	54	930	100	1008	18
Zircon_030	122.8	72.7	0.59	0.071	0.0051	1.66	0.14	0.1696	0.0032	0.22	0.0508	0.0055	1010	18	990	53	966	71	1010	18
Zircon_086	158.2	56.6	0.36	0.0725	0.0052	1.82	0.15	0.1794	0.0034	0.23	0.0514	0.0057	1063	19	1049	56	1020	110	1020	110
Zircon_092	549	147.6	0.27	0.0731	0.0047	1.8	0.14	0.1776	0.003	0.22	0.056	0.006	1054	16	1045	52	1024	77	1024	77
Zircon_038	117.3	35.7	0.30	0.0703	0.0052	1.69	0.15	0.1733	0.0034	0.22	0.0519	0.0059	1030	19	1002	59	957	92	1030	19
Zircon_047	248	89.2	0.36	0.0744	0.005	1.7	0.14	0.1665	0.003	0.22	0.0498	0.0054	993	16	1007	52	1035	84	1035	84

Zircon_023	144.1	56.8	0.39	0.0747	0.0055	1.61	0.13	0.1597	0.0031	0.24	0.0488	0.0054	955	17	977	58	1046	97	1046	97
Zircon_049	311.3	64.8	0.21	0.0748	0.0058	1.85	0.16	0.1819	0.0043	0.27	0.0559	0.0064	1077	24	1063	58	1055	91	1055	91
Zircon_093	276	52	0.19	0.0754	0.0056	1.99	0.18	0.1902	0.0039	0.23	0.0699	0.0082	1122	21	1112	59	1089	71	1089	71
Zircon_066	290.7	101.8	0.35	0.0757	0.0049	1.92	0.16	0.1842	0.0032	0.21	0.054	0.0058	1090	18	1088	54	1100	71	1100	71
Zircon_001	364	138.8	0.38	0.0766	0.005	2.07	0.17	0.1951	0.0044	0.27	0.0582	0.0062	1149	24	1137	55	1104	70	1104	70
Zircon_003	196	80.6	0.41	0.0763	0.0051	1.78	0.15	0.1718	0.003	0.21	0.0539	0.006	1022	17	1042	52	1115	92	1115	92
Zircon_048	156.5	66.8	0.43	0.0768	0.0057	1.7	0.15	0.1647	0.0045	0.31	0.0437	0.0051	983	25	1015	62	1116	86	1116	86
Zircon_069	92.3	50.6	0.55	0.0783	0.0056	2.19	0.19	0.2025	0.0037	0.21	0.0588	0.0064	1189	20	1173	61	1121	74	1121	74
Zircon_054	238	55.9	0.23	0.0766	0.0055	2.1	0.18	0.1991	0.0043	0.25	0.0569	0.0065	1171	23	1149	58	1145	72	1145	72
Zircon_074	84.6	34.4	0.41	0.0776	0.0056	2.15	0.19	0.2005	0.0045	0.25	0.0589	0.0066	1178	24	1162	60	1150	69	1150	69
Zircon_091	192.1	54	0.28	0.0793	0.0059	1.99	0.18	0.1817	0.004	0.24	0.062	0.007	1076	22	1115	57	1180	130	1180	130
Zircon_006	161.4	63.3	0.39	0.0783	0.0055	2.22	0.19	0.2057	0.0043	0.24	0.0589	0.0065	1206	23	1185	62	1181	95	1181	95
Zircon_082	370	95.9	0.26	0.079	0.0052	2.26	0.19	0.2065	0.0037	0.21	0.0609	0.0066	1210	20	1200	58	1185	77	1185	77
Zircon_087	577	135.3	0.23	0.0795	0.0053	2.26	0.18	0.2061	0.0038	0.23	0.0597	0.0065	1208	20	1201	57	1188	56	1188	56
Zircon_072	123.6	30.9	0.25	0.0803	0.0058	2.21	0.19	0.2014	0.0045	0.26	0.0621	0.0069	1185	25	1181	60	1199	72	1199	72
Zircon_025	84.1	28.4	0.34	0.0795	0.0061	2.29	0.21	0.2059	0.0041	0.22	0.0622	0.0069	1207	22	1210	66	1204	88	1204	88
Zircon_041	153.8	157	1.02	0.0786	0.0057	1.68	0.15	0.1516	0.0064	0.47	0.0281	0.0046	910	36	1000	58	1210	120	1210	120
Zircon_029	351	83.9	0.24	0.0808	0.0052	2.27	0.18	0.2051	0.0036	0.22	0.0581	0.0063	1203	19	1204	57	1217	59	1217	59
Zircon_022	70.6	25.2	0.36	0.0814	0.0055	2.33	0.19	0.2112	0.0039	0.23	0.0736	0.0083	1235	21	1229	65	1220	110	1220	110
Zircon_005	365	118	0.32	0.0803	0.0055	1.93	0.19	0.1731	0.0069	0.40	0.0548	0.0061	1029	38	1091	65	1234	92	1234	92
Zircon_088	21.98	16.14	0.73	0.077	0.0099	1.7	0.24	0.1606	0.0052	0.23	0.0419	0.0057	960	29	1023	91	1250	110	1250	110
Zircon_073	361	107.7	0.30	0.0861	0.0057	2.75	0.22	0.2327	0.0045	0.24	0.0656	0.0071	1349	23	1341	61	1320	94	1320	94
Zircon_018	174.2	94.9	0.54	0.0887	0.0059	2.98	0.24	0.2463	0.005	0.25	0.0744	0.008	1419	26	1402	61	1393	65	1393	65
Zircon_090	91	76.1	0.84	0.0892	0.0062	2.81	0.24	0.2319	0.0052	0.26	0.0659	0.0071	1344	27	1361	67	1417	59	1417	59
Zircon_081	1037	377	0.36	0.0946	0.0064	3.33	0.28	0.2544	0.0075	0.35	0.0737	0.008	1461	39	1487	66	1515	74	1515	74
Zircon_083	102.1	25.8	0.25	0.0963	0.0065	3.64	0.3	0.2724	0.0052	0.23	0.0833	0.0094	1553	26	1558	65	1555	72	1555	72
Zircon_070	258.1	131.5	0.51	0.1304	0.0085	6.39	0.51	0.3543	0.0067	0.24	0.1	0.011	1955	32	2031	71	2102	61	2102	61
Zircon_057	158.5	88.9	0.56	0.19	0.014	12.9	1.1	0.489	0.012	0.29	0.129	0.016	2568	52	2668	80	2735	47	2735	47
Zircon_095	110.9	26.51	0.24	0.23	0.014	19.1	1.5	0.602	0.011	0.23	0.163	0.018	3037	43	3048	77	3044	72	3044	72

FORMACIÓN ATZOMPA, MIEMBRO SANTA MARTA, MIS163B

18°47'4.32"N **98° 5'57.14"W** **CORRECTED RATIOS** **CORRECTED AGES (Ma)**

	U (ppm)	Th (ppm)	Th/U	207Pb/206Pb	±1s	207Pb/235U	±1s	206Pb/238U	±1s	208Pb/232Th	±1s	Rho	206Pb/238U	±1s	207Pb/235U	±1s	207Pb/206Pb	±1s	Best age (Ma)	±1s
Zircon_047	902	382	0.42	0.0484	8E-05	0.1256	0.004	0.0189	0.0005	0.0061	0.0012	0.84	120.7	3.1	120.1	3.1	119.2	4.1	120.7	3.1
Zircon_097	676	301	0.45	0.0485	5E-05	0.1261	0.003	0.019	0.0005	0.0058	0.0018	0.74	121.5	3.1	120.6	2.6	122.2	2.4	121.5	3.1
Zircon_023	266.4	83.1	0.31	0.0486	0.0002	0.1275	0.007	0.019	0.0009	0.0048	0.0013	1.00	121.6	5.4	121.8	6.3	126.1	7.3	121.6	5.4
Zircon_048	265.7	103.9	0.39	0.0486	9E-05	0.1277	0.006	0.019	0.0008	0.0052	0.0027	1.00	121.6	5.3	121.9	5.3	128.8	4.3	121.6	5.3
Zircon_010	1019	392	0.38	0.0485	0.0001	0.1277	0.006	0.0191	0.0006	0.00552	0.00088	1.00	121.8	3.5	122	5	125.7	5.3	121.8	3.5
Zircon_033	636	209.8	0.33	0.0485	5E-05	0.1279	0.004	0.0191	0.0005	0.0064	0.0015	1.00	122.1	3.4	122.2	3.1	123.2	2.5	122.1	3.4
Zircon_043	881	417	0.47	0.0485	8E-05	0.1288	0.003	0.0192	0.0004	0.00566	0.00054	0.80	122.6	2.6	123	2.7	124.3	3.7	122.6	2.6
Zircon_046	478	217	0.45	0.0486	6E-05	0.1299	0.004	0.0194	0.0005	0.0062	0.001	1.00	123.8	2.9	124	3.1	126.7	3	123.8	2.9
Zircon_018	604	222.3	0.37	0.0485	6E-05	0.1299	0.004	0.0194	0.0006	0.0056	0.0015	1.00	123.9	3.5	124	3.6	125.2	2.7	123.9	3.5
Zircon_026	362	166.3	0.46	0.0485	7E-05	0.1297	0.004	0.0194	0.0005	0.0058	0.001	0.83	123.9	3.1	123.8	3.5	124.4	3.6	123.9	3.1
Zircon_029	1550	421	0.27	0.0483	0.0003	0.1278	0.005	0.0195	0.0004	0.0056	0.0013	0.48	124.7	2.4	122.1	4.3	115	15	124.7	2.4
Zircon_044	935	396.9	0.42	0.0485	0.0001	0.1307	0.003	0.0196	0.0004	0.00596	0.00096	0.74	125.2	2.4	124.7	2.4	122.8	6.1	125.2	2.4
Zircon_058	803	349	0.43	0.0485	0.0002	0.1343	0.004	0.0198	0.0005	0.00618	0.00093	0.52	126.1	3	127.9	3.7	121.6	9.2	126.1	3
Zircon_083	628	313.6	0.50	0.0486	7E-05	0.1328	0.004	0.0198	0.0005	0.006	0.0011	0.77	126.1	3.1	126.6	3.4	127.4	3.3	126.1	3.1
Zircon_059	708	249	0.35	0.0485	0.0001	0.1325	0.004	0.0198	0.0005	0.0059	0.0014	0.50	126.4	3	126.3	3.6	125.8	5.6	126.4	3
Zircon_080	401	127.2	0.32	0.0486	9E-05	0.1327	0.004	0.0198	0.0005	0.0059	0.0011	0.72	126.6	3.1	126.5	4	128.4	4.2	126.6	3.1
Zircon_035	563	201	0.36	0.049	9E-05	0.1342	0.005	0.0199	0.0007	0.0068	0.0027	1.00	126.8	4.5	127.8	4.8	146.6	4.3	126.8	4.5
Zircon_019	1550	739	0.48	0.0486	0.0001	0.1334	0.006	0.0199	0.0007	0.00607	0.00092	1.00	127	4.4	127.1	5.2	130	5.4	127	4.4
Zircon_057	360	117.9	0.33	0.0486	8E-05	0.1353	0.005	0.0201	0.0006	0.0055	0.0015	0.97	128.2	3.9	128.8	4.1	129.3	3.9	128.2	3.9
Zircon_012	574	158.1	0.28	0.0487	5E-05	0.1364	0.003	0.0203	0.0006	0.005	0.0022	1.00	129.5	3.6	129.8	2.9	134.5	2.4	129.5	3.6
Zircon_039	299.5	114	0.38	0.0487	8E-05	0.137	0.005	0.0204	0.0006	0.0061	0.0013	0.83	130.1	4	130.4	4.2	132.2	3.7	130.1	4
Zircon_017	1193	395	0.33	0.0486	0.0001	0.1367	0.007	0.0204	0.0009	0.0053	0.0019	1.00	130.2	5.8	130.1	6.6	130.2	6.2	130.2	5.8
Zircon_065	228	91.4	0.40	0.0487	9E-05	0.1358	0.005	0.0204	0.0007	0.0047	0.0013	0.91	130.2	4.1	129.3	4	131.3	4.5	130.2	4.1
Zircon_032	874.9	292	0.33	0.0487	6E-05	0.1372	0.004	0.0204	0.0006	0.0064	0.0011	1.00	130.4	3.5	130.5	3.1	132.7	2.7	130.4	3.5
Zircon_098	121.7	34.73	0.29	0.0487	0.0001	0.1373	0.008	0.0204	0.0011	0.006	0.0028	1.00	130.4	6.7	130.6	6.8	134.5	5.6	130.4	6.7
Zircon_024	985	455	0.46	0.0486	0.0001	0.1365	0.004	0.0205	0.0005	0.0058	0.0013	0.61	130.5	2.8	129.9	3.1	128.8	6.6	130.5	2.8

Zircon_004	667	303	0.45	0.0486	0.0002	0.1365	0.005	0.0205	0.0005	0.0063	0.0012	0.77	130.6	3	129.9	4.3	127.6	9.3	130.6	3
Zircon_050	242	93	0.38	0.0487	7E-05	0.1365	0.004	0.0206	0.0006	0.0055	0.0013	0.79	131.1	3.6	129.9	3.4	133.1	3.3	131.1	3.6
Zircon_052	691	493	0.71	0.0487	0.0001	0.1387	0.005	0.0206	0.0005	0.00614	0.00088	0.77	131.4	3	131.9	4.3	131.9	5.2	131.4	3
Zircon_014	821	464	0.57	0.0487	9E-05	0.1383	0.004	0.0207	0.0005	0.00622	0.00085	0.90	131.9	3	131.5	3.8	131.2	4.5	131.9	3
Zircon_038	369	111.8	0.30	0.0487	6E-05	0.137	0.004	0.0207	0.0006	0.0057	0.0021	0.26	132.1	3.5	130.3	3.2	132	2.7	132.1	3.5
Zircon_093	291	153.1	0.53	0.0487	0.0001	0.1393	0.008	0.0207	0.001	0.0061	0.0025	1.00	132.1	6.2	132.3	6.9	135.3	5.7	132.1	6.2
Zircon_054	187.6	125	0.67	0.0487	0.0001	0.1367	0.006	0.0208	0.0006	0.00603	0.00078	0.72	132.6	3.7	130.7	5.6	131.3	5.2	132.6	3.7
Zircon_068	268	74	0.28	0.0487	0.0001	0.1374	0.005	0.0208	0.0007	0.0071	0.0014	0.79	132.6	4.5	130.7	4.7	130.9	6.4	132.6	4.5
Zircon_099	834	413.9	0.50	0.0488	6E-05	0.1396	0.003	0.0208	0.0004	0.00674	0.0008	0.84	132.6	2.6	132.7	2.3	136.1	2.7	132.6	2.6
Zircon_062	707	331.3	0.47	0.0486	0.0002	0.1377	0.004	0.0209	0.0004	0.0061	0.0013	0.18	133.1	2.6	131.5	3.3	127	11	133.1	2.6
Zircon_078	1194	472	0.40	0.0487	0.0001	0.1411	0.005	0.0209	0.0005	0.007	0.001	0.80	133.6	3	134	4.2	132.9	5.7	133.6	3
Zircon_045	635	202.2	0.32	0.0486	0.0001	0.1405	0.004	0.021	0.0005	0.0065	0.0019	0.58	133.9	3.2	133.5	3.8	128.7	4.9	133.9	3.2
Zircon_074	1063	528	0.50	0.0488	7E-05	0.1421	0.004	0.0211	0.0006	0.006	0.0014	1.00	134.6	3.7	134.9	3.9	139.8	3.5	134.6	3.7
Zircon_092	444	290	0.65	0.0487	7E-05	0.1412	0.005	0.0211	0.0006	0.0062	0.0013	0.69	134.6	3.8	134	4.2	134.8	3.6	134.6	3.8
Zircon_021	579	255	0.44	0.0486	0.0001	0.1403	0.006	0.0211	0.0006	0.0065	0.0013	0.75	134.8	3.7	133.3	5.6	130.5	6.8	134.8	3.7
Zircon_020	727	190	0.26	0.0488	1E-04	0.1422	0.005	0.0211	0.0006	0.0062	0.0014	1.00	134.9	3.7	135	4.8	137.1	4.6	134.9	3.7
Zircon_036	335	97.5	0.29	0.0488	8E-05	0.1425	0.005	0.0212	0.0007	0.0057	0.0018	0.93	135.3	4.5	135.2	4.7	137	3.8	135.3	4.5
Zircon_001	418	138	0.33	0.0488	9E-05	0.1428	0.005	0.0212	0.0007	0.008	0.0013	1.00	135.4	4.4	135.5	4.6	136.8	4.2	135.4	4.4
Zircon_090	2070	1020	0.49	0.0487	0.0001	0.143	0.003	0.0213	0.0005	0.00668	0.0004	0.92	135.7	3	135.7	3.1	135.4	6.1	135.7	3
Zircon_034	259.8	130.3	0.50	0.0487	0.0001	0.1411	0.006	0.0213	0.0006	0.0061	0.0013	0.05	135.8	3.9	134	4.9	133.5	6.3	135.8	3.9
Zircon_049	368.6	138.1	0.37	0.0488	0.0001	0.1425	0.004	0.0213	0.0006	0.0065	0.0014	0.71	135.8	3.8	135.2	3.9	136.1	5	135.8	3.8
Zircon_022	467	143	0.31	0.0487	9E-05	0.1413	0.005	0.0214	0.0006	0.0062	0.0016	0.68	136.2	3.5	134.2	4.7	135.3	4.5	136.2	3.5
Zircon_071	567	275	0.49	0.0488	0.0001	0.1437	0.004	0.0214	0.0005	0.0072	0.0011	0.89	136.4	3.3	136.3	3.5	135.7	6.1	136.4	3.3
Zircon_003	308	98.2	0.32	0.0489	0.0001	0.1443	0.006	0.0214	0.0009	0.0089	0.0022	1.00	136.6	5.6	136.8	5.7	140.6	5.2	136.6	5.6
Zircon_008	1110	650	0.59	0.0488	9E-05	0.1439	0.007	0.0215	0.0007	0.007	0.001	0.94	137.1	4.6	136.5	5.9	138.5	4.5	137.1	4.6
Zircon_013	634	257	0.41	0.0489	0.0002	0.1494	0.005	0.0223	0.0007	0.0066	0.0012	0.78	142.2	4.4	141.4	4.8	142.5	7.7	142.2	4.4
Zircon_055	152.1	79.2	0.52	0.0493	0.0001	0.1624	0.009	0.0239	0.001	0.0057	0.002	1.00	152	6.6	152.7	7.5	163.2	6.5	152	6.6
Zircon_070	161	58.1	0.36	0.05	0.0002	0.21	0.013	0.0305	0.0016	0.0095	0.003	1.00	193	10	194	11	197	11	193	10
Zircon_100	160.5	67.9	0.42	0.0515	0.0001	0.2691	0.009	0.0379	0.0014	0.0109	0.0056	1.00	240	8.9	241.9	7.2	261	5.2	240	8.9
Zircon_064	57.67	56.7	0.98	0.0515	0.0005	0.283	0.034	0.0395	0.0044	0.0102	0.0041	1.00	250	27	252	27	265	20	250	27

Zircon_053	42.5	33	0.78	0.0519	0.0003	0.311	0.02	0.0439	0.0021	0.0124	0.0034	0.68	279	13	274	16	282	14	279	13
Zircon_076	112.6	71.1	0.63	0.0524	0.0002	0.345	0.012	0.0478	0.0014	0.0136	0.0028	0.91	300.9	8.5	300.7	8.8	304.5	9	300.9	8.5
Zircon_082	167	129	0.77	0.0552	0.0007	0.53	0.026	0.0698	0.0019	0.0213	0.002	0.56	435	11	433	16	420	28	435	11
Zircon_011	238	103	0.43	0.056	0.0005	0.575	0.02	0.0744	0.0022	0.023	0.0027	0.98	463	13	461	13	453	21	463	13
Zircon_009	1013	408	0.40	0.0563	0.0017	0.595	0.035	0.077	0.0014	0.0245	0.0024	0.55	478.2	8.6	474	23	466	66	478.2	8.6
Zircon_025	746	358	0.48	0.0557	0.0014	0.614	0.044	0.0803	0.0018	0.0242	0.0036	0.31	498	11	485	28	438	55	498	11
Zircon_077	350	48.5	0.14	0.0585	0.0002	0.675	0.016	0.0837	0.0028	0.026	0.015	1.00	518	17	523.6	9.9	548.5	6.2	518	17
Zircon_051	469	406	0.87	0.0579	0.0008	0.704	0.037	0.089	0.0019	0.0265	0.0027	0.61	550	11	541	22	526	30	550	11
Zircon_016	77.2	70.1	0.91	0.0599	0.0012	0.835	0.046	0.1053	0.0034	0.0313	0.0047	0.24	645	20	615	26	598	45	645	20
Zircon_040	127.2	43.9	0.35	0.065	0.0008	1.137	0.051	0.1272	0.0044	0.035	0.011	0.98	772	25	771	24	774	26	772	25
Zircon_037	134.7	76.1	0.56	0.0693	0.0018	1.492	0.089	0.1576	0.0031	0.0483	0.0051	0.40	944	17	926	36	906	55	944	17
Zircon_094	114.3	38.3	0.34	0.07	0.001	1.532	0.085	0.1599	0.0038	0.0497	0.0052	0.38	956	21	942	34	926	30	956	21
Zircon_005	681	13.39	0.02	0.071	0.0016	1.57	0.1	0.1613	0.0034	0.093	0.012	0.65	964	19	957	41	956	46	964	19
Zircon_056	524	131	0.25	0.0708	0.0017	1.572	0.08	0.1623	0.003	0.0485	0.0035	0.54	969	16	961	34	952	49	969	16
Zircon_089	101.6	63.2	0.62	0.0719	0.001	1.596	0.051	0.1627	0.0034	0.0491	0.0035	0.82	972	19	970	19	981	27	972	19
Zircon_002	1106	137.8	0.12	0.0682	0.0013	1.53	0.1	0.1629	0.0037	0.0458	0.0046	0.49	973	20	941	42	874	40	973	20
Zircon_006	122.4	27.5	0.22	0.0714	0.0011	1.611	0.09	0.1646	0.0035	0.0535	0.0056	0.19	982	20	974	35	969	31	982	20
Zircon_095	154.1	61.6	0.40	0.0705	0.0016	1.587	0.069	0.1658	0.0037	0.0522	0.0054	0.53	989	20	964	27	943	49	989	20
Zircon_081	311.4	181.8	0.58	0.0708	0.0019	1.611	0.098	0.1662	0.003	0.0503	0.0049	0.35	991	17	977	38	950	56	991	17
Zircon_091	168.9	43.1	0.26	0.0711	0.0015	1.65	0.11	0.1672	0.0037	0.0513	0.0048	0.52	996	20	988	42	959	44	996	20
Zircon_060	385.5	99.3	0.26	0.0715	0.0017	1.64	0.088	0.1678	0.0031	0.0505	0.0039	0.41	1000	17	985	34	971	49	1000	17
Zircon_072	129.1	66.5	0.52	0.0715	0.0011	1.638	0.098	0.1685	0.0037	0.0496	0.0047	0.44	1004	21	984	38	971	32	1004	21
Zircon_028	112.9	40.5	0.36	0.0713	0.0023	1.69	0.11	0.1738	0.0046	0.0529	0.0039	0.08	1033	25	1015	41	964	67	1033	25
Zircon_042	103	78	0.76	0.0742	0.0013	1.78	0.11	0.1788	0.0045	0.0548	0.0062	0.69	1060	25	1037	41	1045	36	1045	36
Zircon_096	369	164	0.44	0.0761	0.0021	1.922	0.094	0.1857	0.0042	0.0573	0.0055	0.80	1098	23	1088	35	1097	54	1097	54
Zircon_015	374	166.3	0.44	0.0763	0.0018	2.09	0.15	0.1974	0.0041	0.0592	0.0057	0.14	1161	22	1144	50	1104	47	1104	47
Zircon_086	185.2	68.4	0.37	0.0767	0.0017	2.04	0.11	0.1929	0.0037	0.059	0.0054	0.30	1137	20	1129	38	1113	44	1113	44
Zircon_063	70.2	37.8	0.54	0.0764	0.0021	2.04	0.11	0.1967	0.0044	0.0603	0.0069	0.48	1158	24	1128	36	1115	54	1115	54
Zircon_075	287	90	0.31	0.0768	0.0023	2.11	0.15	0.1992	0.0039	0.0636	0.0065	0.43	1171	21	1156	51	1115	59	1115	59
Zircon_041	607	200.1	0.33	0.0773	0.0026	2.24	0.16	0.211	0.0043	0.058	0.0056	0.49	1234	27	1193	49	1127	68	1127	68

Zircon_030	324	137.3	0.42	0.078	0.0026	2.23	0.13	0.2089	0.0042	0.06	0.0057	0.30	1223	22	1189	41	1145	68	1145	68
Zircon_085	144	53	0.37	0.0795	0.0011	2.31	0.1	0.2092	0.0055	0.0666	0.0065	0.66	1224	29	1226	31	1183	27	1183	27
Zircon_069	141	42.4	0.30	0.0797	0.002	2.32	0.13	0.2122	0.0044	0.0647	0.006	0.39	1240	23	1217	40	1187	50	1187	50
Zircon_087	293	104	0.35	0.0814	0.0026	2.44	0.16	0.2169	0.0039	0.0631	0.0064	0.27	1265	21	1254	48	1230	62	1230	62
Zircon_031	248	357	1.44	0.0817	0.0019	2.46	0.15	0.2186	0.0043	0.0643	0.0061	0.24	1275	23	1260	45	1237	45	1237	45
Zircon_066	74.9	19.89	0.27	0.0847	0.0032	2.75	0.19	0.2356	0.006	0.0698	0.0072	0.32	1364	31	1340	50	1306	76	1306	76
Zircon_079	268	143.1	0.53	0.0882	0.0028	2.88	0.27	0.2371	0.0055	0.0704	0.007	0.87	1371	29	1376	70	1386	61	1386	61
Zircon_084	491	243.5	0.50	0.1115	0.0034	5.27	0.34	0.3417	0.0069	0.0986	0.0095	0.31	1895	33	1864	55	1824	56	1824	56
Zircon_067	311.2	141.6	0.46	0.117	0.0046	5.59	0.44	0.3445	0.0093	0.093	0.009	0.32	1908	45	1914	68	1910	70	1910	70
Zircon_088	149.6	97.8	0.65	0.1176	0.0034	5.83	0.38	0.3561	0.0066	0.1028	0.0099	0.30	1963	31	1950	57	1920	52	1920	52

FORMACIÓN ATZOMPA, MIEMBRO SANTA MARTA, CLASTOS DE CONGLOMERADO, MIS136

18°46´46.3´´N **98°7´13´´W** **CORRECTED RATIOS** **CORRECTED AGES (Ma)**

	U (ppm)	Th (ppm)	Th/U	207Pb/206Pb	±1s	207Pb/235U	±1s	206Pb/238U	±1s	208Pb/232Th	±1s	Rho	206Pb/238U	±1s	207Pb/235U	±1s	207Pb/206Pb	±1s	Best age (Ma)	±1s
Zircon_064_083	741.2	529.9	0.6642	0.0504	0.0014	0.1327	0.004	0.0191	0.0003	0.00597	0.00016	0.42	122	2	126	4	213	62	122	2
Zircon_037_051	716.7	397.2	0.515	0.051	0.0015	0.1349	0.004	0.0193	0.0003	0.00567	0.00016	0.48	123	2	128	4	240	62	123	2
Zircon_036_136_050	347.0	218.6	0.5855	0.0588	0.0033	0.1594	0.01	0.0196	0.0004	0.0056	0.00022	0.35	125	3	150	8	558	114	125	3
Zircon_047_063	327.4	131.9	0.3743	0.0557	0.0023	0.1495	0.007	0.0195	0.0003	0.00607	0.00021	0.39	125	2	141	6	442	85	125	2
Zircon_050_066	765.3	448.4	0.5445	0.0501	0.0016	0.1355	0.005	0.0196	0.0003	0.00605	0.00019	0.44	125	2	129	4	199	67	125	2
Zircon_067_087	572.8	241.0	0.391	0.0507	0.0016	0.1378	0.005	0.0198	0.0003	0.00599	0.00019	0.44	126	2	131	4	228	68	126	2
Zircon_046_062	450.0	179.6	0.3708	0.0512	0.0018	0.1408	0.005	0.0201	0.0003	0.00645	0.00023	0.39	128	2	134	5	248	75	128	2
Zircon_059_077	307.0	164.5	0.4978	0.0536	0.0021	0.1471	0.006	0.02	0.0003	0.00624	0.00022	0.36	128	2	139	5	355	84	128	2
Zircon_066_086	369.4	139.9	0.3518	0.0514	0.0021	0.143	0.006	0.0201	0.0003	0.00594	0.00022	0.3	128	2	136	5	261	90	128	2
Zircon_048_064	859.0	460.3	0.4979	0.0509	0.0014	0.1414	0.004	0.0202	0.0003	0.00621	0.00018	0.43	129	2	134	4	234	60	129	2
Zircon_052_069	364.5	164.7	0.4198	0.0544	0.0023	0.1511	0.007	0.0202	0.0003	0.0062	0.00022	0.34	129	2	143	6	386	90	129	2
Zircon_056_074	517.1	217.6	0.3911	0.0518	0.0017	0.1445	0.005	0.0202	0.0003	0.00644	0.0002	0.47	129	2	137	5	275	70	129	2
Zircon_061_080	444.1	170.4	0.3565	0.0524	0.0023	0.1452	0.007	0.0202	0.0003	0.0067	0.00021	0.31	129	2	138	6	302	93	129	2
Zircon_063_082	327.9	154.3	0.4371	0.0528	0.0026	0.1459	0.008	0.0203	0.0004	0.00653	0.00022	0.36	129	2	138	7	319	108	129	2
Zircon_065_084	278.3	162.7	0.5432	0.0569	0.0022	0.1596	0.006	0.0204	0.0003	0.00636	0.0002	0.35	130	2	150	6	488	80	130	2
Zircon_051_068	483.8	287.5	0.5521	0.0502	0.002	0.1407	0.006	0.0206	0.0004	0.00631	0.00019	0.45	131	3	134	5	203	84	131	3
Zircon_040_054	240.8	169.7	0.6548	0.0605	0.0029	0.1712	0.009	0.0207	0.0004	0.00657	0.00022	0.35	132	2	160	8	623	97	132	2
Zircon_041_056	512.7	285.1	0.5167	0.0496	0.002	0.1426	0.006	0.0207	0.0003	0.00639	0.00021	0.32	132	2	135	5	178	88	132	2
Zircon_044_059	503.3	266.0	0.4911	0.0523	0.0017	0.1487	0.005	0.0206	0.0003	0.00652	0.0002	0.38	132	2	141	5	298	70	132	2
Zircon_068_088	299.2	157.4	0.4888	0.0529	0.0025	0.1507	0.008	0.0207	0.0004	0.00658	0.00027	0.34	132	2	143	7	322	102	132	2
Zircon_070_090	393.1	232.3	0.5491	0.0526	0.0021	0.1508	0.006	0.0208	0.0003	0.0066	0.00021	0.38	133	2	143	6	312	84	133	2
Zircon_038_052	298.3	151.4	0.4717	0.0624	0.0028	0.1818	0.009	0.021	0.0003	0.00678	0.00023	0.31	134	2	170	7	689	90	134	2
Zircon_049_065	344.8	131.3	0.3538	0.0518	0.0028	0.1505	0.009	0.0211	0.0003	0.00662	0.00011	0.31	134	2	142	8	278	115	134	2
Zircon_062_081	268.0	144.3	0.5002	0.0493	0.002	0.142	0.006	0.021	0.0003	0.00648	0.00026	0.32	134	2	135	5	161	90	134	2
Zircon_039_053	431.5	173.9	0.3745	0.0511	0.0022	0.1501	0.007	0.0212	0.0003	0.00674	0.00022	0.34	135	2	142	6	247	90	135	2
Zircon_055_072	365.6	146.4	0.3721	0.0486	0.0022	0.141	0.007	0.0212	0.0003	0.0065	0.00021	0.33	135	2	134	6	126	99	135	2

Zircon_042_057	161.0	72.9	0.4205	0.0546	0.0026	0.1599	0.008	0.0213	0.0004	0.00619	0.0003	0.37	136	3	151	7	394	101	136	3
Zircon_058_076	266.3	149.0	0.5199	0.048	0.0023	0.1416	0.007	0.0213	0.0003	0.00633	0.00025	0.32	136	2	134	6	101	100	136	2
Zircon_060_078	591.1	293.1	0.4607	0.0513	0.0016	0.1528	0.005	0.0216	0.0003	0.00694	0.00022	0.39	138	2	144	5	255	68	138	2
Zircon_043_058	174.0	72.1	0.3848	0.0529	0.0029	0.1574	0.009	0.0217	0.0004	0.00621	0.00029	0.28	139	2	148	8	325	117	139	2
Zircon_053_070	173.6	146.9	0.786	0.0559	0.0027	0.166	0.009	0.0218	0.0004	0.00567	0.00023	0.32	139	2	156	7	446	104	139	2
Zircon_057_075	532.7	274.5	0.4789	0.0489	0.0021	0.1489	0.007	0.0221	0.0003	0.00699	0.00012	0.38	141	2	141	6	144	93	141	2
Zircon_054_071	349.3	210.0	0.5585	0.0488	0.0021	0.1549	0.007	0.0231	0.0004	0.0072	0.00029	0.4	147	3	146	6	140	94	147	3
Zircon_045_060	362.9	128.6	0.3293	0.052	0.0017	0.1823	0.007	0.0248	0.0005	0.00905	0.00031	0.54	158	3	170	6	284	70	158	3

ANEXO 3

RESPUESTA A LAS CORRECCIONES REALIZADAS A LA TESIS POR PARTE DEL SINODAL DRA. CLAUDIA CRISTINA MENDOZA ROSALES.

RESPUESTA A LOS COMENTARIOS AL ARTÍCULO:

Sierra-Rojas, M. I., Molina-Garza, R. S., y Lawton, T. F., 2016. The Lower Cretaceous Atzompa Formation in South-Central Mexico: Record of Evolution from Extensional Backarc Basin Margin to Carbonate Platform. Journal of Sedimentary Research, 86(6), 712-733.

Procedencia de sedimentos en areniscas. Figura 6, capitulo 3

CCMR: ¿De dónde salieron estos datos? En mi tesis analicé la procedencia de la Formación La Compañía. Debes de ser más cuidadosa al referir la información de otros autores. Puede ser muy delicado.

En el artículo correspondiente al capítulo 3, graficamos los datos de conteo de puntos realizados en la Formación Atzompa en los diagramas ternarios de discriminación Tectónica de Dickinson (1985). Junto con los nuevos datos, graficamos datos de trabajos anteriores como el de la tesis de licenciatura de Serrano-García et al. (2014) y Mendoza-Rosales, 2010. En la leyenda de las figuras, mencionamos erróneamente que el dato de una muestra corresponde a la Formación Zapotitlán y no a la Formaciones la Compañía.

Magmatismo Alcalino en la Formación Chivillas

En el Artículo correspondiente al capítulo 3 escribimos: "*Aptian mafic rocks in the Cuicateco basin, represented by pillow basalts of the Chivillas Formation, have been interpreted as oceanic tholeiites from a ridge transform intersection (Mendoza-Rosales et al. 2010)"*

CCMR: Este trabajo no dice esto. Revisa el texto y aclara tu cita.

Revisando detenidamente el artículo referenciado, la Dra. Mendoza está en lo cierto. Los autores clasifican geoquímicamente los basaltos de la Formación Chivillas en la serie alcalina, y no sub-alcalina como correspondería a una roca toleítica.

Con respecto a la interpretación tectónica, efectivamente Mendoza-Rosales et al. (2010) favorecen el modelo de intersección entre la dorsal y la falla transformate "*We favor the model on Figs. 6 and 7, in which submarine volcano-sedimentary rocks of the Chivillas Formation are explained as the result of extensional stress at a ridge–transform intersection"*

Edad del magmatismo y depositación de la Formación Chivillas

En el artículo del capítulo 3, Sierra-Rojas et al. (2016) mencionan que el magmatismo de la Formación Chivillas es de edad Aptiano, según los datos reportados por Mendoza-Rosales et al., (2010):

"This interpretation contrasts with that of Mendoza-Rosales et al. (2010), who linked the Aptian magmatism of the Chivillas Formation in the Cuicateco basin to the opening of the Gulf of Mexico"

En otra línea afirmamos:

"Westward propagation of seafloor spreading in the Gulf of Mexico may have contributed to extension, subsidence, and magmatism in the Cuicateco basin early in its history during Valanginian to Berriasian time, but not during Aptian deposition of the Chivillas Formation as proposed by Mendoza-Rosales et al. (2010)."

CCMR: Nosotros no dijimos esto en este artículo. ¿Lo leiste?

Aunque Mendoza-Rosales et al. (2010) nunca dicen que el magmatismo es Aptiano los datos implican esta conclusión. Nosotros luego de leer el artículo en mención, interpretamos que la edad del magmatismo es Aptiana, por los siguientes motivos:

- Los autores reportan una edad máxima de depósito, lo cual corresponde a la componente de edad más joven en una muestra de circones detríticos. Lo anterior implica, que la edad de depósito de la capa representada por dicha población detrítica debe ser más joven que la edad máxima de depósito, en este caso específico la edad del circón más joven.
- Revisando el repositorio de datos de dicho artículo, el circón más joven en la muestra FCH040 es de 125 ± 2 Ma y en la muestra FCH039 es de 126 ± 1 Ma.
- La edad máxima de depósito reportada en el artículo de Mendoza-Rosales et al. (2010), es de ca. 126 Ma, el cual reportan como Barremiano, pero técnicamente corresponde al límite Barremiano-Aptiano (Gradstein et al., 2012).
- Posición estratigráfica. Considerando que las lavas almohadilladas de la Formación Chivillas demostraron ser estériles en circón, y que lo reportado es una edad máxima de depósito en arenas, las lavas almohadilladas que suprayacen los horizontes de areniscas fechados, deben corresponder con la parte inferior del Aptiano.